LOW TEMPERATURE DOLOMITE SYNTHESIS

LOW TEMPERATURE DOLOMITE SYNTHESIS: REACTION KINETICS, UREA CATALYSIS AND ISOTOPIC ANALYSES

By: Bradley Freake, B.Sc. (Hons)

A Thesis Submitted to the School of Graduate Studies in Partial Fulfillment of the Requirements for the Degree Master of Science

McMaster University

Descriptive Note

MASTER OF SCIENCE (2019), McMaster University, Hamilton, Ontario

School of Geography and Earth Sciences

TITLE: Low Temperature Dolomite Synthesis: Reaction Kinetics, Urea Catalysis and Isotopic Analyses

AUTHOR: Bradley Freake

SUPERVISOR: Dr. Sang-Tae Kim

NUMBER OF PAGES: X, 183

Abstract

Dolomite is a naturally abundant carbonate mineral possessing important links to economic mineral deposits, petroleum reservoirs and carbonate geochemistry, yet the geochemical conditions by which it forms remain a mystery. Abundant attempts to synthesis dolomite at temperatures below 100 °C have proved unsuccessful, forming the paradox known as the "dolomite problem". This study demonstrates a newly developed method capable of synthesizing dolomite at temperatures as low as 60 °C. This method, involving the addition of solid phase Na_2CO_3 to Ca-Mg^{2+} cation solutions, seemingly overcomes the kinetic barriers known to inhibit dolomite formation by rapid replacement of Na_2CO_3. Furthermore, although previously proposed to encourage dolomite formation, the role of urea facilitating dolomite synthesis is confirmed. The addition of varying urea concentrations is found to improve the stoichiometry and cation ordering of dolomite between 50 - 80 °C, and notably, dolomite synthesis at 50 °C requires a 252 mmolal urea concentration in solution. These findings provide a foundational tool which will greatly benefit future research into answering the "dolomite problem".

Due to the inability to synthesize dolomite at low temperatures, understanding of isotope fractionation between dolomite and water has been poorly constrained. Therefore, calibrations of the dolomite-water oxygen isotope paleothermometer are scarce, relying on data from either the extrapolation of high temperature (> 100 °C) dolomite studies or protodolomite synthesized at more ambient temperatures. Provided here is a new dolomite-water oxygen isotope fractionation curve, constructed from dolomite synthesized between 50 - 80 °C. Although certain dolomite synthesized by the method developed in this study display apparent isotopic heterogeneity, a correction is applied to more closely resemble isotopic equilibrium fractionation between dolomite and water. Initial investigations into isotope effects associated with dolomite synthesis by the method developed here are promising and should strengthen the role of dolomite in carbonate geochemistry research.

Acknowledgements

First and foremost, much thanks and appreciation go to my wife, Yvette. Your encouragement, support, and the unwavering belief that I could achieve the sometimes ambitious goals I laid out for myself, allowed this project to be possible. Your editorial review of this thesis and guidance with academic writing in general has been greatly beneficial to my academic career.

Appreciation goes to my supervisor, Dr. Sang-Tae Kim. I value your support in allowing me to choose a research direction that I was passionate about and the commitment you displayed for continuing this project, even after many disappointing experiments. I also appreciate your time in reviewing and discussing experimental data and your input on the contents of this thesis. I also thank my committee members, Dr. Gregory Slater and Dr. Henry Schwarcz for their review and improvements to this thesis.

Special thanks is given to Martin Knyf; your guidance with laboratory techniques was crucial for implementing this project and your willingness to answer any geochemistry question was always appreciated. Your continuous positive attitude was infectious and your enthusiasm for science in general has no doubt been instilled in each student you have guided. Thanks goes to Nick Randazzo, our discussions regarding my research were always beneficial, and I appreciate the much-needed advice you have provided for the past two years. Your friendship will be a valued part of my time at McMaster. I also thank Kate Allan for assistance with laboratory procedures and the optimistic approach you brought to our lab group. I thank Victoria Jarvis and James Britten for your instruction in performing XRD techniques, your willingness to assist with any issues that arose, and valuable discussions. I also thank Chris Butcher for help with performing SEM procedures.

Finally, thanks go to my dad for your support throughout my academic career and for being a testament to the values of faith and hard work. Also, to my mom, the determination you have demonstrated throughout your life has been instilled in not only myself, but in all of your children. I hope you realize the role you have played in each of our lives.

Table of Contents

Abstract iii
Acknowledgements iv
List of Figures viii
List of Tables x
CHAPTER 1: INTRODUCTION AND BACKGROUND 2
Section 1.1: Geochemical Overview for Carbonate Minerals 2
Section 1.2: Dolomite Properties 5
Section 1.2.1: Dolomite Stoichiometry and Cation Ordering 5
Section 1.2.2: Protodolomite Characterization and Terminology 8
Section 1.2.3: Dolomitization and Direct Precipitation 9
Section 1.3: Dolomite Formation and Laboratory Synthesis 11
Section 1.3.1: Inhibiting Factors of Dolomite Formation 11
Section 1.3.2: High Temperature Dolomite Synthesis 13
Section 1.3.3: Low Temperature Dolomite Synthesis 15
Section 1.3.4: Microbial and Biotic Protodolomite Synthesis 18
Section 1.3.5: Ostwald's Step Rule 20
Section 1.4: Carbonate-Water Oxygen Isotope Thermometry 21
Section 1.4.1: Isotopic Equilibrium and Influence of Kinetic Effects 22
Section 1.5: Study Purpose 24
Section 1.6: Thesis Outline 25
Figures and Tables 27
References 28
CHAPTER 2: LOW TEMPERATURE DOLOMITE SYNTHESIS: REACTION KINETICS AND UREA CATALYSIS 36
Abstract 36
Section 2.1: Introduction 36
Section 2.2: Materials and Methods 38
Section 2.3: Experimental Results 41
Section 2.4: Discussion 45
Section 2.4.1: Effect of Na_2CO_3 Phase on Dolomite Synthesis 45
Section 2.4.2: Effect of Urea Catalysis on Dolomite Synthesis 48

Section 2.5: Conclusions 51
Figures and Tables 54
CHAPTER 2 APPENDICES 66
Appendix 2.1: Detailed Materials and Methods 66
Appendix 2.1.1: Synthesis of Ca-Mg Carbonates 66
Appendix 2.1.2: Precipitate Crystal Structure Identification 68
Appendix 2.1.3: Analyses of Precipitate Stoichiometry and Cation Ordering 68
Appendix 2.2.4: Carbon Isotope Measurements 71
Appendix 2.2: Detailed Results 72
Appendix 2.2.1: (Proto)Dolomite Crystal Structure 72
Appendix 2.2.2: Cation Ordering and Identification of Dolomite 74
Appendix 2.2.3: (Proto)Dolomite Stoichiometry 77
Appendix 2.2.4: Final Solution pH Trends 81
Appendix 2.2.5: (Proto)Dolomite Carbon Isotopic Signatures 82
Appendix 2.3: Supplementary Discussion 82
Appendix 2.3.1: Effect of $CaCl_2$ Replacement on Dolomite Synthesis 82
Appendix 2.3.2: Effect of Bottle Volume on Dolomite Synthesis 83
Figures and Tables 86
References 99
CHAPTER 3: OXYGEN ISOTOPE EFFECTS IN THE DOLOMITE-WATER SYSTEM 103
Abstract 103
Section 3.1: Introduction 103
Section 3.2: Detailed Materials and Methods 107
Section 3.2.1: Carbonate Synthesis 107
Section 3.2.2: Oxygen Isotope Analyses for Carbonates 108
Section 3.2.3: Oxygen Isotope Analyses for Solutions 109
Section 3.3: Detailed Results and Discussion 110
Section 3.3.1: Time Series of $\delta^{18}O_{Dolomite}$ 110
Section 3.3.2: Effect of Evaporation on Solution $\delta^{18}O$ 111
Section 3.3.3: Effect of Urea on Solution and Carbonate $\delta^{18}O$ 112
Section 3.3.4: Effect of Preparation Method on Carbonate $\delta^{18}O$ 113
Section 3.3.5: Effect of Non-Equilibrium Isotope Effects 114

Section 3.3.6: Temperature Dependence of Oxygen Isotope Fractionation between Dolomite and Water....117
Section 3.3.7: Comparison of Dolomite-Water Fractionation Studies in Literature....118
Section 3.4: Conclusions....120
Figures and Tables....122
References....132
CHAPTER 4: CONCLUSIONS AND FUTURE RESEARCH....135
Section 4.1: Principal Findings....135
Section 4.2: Candidate's Contribution to the Field....137
Section 4.3: Future Research Requirements....138
References....140
Supplementary Information....141

List of Figures

Figure 1.1. The calcite and dolomite crystal structure 27
Figure 2.1. Schematic highlighting the difference in the solution preparation procedure between the aqueous addition and solid addition methods 54
Figure 2.2. XRD patterns for protodolomite (50 °C) and dolomite (60, 70 and 80 °C) precipitated by the solid addition method, containing no urea, and in 250 mL bottles 55
Figure 2.3. XRD patterns displaying the 015 peak for dolomite formed at 60 °C and under varying bottle size and urea concentration 56
Figure 2.4. XRD patterns displaying the 015 peak for protodolomite and dolomite formed under varying conditions at 50 °C. 57
Figure 2.5. XRD patterns for the triplicate dolomite samples precipitated by SAM, in 250 mL bottles, and 252 mM urea 58
Figure 2.6. Influence of urea on $\%MgCO_3$ of synthesized (proto)dolomite at 50, 60, 70, and 80 °C and under identical conditions (solid addition method, 250 mL bottles). 59
Figure 2.7. SEM images of synthesized (proto)dolomite at 60 °C and under various conditions . 60
Figure 2.8. Influence of urea concentration on (proto)dolomite $\delta^{13}C$ at each respective temperature between 50, 60, 70 and 80 °C 61
Figure 2.9. Relationship between urea concentration and the average final solution pH at 50, 60, 70, and 80 °C 61
Figure 2.10. Comparison of the precipitates formed from this study and those from Zhang et al. (2012a) 62
Figure 2.A1. Correlation of initial recorded SEM-EDS $\%MgCO_3$ and values displayed by Aztec software 86
Figure 2.A2. SEM images of selected carbonate samples from this study 87
Figure 2.A3. Comparison of average % cation ordering for solid method precipitates with increasing urea concentration at 70 °C 88
Figure 2.A4. XRD patterns displaying 015 peak for dolomite formed under varying conditions at 70 °C 88
Figure 2.A5. Comparison of average % cation ordering for solid method precipitates with increasing urea concentration at 80 °C 89
Figure 2.A6. Comparison of average % cation ordering for solid method precipitates with increasing urea concentration at 60 °C 89
Figure 2.A7. XRD patterns displaying 015 peak for protodolomite and dolomite formed under varying conditions at 60 °C 90
Figure 2.A8. Comparison of % cation ordering when using the typical $Ca(NO_3)_2$ as the Ca^{2+} ion source and using $CaCl_2$ as the Ca^{2+} ion source 91
Figure 2.A9. Comparison of $\%MgCO_3$ from solid addition method precipitates with aqueous addition method precipitates, with increasing urea concentration and at 50 °C 91
Figure 2.A10. Comparison of $\%MgCO_3$ from precipitates formed at all experimental conditions tested in this study, with increasing urea concentration and at 60 °C. 92
Figure 2.A11. Comparison of $\%MgCO_3$ from precipitates formed at all experimental conditions tested in this study, with increasing urea concentration and at 80 °C. 92

Figure 2.A12. Comparison of the influence of urea concentration on $\%MgCO_3$ for precipitates formed using the solid addition method at 40, 50, 60, 70, and 80 °C. 93
Figure 2.A13. Comparison of $\%MgCO_3$ when using the typical $Ca(NO_3)_2$ as the Ca^{2+} ion source and using $CaCl_2$ as the Ca^{2+} ion source. 93
Figure 2.A14. Comparison of the final solution pH for solid addition method precipitates with increasing urea concentration at 40, 50, 60, 70, and 80 °C. 94
Figure 2.A15. Relation of urea concentration with $\delta^{13}C$ of solid addition method precipitates at 40, 50, 60, 70, and 80 °C. 94
Figure 3.1. Relation of percent yield of CO_2 from dolomite following reaction with phosphoric acid 122
Figure 3.2. Comparison of the $\delta^{18}O_{carb}$ of BF-12-1 and BF-Dol with increasing reaction time with phosphoric acid 123
Figure 3.3. Comparison of $\delta^{18}O_{carb}$ with percent yield for BF-12-1 and BF-Dol 123
Figure 3.4. Change in solution $\delta^{18}O$ with increasing urea concentration over the temperature range 40 - 80 °C 124
Figure 3.5. Comparison of $1000\ln\alpha_{(proto)dolomite\text{-}water}$ for precipitates formed by the solid addition method with increasing urea concentration 125
Figure 3.6. Comparison of $1000\ln\alpha_{(proto)dolomite\text{-}water}$ for precipitates formed by the solid addition method in 250 mL bottles and those formed in 50 mL bottles 126
Figure 3.7. Comparison of $1000\ln\alpha_{carbonate\text{-}water}$ values for solid addition method precipitates and aqueous addition method precipitates from 40 - 80 °C 126
Figure 3.8. Calibration of the initial dolomite-water oxygen isotope fractionation curve developed in this study, as well as the carbonate-water oxygen isotope fraction curve 127
Figure 3.9. Comparison of the uncorrected, “Homogeneity Test`` corrected dolomite-water oxygen isotope curves developed in this study, as well as the carbonate-water curve (protodolomite/HMC) 127
Figure 3.10. Comparison of the dolomite-water oxygen isotope fractionation curve developed from study with previous literature calibrations 128

List of Tables

Table 1.1. Solubilities of common carbonate minerals at 25 °C and 1 bar atmospheric pressure. 27
Table 2.1. Experimental conditions for parent solutions prepared in this study 63
Table 2.2. Average parent solution and precipitate results 64
Table 2.3. XRF results for selected precipitates, including BF-Dol, the internal laboratory dolomite standard 65
Table 2.A1. Experimental conditions for parent solutions prepared in this study 95
Table 2.A2. Average experimental solution and precipitate results 97
Table 2.A3. Comparison of $\%MgCO_3$ values calculated for identical samples analyzed by the Bruker SMART6000 and Bruker D8 with CuKα radiation 98
Table 3.1. Results of the dolomite time series investigation from this study 129
Table 3.2. Detailed parent solution conditions and isotopic results for all samples analyzed, exclusion those displaying an evaporation effect 130

CHAPTER 1: INTRODUCTION AND BACKGROUND

CHAPTER 1: INTRODUCTION AND BACKGROUND

Section 1.1: Geochemical Overview for Carbonate Minerals

Studies of carbonate minerals have provided critical insight into numerous aspects of earth and environmental sciences. Specifically, the understanding of solution chemistry which promotes certain carbonate formation has provided insight into potential environmental conditions that allowed the carbonate to form through geologic history, including solution ionic strength, pH or temperature, or the presence of certain biologic catalysts (e.g., Lippman, 1973; Morse et al., 1997; Vasconcellos et al., 1995). This concept has become especially useful for the most abundant carbonate minerals: calcite, dolomite, and aragonite (e.g., Warren, 2000). Although the solution conditions that enable calcite and aragonite formation have been well-established (e.g., Kim and O'Neil, 1997; Kim et al., 2006), understanding of dolomite formation has remained elusive for more than a century (Land, 1998; Machel, 2004).

Calcite and aragonite commonly form as foraminifera shells, corals, and other marine organisms. Calcite ($CaCO_3$), a rhombohedral mineral, can be readily synthesized in the laboratory through the simple mixture of a calcium salt (e.g., $CaCl_2$) and a carbonate source (e.g., $NaHCO_3$). Aragonite, a calcite polymorph that possesses an orthorhombic crystal structure, can alternatively be synthesized by the addition of Mg^{2+} ions (> 1:1 molar Mg/Ca ratio in seawater above 25 °C) (Morse et al., 1997), which have been found to inhibit calcite growth but do not impede aragonite formation. Dolomite, like calcite, is a rhombohedral carbonate mineral, but contrasting calcite, dolomite contains magnesium (Mg^{2+}) ions within its crystal structure and is typically comprised of

distinct alternating layers of $CaCO_3$ and $MgCO_3$, formed perpendicular to the mineral's c-axis (Figure 1.1) (Lippmann, 1973). This alternating crystal structure defines the $R\bar{3}$ space group, unique from the $R\bar{3}c$ space group of calcite, magnesite, siderite, and other similar carbonate minerals (Lippmann 1973, Gregg et al., 2015). Distinct from calcite and aragonite, dolomite may form either by dolomitization of previously deposited calcite or aragonite (typically limestone), or by direct precipitation from solution. Recent dolomite formation has been restricted to specific environments such as hypersaline sabkhas, lagoons and playa lakes, which contain high alkalinities and salinities (McKenzie, 1981; Arvidson and Mackenzie, 1999). Environments abundant in organic matter have also been associated with modern dolomite formation (e.g., Mazzullo et al., 1987; Compton, 1988). Furthermore, parent solutions at locations in which Holocene dolomite are found generally reach relatively high temperatures, regularly up to 40 °C or higher (Furman et al., 1993).

Numerous advances in the fields of geology and geochemistry have resulted from the ability to synthesize calcite and aragonite (among other carbonates) under well-controlled conditions. For example, carbonate-water oxygen isotope paleothermometry enables an estimation of past climate changes and its calibration requires carbonate synthesis under precise temperatures (e.g., O'Neil et al., 1969; Kim and O'Neil, 1997). As well, the calibration of $\delta^{11}B$ isotopic signatures of borate incorporated into laboratory synthesized carbonates allows an approximation of past ocean pH levels (Vengosh et al., 1991; Pagani et al., 2005). More recently, the development of carbonate clumped isotope research provides a new carbonate paleothermometer that has the potential to be highly

valuable, as it does not require knowledge of oxygen isotopic compositions of past water bodies in which carbonates formed, which is necessary for the carbonate-water oxygen isotope paleothermometer (Ghosh et al., 2006; Eiler, 2011). Similarly, calibrations of the carbonate clumped isotope paleothermometry would not be possible without carbonate synthesis under highly accurate temperatures.

Although carbonate mineral research has provided an understanding of many aspects of paleoclimates, the inability to synthesize dolomite at temperatures representative of those in nature has left a sizeable gap in the field's knowledge. The discovery of a method, or experimental solution conditions, that facilitate dolomite synthesis at near-ambient conditions would provide critical insight into to numerous geological issues. These issues include: the mysteries concerning dolomite-rich oceans that existed during the Pre-Cambrian, but dolomite scarcity in present oceans (Warren, 2000); the difficulty in establishing an accurate dolomite-water oxygen isotope paleothermometer below 100 °C (Schmidt et al., 2005; Horita, 2014); and uncertainties in the calibrations for dolomite clumped isotope paleothermometer (see Bonifacie et al. (2017) for the most recent (proto)dolomite calibration). The clarity of dolomite formation also has economic implications, as its understanding would provide clues for the formation conditions of dolomite-hosted Mississippi Valley-Type (MVT) deposits and dolomite oil and gas reservoirs (Braithwaite et al., 2004; Machel, 2004).

Section 1.2: Dolomite Properties

Section 1.2.1: Dolomite Stoichiometry and Cation Ordering

Stoichiometry and cation ordering are the primary properties of dolomite used for distinction from calcite and other similar carbonate minerals. Stoichiometry defines the proportion of Ca^{2+} and Mg^{2+} (or in some instances Fe^{2+} and Mn^{2+}) that comprise the dolomite structure. In the ideal case, dolomite stoichiometry is 50 % $CaCO_3$ and 50 % $MgCO_3$; however, many natural dolomites have compositions that deviate from perfect stoichiometry (e.g., Rosen et al., 1989; Gregg et al., 1992). Commonly, natural dolomites are Ca-rich in composition, especially younger samples formed during periods such as the Miocene and Holocene, due to slow reaction kinetics and the preferential incorporation of Ca^{2+} ions (Gregg et al., 1992; Warren, 2000). However, occurrences of slightly Mg-rich dolomite (%$MgCO_3$ between 50 and 55 %) have been documented as well, although these instances have been rare (Rosen et al., 1989). Stoichiometric dolomite composition implies more complete dolomite formation, as stoichiometric dolomite is more thermodynamically stable than Ca-rich dolomite (Lippmann, 1973; Carpenter, 1980). In the case of laboratory synthesis, %$MgCO_3$ has been utilized as an indicator of conditions, such as parent solution chemistry or catalysts, that facilitate dolomite formation (e.g., Kaczmarek et al., 2011; Zhang et al., 2012a,b).

Dolomite stoichiometry is commonly determined by powder X-Ray diffraction (XRD) analysis, due to its simplicity and low cost (Jones et al, 2001; Kaczmarek and Sibley, 2011). Chave (1952) first discovered, through XRD analyses, that calcite 2θ values (angle between incident X-Ray beam and detector) for the 104 diffraction peak

increased (or shifted to greater 2θ value) with an increasing proportion of Mg^{2+}. The shift in 2θ is caused by smaller Mg^{2+} ions substituting for Ca^{2+} ions and thereby reducing the unit cell size (Gregg et al, 2015). A similar diffraction peak shift occurs in dolomite analyses, which allows the proportion of Ca^{2+} and Mg^{2+} to be determined qualitatively based on the 2θ value of the dolomite 104 peak. Lumsden and Chimahusky (1980) developed an equation enabling the stoichiometry of dolomite to be quantified based on the 104 peak location. The equation is as follows:

$$\%CaCO_3 = 333.33d - 911.99 \qquad \text{(Equation 1.1)}$$

where d is the d-spacing of the dolomite 104 peak from CuKα radiation XRD analysis, which is directly proportional to the 2θ value. The $\%MgCO_3$ is then calculated by the difference between $\%CaCO_3$ and 100 %, but assumes there is no incorporation of other cations (i.e. Fe^{2+}, Mn^{2+}, or Na^{2+}). Although a sizable error of 1 - 3 $\%MgCO_3$ can be associated with the Lumsden and Chimahusky (1980) equation, this method is widely utilized by researchers, especially for analyzing large data sets (Kaczmarek and Sibley, 2011; Gregg et al., 2015).

Other methods for determining dolomite stoichiometry include: scanning electron microscope energy dispersive X-Ray spectroscopy (SEM-EDS), transmission electron microscope (TEM)-EDS, X-Ray fluorescence (XRF), and inductively coupled plasma mass spectrometry (ICP-MS) (e.g., Sanchez-Roman et al., 2008; Zhang et al., 2012a,b). Examples in which XRF is used to estimate dolomite stoichiometry are rare, due to the requirement for pure dolomite powders that contain no other mineral phases.

Dolomite cation ordering refers to the fraction of Ca^{2+} and Mg^{2+} ions that are occupied within the appropriate CO_3^{2-} layers in the crystal structure (Lippmann, 1973). As previously discussed, dolomite is comprised of alternating layers of $CaCO_3$ and $MgCO_3$ relative to the c-axis. Perfect cation order indicates that all Ca^{2+} and Mg^{2+} ions are bonded within their respective layer. In other words, there is no replacement of Ca^{2+} ions for Mg^{2+} in the $MgCO_3$ layer, or vice-versa.

In order for a carbonate mineral to be termed "dolomite", evidence of cation ordering is required (Land, 1980; Gregg et al., 2015), as cation ordering produces the distinction between the $R\bar{3}$ space group for dolomite and the calcite $R\bar{3}c$ group (Lippmann, 1973). Commonly, dolomite cation ordering is identified by the presence of "ordering" diffraction peaks in XRD analyses (Gregg et al., 2015). A carbonate mineral cannot be labelled dolomite if the ordering peaks (the 015, 101, and 021 peaks) are absent, regardless of the stoichiometry. $CaCO_3$ minerals that contain > 4 %$MgCO_3$, and display no cation ordering, are typically termed either high-magnesium calcite (HMC) or protodolomite (Gregg et al., 2015) (discussed further in Section 1.2.2).

A quantitative analysis for dolomite cation ordering is possible through comparison of the relative intensities of the 015 and the 101 dolomite diffraction peaks, termed the cation ordering ratio (Goldsmith and Graf, 1958; Kaczmarek and Sibley, 2011). Alternatively, the cation ordering ratio is represented as % cation ordering by multiplying the ordering ratio by 100. Perfectly ordered dolomite has equal intensities of the 015 and 101 peaks, and therefore the % cation ordering is equal to 100 %. Many natural dolomites, as well as most laboratory synthesized dolomite, possess cation

ordering that is less than ideal (Warren, 2000), and similar to stoichiometry, partial ordering is common for dolomite formed in recent geologic history, including samples collected from the well-studied Coorong Region, Australia (Rosen et al., 1989).

Section 1.2.2: Protodolomite Characterization and Terminology

A discrepancy exists for the terms used to describe carbonate minerals that resemble dolomite but fail to meet the requirements for stoichiometry and cation ordering (Gregg et al., 2015). In order for a carbonate mineral to be termed dolomite, established criteria include a sufficient proportion of $MgCO_3$ (generally above 43%) and evidence of cation ordering (e.g., Land, 1980; Gregg et al., 2015). If one or both criteria fail to be met, the mineral cannot be termed dolomite. However, the terms used to label minerals with near-dolomite compositions are inconsistent and lack a clear definition (Gregg et al., 2015).

Carbonate minerals that possess a calcite structure but contain a high proportion of Mg^{2+} ions (> 4 mol %$MgCO_3$) are referred to as HMC (Tucker and Wright, 1990; Gregg et al., 2015). Although natural occurrences of HMC have been found at Earth's surface conditions (Goldsmith et al., 1955), HMC is thermodynamically unstable in relation to calcite and dolomite (Land, 1982). As well, laboratory synthesis of HMC is easily achievable, including low temperature experiments (Graf and Goldsmith, 1956).

The term protodolomite was first introduced by Graf and Goldsmith (1956) to describe stable Ca-Mg carbonates possessing either a composition that deviates from ideal dolomite stoichiometry, is disordered, or a combination of both. However,

subsequent studies argued or rejected the "protodolomite" terminology. Gaines (1977) proposed that protodolomite should define carbonates with a large discrepancy from ideal dolomite stoichiometry and have minor cation ordering, and instead used the term "pseudodolomite" for carbonates with a near-ideal $\%MgCO_3$ composition and the absence of cation ordering. Other studies have instead used a variety of terms to describe Ca-Mg carbonates that cannot be labelled dolomite, including: "very high magnesium calcite" (Sibley et al., 1994; Zhang et al., 2010); "unordered dolomite" (Zempolich and Baker, 1993); "non-stoichiometric dolomite" (Sibley et al., 1994); and "disordered dolomite" (Zhang et al., 2010; Kaczmarek and Sibley, 2011).

For the purpose of consistency, the term "protodolomite" will be used in this study to describe carbonates with near dolomite stoichiometry (> 43 $\%MgCO_3$), but with no indication of cation ordering. If a carbonate contains < 43 $\%MgCO_3$, it will be referred to as HMC. Since cation ordering distinguishes the dolomite structure from that of calcite, and following the definitions by Land (1980) and Gregg et al. (2015), a carbonate mineral containing > 43 $\%MgCO_3$ and displaying evidence of cation ordering will be labelled dolomite.

Section 1.2.3: Dolomitization and Direct Precipitation

Dolomite formation is possible by either dolomitization of existing calcium carbonate or direct precipitation from a parent solution (Graf and Goldsmith, 1956; Warren, 2000). Dolomitization is likely the most dominant dolomite formation process throughout geologic history (Machel, 2004; Horita, 2014), and typically, limestone deposits are dolomitized after burial to greater depth, due to elevation in temperature and

pressure (Machel, 2004). Dolomitization requires high temperatures, generally greater than 100 °C, and a fluid source of concentrated Mg^{2+} ions (Katz and Matthews, 1977; Kaczmarek and Sibley, 2011). Dolomitization has been demonstrated to proceed from initial calcium carbonate replacement with high magnesium carbonate, to formation of disordered dolomite (protodolomite) with a high $\%MgCO_3$ composition, and finally recrystallization to dolomite (Kaczmarek and Sibley, 2014).

Direct dolomite precipitation from seawater and other carbonate forming environments is rare, due to the slow kinetics involved for the reaction at low temperatures (Arvidson and Mackenzie, 1999). Calcite and aragonite are favored to precipitate from solution because Ca^{2+} ions readily react with CO_3^{2-} ions to form $CaCO_3$, which is thermodynamically more stable than high-magnesium calcite or protodolomite (Lippmann, 1973). Dolomite precipitation is also inhibited by the hydration of Mg^{2+} ions, which hinder Mg^{2+} incorporation (Lippmann, 1973). The exact mechanisms which inhibit direct dolomite precipitation are outlined in Section 1.3.1.

Direct dolomite precipitation has been proposed to explain certain cases of natural dolomite formation, primarily in evaporitic environments (Rosen et al., 1989; Warren, 2000 and references within). In these geologic settings, direct precipitation of dolomite is proposed to occur by elevated reaction kinetics caused by rapid evaporation. When evaporation occurs quickly, precipitation of calcite, gypsum ($CaSO_4 \bullet 2H_2O$) and anhydrate ($CaSO_4$) is favored and, as a result, fluid molar Mg/Ca ratios readily increase (Patterson and Kinsman, 1982; Rosen et al., 1989). Sufficiently high solution molar

Mg/Ca ratio allows reaction kinetics to proceed rapidly enough to form dolomite by direct precipitation (Rosen et al., 1989).

As a specific example, Rosen et al. (1989) provided multiple lines of evidence to support dolomite direct precipitation out of evaporitic brines from the Coorong Lakes, Australia. Dolomite samples suspected to directly precipitate, labelled Type-A dolomites and suggested to have formed near basin centers, possessed: 1) an enrichment of Mg^{2+}; 2) identifiable heterogeneous microstructures, visible by TEM analyses, indicating rapid precipitation and crystal growth; and 3) relatively ^{18}O enriched, likely resulting from evaporation of the lighter ^{16}O. In comparison, nearby Type-B dolomite which formed at lake margins, was Ca-rich, lacked heterogeneous microstructures, and was relatively depleted in ^{18}O (Rosen et al., 1989).

Section 1.3: Dolomite Formation and Laboratory Synthesis

Section 1.3.1: Inhibiting Factors of Dolomite Formation

The issues surrounding conditions that inhibit natural and laboratory dolomite formation are attributed to several established factors (Lippmann, 1973; Arvidson and Mackenzie, 1999; Petrash et al., 2017). First, the kinetics involved for dolomite nucleation and growth at low temperatures may prevent the mineral from forming on relatively short time scales (Land, 1998; Arvidson and Mackenzie, 1999). For example, Land (1998) failed to precipitate dolomite following an allocated growth time of 32 years at ambient temperatures and “1000-fold oversaturation” of dolomite. Subsequently, Arvidson and Mackenzie (1999), by means of dolomite growth rate calculations using temperature and solution saturation state as variables, stated that it likely not feasible to

synthesize dolomite at ~ 25 °C. Furthermore, the associated sluggish reaction rates and sufficient growth time for dolomite formation is evidenced by its scarcity in recent sedimentary environments (i.e., Miocene to Holocene), yet its abundance throughout certain geologic periods (i.e., Pre-Cambrian) (Warren, 2000; Machel, 2004).

Second, the difficulty for Mg^{2+} ion incorporation into a growing dolomite crystal structure is considered to be rate determining for dolomite formation (Lippmann, 1973; Oomori and Kitano, 1987; Zhang et al., 2012a). Mg^{2+} ions possess a double hydration shell that can inhibit incorporation and favor the adsorption of Ca^{2+} or other available cations (Lippman, 1973). If Mg^{2+} ions are incorporated, the hydration shell charge can influence the carbonate structure and hinder further growth (Lippman, 1973; Mucci and Morse, 1983). Third, insufficient parent solution alkalinity likely prevents dolomite formation (Lippmann, 1973; Petrash et al., 2017), as raised alkalinity provides the necessary free energy required to overcome the issue of Mg^{2+} ion hydration (Lippmann, 1973; Machel and Mountjoy, 1986). Furthermore, Morrow and Ricketts (1988) found that an increase in the carbonate concentration of parent solutions accelerated the rate of dolomitization.

Finally, an inhibiting role of sulfate on dolomite formation has been widely debated and remains controversial (Baker and Kastner, 1981; Brady et al., 1996; Sanchez-Roman et al., 2009). Baker and Kastner (1981) first discovered that sulfate hindered the dolomitization of calcite in their laboratory experiments at 200 °C. This effect results from the formation of strong bonds between Mg^{2+} ions and SO_4^{2-} ions, which slows or prevents Mg^{2+} incorporation into the carbonate (Slaughter and Hill, 1991). Similarly,

Morrow and Ricketts (1988) displayed that sulfate concentrations of ~ 4 mM inhibited dolomitization of calcite, whereas dolomitization occurred more slowly < 4 mM sulfate than in the absence of sulfate. However, experiments conducted by Brady et al. (1996) found that only sulfate concentrations < 5 mM inhibit dolomite formation and proposed that concentrations > 5 mM may instead accelerate formation. Subsequently, Sanchez-Roman et al. (2009) also failed to observe an inhibiting effect from sulfate, regardless of concentration, in experiments associated with aerobic bacteria. Recently, the majority of low temperature dolomite synthesis studies have investigated use of sulfate-reducing bacteria as a catalyst, with the belief that sulfate reduction to sulfide may facilitate dolomite formation (Vasconcelos et al., 1995) (discussed further in section 1.3.4).

Section 1.3.2: High Temperature Dolomite Synthesis

Due to the inability to successfully synthesize dolomite at low temperatures, much of the knowledge for conditions that facilitate dolomite formation have been obtained from high temperature (> 100 °C) synthesis experiments (e.g., Kaczmarek and Sibley, 2011, 2014; Kaczmarek and Thornton, 2017). Although the bulk of these studies synthesize dolomite through dolomitization, numerous favorable solution chemistry and other conditions have been demonstrated to be applicable, or provide valuable insight, to low temperature dolomite formation as well.

High temperature dolomitization experiments have shown that the initial solution molar Mg/Ca ratio is a primary controlling factor in dolomite formation (Gaines, 1974; Sibley, 1990; Kaczmarek and Sibley, 2011). Sibley (1990) found that protodolomite, formed at 218 °C, increased in $\%MgCO_3$ from ~ 35 % to ~ 40 % when the initial solution

molar Mg/Ca ratio was increased from 0.66 to 1. Kaczmarek and Sibley (2011), conducting similar dolomitization experiments as Sibley (1990) at 218 °C, found that dolomite stoichiometry is more dependent on initial solution molar Mg/Ca ratio than previously understood. The authors showed that dolomite stoichiometry correlated directly with the initial solution molar Mg/Ca ratio until dolomite had replaced ~ 95 % of the initial $CaCO_3$. However, after the 95 % threshold was elapsed, stoichiometry increased readily (Kaczmarek and Sibley, 2011). In other words, dolomite stoichiometry reflected the initial solution molar Mg/Ca ratio until $CaCO_3$ was almost entirely replaced. Therefore, the authors proposed that the initial solution molar Mg/Ca ratio provides a template for which dolomite follows until the reaction is nearly complete. It has yet to be confirmed if the stoichiometry of dolomite formed by direct precipitation has a comparable relationship with initial solution molar Mg/Ca ratio.

Kaczmarek and Sibley (2011) also found, in contrast to stoichiometry, that dolomite cation ordering develops independently of initial solution molar Mg/Ca ratio. Alternatively, cation ordering steadily increases with the progression of dolomitization, and also increases with an elevation in dolomitization reaction rate. Furthermore, dolomite cation ordering was displayed to have no correlation with stoichiometry, with the exception of samples with > 95 % dolomite replacement (Kaczmarek and Sibley, 2011).

High temperature dolomitization experiments have determined a number of factors that increase the dolomitization induction rate. Induction rate refers to the time required for an initial replacement of $CaCO_3$ with dolomite, which is commonly

identified by XRD analyses (Sibley et al., 1987; Kaczmarek and Sibley, 2011). Greater reactant ($CaCO_3$) surface area was found by Sibley and Bartlett (1987) to significantly raise the induction rate for dolomitization of calcite at 175 °C. As well, multiple studies have indicated that dolomitization proceeds more rapidly when replacing aragonite instead of calcite, due to the higher solubility of aragonite (Baker and Kastner, 1981; Kaczmarek and Sibley, 2014). It has been established that the dolomitization induction rate also increases with elevated temperatures (Graf and Goldsmith, 1956; Arvidson and Mackenzie, 1999), with increasing alkalinity (Morrow and Rickets, 1988), and at lower solution pH values (Sibley et al., 1987).

Section 1.3.3: Low Temperature Dolomite Synthesis

Abundant attempts have been made to synthesize dolomite at low temperatures (e.g., Graf and Goldsmith, 1956; Siegel, 1961; Liebermann, 1967; Oomori and Kitano, 1987; Deelman, 1999; Kelleher and Redfern, 2002; Zhang et al., 2012a,b), but each study have proved unsuccessful, typically producing HMC, protodolomite, or a series of irreproducible results. Nevertheless, insight into solution chemistry and potential catalysts that facilitate pure protodolomite formation or raised $\%MgCO_3$ compositions have been gained from the experimental studies.

Employing a somewhat unique approach in attempts to synthesize dolomite at low-temperatures, Liebermann (1967) developed a dissolution-reprecipitation method, using solutions with 1 - 6 times the salinity of seawater. This method consisted of repeated cycles of precipitation and dissolution that aimed to dissolve unstable carbonate minerals and eventually precipitate only stable dolomite. The repeated cycles involved the

bubbling of CO_2 into parent solutions at room temperature for approximately 12 hours (to dissolved unstable carbonates), followed by small additions of Na_2CO_3 or NH_4OH to raise pH to ~ 8.0, and finally the placement of parent solutions into a drying oven at 43 ± 2 °C. Liebermann (1967) claimed to have synthesized a mixture of dolomite and HMC, following an experiment using solutions that were 6 times the normal salinity of seawater and employing a total of 14 cycles. However, the presence of cation ordering was not clear, especially due to the lack of XRD patterns for the synthesized minerals. Other similar experiments resulted in the synthesis of HMC or apparent protodolomite.

Oomori and Kitano (1987) synthesized pure protodolomite from sea water with an molar Mg/Ca ratio of 4.9 and small additions of dioxane. The authors proposed that dioxane acted as a catalyst for protodolomite formation by lowering the dielectric constant of solution and thereby causing Mg^{2+} ions to dehydrate. Kelleher and Redfern (2002) synthesized a hydrous protodolomite with a composition of $Ca_{1.056}Mg_{0.944}(SO_4)_{0.035}(CO_3)_{1.965}{\cdot}0.26H_2O$ by mixing $MgSO_4{\cdot}7H_2O$, $Ca(NO_3)_2{\cdot}4H_2O$ and Na_2CO_3 solutions, with a molar Mg/Ca ratio of 1.22, at 40 °C, 61 °C, and 81 °C for a maximum growth time of 23 days. The authors suggested this hydrous protodolomite is likely a precursor mineral for natural dolomite, and that the mineral would eventually recrystallize into dolomite through continued dissolution-reprecipitation processes. More recently, Horita (2014) repeated the methods of Kelleher and Redfern (2002) at 80 °C, but for an extended period of 41 days, and precipitated a single protodolomite sample. The protodolomite sample was slightly Ca-rich (~ 49 %$MgCO_3$), but the XRD results failed to display evidence of the dolomite cation ordering peaks.

Deelman (1999) claimed to have formed dolomite in low temperature experiments (40 and 60 °C) by repeating the experimental methods of Liebermann (1967), but with an addition of 50.5 mM urea. The concept of urea catalysis was previously proposed by Mansfield (1980), following the discovery of a dolomite bladder stone that formed within a Dalmatian dog. However, the assertion by Deelman (1999) that dolomite synthesis was attained at 40 °C appears unsubstantiated, with questionable evidence for cation ordering. The study also displayed irreproducible results for experiments in the absence of urea, which included HMC, hydromagnesite ($(MgCO_3)_4(OH)_2 \cdot 4H_2O$), and magnesite ($MgCO_3$), and only a single experiment tested possible urea catalysis on dolomite formation.

Zhang et al. (2012a) determined that the addition of sulfide to solutions containing a molar Mg/Ca ratio similar to seawater produced HMC and protodolomite (the authors used the term disordered dolomite) at 25 °C. The catalytic ability of sulfide was shown by an evident increase in $\%MgCO_3$ with increasing sulfide concentration. Although the sulfide addition also led to an increase in solution pH, which has been speculated to facilitate dolomite formation by encouraging the dehydration of Mg^{2+} ions (Slaughter and Hill, 1991), control experiments were carried out that contained sulfide and amounts of HCl to lower solution pH values. These control experiments produced HMC with similar $\%MgCO_3$ as solutions containing without HCl. Therefore, sulfide is a potential catalyst for dolomite formation in certain natural environments, especially those that coincide with high values of pH (> 8.5), including environments in which bacterial sulfate

reduction (BSR) produces high solution pH (Zhang et al., 2012a) (discussed further in section 1.3.4).

Zhang et al. (2012a) also found that the addition of calcite seeds to experimental solutions containing dissolved sulfide produced protodolomite, with upwards of 43 $\%MgCO_3$ at 25 °C. In relation, solutions containing calcite seeds and no sulfide produced HMC with a maximum 26 $\%MgCO_3$. The authors also displayed that this "calcite seed effect" prevented aragonite and monohydrocalcite formation (precipitated in the absence of calcite seeds) and instead encouraged formation of HMC or protodolomite (Zhang et al., 2012a). Zhang et al. (2012a) suggested the calcite seed effect as a possible explanation for certain natural dolomite examples, such as dolomite recovered from the Miocene Monterey Formation (Compton and Siever, 1984) and dolomite laminae found within cores from ODP sites 680 and 686 (Kemp, 1990).

Section 1.3.4: Microbial and Biotic Protodolomite Synthesis

Research devoted to understanding dolomite formation drastically shifted following the published findings of Vasconcelos et al. (1995), commencing a focus on microbial catalysis on dolomite formation (e.g., Van Lith et al., 2003; Vasconcelos et al., 2005; Sanchez-Roman et al., 2008; Roberts et al., 2013). Vasconcelos et al. (1995) seemingly discovered that dolomite synthesis was possible in the presence of sulphate-reducing bacteria (SRB) under anoxic conditions. Subsequent studies concentrated on understanding the interaction between SRB and dolomite, as well as other possible microorganism catalysts, and the associated altered solution chemistry which promote dolomite formation (see Petrash et al., 2017 and references within). For example, Roberts

et al. (2004) suggested that both natural and laboratory (25 °C) dolomite formation could be influenced by methanogens, which interact with basalt rock, producing Mg^{2+} and Ca^{2+} ions, and facilitating dolomite precipitation on the organism's cell walls. Roman-Sanchez et al. (2008) claimed that dolomite could be directly precipitated by two strains of aerobic bacteria at 25 and 35 °C, by nucleation directly on the microorganism cell walls. Notably, the study also showed that the aerobic microorganisms caused associated changes in experimental solution chemistry, such as raised pH from ~ 7 to 8.5 – 9 and dissolved CO_2 production, which subsequently formed HCO_3^- or CO_3^{2-} (Sanchez-Roman et al., 2008). Finally, Krause et al. (2012) claimed that the combination of sulfate-reducing bacteria and extracellular polymetric substances resulted in dolomite precipitation under anoxic conditions at 21 °C. Numerous other studies also displayed similar results from dolomite synthesis experiments in the presence of microorganisms (e.g., Warthmann et al., 2000; Van Lith et al., 2003; Bontognali et al., 2014).

The assertion of microbial mediation as an answer for the widely debated "dolomite problem" has since been disproven (Zhang et al., 2012b, Gregg et al., 2015; Kaczmarek et al., 2017). Numerous instances of claimed dolomite synthesis by SRB or other biogenic sources were thoroughly evaluated by Gregg et al. (2015) and a deficiency in the experimental results were outlined for each case. The reoccurring problem surrounding the dolomite synthesis claims was the failure to effectively demonstrate evidence of dolomite cation ordering, with XRD patterns lacking evident ordering diffraction peaks (Zhang et al., 2012b; Gregg et al., 2015). Therefore, microbial

mediation likely has yet to facilitate dolomite formation, instead producing HMC or protodolomite (Gregg et al., 2015; Petrash et al., 2017).

Although dolomite has not been synthesized by microbial mediation, beneficial evidence for conditions that facilitate dolomite formation and growth can be inferred from the associated studies (Petrash et al., 2017). Microorganisms have been shown to increase solution alkalinity and pH, as well as maintain higher pH values (Slaughter and Hill, 1991). Studies of microbial influences on dolomite formation has also revealed the importance of the initial nucleation stage, indicating that factors that promote nucleation are likely significant to low temperature dolomite synthesis (Petrash et al., 2017).

Section 1.3.5: Ostwald's Step Rule

Ostwald's Step Rule has been suggested as the process by which dolomite typically forms (Kelleher and Redfern, 2002; Gregg et al., 2015; Rodriguez-Blanco et al., 2015). First proposed by Ostwald (1897), Ostwald's Step Rule states that the initial reaction products continuously undergo a series of reactions to form products each less soluble than the preceding product. Kelleher and Redfern (2002) proposed that Ostwald's Step rule explained why the authors obtained a hydrous protodolomite precipitate in direct precipitation experiments at 40, 61, and 81 °C. The authors suggested that with further reaction time, the hydrous protodolomite would undergo a series of dissolution and reprecipitation steps until dolomite formed (Kelleher and Redfern, 2002). Previously, Navrotsky and Capobianco (1987) showed that protodolomite, displaying no cation ordering, is more soluble than dolomite and Carpenter (1980) found that Ca-rich dolomite is more soluble than stoichiometric dolomite (Table 1.1)

More recently, Rodriguez-Blanco et al. (2015) carefully investigated (proto)dolomite formation by direct precipitation over the temperature range 60 - 220 °C. The authors observed that dolomite forms by a distinct three-stage reaction pathway. First, a hydrous amorphous Ca-Mg carbonate is initially formed, followed by partial dehydration and rapid recrystallization to Ca-rich protodolomite (Rodriguez-Blanco et al., 2015). Finally, in stage three, a relatively longer time period is required to recrystallize protodolomite into ordered, and stoichiometric, dolomite. Rodriguez-Blanco et al. (2015) proposed that stage three occurs following Ostwald's Step Rule, as the final dolomite product only formed after undergoing the dissolution and reprecipitation processes.

Section 1.4: Carbonate-Water Oxygen Isotope Thermometry

Since the 1950's, oxygen isotopes of carbonates have become a value tool which enables the reconstruction of climate temperatures for past carbonate depositional environments (Epstein et al., 1951,1953; Tarutani et al., 1969). The method is founded upon the temperature dependent oxygen isotopic exchange between carbonates and parent solution during carbonate formation. Therefore, by establishing a calibration between the formation temperature and oxygen isotope ratios of synthesized carbonates, past climate temperatures can be estimated based on oxygen isotopic compositions of natural carbonates. Calibrations for carbonate minerals have typically been developed through inorganic mineral synthesis at accurately controlled temperatures, including generally accepted low temperature calibrations for calcite (Kim and O'Neil, 1997) and aragonite (Kim et al., 2007).

Oxygen isotope carbonate-water thermometry requires knowledge of the initial oxygen isotopic composition of the solution in which the carbonate formed, and that isotopic equilibrium was attained between the carbonate and solution during mineral formation (e.g., Kim and O'Neil, 1997; Coplen, 2007). In the absence of isotopic equilibrium, nonequilibrium effects (i.e. kinetic effects) cause deviations from the true equilibrium value. In nature, vital effects also cause oxygen isotope variations in carbonates produced by aquatic organisms, likely due to kinetic effects during CO_2 hydration and hydroxylation (McConnaughey, 1989a,b).

Section 1.4.1: Isotopic Equilibrium and Influence of Kinetic Effects

Isotopic equilibrium refers to the point in which two distinct chemical compounds no longer exchange stable isotopes. The requirement of isotopic equilibrium has been demonstrated for effective calculation of the temperature-dependent incorporation of oxygen isotopes into precipitating carbonates (Kim and O'Neil, 1997; Kim et al., 2007; Coplen, 2007). In addition, oxygen isotopic exchange between carbonates and water is dependent on the carbonate minerology (i.e. calcite, aragonite, dolomite) and carbonate composition (e.g., O'Neil et al., 1969; Kim and O'Neil, 1997). If isotopic equilibrium has not been attained between a carbonate and its parent solution, kinetic effects influence oxygen isotope exchange and result in a value deviated from the equilibrium value (e.g., Beck et al., 2005; Kim et al., 2006).

Kinetic effects influencing carbonate formation were described by Given and Wilkinson (1985), suggesting that carbonate nucleation kinetics and carbonate ion concentrations can control the carbonate composition. Zeebe (1999) claimed that the

kinetic effects existed between calcite and water due to variations in solution pH. Subsequently, it was discovered by Beck et al. (2005) that equilibration between dissolved inorganic carbon (DIC) species and water is required prior to carbonate formation. The authors found that the oxygen isotope equilibrium values between DIC and water vary depending on the carbon species (i.e., HCO_3^-, CO_3^{2-}, and $CO_{2(aq)}$) and temperature. For example, Beck et al. (2005) determined an $1000\ln\alpha_{HCO3\text{-}H20}$ value of 31.03 and an $1000\ln\alpha_{CO3\text{-}H20}$ value of 24.19 at 25 °C. If equilibrium is not attained, DIC and water may continue to exchange oxygen isotopes while carbonates form and the determined $1000\ln\alpha_{carbonate\text{-}water}$ following carbonate synthesis may not be representative of an equilibrium exchange between carbonate and water.

The carbonate precipitation rate has also been demonstrated to produce kinetics effects (Zuddas and Mucci, 1994; Kim et al., 2006). If a carbonate forms rapidly, it may incorporate the isotopic signature of the DIC source closest to its nucleation site, and as a result, incorporate the oxygen isotope composition of that DIC species (Beck et al., 2005). In addition, Kim et al. (2006) determined that CO_3^{2-}, as opposed to HCO_3^-, is preferentially incorporated into growing carbonates. Kim et al., (2006) also found that HCO_3^- will breakdown to CO_3^{2-}, and the produced CO_3^{2-} ions require further equilibrium with water. Otherwise, CO_3^{2-} ions will contain the isotopic signature of the HCO_3^- from which it originated. As a result, rapid carbonate precipitation may lead to kinetic isotope effects if the parent solution DIC is not effectively equilibrated. Furthermore, Kim and O'Neil (1997) found nonequilibrium effects for calcite, witherite, and otavite synthesis experiments at 10, 25, and 40 °C. The authors determined that elevated initial cation and

HCO_3^- concentrations resulted in oxygen isotope fractionation factors with considerable variation and therefore proposed that the smaller, and more reproducible, oxygen fractionation values were representative of isotopic equilibrium. Raised cation and HCO_3^- concentration may have increased the carbonate formation rate, and thereby resulted in kinetic isotope effects.

Section 1.5: Study Purpose

This study aimed at developing a method to reproducibly synthesize dolomite at temperatures below 100 °C, and by extension, provide insight into the environmental conditions that promote dolomite formation. The long-standing "dolomite problem" has puzzled the scientific community for more than a century and any potential evidence for solution conditions that facilitate dolomite formation and growth are therefore invaluable. A method, or solution chemistry, capable of synthesizing dolomite would also provide an ability to more effectively evaluate geochemical tools, such as the oxygen isotope dolomite-water thermometer and dolomite clumped isotope thermometer.

Investigated in this study are multiple conditions which may promote dolomite synthesis. First, this study examines the influence of two distinct solution preparation methods, and the associated kinetics effects, on dolomite formation and subsequent growth. The methods differ by the phase of carbonate ions (CO_3^{2-}) at the time of solution preparation, with $NaCO_3$ added to Ca-Mg solutions as either a dissolved solution or solid Na_2CO_3 salt. Second, a potential effect from varying urea concentrations is thoroughly studied. Urea has been proposed as a catalyst for dolomite formation in the past, due to the discovery of a dolomite bladder stone that formed within a Dalmatian dog (Mansfield,

1980), and subsequent low temperature dolomite synthesis attempts with 50.5 mM urea concentrations (Deelman, 1999). However, the experiments by Deelman (1999) were inconclusive, and therefore a comprehensive investigation of possible urea catalysis is targeted here. Third, after Deelman (1999) proposed that urea facilitates dolomite growth by hindering chlorine ion absorption to the dolomite crystal structure and encouraging CO_3^{2-} ion incorporation, $CaCl_2$ is substituted for $Ca(NO_3)_2$ in select experimental solutions containing urea. Finally, reduction in solution bottle volume, from 250 mL to 50 mL while maintaining a constant 50 mL solution volume, is performed to examine a possible influence of larger headspace.

Following successful low temperature dolomite synthesis, this study targeted to develop an accurate dolomite-water oxygen isotopic paleothermometer calibration. Previous dolomite-water calibrations below 100 °C are complicated by the inability to synthesize dolomite, and subsequently measured protodolomite precipitates (Vasconcelos et al., 2005; Schmidt et al., 2005; Horita, 2014). By refining the dolomite-water paleothermometer calibration at low-temperatures, attempts to successfully reconstruct past environmental conditions for dolomite formation will be greatly enhanced. Furthermore, possible isotopic kinetic effects produced by the dolomite synthesis methods developed here are investigated.

Section 1.6: Thesis Outline

Chapter 1 consists of the fundamental background information required for an understanding of dolomite formation, the related advances, and unresolved issues. This chapter also introduces the focus of this study and its intended purpose. Chapter 2

describes an in-depth experimental study which developed a method that enables successful dolomite synthesis at temperatures between 50 °C and 80 °C, and outlines clear evidence of urea catalysis on dolomite synthesis. Chapter 2 is prepared in a condensed format in preparation for submission to Geology, and as a result, describes the primary findings of dolomite synthesis experiments. Chapter 2 Appendices provides a more comprehensive description for the methods and results of this dolomite synthesis study, as well as an investigation of the effects of $CaCl_2$ substitution for $Ca(NO_3)_2$ and the reduction in experimental solution bottle volume on dolomite synthesis. Chapter 3 presents the establishment of a refined oxygen isotope dolomite-water paleothermometer calibration, and its relation to both previously developed low temperature protodolomite-water calibrations and high temperature dolomite-water calibrations. Furthermore, possible kinetic isotope effects associated with dolomite formed by the solid addition method are outlined and discussed. To conclude this thesis, Chapter 4 details the principal conclusions obtained by this study, how the candidate's findings will impact the scientific field, and the necessary research required to further develop the scientific contributions established here.

Figures and Tables

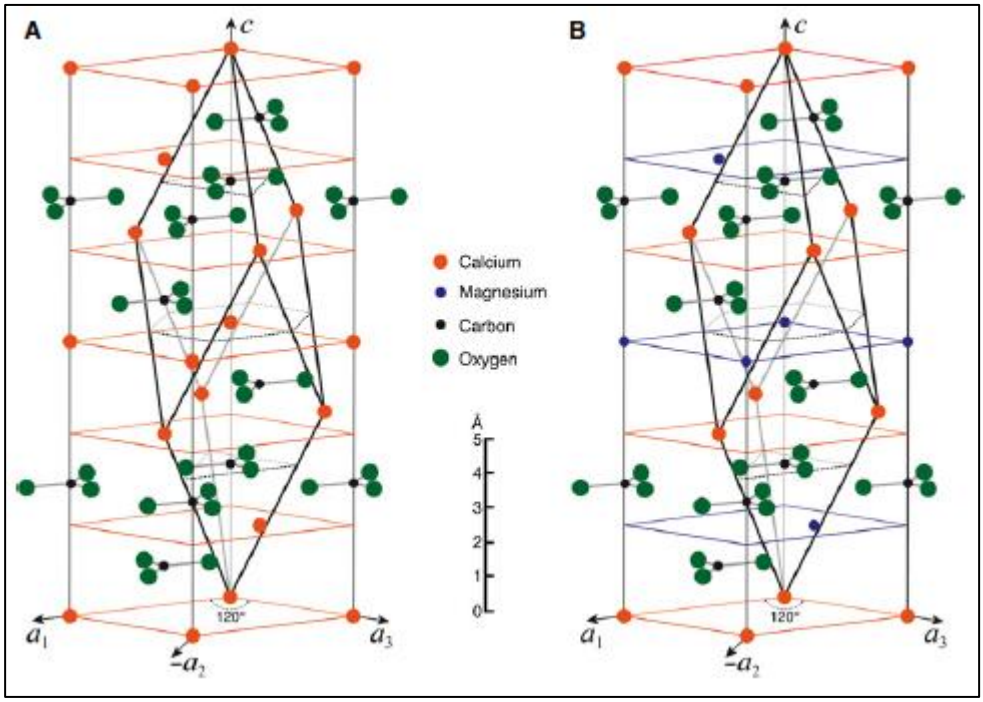

Figure 1.1. The calcite (A) and dolomite (B) crystal structure. Black lines represent the rhombohedral unit cell for both mineral crystal structures. Taken from Gregg et al. (2015).

Table 1.1. Solubilities of common carbonate minerals at 25 °C and 1 bar atmospheric pressure. Solubility values for calcite are taken from Busenburg and Plummer (1989) and Nordstrom et al. (1990), and values for aragonite, protodolomite and dolomite are taken from Nordstrom et al. (1990).

Mineral Name	Chemical Formula	$-\log K_{sp}$
Calcite	$CaCO_3$	8.33-8.48
Aragonite	$CaCO_3$	8.34
Protodolomite	$CaMg(CO_3)_2$	16.54
Dolomite	$CaMg(CO_3)_2$	17.09

References

Arvidson, R., & Mackenzie, F. (1999). The dolomite problem: Control of precipitation kinetics by temperature and saturation state. American Journal of Science, 299(4), 257-288.

Baker, P. A., & Kastner, M. (1981). Constraints on the formation of sedimentary dolomite. Science, 213(4504), 214-216.

Beck, W. C., Grossman, E. L., & Morse, J. W. (2005). Experimental studies of oxygen isotope fractionation in the carbonic acid system at 15, 25, and 40 C. Geochimica et Cosmochimica Acta, 69(14), 3493-3503.

Bonifacie, M., Calmels, D., Eiler, J. M., Horita, J., Chaduteau, C., Vasconcelos, C., & Bourrand, J. J. (2017). Calibration of the dolomite clumped isotope thermometer from 25 to 350° C, and implications for a universal calibration for all (Ca, Mg, Fe) CO_3 carbonates. Geochimica et Cosmochimica Acta, 200, 255-279.

Busenberg, E., & Plummer, L. N. (1989). Thermodynamics of magnesian calcite solid-solutions at 25 °C and 1 atm total pressure. Geochimica et Cosmochimica Acta, 53(6), 1189-1208.

Brady, P. V., Krumhansl, J. L., & Papenguth, H. W. (1996). Surface complexation clues to dolomite growth. Geochimica et Cosmochimica Acta, 60(4), 727-731.

Braithwaite, C. J., Rizzi, G., & Darke, G. (2004). The geometry and petrogenesis of dolomite hydrocarbon reservoirs. Geological Society of London.

Carpenter, A. B. (1980). The Chemistry of Dolomite Formanon I: The Stability of Dolomite. (Eds. Zenger D. H., Dunham J.B., and Ethington R. L), SEPM Spec. Publ., 28, 111-121.

Chave, K. E. (1952). A solid solution between calcite and dolomite. The Journal of Geology, 60(2), 190-192.

Compton, J.S. (1988). Sediment Composition and Precipitation of Dolomite and Pyrite in the Neogene Monterey and Sisquoc Formations Santa Maria Basin Area California. In: Sedimentology and Geochemistry of Dolostones (Ed. Baker, P.A.), Society of Economic Paleontologists and Mineralogists Special Publication 43, 53-64, Tulsa.

Coplen, T. B. (2007). Calibration of the calcite–water oxygen-isotope geothermometer at Devils Hole, Nevada, a natural laboratory. Geochimica et Cosmochimica Acta, 71(16), 3948-3957.

Deelman J. C. (1999). Low-temperature nucleation of magnesite and dolomite. Neues Jahrbuch Fur Mineralogie-Monatshefte, 7, 289–302.

Eiler, J. M. (2011). Paleoclimate reconstruction using carbonate clumped isotope thermometry. Quaternary Science Reviews, 30(25-26), 3575-3588.

Epstein, S., Buchsbaum, R., Lowenstam, H., & Urey, H. C. (1951). Carbonate-water isotopic temperature scale. Geological Society of America Bulletin, 62(4), 417-426.

Epstein, S., Buchsbaum, R., Lowenstam, H. A., & Urey, H. C. (1953). Revised carbonate-water isotopic temperature scale. Geological Society of America Bulletin, 64(11), 1315-1326.

Gaines, A. M. (1974). Protodolomite synthesis at 100 °C and atmospheric pressure. Science, 183(4124), 518-520.

Gaines, A. M. (1977). Protodolomite redefined. Journal of Sedimentary Research, 47(2), 543-546.

Ghosh, P., Adkins, J., Affek, H., Balta, B., Guo, W., Schauble, E. A., ... & Eiler, J. M. (2006). 13C–18O bonds in carbonate minerals: a new kind of paleothermometer. Geochimica et Cosmochimica Acta, 70(6), 1439-1456.

Goldsmith, J. R., & Graf, D. L. (1958). Structural and compositional variations in some natural dolomites. The Journal of Geology, 66(6), 678-693.

Graf, D.L. and Goldsmith, J.R. (1956). Some hydrothermal syntheses of dolomite and protodolomite. J. Geol., 64, 173–186.

Gregg, J., Bish, D., Kaczmarek, S., & Machel, H. (2015). Mineralogy, nucleation and growth of dolomite in the laboratory and sedimentary environment: A review. Sedimentology, 62(6), 1749-1769.

Gregg, J. M., Howard, S. A., & Mazzullo, S. J. (1992). Early diagenetic recrystallization of Holocene (< 3000 years old) peritidal dolomites, Ambergris Cay, Belize. Sedimentology, 39(1), 143-160.

Furman, F.C., Woody, R.E., Rasberry, M.A., Keller, D.J. and Gregg, J.M. (1993). Carbonate and evaporite mineralogy of Holocene (<1900 RCYBP) sediments at Salt Pond, San Salvador Island, Bahamas: preliminary study. In: Sixth Symposium on the Geology of the Bahamas (Ed. White, B.), 67–74.

Horita, J. (2014). Oxygen and carbon isotope fractionation in the system dolomite-water-CO_2 to elevated temperatures. Geochimica et Cosmochimica Acta, 129, 111-124.

Jones, B., Luth, R. W., & MacNeil, A. J. (2001). Powder X-ray diffraction analysis of homogeneous and heterogeneous sedimentary dolostones. Journal of Sedimentary Research, 71(5), 790-799.

Kaczmarek, & Sibley. (2011). On the evolution of dolomite stoichiometry and cation order during high-temperature synthesis experiments: An alternative model for the geochemical evolution of natural dolomites. Sedimentary Geology, 240(1), 30-40.

Kaczmarek, S. E., & Sibley, D. F. (2014). Direct physical evidence of dolomite recrystallization. Sedimentology, 61(6), 1862-1882.

Kaczmarek, & Thornton. (2017). The effect of temperature on stoichiometry, cation ordering, and reaction rate in high-temperature dolomitization experiments. Chemical Geology, 468, 32-41.

Katz, A., & Matthews, A. (1977). The dolomitization of CaCO3: an experimental study at 252–295 C. Geochimica et Cosmochimica Acta, 41(2), 297-308.

Kelleher, I. J., & Redfern, S. A. (2002). Hydrous calcium magnesium carbonate, a possible precursor to the formation of sedimentary dolomite. Molecular simulation, 28(6-7), 557-572.

Kim, S. T., & O'Neil, J. R. (1997). Equilibrium and nonequilibrium oxygen isotope effects in synthetic carbonates. Geochimica et Cosmochimica Acta, 61(16), 3461-3475.

Kim, S. T., O'Neil, J. R., Hillaire-Marcel, C., & Mucci, A. (2007). Oxygen isotope fractionation between synthetic aragonite and water: influence of temperature and Mg2+ concentration. Geochimica et Cosmochimica Acta, 71(19), 4704-4715.

Kim, S. T., Hillaire-Marcel, C., & Mucci, A. (2006). Mechanisms of equilibrium and kinetic oxygen isotope effects in synthetic aragonite at 25 C. Geochimica et Cosmochimica Acta, 70(23), 5790-5801.

Land, L. S. (1980). The isotopic and trace element geochemistry of dolomite: the state of the art. SEPM Spec: Publ., 28, 87-110.

Land, L. S. (1982). Dolomitization. American Association of Petroleum Geologists, Tulsa.

Land, L. (1998). Failure to Precipitate Dolomite at 25 °C from Dilute Solution Despite 1000-Fold Oversaturation after 32 Years. Aquatic Geochemistry, 4(3), 361-368.

Liebermann, O. (1967). Synthesis of dolomite. Nature, 213(5073), 241.

Lippmann, F. (1973). Sedimentary Carbonate Minerals, Rocks, and Inorganic Materials. Monograph Series of Theoretical and Experimental Studies Vol. 4 Springer-Verlag, Berlin (228 p).

Lumsden, D. N., & Chimahusky, J. S. (1980). Relationship between dolomite nonstoichiometry and carbonate facies parameters. In: Concepts and Models of Dolomitization (Eds. Zenger D. H., Dunham J.B., and Ethington R. L), SEPM Spec. Publ. 28, 123–137.

Machel, H. G. (2004). Concepts and models of dolomitization: a critical reappraisal. Geological Society, London, Special Publications, 235(1), 7-63.

Machel, H. G., & Mountjoy, E. W. (1986). Chemistry and environments of dolomitization—a reappraisal. Earth-Science Reviews, 23(3), 175-222.

Mansfield, C. F. (1980). A urolith of biogenic dolomite - another clue in the dolomite mystery. Geochimica et Cosmochimica Acta, 44(6), 829-839.

Mazzullo, S.J., Reid, A.M. (1988). Sedimentary textures of recent Belizean peritidal dolomite. J. Sediment. Res. 58, 479-488.

McConnaughey, T. (1989a). 13C and 18O isotopic disequilibrium in biological carbonates: I. Patterns. Geochimica et Cosmochimica Acta, 53(1), 151-162.

McConnaughey, T. (1989b). 13C and 18O isotopic disequilibrium in biological carbonates: II. In vitro simulation of kinetic isotope effects. Geochimica et Cosmochimica Acta, 53(1), 163-171.

McKenzie, J. A. (1981). Holocene dolomitization of calcium carbonate sediments from the coastal sabkhas of Abu Dhabi, UAE: a stable isotope study. The Journal of Geology, 89(2), 185-198.

Morrow, D.W. & Rickets, B.D. (1988) Experimental investigation of sulfate inhibition of dolomite and its mineral analogues. In: Sedimentology and Geochemistry of Dolostones (Eds. V. Shukla and P.A. Baker), SEPM Spec. Publ., 43, 25–38.

Morse, J. W., Wang, Q., & Tsio, M. Y. (1997). Influences of temperature and Mg: Ca ratio on CaCO3 precipitates from seawater. Geology, 25(1), 85-87.

Mucci, A., & Morse, J. W. (1983). The incorporation of Mg2+ and Sr2+ into calcite overgrowths: influences of growth rate and solution composition. Geochimica et Cosmochimica Acta, 47(2), 217-233.

Navrotsky, A., & Capobianco, C. (1987). Enthalpies of formation of dolomite and of magnesian calcites. American Mineralogist, 72(7-8), 782-787.

Nordstrom, D. K., Smellie, J. A. T., & Wolf, M. (1990). Chemical and isotopic composition of groundwaters and their seasonal variability at the Osamu Utsumi and Morro do Ferro analogue study sites, Poços de Caldas, Brazil (No. NAGRA-NTB--90-24). Nationale Genossenschaft fuer die Lagerung Radioaktiver Abfaelle (NAGRA).

O'Neil, J. R., Clayton, R. N., & Mayeda, T. K. (1969). Oxygen isotope fractionation in divalent metal carbonates. The Journal of Chemical Physics, 51(12), 5547-5558.

Oomori, T., & Kitano, Y. (1987). Synthesis of protodolomite from sea water containing dioxane. Geochemical Journal, 21(2), 59-65.

Ostwald, W.Z., (1897). Studien uber die Bildung und Umwaldung fester Korper. 1. Abhandlung: Ubersattigung and Uberkaltung. Z. Physik. Chem., 22, 289–330.

Pagani, M., Lemarchand, D., Spivack, A., & Gaillardet, J. (2005). A critical evaluation of the boron isotope-pH proxy: The accuracy of ancient ocean pH estimates. Geochimica et Cosmochimica Acta, 69(4), 953-961.

Patterson, R. J., & Kinsman, D. J. J. (1982). Formation of diagenetic dolomite in coastal sabkha along Arabian (Persian) Gulf. AAPG Bulletin, 66(1), 28-43.

Petrash, D. A., Bialik, O. M., Bontognali, T. R., Vasconcelos, C., Roberts, J. A., McKenzie, J. A., & Konhauser, K. O. (2017). Microbially catalyzed dolomite formation: from near-surface to burial. Earth-Science Reviews, 171, 558-582.

Roberts, J. A., Kenward, P. A., Fowle, D. A., Goldstein, R. H., González, L. A., & Moore, D. S. (2013). Surface chemistry allows for abiotic precipitation of dolomite at low temperature. Proceedings of the National Academy of Sciences, 201305403.

Rodriguez-Blanco, J. D., Shaw, S., & Benning, L. G. (2015). A route for the direct crystallization of dolomite. American Mineralogist, 100(5-6), 1172-1181.

Rosen, M. R., Miser, D. E., Starcher, M. A., & Warren, J. K. (1989). Formation of dolomite in the Coorong region, South Australia. Geochimica et Cosmochimica Acta, 53(3), 661-669.

Sánchez-Román, M., McKenzie, J. A., Wagener, A. D. L. R., Rivadeneyra, M. A., & Vasconcelos, C. (2009). Presence of sulfate does not inhibit low-temperature dolomite precipitation. Earth and Planetary Science Letters, 285(1-2), 131-139.

Sánchez-Román, M., Vasconcelos, C., Schmid, T., Dittrich, M., McKenzie, J. A., Zenobi, R., & Rivadeneyra, M. A. (2008). Aerobic microbial dolomite at the nanometer scale: Implications for the geologic record. Geology, 36(11), 879-882.

Schmidt, M., Xeflide, S., Botz, R., & Mann, S. (2005). Oxygen isotope fractionation during synthesis of CaMg-carbonate and implications for sedimentary dolomite formation. Geochimica et Cosmochimica Acta, 69(19), 4665-4674.

Siegel, E. (1961). Factors influencing the precipitation of dolomitic carbonates. State Geol. Surv. Kansas. Bull. 152, 127-158.

Sibley, D. F. (1990). Unstable to stable transformations during dolomitization. The Journal of Geology, 98(5), 739-748.

Sibley, D. F., Dedoes, R. E., & Bartlett, T. R. (1987). Kinetics of dolomitization. Geology, 15(12), 1112-1114.

Sibley, D. F., Nordeng, S. H., & Borkowski, M. L. (1994). Dolomitization kinetics of hydrothermal bombs and natural settings. Journal of Sedimentary Research, 64(3a), 630-637.

Slaughter, M., & Hill, R. J. (1991). The influence of organic matter in organogenic dolomitization. Journal of Sedimentary Research, 61(2), 296-303.

Tarutani, T., Clayton, R. N., & Mayeda, T. K. (1969). The effect of polymorphism and magnesium substitution on oxygen isotope fractionation between calcium carbonate and water. Geochimica et Cosmochimica Acta, 33(8), 987-996.

Tucker, M.E. and Wright, V.P. (1990) Carbonate Sedimentology. Blackwell Scientific Publications, Boston, (482 p).

Wright, V. P., & Tucker, M. E. (1990). Carbonate sedimentology (pp. 1-27). Blackwell scientific publications.

Vasconcelos, C., McKenzie, J. A., Bernasconi, S., Grujic, D., & Tiens, A. J. (1995). Microbial mediation as a possible mechanism for natural dolomite formation at low temperatures. Nature, 377(6546), 220.

Vasconcelos, C., McKenzie, J. A., Warthmann, R., & Bernasconi, S. M. (2005). Calibration of the δ18O paleothermometer for dolomite precipitated in microbial cultures and natural environments. Geology, 33(4), 317-320.

Van Lith, Y., Warthmann, R., Vasconcelos, C., & Mckenzie, J. A. (2003). Sulphate-reducing bacteria induce low-temperature Ca-dolomite and high Mg-calcite formation. Geobiology, 1(1), 71-79.

Vengosh, A., Kolodny, Y., Starinsky, A., Chivas, A. R., & McCulloch, M. T. (1991). Coprecipitation and isotopic fractionation of boron in modern biogenic carbonates. Geochimica et Cosmochimica Acta, 55(10), 2901-2910.

Warren, J. (2000). Dolomite: Occurrence, evolution and economically important associations. Earth Science Reviews, 52(1), 1-81.

Zeebe, R. E. (1999). An explanation of the effect of seawater carbonate concentration on foraminiferal oxygen isotopes. Geochimica et Cosmochimica Acta, 63(13-14), 2001-2007.

Zempolich, W. G., & Baker, P. A. (1993). Experimental and natural mimetic dolomitization of aragonite ooids. Journal of Sedimentary Research, 63(4), 596-606.

Zhang, F., Xu, H., Konishi, H., & Roden, E. E. (2010). A relationship between d 104 value and composition in the calcite-disordered dolomite solid-solution series. American Mineralogist, 95(11-12), 1650-1656.

Zhang, F., Xu, H., Konishi, H., Shelobolina, E., & Roden, E. (2012a). Polysaccharide-catalyzed nucleation and growth of disordered dolomite: A potential precursor of sedimentary dolomite. The American Mineralogist, 97(4), 556-567.

Zhang, F., Xu, H., Konishi, H., Kemp, J., Roden, E., & Shen, Zhizhang. (2012b). Dissolved sulfide-catalyzed precipitation of disordered dolomite: Implications for the formation mechanism of sedimentary dolomite. Geochimica Et Cosmochimica Acta, 97, 148-165.

Zuddas, P., & Mucci, A. (1994). Kinetics of calcite precipitation from seawater: I. A classical chemical kinetics description for strong electrolyte solutions. Geochimica et Cosmochimica Acta, 58(20), 4353-4362.

CHAPTER 2: LOW TEMPERATURE DOLOMITE SYNTHESIS: REACTION KINETICS AND UREA CATALYSIS

CHAPTER 2: LOW TEMPERATURE DOLOMITE SYNTHESIS: REACTION KINETICS AND UREA CATALYSIS

Abstract

The understanding of geochemical conditions that facilitate dolomite formation at low temperatures (< 100 °C) has remained a mystery since dolomite was first discovered, forming the basis of the "dolomite problem". Abundant attempts to synthesize dolomite at temperatures below 100 °C have proved to be unsuccessful, although recent studies have shed light on potential chemical conditions which promote dolomite formation, including catalysis by biotic compounds, bacterial-mediation, and elevated pH. This study presents, to the best of our knowledge, the first-known synthesis of dolomite at temperatures below 100 °C, which was achieved by employing a developed method that leads to precipitation of partially-ordered dolomite at temperatures as low as 50 °C, following a ~ 42 day growth period. This "solid addition method" involves the addition of a solid phase Na_2CO_3 to Na–Ca–Mg–CO_2-NO_3-SO_4 solutions, which appears to sufficiently accelerate reaction kinetics to produce dolomite over relatively short time periods. This study also demonstrates that added urea concentrations promote dolomite formation at 50 - 80 °C, including a 252 mmolal urea concentration that is necessary for dolomite formation at 50 °C. These findings provide a breakthrough for the understanding of dolomite formation and a foundational method that will enable continued progress by future research.

Section 2.1: Introduction

Despite the abundance of dolomite throughout geologic history, understanding of the geochemical conditions favorable for dolomite formation at Earth's surface temperatures has plagued researchers for over a century (Graf and Goldsmith, 1956; Land

1998; Warren, 2000; Gregg et al., 2015). The “dolomite problem”, referring to the inability for dolomite synthesis in a laboratory setting at temperatures below 100 °C, has developed into a well-known mystery (Land, 1998; Arvidson and Mackenzie, 1999). This is especially puzzling, considering the ubiquity of dolomite formation in nature throughout the geologic record, and present-day oceans that are supersaturated with respect to dolomite (Warren, 2000). As a result, much of the knowledge regarding geochemical conditions that facilitate low temperature dolomite formation rely on experimental studies from elevated temperatures (> 100 °C) (e.g., Kaczmarek and Sibley, 2007, 2011; Kaczmarek and Thornton, 2017).

Laboratory synthesis studies have shown that numerous chemical conditions facilitate dolomite precipitation and dolomitization at temperatures above 100 °C. These include the molar Mg/Ca ratio, alkalinity, salinity, and the presence of sulfate ions, among others (see Gregg et al., 2015 and references within). Several low temperature experiments have investigated the role of biotic catalysts, such as dioxane (Oomori and Kitano, 1987) and urea (Deelman, 1999) for dolomite synthesis. However, these efforts were unsuccessful in reproducibly synthesizing dolomite and instead produced protodolomite that lacked evidence of cation ordering. More recently, sulfate-reducing bacteria, and other similar bacterial catalysts, seemingly overcame the kinetic barriers of dolomite formation and thus received the bulk of experimental focus (e.g., Vasconcelos et al., 1995; Sanchez-Román et al, 2008; Krause et al., 2012). However, microbial-mediation as an answer to the “dolomite problem” has been disproven (Zhang et al., 2012a; Gregg et al., 2015; Petrash et al., 2017) because these studies produced, at best,

near-stoichiometric but disordered, protodolomite. Additional cases of (proto)dolomite formation in nature have yet to be fully understood, such as partially-ordered dolomite formation as a bladder stone in a Dalmatian dog (Mansfield, 1980) and the rapid formation of protodolomite teeth by sea urchins (Wang et al., 1997; Goetz et al., 2014).

This study discusses the first known reproducible synthesis method for dolomite at temperatures below 100 °C. The key experimental conditions for dolomite synthesis found in this study are two-fold: (1) the addition of Na_2CO_3 as a solid phase to the experimental solution (as opposed to an aqueous CO_3^{2-} source); and (2) the inclusion of urea as a catalyst for dolomite formation. The combination of these two conditions facilitate reproducible dolomite synthesis at temperatures as low as 50 °C, following a ~ 42-day growth period. These findings will significantly help us to understand geochemical conditions for dolomite formation in nature and provide a foundational tool for future research on dolomite.

Section 2.2: Materials and Methods

Ca-Mg carbonates were synthesized through modified methods of those used by Kelleher and Redfern (2002) over the temperature range of 50 - 80 °C, at 10 °C increments with a typical growth period of ~ 42 days (a maximum range between 33 and 56 days). Measured amounts of ACS-grade 256 mmolal $MgSO_4 \cdot 7H_2O$, 238 mmolal $Ca(NO_3)_2 \cdot 4H_2O$, 483 mmolal Na_2CO_3, and varying $CO(NH_2)_2$ (urea) concentrations (0 - 252 mmolal) were added to 50 mL of 18.2 Ω deionized water within capped 250 mL glass bottles. For all experiments, Na_2CO_3 was the final chemical reagent added to the parent solution. Each solution was shaken vigorously by hand for 2 minutes following the

Na_2CO_3 addition and immediately placed in a convection drying oven (~ ±1 °C). Each parent solution was shaken for 1 minute, 5 to 6 times per week with a minimum 24-hour interval. Once the growth period elapsed, the pH of the parent solution was measured and the precipitates were collected through vacuum filtration using a 0.45 μm membrane disc filter, then rinsed with a minimum of 150 mL deionized water and a small amount of methanol, and finally dried at room temperature for a minimum of 48 hours.

Detailed experimental conditions are shown in Table 2.1. Consistent concentration of 256 mmolal $MgSO_4 \cdot 7H_2O$ and 238 mmolal $Ca(NO_3)_2 \cdot 4H_2O$ were used for all parent solutions and therefore the molar Mg/Ca ratio was held constant at 1.22 (Kelleher and Redfern, 2002).In the ideal case, if all chemical reagents were dissolved, this solution is supersaturated with respect to several minerals, including dolomite, calcite, aragonite and magnesite. The influence of Na_2CO_3 phase on the synthesis of dolomite was investigated by adding either Na_2CO_3 solution (e.g., Kelleher and Redfern, 2002) or solid Na_2CO_3 to the parent solution (Figure 2.1). In addition, the catalytic ability of $CO(NH_2)_2$ (urea) was examined by varying its concentration, as well as its exclusion, in selected parent solutions. Finally, whereas most parent solutions in this study were prepared in 250 mL glass bottles, a selection of parent solutions were prepared in 50 mL bottles (with a consistent solution volume of 50 mL) to confirm that elevated headspace was not a determining factor for dolomite formation in this study and to test the influence of reduced headspace.

To identify the mineralogy of the precipitates and their respective chemical compositions, powder X-ray diffraction (XRD) analyses were performed for all samples

reported, using either a Bruker SMART6000 equipped with CuKα radiation, Bruker D8 Discover with CuKα radiation, or a Bruker D8 Discover with CoKα radiation. Carbonate stoichiometry and cation ordering values were calculated through Lumsden and Chimahusky (1980)'s equation based on the d-value of the dolomite 104 diffraction peak and the intensity ratio of the dolomite 015/110 diffraction peaks, respectively. It was found that $\%MgCO_3$ values calculated from XRD data collected by the Bruker D8 Discover with CuKα radiation were noticeably lower (1 - 2 %) than the values collected from the two other XRD instruments. To account for this discrepancy and allow an effective comparison of all collected $\%MgCO_3$ data, a correction was applied for precipitates analyzed by the Bruker D8 Discover with CuKα radiation. A more detailed description of this correction is outlined in Appendix 2.1.3. Scanning electron microscopy (SEM) was performed on a JEOL 6610LV and a JEOL JSM-7000F to examine the crystal morphology of the precipitates. SEM-energy dispersive X-Ray spectroscopy (SEM-EDS) and X-Ray fluorescence (XRF) were also performed to confirm the mineral composition results obtained from XRD analyses.

A precipitate was labelled dolomite if it contained > 43 $\%MgCO_3$ and displayed evidence of cation ordering (primarily the 015 peak) (Land, 1980; Gregg et al., 2015). The term "protodolomite" was used in this study to describe carbonates with near dolomite stoichiometry (> 43 $\%MgCO_3$), but with no indication of cation ordering. Carbonates that contained < 43 $\%MgCO_3$ are referred to as HMC.

The $\delta^{13}C$ values of precipitates were determined using a Thermo Finnigan Delta plus XP isotope mass spectrometer equipped with a Gas Bench II headspace autosampler.

A minimum 2 day reaction time was given to ensure a sufficient CO_2 yield from the precipitates (see Section 3.3.1). The collected $\delta^{13}C$ values were calibrated to standard values for NBS 18 (-5.01 ‰) and NBS 19 (+1.95 ‰) on the VPDB scale. The $\delta^{13}C$ values of urea used in this study were measured using a Thermo Finnigan Delta plus XP isotope mass spectrometer equipped with an Elemental Analyzer.

Section 2.3: Experimental Results

All quantitative experimental results (e.g., stoichiometry and cation ordering) for individual precipitates are in Table 2.1 and the average results for each tested condition (e.g., temperature, precipitation method, urea concentration) are shown in Table 2.2. Dolomite was synthesized at 60, 70, and 80 °C, without the addition of urea, by adding Na_2CO_3 as a solid phase to the parent solutions (hereafter referred to as the "solid addition method"), which is confirmed by distinct evidence of cation ordering peaks (101, 015 and 021 XRD reflections) (Figure 2.2). Precipitates formed at 50 °C by the solid addition method were protodolomite lacking evidence of cation ordering. The synthesis experiments in which Na_2CO_3 was added as an aqueous phase to parent solutions (hereafter referred to as the "aqueous addition method") under the identical temperature and solution chemistry produced protodolomite with no indication of cation ordering at all tested temperatures (Table 2.1). These protodolomite precipitates appear structurally identical to those synthesized in previous studies employing a similar method (Kelleher and Redfern, 2002; Schmidt et al., 2005; Horita, 2014). (Proto)dolomite precipitated by the solid addition method always contained a higher $\%MgCO_3$ concentration than those from the aqueous addition method. For instance, the solid addition method yielded

dolomite with an average 48.4 %$MgCO_3$ whereas the protodolomite produced by the aqueous addition method contained an average of 45.7 %$MgCO_3$ at 60 °C (Table 2.2). Dolomite was also formed in 50 mL bottles at 60 °C and 80 °C by the solid addition method (Figure 2.3) (Table 2.A1), confirming that increased headspace was not the determining factor facilitating dolomite precipitation in this study.

The addition of various amounts of urea in parent solutions was found to facilitate an increase in cation ordering for dolomite formed at 50 - 80 °C (Table 2.1). Furthermore, at 50 °C, dolomite cation ordering was evident solely with an added urea concentration of 252 mmolal to solutions prepared by the solid addition method (Figure 2.4). Although the 015 peaks of the triplicate samples formed with 252 mmolal urea concentration added are distinctly attenuated in relation to those displayed by dolomite precipitated at elevated temperatures (i.e. 60, 70, 80 °C), each sample appears to display a small broad peak at the expected location for the 015 reflection ($2\theta = 35.4$ °) (Figure 2.5). Parent solutions at 50 °C containing less than 252 mmolal failed to produce dolomite.

Increasing the urea concentration was also found to increase the %$MgCO_3$ of (proto)dolomite at each temperature tested, regardless of the solution preparation method employed in this study (Table 2.1, Table 2.2). This finding is best highlighted at 80 °C, in which average %$MgCO_3$ of the dolomite precipitates increased from 48.5 % in the absence of urea, to 49.5 % with 50.5 mmolal of urea, and further increased to 50.6 % $MgCO_3$ with 101 mmolal urea (Figure 2.6). However, while the addition of 50.5 mmolal urea to parent solutions prepared by the aqueous addition method did increase the

stoichiometry of protodolomite formed at all tested temperatures, only samples grown at 80 °C precipitated dolomite (Table 2.1).

SEM-EDS analyses confirmed the near-stoichiometric composition of dolomite synthesized in this study (49.3 – 54.0 %$MgCO_3$) (Table 2.1). Although there is a somewhat sizable discrepancy in %$MgCO_3$ (~ 2 - 4 %) between those obtained from SEM-EDS (49.3 – 54.0 %) and calculated from XRD analyses (47.3 – 50.5 %), the trends for $MgCO_3$ outlined in this study are consistent from the results of both analytical methods. It should be noted that a correction was applied to certain SEM-EDS %$MgCO_3$ values, which is detailed in the Appendix 2.1.3. XRF analyses also validate the assertion of near-stoichiometric dolomite for selected samples in this study (Table 2.3), although quantitative comparisons to XRD and SEM-EDS data is not possible by this method, due to the lack of an established procedure.

SEM analyses of the (proto)dolomite precipitates indicate a substantial difference in morphology between precipitates synthesized by the solid addition method and the aqueous addition method (Figure 2.7). Dolomite formed through the solid addition method ranged from ~ 0.1 - 1 µm and display an elongated “rod-like” structure. In contrast, (proto)dolomites formed by the aqueous addition method were larger spherical aggregates ranging in size from ~ 2 - 50 µm. There was no discernable difference in the morphology of precipitates formed by the solid addition method, regardless of urea concentration (Figure 2.7). Similarly, aqueous addition method precipitates possessed an identical spherical morphology regardless of urea addition.

Carbon isotope compositions of (proto)dolomite precipitates were measured to investigate the effect of urea on dolomite synthesis. In our parent solutions, Na_2CO_3 ($\delta^{13}C$ = -1.86 ‰ (VPDB)) and urea ($\delta^{13}C$ = -41.04 ‰ (VPDB)) were the two sources of carbon. Therefore, carbonates precipitated from parent solutions without urea should reflect only the carbon isotope signature of the Na_2CO_3 used, whereas carbonates precipitated from parent solutions containing urea should have carbon isotope signatures of both carbon sources. An increase in urea concentration in the parent solution resulted in a strong temperature-dependent linear ^{13}C depletion in the precipitating (proto)dolomite (Figure 2.8). Furthermore, as the formation temperature increased, the degree of ^{13}C depletion in (proto)dolomite was increased, for each respective urea concentration (Figure 2.8). For example, the average $\delta^{13}C$ value (-4.80 ‰) for dolomite formed at 60 °C and with 101 mmolal urea concentration indicated that 12.2 % of incorporated carbon in the dolomite was from the source urea, whereas urea carbon accounted for 23.8 % of the dolomite carbon ($\delta^{13}C$ = -9.32 ‰) formed at 80 °C and with 101 mmolal urea.

Measured final solution pH values revealed a distinct trend of raised pH with increasing urea concentration (Figure 2.9). Similar to $\delta^{13}C$ signatures, average final pH values were generally dependent on urea concentration. More specifically, final pH was higher with increasing urea concentration and the influence of urea concentration was promoted by elevated temperatures, which is evident by higher trend line slopes with increasing temperatures (Figure 2.9).

Section 2.4: Discussion

Section 2.4.1: Effect of Na_2CO_3 Phase on Dolomite Synthesis

Dolomite was synthesized between 50 and 80 °C by employing the solid addition method; therefore, formation is primarily attributed to the addition of the carbonate ion (CO_3^{2-}) as a solid phase. When employing the aqueous addition method, dolomite was precipitated only at 80 °C with the addition of 50.5 mmolal urea. To the best of our knowledge, no previous study has successfully synthesized dolomite at low temperatures (< 100 °C) through the addition of either $NaHCO_3$ or Na_2CO_3 as a solid phase.

A potential dolomite formation model is proposed here to explain the influence of the solid addition method. Through the solid addition method, Ca^{2+} and Mg^{2+} ions may quickly replace Na^{2+} ions without allowing the Na_2CO_3 crystals to entirely dissolve, as a rapid "pseudo-dolomitization" replacement. It appears that crystal growth was inhibited within the parent solution, which is evident by generally consistent dolomite crystal size regardless of temperature (Appendix Figure 2.A2). As a result, cation ordering would occur within the dolomite precursor crystals, as the crystal grains are recrystallized following Ostwald's Step Rule when further growth no longer occurs (Kelleher and Redfern, 2002; Rodriguez-Blanco et al., 2015). Ostwald's Step Rule describes the process by which the eventual formation of a final mineral product, in this case dolomite, is preceded by a series of more soluble minerals (i.e. HMC, protodolomite), each less soluble than the mineral produced previously. HMC has been demonstrated to be more soluble than protodolomite, and protodolomite more soluble than dolomite possessing cation ordering (Navrotsky and Capobianco, 1987).

This model is largely supported by the findings of Kaczmarek and Sibley (2011). The study demonstrated that, through high temperature (218 °C) dolomitization experiments, whereas dolomite stoichiometry is dictated by parent solution chemistry, cation ordering is independent of initial solution chemistry and evolves with reaction progress ($CaCO_3$ replacement). Therefore, dolomite formed in this study may be facilitated by an increase in reaction kinetics by the rapid replacement of Na_2CO_3 with $CaMg(CO_3)_2$ without Na_2CO_3 dissolution, which would accelerate the reaction progress and, by extension, accelerate cation ordering. Insufficient reaction kinetics for dolomite nucleation and growth have been widely proposed as a primary inhibiting factor (Land, 1998; Arvidson and Mackenzie, 1999). Therefore, this form of "rapid pseudo-dolomitization" may sufficiently elevate the reaction rate to achieve cation ordering that would normally require exceedingly lengthy time periods (potentially decades to centuries) when employing aqueous addition methods. Alternatively, the rapid replacement of Na_2CO_3 may bypass the rate-limiting nucleation step entirely and similarly allow more efficient dolomite growth.

This proposed model is also supported by the findings of Zhang et al. (2012a). The authors, investigating the influence of dissolved sulfide (HS^- and H_2S) on dolomite formation, showed that the addition of sub-micron calcite seeds to parent solutions at 25 °C facilitated HMC formation in the absence of sulfide, and protodolomite in solutions containing sulfide. In contrast, solutions without calcite seeds produced aragonite and HMC without sulfide and with dissolved sulfide, respectively (Zhang et al., 2012a). The authors did not discuss the kinetics that may be associated with this "calcite seed effect",

but attributed certain dolomite deposits, such as the Miocene Monterey Formation (Compton and Siever, 1984) and the ODP Sites 680 and 686 (Kemp, 1990), to a similar effect. Importantly, the HMC produced by Zhang et al. (2012a) in dissolved sulfide solutions without calcite seeds appear visibly identical to the precipitates formed by the aqueous addition method in this study, and notably, the protodolomite produced in sulfide solutions containing calcite seeds display a similar "rod-like" crystal structure to the dolomite formed in this study by the solid addition method (Figure 2.10). If Na_2CO_3 grains cause a comparable "seed effect" as calcite, which may result from an increase in reaction kinetics, then the effect would be expedited for Na_2CO_3 due its appreciably greater solubility in comparison to calcite.

Natural examples of dolomite formation further support cation ordering development with reaction progress. Numerous recent (e.g., Miocene, Holocene) dolomite samples have been studied which display partial ordering (e.g., Sibley et al., 1989; Gregg et al., 1992). In relation, older dolomite samples (e.g., Pre-Cambrian), display stronger ordering (e.g., Gregg and Shelton, 1990), indicating that cation ordering increases with time. Moreover, Gregg et al. (1992) found that Holocene dolomite from Ambergris Cay, Belize, had increasing cation ordering that correlated with burial depth. Therefore, extended formation progress is directly related to the degree of cation ordering.

Our formation model is also supported by observed evidence from this study. First, regardless of formation temperature (50 °C - 80 °C), all precipitates from the solid addition method grew to approximately the same crystal size (~1 µm in length), implying

a limitation in a crystal growth (Appendix Figure 2.A2). In contrast, aqueous addition method precipitates largely varied in crystal size, generally between 2 and 50 µm at each temperature studied. Second, the solid addition method produced a significantly larger crystal quantity with respect to the precipitates from the aqueous addition method, even though the total collected precipitate weights for both methods were approximately the same.

Section 2.4.2: Effect of Urea Catalysis on Dolomite Synthesis

Urea (CH_4N_2O) was found to improve the stoichiometry and cation ordering of the dolomite precipitates obtained in this study, regardless of the formation temperature. This finding is likely the result of urea hydrolysis following the chemical equations:

$$CH_4N_2O + H_2O = 2NH_3 + CO_2 \quad \text{(Equation 2.1)}$$

$$NH_3 + H_2O = NH_4OH \quad \text{(Equation 2.2)}$$

$$CO_2 + H_2O = H_2CO_3 \quad \text{(Equation 2.3)}$$

in which urea hydrolysis increases the solution pH by the further hydrolysis of NH_3 into NH_4OH, a strong base (Mansfield, 1980). Due to the pH range of the parent solutions used in this study (6.91 – 8.97), the H_2CO_3 produced by the hydrolysis of CO_2 would rapidly dissociate to HCO_3^- or CO_3^{2-} (Beck et al., 2005; Kim et al., 2006). Because H_2CO_3 is a weak acid, the elevation of pH with increasing urea concentration suggests that NH_4OH production has a greater influence on pH than H_2CO_3 production (Figure 9).

Increased solution pH has previously been proposed to facilitate dolomite growth by causing a dehydration of Mg^{2+} ions (Lippman, 1973), and recent experimental results have supported this hypothesis (Zhang et al., 2012a,b). The dehydration of Mg^{2+} ions has been a well-documented inhibitor of dolomite formation due to the greater hydration energy of Mg^{2+} ions than that of Ca^{2+} ions (Oomori and Kitano, 1987; Zhang et al., 2012a,b). Mg^{2+} ions possess a double hydration shell that can inhibit incorporation and favor the adsorption of Ca^{2+} or other available cations. Hydrated Mg^{2+} ions which are incorporated into a dolomite crystal structure, alter the charge of the carbonate and hinder further growth (Lippmann, 1973).

Urea catalysis led to an increase in dolomite stoichiometry (%$MgCO_3$) (Figure 2.6) and cation ordering (Table 2.2) for all temperatures tested in this study and its role is evidenced by two factors. First, a comparison of final pH for all parent solutions forms a linear trend that is dependent on urea concentration (Figure 2.9). This supports the effect of urea hydrolysis, leading to NH_4OH and H_2CO_2 formation (as discussed above) and the resulting increase in solution pH. Second, $\delta^{13}C$ values of the (proto)dolomite precipitates display a strong correlation with urea concentration in the parent solution (Figure 2.8). These stable isotope compositions likely provide a direct indication of the degree of urea catalysis over the course of (proto)dolomite precipitation, reflecting the proportion of CO_3^{2-} ions produced from urea hydrolysis that is incorporated into the precipitate. These CO_3^{2-} ions would carry the lower $\delta^{13}C$ value of urea ($\delta^{13}C$ = -41.04 ‰ (VPDB)) and cause the increasingly negative $\delta^{13}C$ values with increasing urea concentration (Figure 2.8).

It is noteworthy that the degree to which urea promotes cation ordering and an increase in stoichiometry is promoted at higher temperatures, evidenced by more significant depletions in ^{13}C (Figure 2.8) and greater final solution pH values (Figure 2.9) as formation temperature increased. This finding is likely the result of thermal hydrolysis of urea. Previously, Meldlin (1959) displayed that thermal hydrolysis of urea was possible at 210 - 230 °C, which may have encouraged dolomite synthesis. The results of this study demonstrate that thermal hydrolysis of urea is possible at temperatures as low as 50 °C. However, with decreasing temperature, notably 50 °C, urea hydrolysis occurs to a lesser degree, evident by the slight depletion of ^{13}C with increasing urea concentration (Figure 2.8). As a result, a minimum of 252 mmolal urea concentration was required to facilitate dolomite formation at 50 °C.

Considering the available evidence, urea hydrolysis may promote dolomite formation by one or more of a series of potential factors, including: 1) increasing pH, which has been proposed to decreased hydration of Mg^{2+} ions and thus promote Mg^{2+} ion incorporation into the dolomite crystal structure (Lippmann, 1973); 2) increasing alkalinity, previously shown to increase the induction rate of dolomitization by increasing reaction kinetics (Morrow and Rickets, 1988; Arvidson and Mackenzie, 1997); or 3) urea, as a biotic compound, produces a similar influence on dolomite formation as other organic substances, such as sulfate-reducing bacteria (Vasconcelos et al., 1995), dioxane (Oomori and Kitano, 1987) or polysaccharides (Zhang et al., 2012b), which have been shown to facilitate protodolomite growth at ambient temperatures (25 - 40 °C), but have

yet to be fully understood for their role in facilitating (proto)dolomite formation (Petrash et al., 2017 and references within).

By confirming the catalytic role of urea for dolomite formation, urea may be a potential analog for natural dolomite formation throughout geological history. In nature, urea readily undergoes hydrolysis, catalyzed by the enzyme urease (Mansfield, 1980). Therefore, urea rarely exists as a component in seawater or other carbonate forming fluids. However, urea production into marine environments by organism's urine and feces (Mansfield, 1980) would undergo hydrolysis driven by urease, or thermal hydrolysis as seen in this study, and potentially lead to an increase in dolomite %$MgCO_3$ and cation ordering. Further research determining a possible correlation exists between periods of increased urea production and elevated dolomite formation is required, as well as natural studies of the relation between solution pH and dolomite formation, in cases of both direct precipitation and dolomitization.

Section 2.5: Conclusions

Dolomite was successfully synthesized by the solid addition method in this study without urea addition (60 - 80 °C) and by urea catalysis (50 - 80 °C). Mineral identification was confirmed by distinct cation ordering peaks for dolomite, visible through XRD analyses, as well as near-stoichiometric composition by XRD, XRF and SEM-EDS techniques. Essential to dolomite formation in the laboratory at low temperatures is the phase of the CO_3^{2-} ions at the time of parent solution preparation and the resulting change in carbonate precipitation kinetics. (Proto)dolomite precipitates obtained by adding a solid phase Na_2CO_3 to Na–Ca–Mg–CO_2-NH_2-NO_3-SO_4 solutions

were significantly different, both structurally and compositionally, from those synthesized by the typical aqueous addition method. Investigations into the role of an increased headspace indicate that the variation in parent solution preparation method, not larger headspace, was the dominant altered conditions in this study, in comparison to previous similar synthesis experiments. Evidence suggests that the solid addition method developed in this study alters the reaction kinetics for mineral precipitation, facilitating a rapid reaction rate for protodolomite formation, followed by dolomite recrystallization through Ostwald's Step Rule.

Dolomite formation at 50 °C using the solid addition method requires a minimum urea concentration of 252 mmolal in the parent solution. Carbonate parent solutions with an absence of urea lacked evidence of cation ordering reflections. Increasing concentrations of urea also proved to facilitate an increase in (proto)dolomite $\%MgCO_3$ at each temperature studied between 50 and 80 °C. Although the exact mechanism by which urea facilitates cation ordering and dolomite formation is currently unclear, its role may be related to increased pH or alkalinity, or urea may influence dolomite formation analogously to other organic substances, for which the reaction mechanisms have yet to be fully understood.

This newly developed method for dolomite synthesis at Earth's surface temperatures will allow subsequent researchers to further investigate solution conditions that facilitate dolomite growth, and specifically, an increased degree of cation ordering. Such studies, as well as a more thorough examination of the reaction mechanisms produced by this solid addition method, will produce a clearer understanding of how

dolomite formed abundantly in past geologic settings and finally provide answers to the widely debated “dolomite problem.”

Figures and Tables

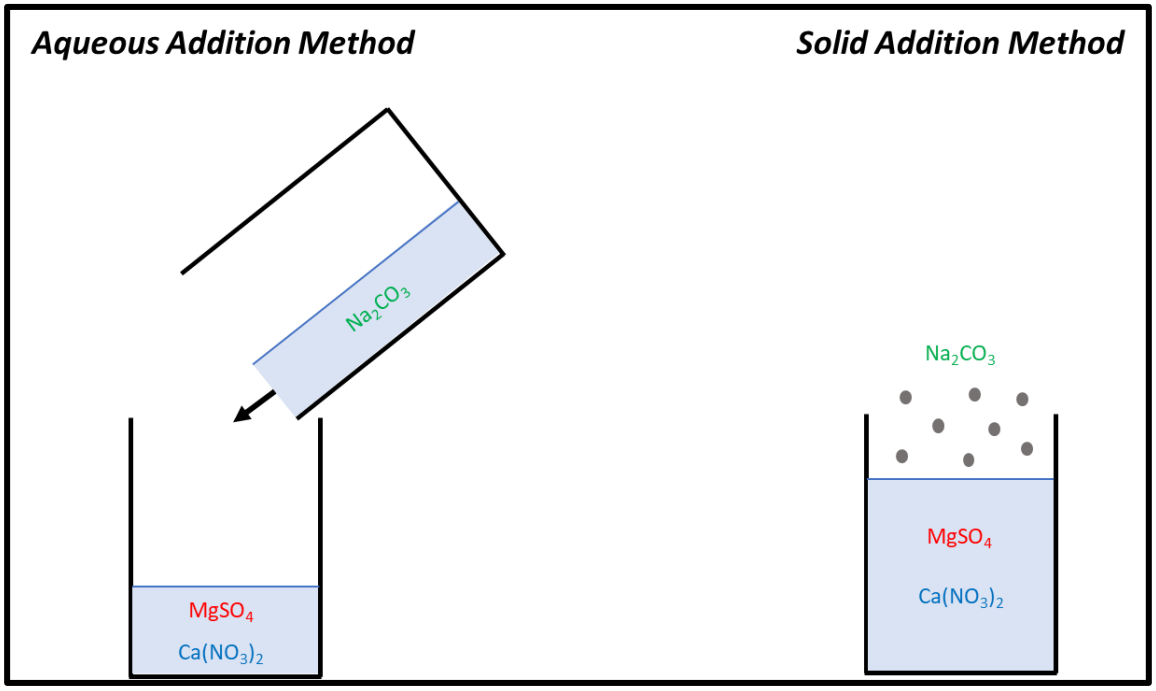

Figure 2.1. Schematic highlighting the difference in the solution preparation procedure between the aqueous addition and solid addition methods.

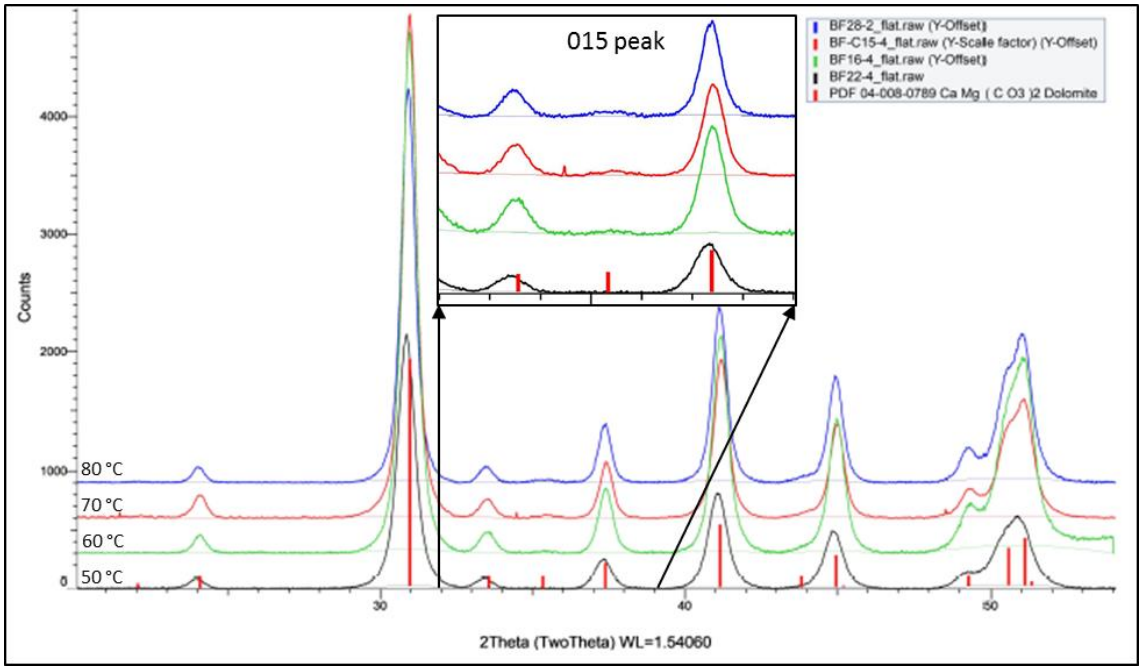

Figure 2.2. XRD patterns for protodolomite (50 °C) and dolomite (60, 70 and 80 °C) precipitated by the solid addition method, containing no urea, and in 250 mL bottles. Black pattern 50 °C, green pattern 60 °C, red pattern 70 °C, blue pattern 80 °C. Red bars represent ideal peak locations of the "Star" dolomite calibration from the PDF-4^{+} XRD database.

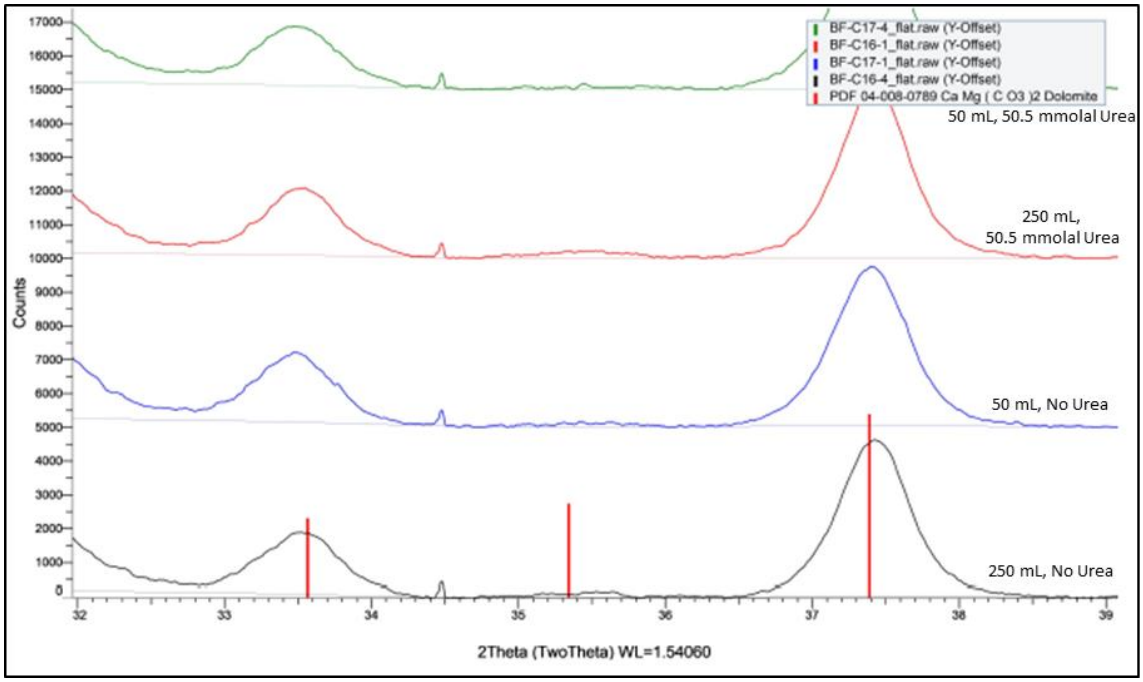

Figure 2.3. XRD patterns displaying the 015 peak for dolomite formed at 60 °C and under varying bottle size and urea concentration. From bottom to top: 250 mL bottle and no urea (black), 50 mL bottle and no urea (blue), 250 mL bottle and 50.5 mmolal urea (red), and 50 mL bottle and 50.5 mmolal urea (green). Notice that the 015 peak is present for precipitates grown in both 250 mL and 50 mL bottles.

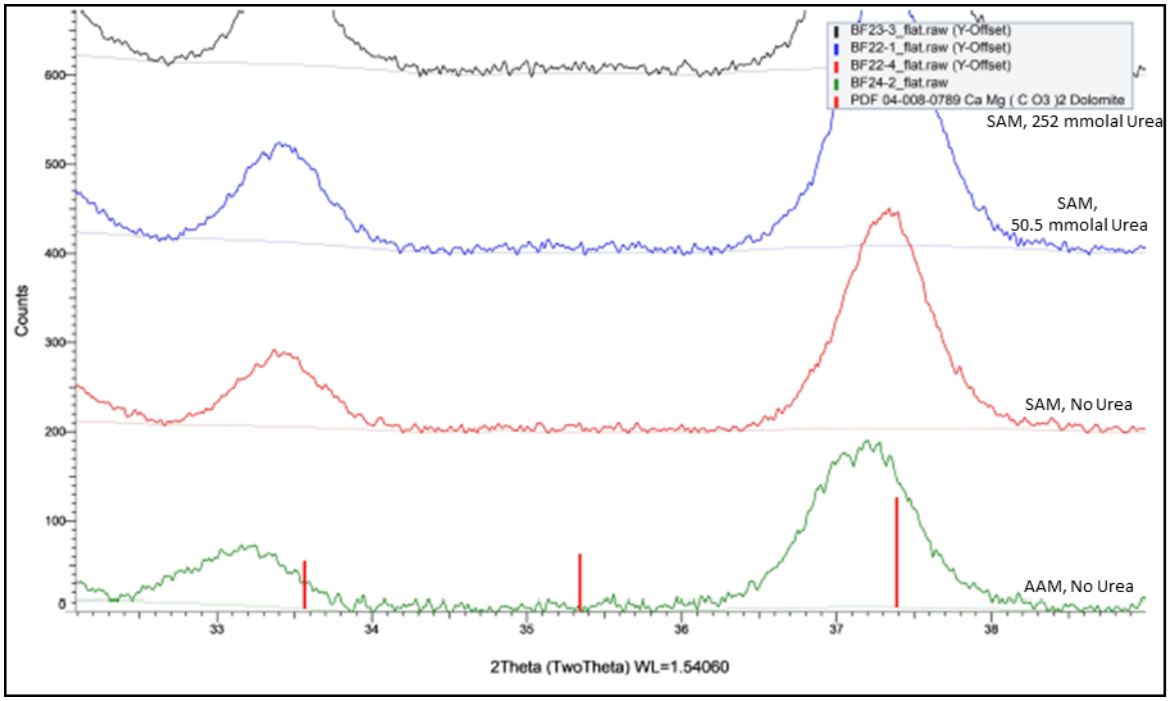

Figure 2.4. XRD patterns displaying the 015 peak for protodolomite and dolomite formed under varying conditions at 50 °C. From bottom to top: aqueous addition method (AAM) and no urea (green), solid addition method (SAM) and no urea (red), SAM and 50.5 mmolal urea (blue), and SAM and 252 mmolal urea (black). At 50 °C, dolomite was only formed with the addition of 252 mmolal urea to the parent solution (black).

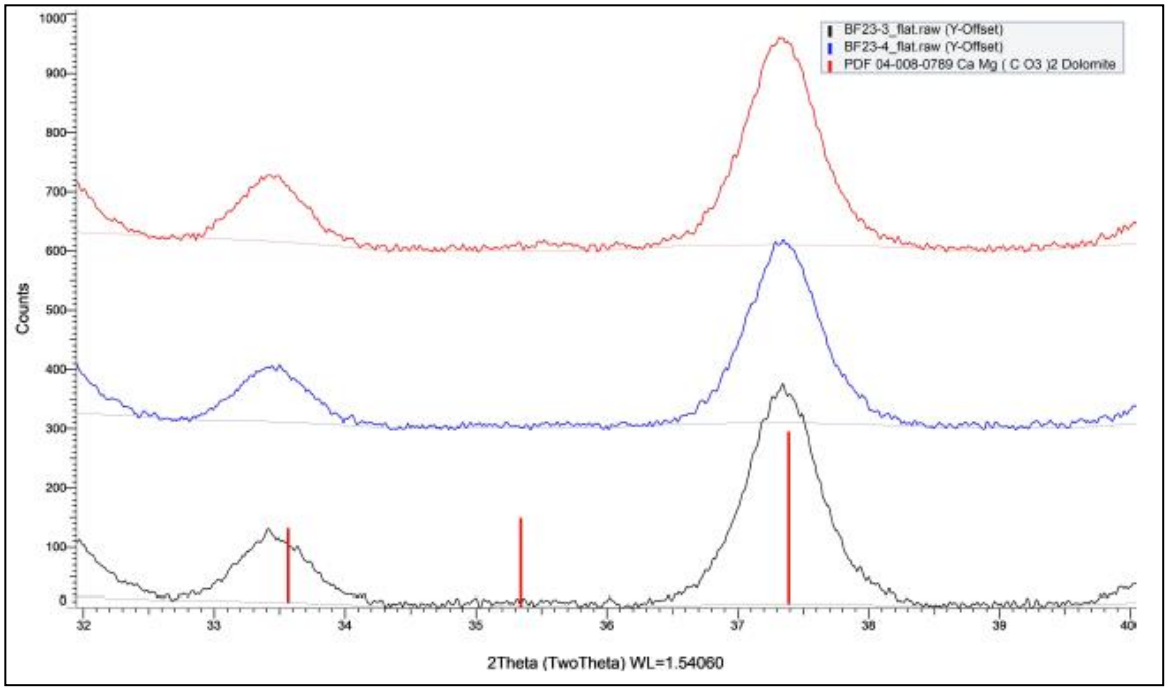

Figure 2.5. XRD patterns for the triplicate dolomite samples precipitated by SAM, in 250 mL bottles, and 252 mmolal urea. From bottom to top: BF-23-3 (black), BF-23-4 (blue), BF-25-4 (red).

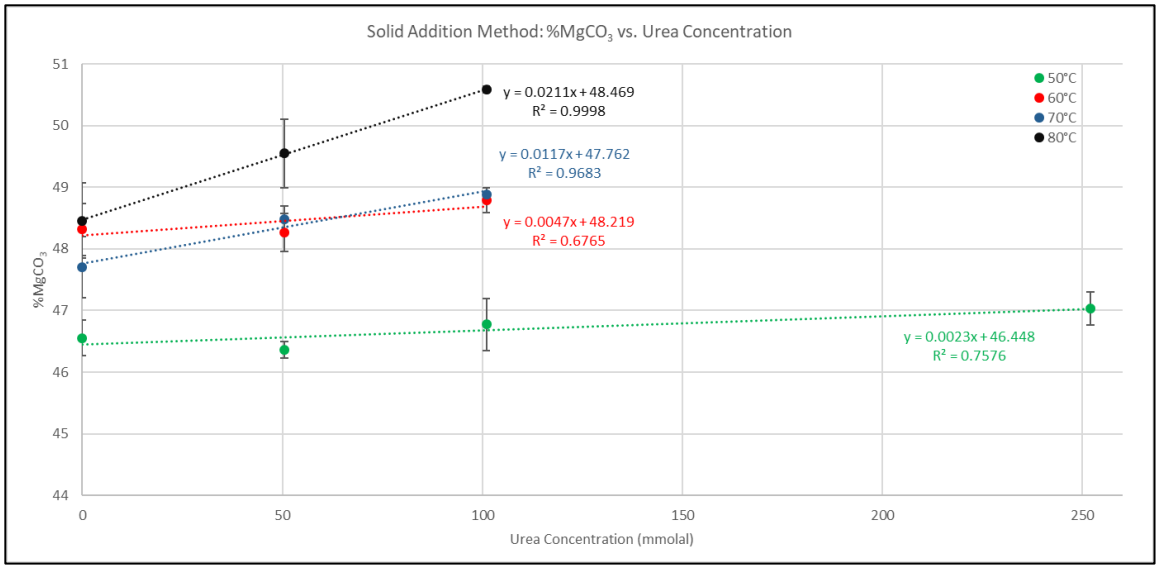

Figure 2.6. Influence of urea on $\%MgCO_3$ of synthesized (proto)dolomite at 50, 60, 70, and 80 °C and under identical conditions (solid addition method, 250 mL bottles).

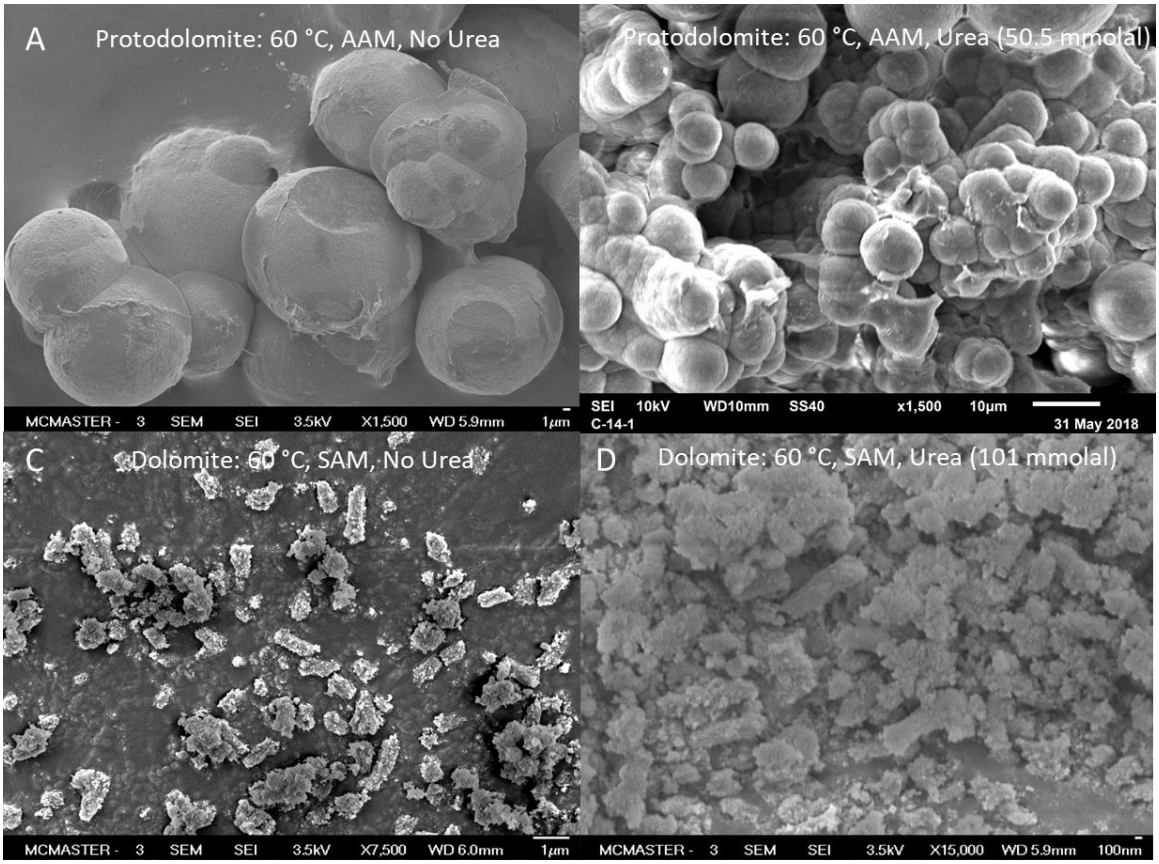

Figure 2.7. SEM images of synthesized (proto)dolomite at 60 °C and under various conditions (highlighted in white). Top left image is of sample BF-14-3, top right is of BF-14-1, bottom left is of BF-9-3, and bottom right is of BF-12-1.

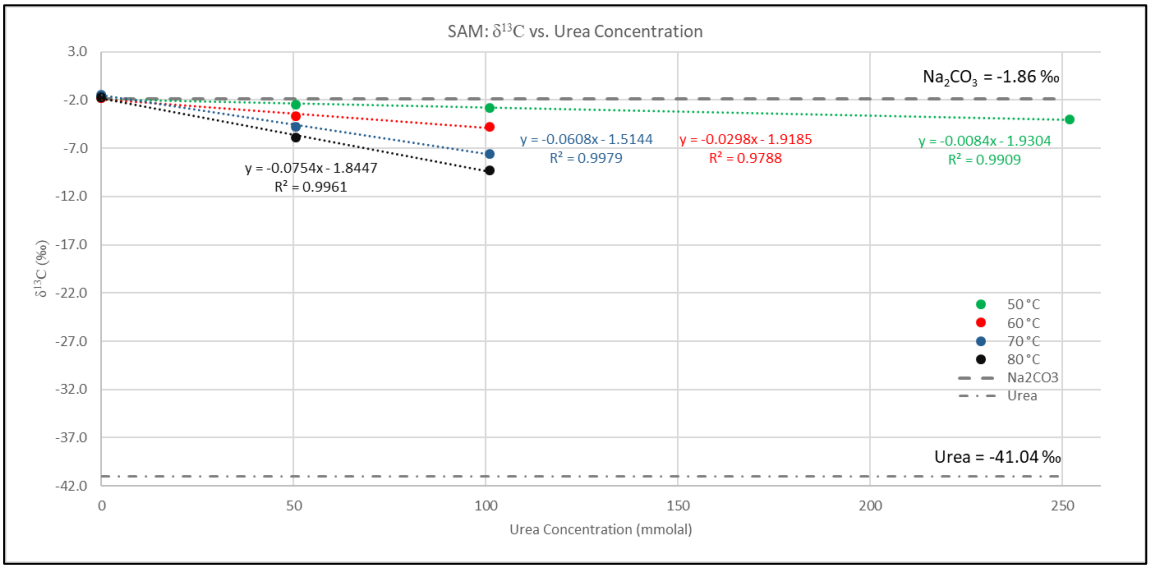

Figure 2.8. Influence of urea concentration on (proto)dolomite $\delta^{13}C$ at each respective temperature between 50, 60, 70 and 80 °C. Notice that $\delta^{13}C$ decreases with increasing urea concentration, as urea carbon is incorporated into the carbonate. Also, the degree to which $\delta^{13}C$ decreases is greater with increasing temperature.

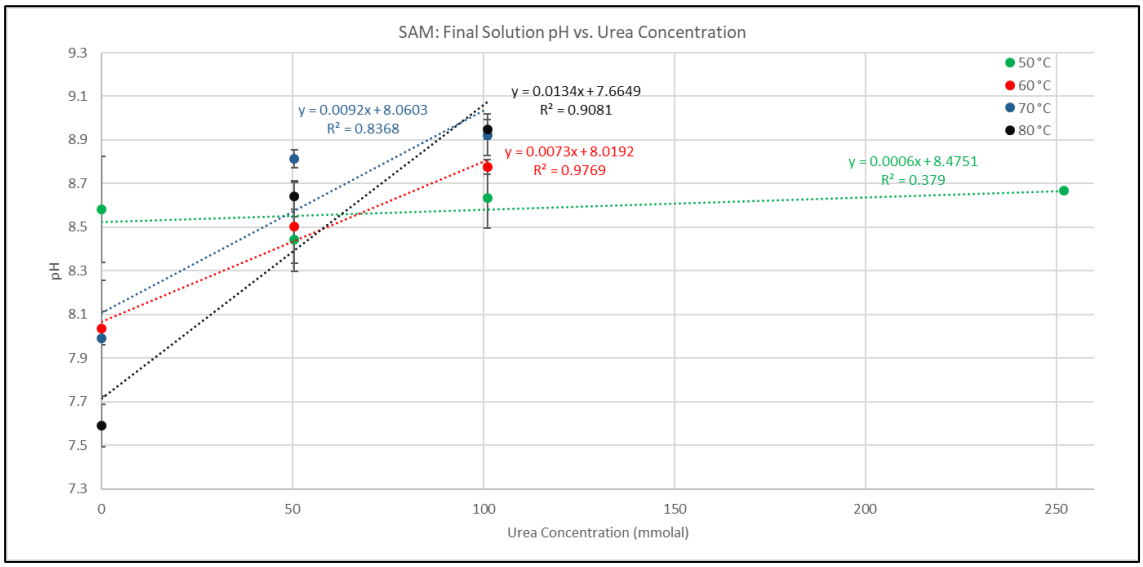

Figure 2.9. Relationship between urea concentration and the average final solution pH at 50, 60, 70, and 80 °C. Notice that pH always increases with increasing pH, and that as temperatures increases, the influence of urea concentration is more significant.

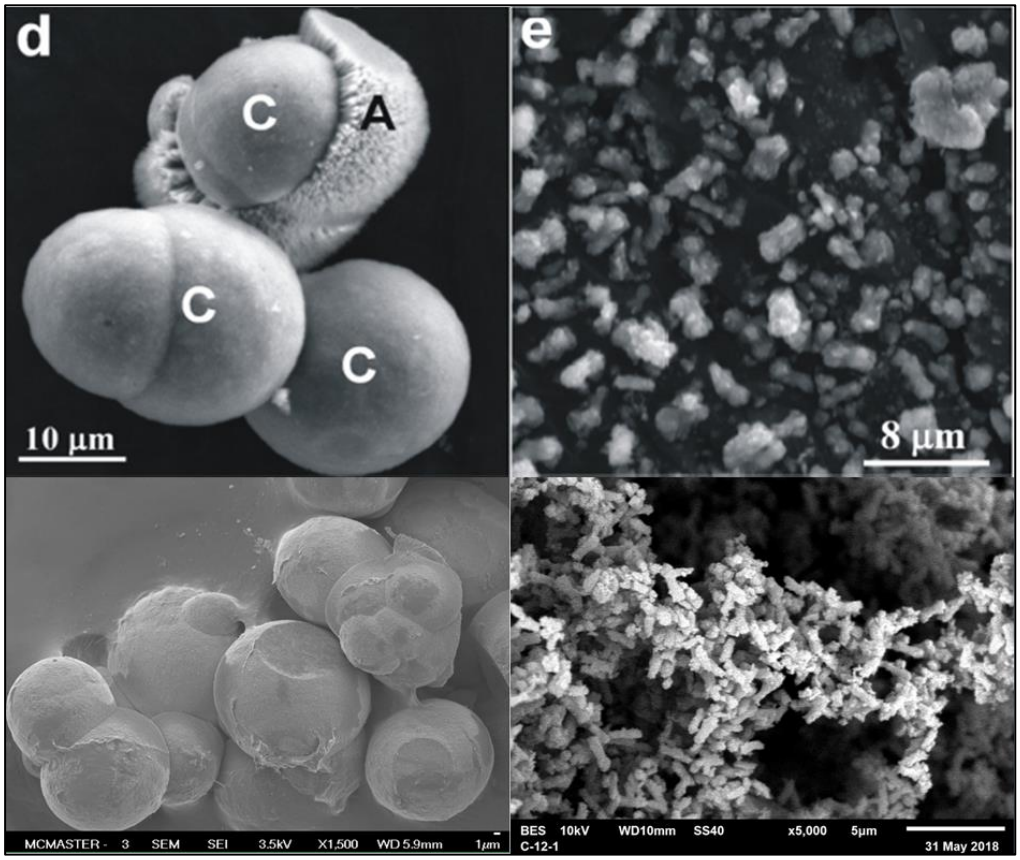

Figure 2.10. Comparison of the precipitates formed from this study and those from Zhang et al. (2012a). Images in top left and top right were modified from Zhang et al. (2012a). Top left: HMC (C) and aragonite (A) produced by Zhang et al. (2012a) from solutions containing dissolved sulfite and an absence of calcite seeds at 25 °C; top right: protodolomite produced by Zhang et al. (2012a) from solutions containing sulfate and calcite seeds at 25 °C; bottom left: protodolomite formed in this study from solutions prepared by the aqueous addition method, containing no urea and at 60 °C; bottom right: dolomite formed in this study from solutions prepared by the solid addition method, containing 101 mmolal urea and at 60 °C. Notice that the precipitates formed by Zhang et al. (2012a) from solutions with an absence of calcite seeds resemble those formed by the aqueous addition method in this study, and that precipitates formed by Zhang et al. (2012a) in solutions containing calcite seeds resemble those formed by the solid addition method in this study.

Table 2.1. Experimental conditions for parent solutions prepared in this study. All solutions contained 238 mmolal $Ca(NO_3)_2$, 256 mmolal $MgSO_4$, and 483 mmolal Na_2CO_3. XRD $\%MgCO_3$ collected from Bruker D8 Discover with CuKα ([b]) were corrected as outlined in Appendix 2.1.3.

Sample I.D	Condition	Temperature (°C)	Preparation Method	Growth Period (Days)	Urea (mmolal)	XRD $\%MgCO_3$	EDS $\%MgCO_3$	% Cation Ordering	pH	$\delta^{13}C$ (‰)	Product Mineralogy
BF-22-3	No U	50	SAM	42	0	46.7[b]		N/A	8.86	-1.87	P
BF-22-4	No U	50	SAM	42	0	46.2[b]	48.6[d]	N/A	8.46	-1.80	P
BF-25-1	No U	50	SAM	42	0	46.8[b]		N/A	8.28	-1.82	P
BF-22-1	U	50	SAM	42	50.5	46.3[b]		N/A	8.54	-2.33	P,A
BF-22-2	U	50	SAM	42	50.5	46.6[b]		N/A	8.29	-2.57	P
BF-25-2	U	50	SAM	42	50.5	46.3[b]		N/A	8.35	-2.43	P
BF-23-1	2X U	50	SAM	42	101	46.6[b]		N/A	8.47	-2.96	P
BF-23-2	2X U	50	SAM	42	101	47.3[b]		N/A	8.51	-2.96	P
BF-25-3	2X U	50	SAM	42	101	46.4[b]		N/A	8.78	-2.59	P
BF-23-3	5X U	50	SAM	42	252	47.1[b]		1.92[b]	8.63	-4.09	D
BF-23-4	5X U	50	SAM	42	252	47.3[b]	49.3[d]	1.18[b]	8.66	-3.93	D
BF-25-4	5X U	50	SAM	42	252	46.7[b]		2.59[b]	8.57	-4.02	D
BF-24-1	AAM	50	AAM	42	0	40.8[b]	40.6[d]	N/A	7.32	N/A	H
BF-24-2	AAM	50	AAM	42	0	40.4[b]		N/A	7.34	N/A	H
BF-24-3	AAM+U	50	AAM	42	50.5	40.8[b]		N/A	7.41	N/A	H
BF-24-4	AAM+U	50	AAM	42	50.5	40.8[b]		N/A	7.42	N/A	H
BF-9-4	No U	60	SAM	42	0	47.6[b]	51.9	2.45[b]	8.02	-1.83	D
BF-16-3	No U	60	SAM	42	0	48.5[a]		3.55[a]	7.91	-1.82	D
BF-16-4	No U	60	SAM	42	0	48.3[a]		2.54[a]	7.92	-1.72	D
BF-20-2	No U	60	SAM	42	0	48.8[b]		1.82[b]	8.09	-1.78	D
BF-9-1	U	60	SAM	42	50.5	47.8[b]		2.34[b]	8.39	-3.74	D
BF-16-1	U	60	SAM	42	50.5	48.3[a]		3.89[a]	8.30	-3.77	D
BF-16-2	U	60	SAM	42	50.5	48.6[a]		3.06[a]	8.32	-3.64	D
BF-20-1	U	60	SAM	42	50.5	48.4[b]		3.13[b]	8.81	-3.58	D
BF-12-1	2X U	60	SAM	42	101	49.1[a]	54.0[d]	3.41[a]	8.68	-4.79	D
BF-12-2	2X U	60	SAM	42	101	48.7[b]	50.7[d]	2.23[b]	8.77	-4.71	D
BF-20-3	2X U	60	SAM	42	101	48.6[b]		1.21[b]	8.73	-4.90	D
BF-14-3	AAM	60	AAM	42	0	46.0[a]		N/A	7.49	N/A	P
BF-14-4	AAM	60	AAM	42	0	45.5[a]	46.1[d]	N/A	7.84	N/A	P
BF-14-1	AAM+U	60	AAM	42	50.5	46.2[a]		N/A	8.25	N/A	P
BF-14-2	AAM+U	60	AAM	42	50.5	46.3[a]		N/A	8.49	N/A	P
BF-15-3	No U	70	SAM	42	0	47.2[a]		4.07[a]	8.21	-1.33	D
BF-15-4	No U	70	SAM	42	0	48.2[a]		3.64[a]	7.67	-1.54	D
BF-15-1	U	70	SAM	42	50.5	48.7[a]		5.33[a]	8.72	-5.04	D
BF-15-2	U	70	SAM	42	50.5	48.3[a]		5.35[a]	8.81	-4.46	D
BF-18-1	2X U	70	SAM	42	101	48.9[a]		5.44[a]	8.78	-7.74	D
BF-18-2	2X U	70	SAM	42	101	48.9[a]		5.60[a]	8.97	-7.42	D
BF-1-1	No U	80	SAM	33	0	49.1[c]	52.1[d]	4.29[c]	7.56	-1.83	D
BF-1-2	No U	80	SAM	33	0	47.6[c]		2.52[c]	7.53	-1.79	D
BF-28-1	No U	80	SAM	38	0	48.1[b]		3.47[b]	7.67	-1.46	D
BF-28-2	No U	80	SAM	38	0	49.0[b]		4.60[b]	7.40	-1.74	D
BF-1-3	U	80	SAM	33	50.5	49.7[c]		4.26[c]	8.60	-5.89	D
BF-1-4	U	80	SAM	33	50.5	50.1[c]		6.66[c]	8.67	-5.91	D
BF-6-1	U	80	SAM	41	50.5	48.8[c]		4.35[c]	8.51	-5.98	D
BF-6-2	U	80	SAM	41	50.5	48.3[c]		5.37[c]	8.53	-5.95	D
BF-6-5	2X U	80	SAM	41	101	50.5[a]	53.6	6.56[a]	8.85	-9.28	D
BF-6-6	2X U	80	SAM	41	101	50.6[b]		5.94[b]	8.94	-9.36	D
BF-7-3	AAM	80	AAM	41	0	47.3[a]	42.2[d]	N/A	6.91	-1.60	P,A
BF-7-4	AAM	80	AAM	41	0	46.3[a]		N/A	6.98	-1.52	P,A
BF-7-1	AAM+U	80	AAM	41	50.5	45.5[a]		N/A	8.06	-4.70	D,A
BF-7-2	AAM+U	80	AAM	41	50.5	44.8[a]		N/A	8.28	-4.36	D.A

D = dolomite; P = protodolomite; H = high magnesium calcite; A = aragonite; M = magnesium adipate glycinate

[a]: Bruker SMART6000 (CuKα); [b]: Bruker D8 Discover (CuKα); [c]: Bruker D8 Discover (CoKα); [d]: SEM Corrected

Table 2.2. Average parent solution and precipitate results.

Temperature (°C)	Condition	Urea (mmolal)	Avg. $\%MgCO_3$ (XRD)	$\%MgCO_3$ St. Dev	$\%MgCO_3$ (EDS)	Avg. Cation Ordering	Cation Ordering St. Dev	Avg. pH	Avg. pH St. Dev	Avg. $\delta^{13}C$	$\delta^{13}C$ St. Dev	Product Mineralogy
50.0	No U	0	46.6	0.29	48.6	N/A	N/A	8.53	0.24	-1.83	-1.83	P
50.0	U	50.5	46.4	0.14		N/A	N/A	8.39	0.11	-2.44	-2.44	P
50.0	2X U	101	46.8	0.42		N/A	N/A	8.58	0.14	-2.84	-2.84	P
50.0	5X U	252	47.0	0.27	49.3	1.90	0.57	8.62	0.04	-4.01	-4.01	D
50.0	AAM	0	40.6	0.17		N/A	N/A	7.33	0.01	N/A	N/A	H
50.0	AAM+U	50.5	40.8	0.01	40.6	N/A	N/A	7.42	0.00	N/A	N/A	H
60.0	No U	0	48.3	0.43	51.9	2.60	0.71	7.97	0.08	-1.78	0.04	D
60.0	U	50.5	48.3	0.30		3.10	0.55	8.48	0.21	-3.66	0.08	D
60.0	2X U	101	48.8	0.20	52.4	2.30	0.90	8.73	0.03	-4.80	0.08	D
60.0	AAM	0	45.7	0.25	46.1	N/A	N/A	7.66	0.18	N/A	N/A	P
60.0	AAM+U	50.5	46.3	0.05		N/A	N/A	8.37	0.12	N/A	N/A	P
60.0	50mL	0	47.4	0.22		2.10	0.52	7.81	0.10	-1.76	0.04	D
60.0	50mL+U	50.5	47.6	0.31		1.50	0.33	8.53	0.28	-3.47	0.33	D
60.0	50mL+2X U	101	47.7	0.16		1.70	0.17	8.73	0.07	-4.90	0.05	D
70.0	No U	0	47.7	0.50		3.86	0.21	7.94	0.27	-1.43	0.11	D
70.0	U	50.5	48.5	0.22		5.34	0.01	8.76	0.04	-4.75	0.29	D
70.0	2X U	101	48.9	0.00		5.52	0.08	8.87	0.10	-7.58	0.16	D
80.0	No U	0	48.5	0.61	52.1	3.72	0.81	7.54	0.10	-1.71	0.14	D
80.0	U	50.5	49.5	0.55		5.09	1.11	8.59	0.06	-5.92	0.04	D
80.0	2X U	101	50.6	0.05	53.6	6.25	0.31	8.90	0.05	-9.32	0.04	D
80.0	AAM	0	46.8	0.50	42.2	N/A	N/A	6.95	0.03	-1.56	0.04	D,A
80.0	AAM+U	50.5	45.2	0.37		N/A	N/A	8.17	0.11	-4.53	0.17	D,A
80.0	50mL	0	49.1	0.21		4.89	0.34	7.52	0.11	-1.70	0.06	D
80.0	50mL+U	50.5	50.3	0.00		4.56	0.05	8.63	0.02	-5.71	0.04	D

D = dolomite; P = protodolomite; H = high magnesium calcite; A = aragonite; M = magnesium adipate glycinate

Table 2.3. XRF results for selected precipitates, including BF-Dol, the internal laboratory dolomite standard.

Analyte Symbol	Co3O4	CuO	NiO	SiO2	Al2O3	Fe2O3(T)	MnO	MgO	CaO	Na2O	K2O	TiO2	P2O5	Cr2O3	V2O5	LOI	Total
Unit Symbol	%	%	%	%	%	%	%	%	%	%	%	%	%	%	%	%	%
Detection Limit	0.005	0.005	0.003	0.01	0.01	0.01	0.001	0.01	0.01	0.01	0.01	0.01	0.01	0.01	0.003		0.01
Analysis Method	FUS-XRF	FUS-XRF	FUS-XRF	FUS-XRF	FUS-XRF	FUS-XRF	FUS-XRF	FUS-XRF	FUS-XRF	FUS-XRF	FUS-XRF	FUS-XRF	FUS-XRF	FUS-XRF	FUS-XRF	FUS-XRF	FUS-XRF
Ideal Dolomite								21.86	30.41							47.73	100
BF-Dol	< 0.005	0.006	< 0.003	0.2	0.34	0.02	0.013	21.09	30.64	< 0.01	< 0.01	0.02	0.03	< 0.01	0.004	45.52	97.88
BF-1-1	< 0.005	< 0.005	< 0.003	0.61	0.33	< 0.01	< 0.001	21.5	28.94	0.07	0.01	0.01	0.02	< 0.01	< 0.003	47.74	99.23
BF-6-5	< 0.005	< 0.005	< 0.003	0.75	0.34	< 0.01	< 0.001	21.91	28.29	< 0.01	< 0.01	0.01	0.01	< 0.01	< 0.003	48	99.31
BF-9-4	< 0.005	< 0.005	< 0.003	0.13	0.35	< 0.01	0.001	21.22	29.17	0.03	< 0.01	0.01	0.01	< 0.01	< 0.003	49.08	100
BF-12-1	< 0.005	< 0.005	< 0.003	< 0.01	0.34	< 0.01	0.006	21.24	27.99	0.01	< 0.01	0.01	0.01	< 0.01	< 0.003	49.94	99.53
BF-14-4	< 0.005	0.006	< 0.003	0.76	0.34	< 0.01	< 0.001	19.4	27.95	0.3	0.02	< 0.01	0.02	< 0.01	< 0.003	49.84	98.63
BF-23-4	< 0.005	0.015	< 0.003	< 0.01	0.33	< 0.01	< 0.001	20.37	27.5	< 0.01	< 0.01	0.01	0.01	< 0.01	< 0.003	51.37	99.61

CHAPTER 2 APPENDICES

Appendix 2.1: Detailed Materials and Methods

Appendix 2.1.1: Synthesis of Ca-Mg Carbonates

Ca-Mg carbonates were synthesized through a modified method used by Kelleher and Redfern (2002) over the temperature range of 50 - 80 °C, at 10 °C increments with a typical growth period of ~ 42 days (a maximum range between 33 and 56 days). A selection of samples were also grown at 40 °C to test the lowest temperature that dolomite synthesis was possible by this method. Measured amounts of ACS-grade 256 mmolal $MgSO_4 \cdot 7H_2O$, 238 mmolal $Ca(NO_3)_2 \cdot 4H_2O$, 483 mmolal Na_2CO_3, and varying $CO(NH_2)_2$ (urea) concentrations (0 - 252 mmolal) were added to 50 mL of 18.2 Ω deionized water within capped 250 mL glass bottles. For all experiments, Na_2CO_3 was the final compound added to the solution. Following the Na_2CO_3 addition, the solutions were shaken vigorously by hand for 2 minutes and immediately placed in a convection drying oven (~ ±1 °C). Each parent solution was shaken for 1 minute, 5 to 6 times per week with a minimum 24-hour interval. Once the mineral growth time elapsed, solution pH was measured. The precipitates were then collected through suction filtration, rinsed with a minimum of 150 mL deionized water and a small amount of methanol, and dried at room temperature for a minimum of 48 hours.

Detailed experimental conditions are given in Table 2.A1. Consistent molal concentrations of 256 mmolal $MgSO_4 \cdot 7H_2O$, 238 mmolal $Ca(NO_3)_2 \cdot 4H_2O$ and 483 mmolal Na_2CO_3 were used for most parent solutions. Therefore, the parent solution molar Mg/Ca ratio was held constant at 1.22. The influence of the Na_2CO_3 phase added was

investigated by the addition of either dissolved Na_2CO_3 solution, as performed by Kelleher and Redfern (2002) or solid Na_2CO_3 salt. More specifically, 25 mL of dissolved Na_2CO_3 was added to a separate 25 mL solution containing $Ca(NO_3)_2$ and $MgSO_4$ (hereafter referred to as the "aqueous addition method") (Figure 2.1). The $Ca(NO_3)_2$-$MgSO_4$ solution was cloudy prior to the dissolved Na_2CO_3 addition and, regardless of mixing time, the $Ca(NO_3)_2$ and $MgSO_4$ could not be entirely dissolved. The Na_2CO_3 addition produced a thick, "milky" solution, indicating the instantaneous nature of the reaction. Alternatively, parent solutions were prepared in a single 50 mL solution, in which $MgSO_4$ and $Ca(NO_3)_2$ were always added first and Na_2CO_3 salt added last (hereafter referred to as the "solid addition method" (Figure 2.1)

The catalytic ability of urea ($CO(NH_2)_2$) was examined by its addition, and varying concentration, in selected solutions. Urea was always added after $Ca(NO_3)_2$ and $MgSO_4$, but prior to the Na_2CO_3 addition. Urea concentration ranged from 0 mmolal to 50.5 mmolal for experiments at 40, from 0 mmolal to 101 mmolal for experiments at 60, 70, and 80 °C and from 0 mmolal to 252 mmolal at 50 °C (Table 2.A1). The replacement of $Ca(NO_3)_2$ with $CaCl_2$ for parent solutions containing 50.5 mmolal urea, was also performed. This replacement intended to investigate whether urea addition would prevent the adsorption of Cl^- anions to a growing dolomite crystal structure, and encourage CO_3^{2-} ion absorption, as proposed by Deelman (1999). Finally, whereas most parent solutions in this study were prepared in 250 mL bottles, a selection of solutions were prepared in 50 mL bottles (with a consistent solution volume) to test the influence of reduced headspace on dolomite formation and growth. The primary purpose for this investigation was to

confirm that increased headspace (50 mL solution in 250 mL bottle) was not the determining factor for dolomite formation, and therefore the solid addition method promoted dolomite formation, as most previously studies have generally used minimal headspace (e.g., 50 mL solution volume in 50 mL bottle).

Appendix 2.1.2: Precipitate Crystal Structure Identification

Scanning electron microscopy (SEM) was performed on a JEOL 6610LV and a JEOL JSM-7000F to identify mineral crystal structure. Images were taken with magnifications up to 30,000. Carbonate samples were prepared for SEM imaging by adhesion to carbon film attached to a metal mount, to which a thin layer of gold coating was applied.

Appendix 2.1.3: Analyses of Precipitate Stoichiometry and Cation Ordering

To identify synthesized minerals and their respective chemical compositions, powder X-ray diffraction (XRD) analyses were performed for all samples reported, using either a Bruker SMART6000 equipped with CuKα radiation, Bruker D8 Discover with CuKα radiation, or a Bruker D8 Discover with CoKα radiation. All XRD data collection and analyses were performed at the McMaster Analytical X-Ray Diffraction Facility. The variation in instruments used was due to unforeseen mechanical failures during the analysis process. Samples analyzed on the Bruker D8 Discover with CoKα radiation were prepared by compaction of the mineral powder to a mound on a metal plate, which were flattened, and then analyzed. Samples analyzed on each instrument using CuKα radiation were prepared by mounting mineral powers on a small glass rod, which were also flatten prior to analysis.

Raw diffraction data obtained from XRD analyses were integrated into 2θ versus intensity patterns, typically used for mineral identification and compositional analyses, using DIFFRAC.EVA software. Mineral phases were identified using the ICDD PDF-4^{+} 2018 Diffraction Database. The stoichiometry of all carbonate precipitates was calculated by the 2θ value of the dolomite 104 peak, which was accurately determined by peak modeling using Topas software. Similarly, all precipitate % cation ordering values were calculated by the respective peak intensities of the modelled 015 and 110 dolomite peaks (Goldsmith and Graf, 1958; Kaczmarek and Sibley, 2011). The 015 and 110 peaks are chosen for comparison because the 015 peak is a primary indicator of dolomite cation ordering, whereas the 110 peak intensity is independent of cation ordering (Kaczmarek and Sibley, 2011).

Carbonate stoichiometry and cation ordering values were calculated through the Lumsden and Chimahusky (1980) equation, based on the d-value of the dolomite 104 diffraction peak, and the ratio of the dolomite 015/110 diffraction peaks, respectively (see Equation 1.1, Section 1.2.1). Since the Lumsden and Chimahusky (1980) equation requires 104 peak d-values, carbonates measured using the Bruker D8 Discover with CoKα radiation had d-values recalculated to CuKα values following the equation:

$$d_{Cu}=(2\theta_{Co}/(2*SIN(0.5*N*\pi/180) \qquad \text{(Equation 2.A1)}$$

where d_{Cu} is the d-value for CuKα radiation analyses, $2\theta_{Co}$ is the 2θ values obtained from CoKα radiation analysis, and N is the CoKα radiation wavelength constant equal to 1.79026.

The recalculated values for samples analyzed by CoKα radiation correlated well with samples analyzed by CuKα radiation. However, a consistent sizeable error was associated with XRD analyses between the two CuKα radiation instruments, which was larger than the measured error measured from rerunning a single sample (~ 0.6 $\%MgCO_3$). To correct for this error, and allow for more accurate comparison between carbonate $\%MgCO_3$ measurements between the two CuKα radiation instruments, correction values were established by calculating the difference in $\%MgCO_3$ for samples analyzed by both instruments. The results for these analyses are shown in Table 2.A3. Interestingly, two distinct groups were found, in which carbonates formed at 80 °C had an average $\%MgCO_3$ difference of 2.32 between analyses from both instruments, whereas those formed at 60 °C had a smaller average difference of 1.24. Therefore, samples analyzed by the Bruker D8 with CuKα radiation at 60 °C were corrected by +1.24 $\%MgCO_3$ and 80 °C samples corrected with +2.32 $\%MgCO_3$, for more accurate comparison with samples previously analyzed by the Bruker SMART6000 with CuKα radiation. Due to the inability to calculate an error for samples analyzed by the Bruker D8 with CuKα radiation at 50 °C, the smaller correction of +1.24 % was also applied to these samples. For consistency, all XRD analyses using the Bruker D8 Discover with CuKα were corrected with one of the two calculated values.

Scanning electron microscopy with energy dispersive X-Ray spectroscopy (SEM-EDS) on a JEOL 6610LV was also utilized to confirm the mineral compositions obtained from XRD analyses. SEM and SEM-EDS analyses were performed either by the candidate or Chris Butcher, at the Canadian Centre for Electron Microscopy (CCEM) and

the results are shown in Table 2.A1. Carbonate samples were prepared for SEM-EDS analyses by adhesion to carbon film attached to a metal mount. In contrast to samples that were solely analyzed for SEM imaging, carbonate samples prepared for SEM-EDS were applied with a thin layer of carbon coating as opposed to gold coating. Furthermore, mineral compositions of a select number of samples were also obtained by X-Ray fluorescence, which was carried out by Activation Laboratories Ltd (Table 2.3).

A correction was also required for $\%MgCO_3$ values collected from SEM-EDS analyses. During SEM-EDS data collection, seemingly accurate ratios for carbonate elemental compositions (used to calculate $\%MgCO_3$), were recorded. However, compositional data stored in AZTEC software, analyzed following data collection, displayed significantly lower $\%MgCO_3$ values. To correct for this issue, a linear correlation was calculated by comparing the initial $\%MgCO_3$ values recorded during SEM-EDS analyses and the values stored in AZTEC software (Figure 2.A1). The equation from this correlation was subsequently applied to correct all values from AZTEC software that did not have initial values recorded. The validity for this correction was confirmed by a similar error associated with a near-stoichiometric natural dolomite sample (BF-Dol, internal dolomite standard), as well as the agreement with compositional data obtained by XRD and XRF analyses (Table 2.A1).

Appendix 2.2.4: Carbon Isotope Measurements

Ca-Mg carbonates were prepared for isotopic analysis by thorough grounding using a mortar and pestle. Small proportions of the ground powder (~ 150 µm) were then weighed on a Mettler Toledo analytical balance and deposited into glass tubes

(Exetainer). The sample $\delta^{13}C$ signatures were determined using a Thermo Finnigan Delta plus XP isotope mass spectrometer equipped with a Gas Bench II headspace autosampler. This instrument has a typical analytical $\delta^{18}O$ precision of ± 0.08 ‰. The tubes were first flushed and filled with He gas, and following the flush and fill procedure, 5 drops (check volume) of 105 % phosphoric acid were injected into each tube to react with sample powders and produce CO_2. All samples were reacted within a block heated to a constant 25 °C (± 0.1 °C). A minimum 2 day reaction time was given to ensure a sufficient CO_2 yield from the (proto)dolomite samples (see Section 3.3.1). Once the allotted reaction time elapsed, CO_2 isotopic mass ratios were measured. All Ca-Mg carbonates were analyzed in duplicate. The collected $\delta^{13}C$ values were calibrated to standard values for NBS 18 (-5.01 ‰) and NBS 19 (+1.95 ‰) on the VPDB scale.

Appendix 2.2: Detailed Results

Appendix 2.2.1: (Proto)Dolomite Crystal Structure

Scanning electron microscope (SEM) images provided carbonate crystal structure information. An obvious difference in mineral crystal structure was found between (proto)dolomite formed by the solid addition method and those formed by the aqueous addition method (Figure 2.A2). (Proto)dolomite formed by the solid addition method were rod-shaped crystals, whereas the aqueous addition method produced distinct spherical aggregates. Furthermore, rod-shaped crystals (≤ 1 µm) precipitated by the solid addition method were considerably smaller than spherical crystals (~ 2 - 50 µm) (Figure 2.A2). Notably, solid addition method carbonates were tightly clumped together following the 48 hour drying period, whereas aqueous addition method carbonates were

larger grainy crystals that remained separated. Seemingly identical crystal structure, corresponding to the method employed, was consistent at all temperatures tested (Figure 2.A2). The total precipitate yield collected from both methods was indistinguishable and ranged from ~ 2.2 - 2.4 grams.

The addition of varying urea concentrations for solutions prepared by both the solid addition and aqueous addition method produced no discernable difference in (proto)dolomite precipitate crystal structure (Figure 2.A2). The crystal structure of precipitates produced by the replacement of $Ca(NO_3)_2$ with $CaCl_2$, and the reduction in bottle size to 50 mL, were not investigated by SEM imaging. However, given that precipitates produced by these conditions were visibly identical to the solid addition method precipitates which were analyzed by SEM imaging (i.e. $Ca(NO_3)_2$ calcium source, 250 mL bottle), which were distinctly unique in relation to aqueous addition method precipitates (larger grainy crystals that did not clump together), it is assumed that $CaCl_2$ replacement of $Ca(NO_3)_2$ and bottle size reduction produced no significant change in crystal structure. Therefore, the change in solution preparation method was the sole condition that produced a change in (proto)dolomite mineral structure in this study.

All solid addition method precipitates from this study, regardless of experimental conditions, produced either pure protodolomite ($\geq$ 43 %$MgCO_3$, no evidence of cation ordering) or dolomite (Table 2.A1; Table 2.A2). In other words, solely one identifiable phase was precipitated when the solid addition method was employed. In contrast, certain aqueous addition method experiments produced multiple minerals (Table 2.A1; Table 2.A2). Specifically, all aqueous addition method precipitates formed at 80 °C were a

mixture of either protodolomite and aragonite (no urea added; BF-7-3, BF-7-4) or dolomite and aragonite (50.5 mmolal urea; BF-7-1, BF-7-2). Similarly, precipitates from the same method and grown at 40 °C, were either a mixture of protodolomite and aragonite (no urea added; BF-11-3, BF-11-4) or protodolomite, aragonite, and magnesium adipate glycinate (50.5 mmolal urea; BF-11-1, BF-11-2). In contrast, aqueous addition method precipitates grown at 50 °C were pure HMC (< 43 %$MgCO_3$), and those grown at 60 °C were pure protodolomite (Table 2.A1).

Appendix 2.2.2: Cation Ordering and Identification of Dolomite

The ability to synthesize dolomite at temperatures below 100 °C was the fundamental finding of this study. XRD patterns were used to identify the presence of required dolomite cation ordering peaks for all dolomite samples formed, which are the 015, 101, and 021 dolomite diffraction peaks. The 015 dolomite peak was the primary peak investigated in this study due to its greater intensity in relation to the 101 and 021 peaks, as well as the focus given to its identification from previous studies (see Gregg et al., 2015 and references within). Table 2.A1 details an overview of the parent solution conditions used for all synthesized samples, as well as the respective %$MgCO_3$, % cation ordering, and minerals identified. Table 2.A2 displays the average experimental results for each investigated condition. The XRD patterns for all precipitated samples are provided in the Supplementary Information.

Precipitates formed by the aqueous addition method, and an absence of urea, did not display evidence of cation ordering at all temperatures tested (40 - 80 °C). Similarly, the addition of 50.5 mmolal urea to solutions prepared by the aqueous addition method

did not produce precipitates with cation ordering at 40, 50, or 60 °C. However, dolomite was synthesized at 80 °C by the aqueous addition method with 50.5 mmolal urea concentration added to the parent solutions.

The solid addition method did not produce dolomite at 40 °C, regardless of 0 mmolal, or 50.5 mmolal urea concentrations. At 50 °C, the solid addition method solely produced dolomite in combination with a 252 mmolal urea concentration addition (Figure 2.4). Although the 015 peaks of the triplicate samples formed by this condition are clearly attenuated in relation to those displayed by dolomite precipitated at elevated temperatures (i.e. 60, 70, 80 °C), each sample appears to display a small broad peak at the expected location for the 015 reflection (2θ = ~ 35.4 °) (Figure 2.5), which is not visible for precipitates with urea concentrations < 252 mmolal. Parent solutions containing 50.5 and 101 mmolal urea concentrations, as well as an absence of urea, failed to dolomite displaying evidence of cation ordering at 50 °C (Figure 2.4). All parent solutions prepared by the solid addition method at 60, 70, and 80 °C resulted in dolomite synthesis. These included solutions containing no urea, 50.5 mmolal urea, or 101 mmolal urea concentration, solutions containing $CaCl_2$ replacement of $Ca(NO_3)_2$, and solutions prepared in 50 mL bottles (Table 2.A1).

The addition of varying urea concentrations to parent solutions was found to increase the 015 peak intensity, and therefore the degree of dolomite cation ordering. This finding is best represented quantitatively through the comparison of cation ordering ratios for each dolomite precipitate (Table 2.A1; Table 2.A2). For example, the cation ordering of dolomite synthesized at 70 °C by the solid addition method display a strong linear

correlation with urea concentration, with average % cation ordering increasing from 3.86 with no urea, to 5.34 with 50.5 mmolal urea, and to 5.52 with 101 mmolal urea added (Figure 2.A3). XRD patterns for dolomite formed at 70 °C likewise display a greater intensity of the 015 diffraction peak with increasing urea concentration (Figure 2.A4). Similarly, for dolomite synthesized at 80 °C, average % cation ordering increased from 3.72 with no urea, to 5.09 with 50.5 mmolal urea, to 6.25 with 101 mmolal urea added (Figure 2.A5). Due to the variation in XRD instruments used at 80 °C (CuKα and CoKα), comparison of XRD patterns with increasing urea concentration was not possible. Dolomite formed at 60 °C did not display a definitive correlation between cation ordering and urea concentration (Figure 2.A6; Figure 2.A7). This may be due to the variation in XRD instruments used to analyze dolomite formed at this temperature over the course of this study, or because thermal urea hydrolysis only weakly occurred at this lower temperature (discussed in detail in Section 2.4.2).

The replacement of $Ca(NO_3)_2$ with $CaCl_2$, in solutions that also contained 50.5 mmolal urea, resulted in lower dolomite cation ordering peak intensities than those calculated from dolomite formed when $Ca(NO_3)_2$ was used (Figure 2.A8). Specifically, solutions containing $Ca(NO_3)_2$ had average ordering percentages of 3.10, 5.34, and 5.09 at 60, 70 and 80 °C, whereas solutions containing $CaCl_2$ had average ordering percentages of 2.06, 3.44, and 3.76 (Table 2.A2).

Finally, dolomite synthesized in 50 mL bottles, as opposed to 250 mL bottles, displayed noticeably lower % cation ordering at 60 °C (Figure 2.A6; Figure 2.3). Dolomite formed at 60 °C and in 250 mL bottles displayed % cation ordering values of

2.59, 3.10, and 2.28 with no urea, 50.5 mmolal urea, and 101 mmolal urea added, respectively. In contrast, dolomite formed in 50 mL the same temperature possessed values of 2.07, 1.54 and 1.66 with no urea, 50.5 mmolal urea and 101 mmolal urea added, respectively. However, no discernable difference was found between dolomite synthesized by either bottle size at 80 °C (Figure 2.A5). At 80 °C, dolomite formed in 250 mL bottes had % cation ordering values of 3.72 and 5.09 with no urea and 50.5 mmolal urea added respectively, whereas those formed in 50 mL bottles had ratios of 4.89 with no urea and 4.56 with 50.5 mmolal urea.

To summarize the experimental conditions favorable for dolomite growth found in this study: at 60, 70 and 80 °C, dolomite was always synthesized by the solid addition method, regardless of solution chemistry conditions investigated in this study or the bottle size. Dolomite was also formed at 80 °C by employing the aqueous addition method when 50.5 mmolal urea was also added to the parent solution. At 50 °C, dolomite was only synthesized by employing the solid addition method in 250 mL bottles with a 252 mmolal urea concentration.

Appendix 2.2.3: (Proto)Dolomite Stoichiometry

The influence of each tested experimental and chemical condition on (proto)dolomite formation from this study was investigated by comparing the $\%MgCO_3$ of synthesized (proto)dolomite. Primarily, the calculated $\%MgCO_3$ value was used, following the equation established by Lumsden and Chimahusky (1980) (see Equation 1.1 discussion in Section 1.2.2). Values of $\%MgCO_3$ obtained through SEM-EDS analyses are also presented for a select number of samples, to confirm the accuracy and reliability

of the calculated values (Table 2.A1). Furthermore, XRF analyses data is presented in Table 2.3, however quantitative $\%MgCO_3$ values were unable to be calculated from the collected data.

An obvious correlation was observed between (proto)dolomite $\%MgCO_3$ and preparation method. The use of the solid addition method resulted in substantially higher $\%MgCO_3$ values, in relation to the aqueous addition method, at all temperatures tested. For samples formed at 50 °C, average $\%MgCO_3$ increased considerably from 39.4 % to 45.3 % (Figure 2.A9). Precipitates at 60 °C displayed a smaller increase from 45.7 % 48.5 % to (Figure 2.A10). Finally, at 80 °C, a precipitate $\%MgCO_3$ increased from 46.8 % to 48.3 % (Figure 2.A11). Samples formed at 40 °C and 80 °C by the aqueous addition method are affected by the presence of other phases that appear to cause unreliable protodolomite $\%MgCO_3$ values, therefore a comparison between the two methods may be inaccurate.

The influence of urea catalysis on (proto)dolomite stoichiometry is clear. Raised parent solution urea concentrations generally produced greater $\%MgCO_3$ values; however the effect of urea greatly increased at elevated temperatures (70 and 80 °C). Protodolomite synthesized at 40 °C by the solid addition method possessed $\%MgCO_3$ values that marginally increased from 45.3 % with no urea to 45.7 % with 50.5 mmolal urea (Figure 2.A12). Experiments at 50 °C produced protodolomite with an average $\%MgCO_3$ of 45. 3 %, 45.1 % and 45.5 % with added urea concentrations of 0 mmolal, 50.5 mmolal and 101 mmolal, respectively (Figure 2.A12). However, with 252 mmolal urea added at 50 °C, dolomite was formed with a slightly higher average $\%MgCO_3$ of

45.8 %. Precipitates synthesized at 60 °C displayed a weaker correlation between urea concentration and %$MgCO_3$ (Figure 2.A12). At this temperature, %$MgCO_3$ was nearly identical with no urea and 50.5 mmol, possessing 48.5 % and 48.4 %, respectively, but increasing the urea concentration to 101 mmolal slightly raised the %$MgCO_3$ to 48.8 %. At 70 °C, dolomite %$MgCO_3$ increased from 47.7 % with no urea, to 48.5 % with 50.5 mmolal urea and to 48.9 % with 101 mmolal urea added (Figure 2.A12). Similarly, at 80 °C, average XRD %$MgCO_3$ increased from 48.3 % with no urea, to 49.5 % with 50.5 mmolal urea and further increased to 50.5 % with 101 mmolal urea added (Figure 2.A12).

The addition of 50.5 mmolal urea to parent solutions prepared by the aqueous addition method, as opposed to the solid addition method, also generally resulted in higher precipitate %$MgCO_3$ (Table 2.A2). Precipitates synthesized at 50 °C had %$MgCO_3$ values that slightly increased from 40.6 % to 40.8 % (Figure 2.A9). At 60 °C, protodolomite %$MgCO_3$ increase from 45.7 % with no urea to 46.3 % with 50.5 mmolal urea (Figure 2.A10). Finally, as opposed to lower temperatures protodolomite formed at 80 °C by the aqueous addition method and no urea had an average %$MgCO_3$ of 46.8 %, but dolomite formed by the same method with 50.5 mmolal urea had an average %$MgCO_3$ of 45.2 % (Figure 2.A11). As previously stated, these 80 °C %$MgCO_3$ values may be unreliable due to the precipitation of both (proto)dolomite and aragonite (Table 2.A1).

The replacement of $Ca(NO_3)_2$ with $CaCl_2$ in solutions prepared by the solid addition method, and containing 50.5 mmolal urea, produced a noticeable reduction in %$MgCO_3$ at all each temperature tested (60, 70 and 80 °C) (Figure 2.A13). Precipitates

formed at 60 °C displayed a small decrease from 48.4 % to 48.0 %. At 70 °C, a more sizeable decrease from 48.5 % to 47.7 % was observed. Finally, at 80 °C, $\%MgCO_3$ decreased from 49.5 % to 48.5 % when $CaCl_2$ replaced $Ca(NO_3)_2$ in parent solutions.

A temperature-dependent effect was found for precipitates grown in 50 mL bottles, as opposed to 250 mL bottles. Precipitates formed at 60 °C in 50 mL bottles had $\%MgCO_3$ values of 47.4 %, 47.6 % and 47.7 % with no urea, 50.5 mmolal urea and 101 mmolal urea, respectively (Figure 2.A10). These values are notable lower than precipitates formed under the same conditions, but in 250 mL bottles, which had values of 48.3 %, 48.3 %, and 48.8 % with no urea, 50.5 mmolal urea and 101 mmolal urea, respectively (Figure 2.A10). However, at 80 °C and using 50 mL, average dolomite $\%MgCO_3$ values were 49.1 % with no urea and 50.3 % with 50.5 mmolal, higher than dolomite synthesized in 250 mL bottles, which had values of 48.5 % with no urea and 49.5 % with 50.5 mmolal urea (Figure 2.A11).

SEM-EDS results also indicate near-stoichiometric composition for dolomite synthesized in this study (Table 2.A2). Generally, SEM-EDS values were ~ 2 - 4 $\%MgCO_3$ greater than the calculated XRD values. Despite this difference, the trends observed from altered experiment conditions (e.g. method employed or urea addition) are supported. The true value of $\%MgCO_3$ is likely closer to the calculated XRD value, due to XRD analyses providing a more average value in relation to SEM-EDS, which analyzed smaller sample sizes. The compositional data collected by XRF is difficult to compare directly with calculated XRD and SEM-EDS data, due to the lack of a method to obtain $\%MgCO_3$ values from XRF compositions. Nevertheless, the selected synthesized

(proto)dolomite samples from this study that were analyzed by XRF display compositions that are similar to those of the internal dolomite laboratory standard (BF-Dol) and an ideal dolomite composition (Table 2.3).

Appendix 2.2.4: Final Solution pH Trends

Two distinct trends are displayed when analyzing the final parent solution pH values. Comparison of final pH values from parent solutions prepared by the solid addition method display a linearly decreasing trend between the final pH and increasing temperature (Figure 2.A14). More specifically, solid addition method solution average pH ranged from 8.34 at 40 °C to 7.55 at 80 °C, whereas aqueous addition method solution values declined from 8.41 at 40 °C to 6.95 at 80 °C. In addition, the aqueous addition method final solution pH values were, in general, considerably lower than identical solutions prepared by the solid addition method (Table 2.A1).

A more evident correlation was found between solid addition method final pH with increasing urea concentration. At all temperatures tested (40 - 80 °C), increasing urea concentrations caused an elevation in final pH (Figure 2.A14). Furthermore, the slopes of the trendlines also increased with elevated temperatures, seemingly providing an indication of the degree to which urea concentration influenced final solution pH. For 40 and 50 °C solutions, the slopes were nearly identical at 0.0007 and 0.006, respectively. Average final pH values at 60 °C display a steeper slope of 0.0074. Finally, at 70 and 80 °C, increasing urea concentration resulted in increasingly steeper slopes values of 0.0092 and 0.0129, respectively. Notably, the pH values of 8.87 and 8.85, under the conditions

70 °C and 80 ° with 101 mmolal urea concentration respectively, were the highest average pH values recorded in this study.

Appendix 2.2.5: (Proto)Dolomite Carbon Isotopic Signatures

Ca-Mg carbonate $\delta^{13}C$ values display a similar correlation with urea concentration as final solution pH. The relation of $\delta^{13}C$ values with increasing concentration, for each temperature tested, is shown in Figure 2.A15. First, parent solutions with an absence of urea formed (proto)dolomite with nearly identical $\delta^{13}C$ values to the initial Na_2CO_3 (-1.86 ‰). As the solution urea concentration increased, the $\delta^{13}C$ values were lowered accordingly, progressing toward the urea value (-41.04 ‰). This trend occurred at each tested temperature (Figure 2.A15). Second, similar to the trend shown by final solution pH, the degree of (proto)dolomite ^{13}C depletion depended on the formation temperature, with a greater depletion as temperature increased. For example, a minor depletion in protodolomite ^{13}C occurred at 40 °C, as $\delta^{13}C$ values decreased from -1.78 ‰ with no urea, to -2.03 ‰ with 101 mmolal urea added. In contrast, $\delta^{13}C$ values were greatly lower at 80 °C, decreasing from a value of -1.80 ‰ with no urea to -9.32 ‰ with 101 mmolal urea. Other altered experimental conditions, the reduction in bottle size from 250 mL to 50 mL and replacement of $Ca(NO_3)_2$ caused no discernable change in the (proto)dolomite $\delta^{13}C$ value (Table 2.A2).

Appendix 2.3: Supplementary Discussion

Appendix 2.3.1: Effect of $CaCl_2$ Replacement on Dolomite Synthesis

The replacement of $Ca(NO_3)_2$ in selected solutions that contained 50.5 mmolal urea, was performed to investigate any influence of urea on Cl^- ion adsorption into the

dolomite crystal structure. However, the small sample size tested indicate that dolomite formed by solutions containing $Ca(NO_3)_2$ possessed slightly stronger cation ordering (Figure 2.A8) and slightly higher $\%MgCO_3$ (Figure 2.A13). The minor increase in both dolomite properties may result from a lower ionic strength when $CaCl_2$ is used. Regardless of a potential influence from the Ca^{2+} ion chemical compound used during solution preparation, it appears unlikely that the cause for urea catalysis on dolomite synthesis is due to the mitigation of Cl^{2-} ion adsorption, and associated encouraged CO_3^{2-} ion adsorption, as stated by Deelman (1999). Nevertheless, the possibility that urea discourages the adsorption of multiple types of anions, not solely Cl^- ions, remains and requires further investigation.

Appendix 2.3.2: Effect of Bottle Volume on Dolomite Synthesis

Primarily, precipitate growth in 50 mL bottles was tested to determine if dolomite synthesis in this study was attributed to the developed solid addition method or to the large headspace use in the 250 mL bottles. Results collected from this study indicate that solution preparation method has a much greater influence on dolomite formation than a change in headspace (e.g., Figure 2.A10; Figure 2.A11). However, it was found that smaller headspace resulted in lower $\%MgCO_3$ (Figure 2.A10), as well as weaker cation ordering (Figure 2.A6), for precipitates formed at 60 °C. This trend was consistent regardless of the added urea concentration (50.5 mmolal or 101 mmolal). Therefore, with the number of samples tested (minimum duplicates for each condition; Table 2.A1), the difference observed is greater than the expected analytical error for individual samples (~ 0.6 %).

With the lack of investigation of similar conditions by previous studies, the influence of an increased headspace on dolomite synthesis is unclear. However, one possible explanation may result from the increase in surface area at the solution-air boundary during daily mixing periods. This increase in surface area would result in a more efficient mixing of the Ca^{2+}, Mg^{2+} and CO_3^{2-} ions and may encourage Mg^{2+} ion incorporation into the dolomite crystal structure. Furthermore, the higher bottle surface area may facilitate separation of Ca^{2+} and Mg^{2+} into alternating layers and thereby increase cation ordering of the dolomite precipitates. This proposal is supported by the observation that precipitates formed in the 50 mL bottles generally remained clumped together during the daily shaking periods. In contrast, precipitates formed in 250 mL bottles, and prepared under identical conditions, separated more quickly while shaking occurred. Therefore, raised headspace may cause a greater influence on mineral synthesis than previously thought.

Nevertheless, dolomite synthesized in 50 mL bottles at 80 °C displayed both higher $\%MgCO_3$ (Figure 2.A11) and % cation ordering than dolomite grown in 250 mL bottles (Figure 2.A5). In this case the higher values may be a result of XRD instrument used for analyses, with most precipitates formed in 250 mL bottles analyzed by the CoKα instrument and all 50 mL precipitates analyzed by the CuKα instrument (Table 2.A1). However, despite accounting for the error associated with instruction variation, dolomite precipitated from 50 mL bottles are unlikely to possess significantly lower $\%MgCO_3$ and cation ordering, to the degree found at 60 °C. Therefore, the inhibiting mechanism (i.e. reduction in solution-air boundary surface area) observed at 60 °C appears negligible at

elevated temperatures. This may be due to the raised thermodynamic energy caused by increased temperatures which may allow the precipitates to separate more easily than at lower temperatures.

Figures and Tables

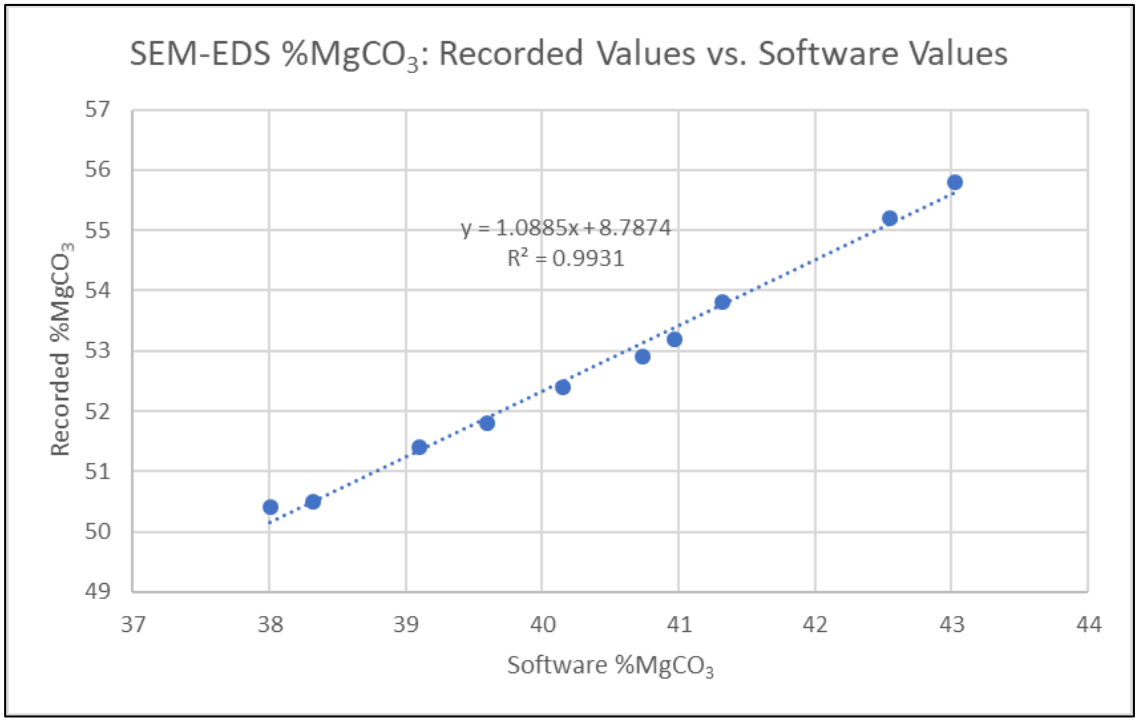

Figure 2.A1. Correlation of initial recorded SEM-EDS $\%MgCO_3$ and values displayed by Aztec software (for samples BF-9-4 and BF-6-5). Values are those collected from multiple EDS analyses of the two samples. Equation of line was used to correct for previously collected SEM-EDS values for which initial values were not recorded (all other samples).

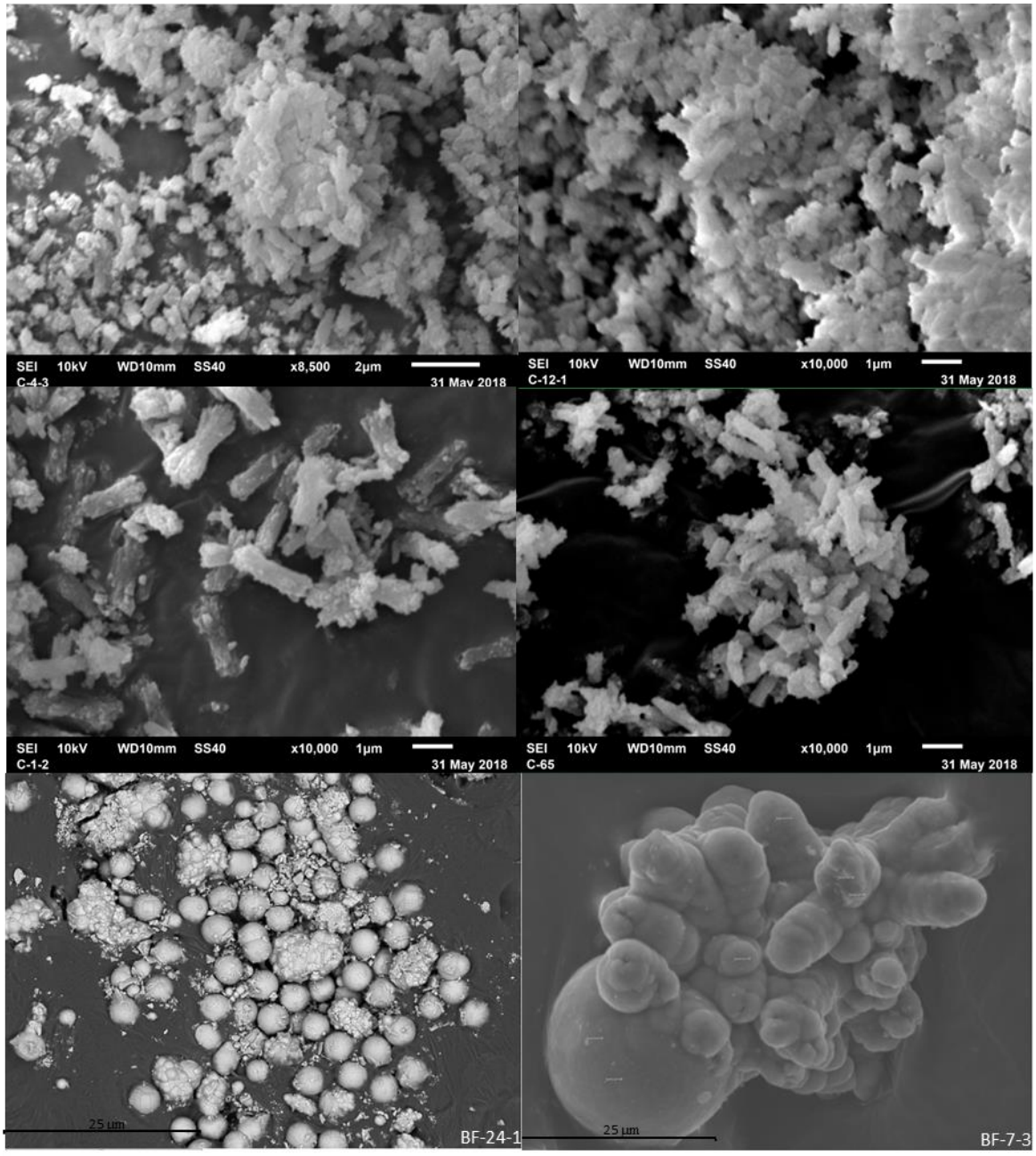

Figure 2.A2. SEM images of selected carbonate samples from this study. Top left: BF-4-3 (protodolomite: 40 °C, SAM, 101 mmolal urea); top right: BF-12-1 (dolomite: 60 °C, SAM, 101 mmolal urea); middle left: BF-1-2 (dolomite: 80 °C, SAM, no urea); middle right: BF-6-5 (dolomite: 80 °C, SAM, 101 mmolal urea); bottom left: BF-24-1 (HMC: 50 °C, AAM, no urea); bottom right: BF-7-3 (protodolomite: 80 °C, AAM, no urea).

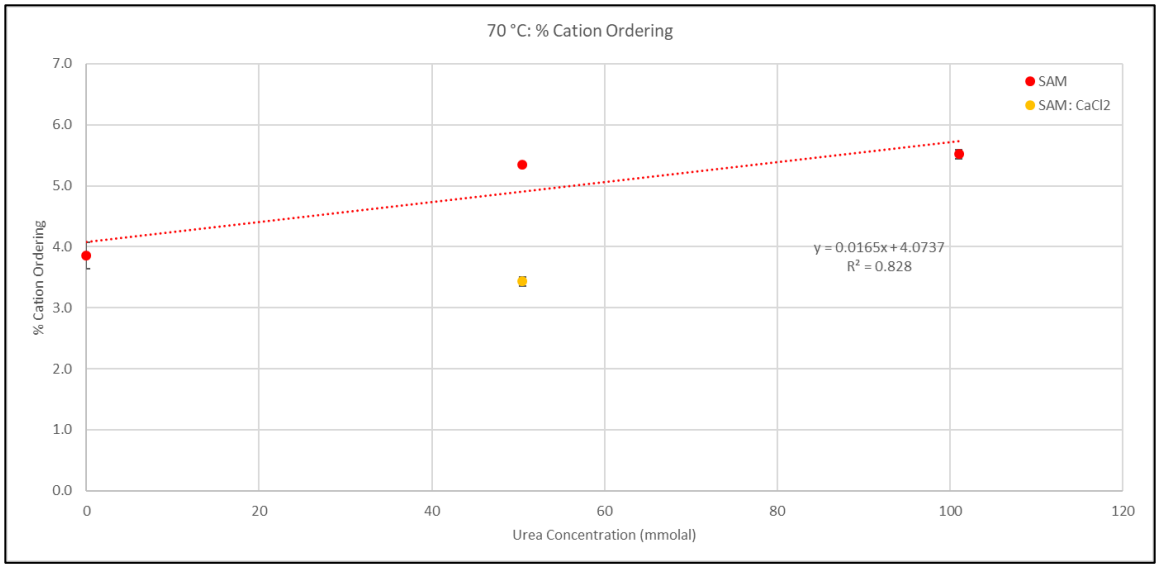

Figure 2.A3. Comparison of average % cation ordering for solid method precipitates with increasing urea concentration at 70 °C. Value is also displayed for $CaCl_2$ replacement precipitates.

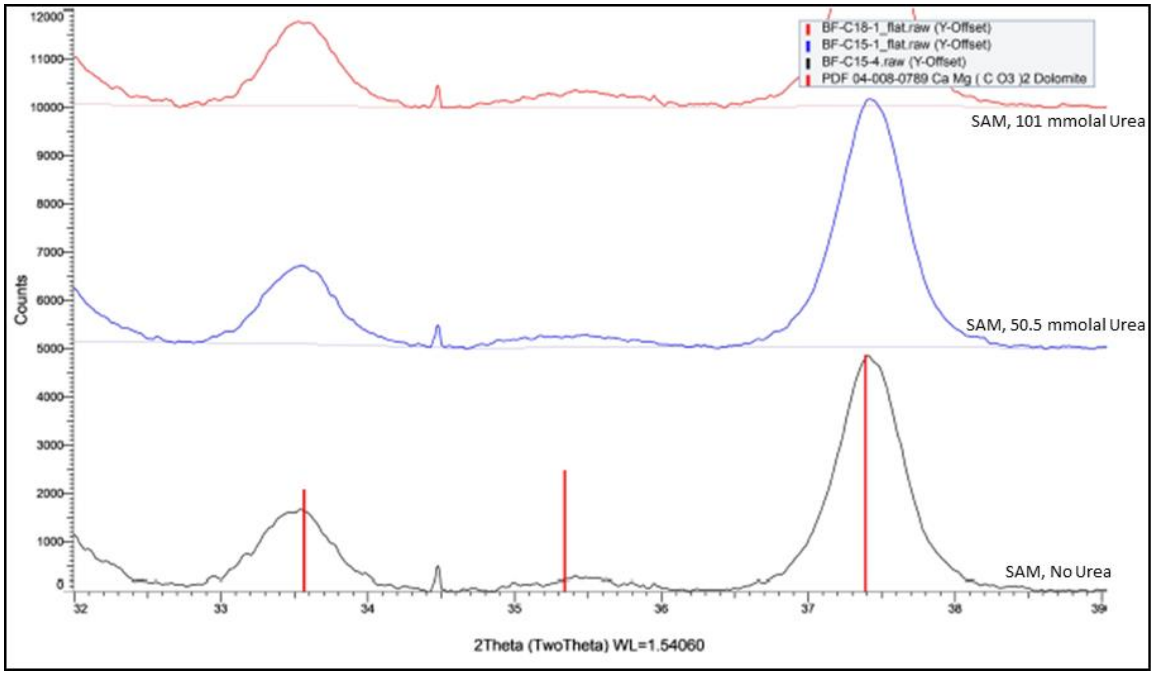

Figure 2.A4. XRD patterns displaying 015 peak for dolomite formed under varying conditions at 70 °C. From bottom to top: solid addition method (SAM) and no urea (black), SAM and 50.5 mmolal urea (blue), and SAM and 101 mmolal urea (red). Notice the increasing intensity of the 015 peak with increasing urea concentration (increasing cation ordering).

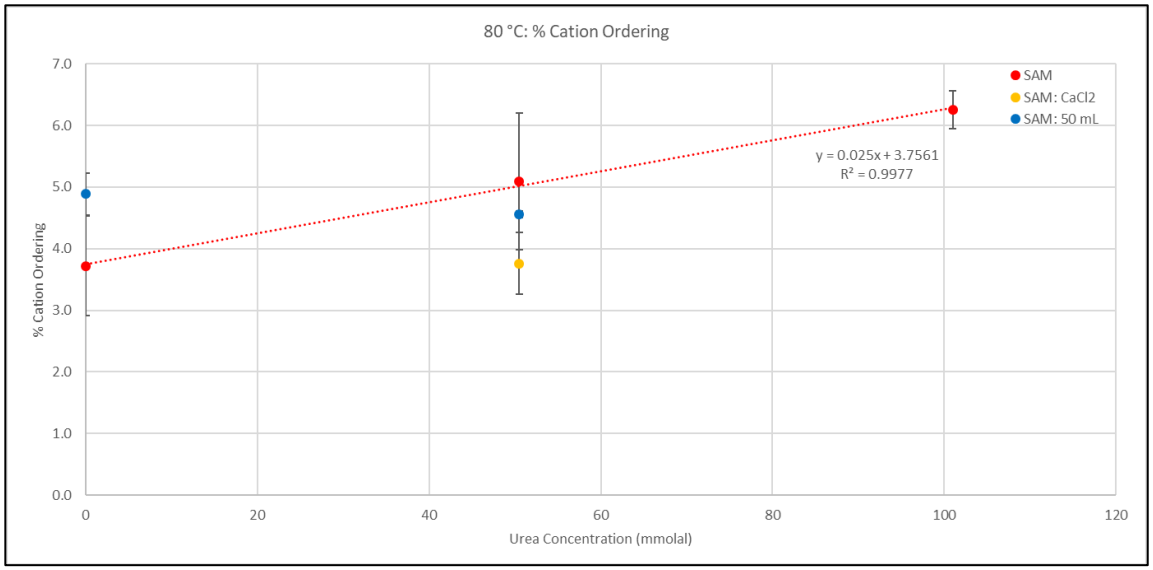

Figure 2.A5. Comparison of average % cation ordering for solid method precipitates with increasing urea concentration at 80 °C. Values are displayed for precipitates grown in 50 mL bottles and for $CaCl_2$ replacement precipitates as well.

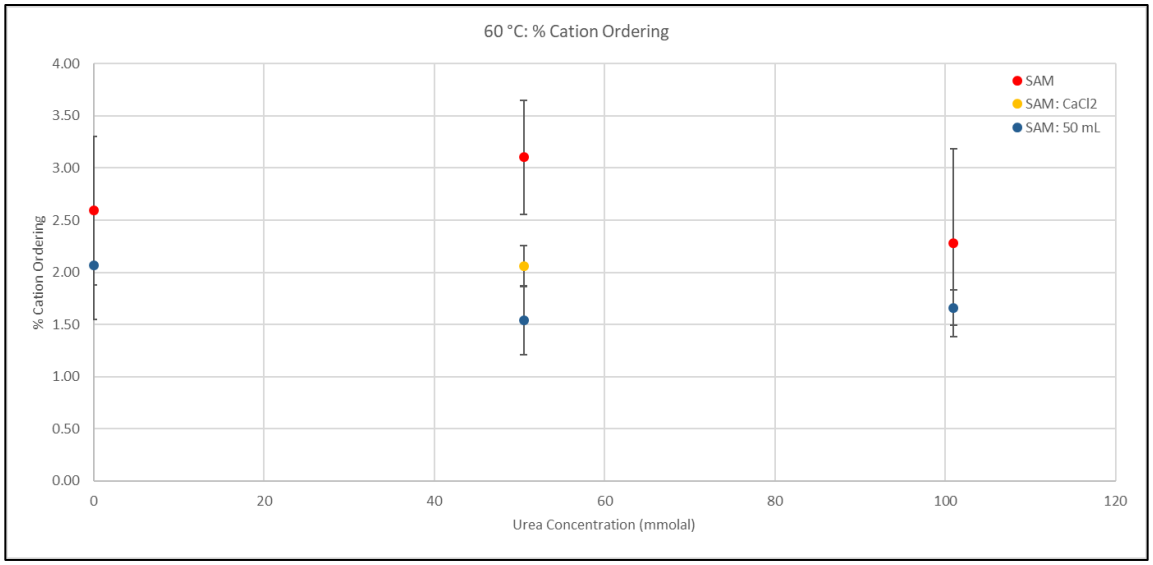

Figure 2.A6. Comparison of average % cation ordering for solid method precipitates with increasing urea concentration at 60 °C. Values are displayed for precipitates grown in 50 mL bottles and for $CaCl_2$ replacement precipitates as well.

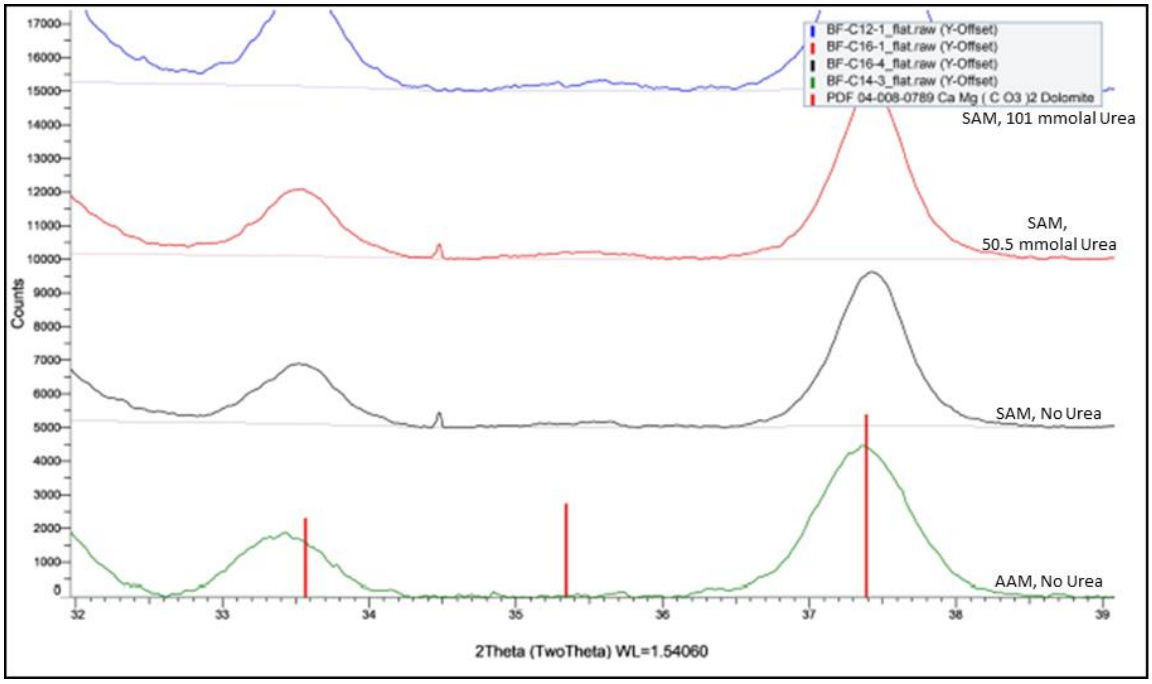

Figure 2.A7. XRD patterns displaying 015 peak for protodolomite and dolomite formed under varying conditions at 60 °C. From bottom to top: aqueous addition method (AAM) and no urea (green), solid addition method (SAM) and no urea (black), SAM and 50.5 mmolal urea (red), and SAM and 101 mmolal urea (blue). At 60 °C, protodolomite was formed when using the AAM (green) and dolomite was formed when using the SAM (black, red and blue). Furthermore, the 015 peak increased in intensity with increasing urea concentration.

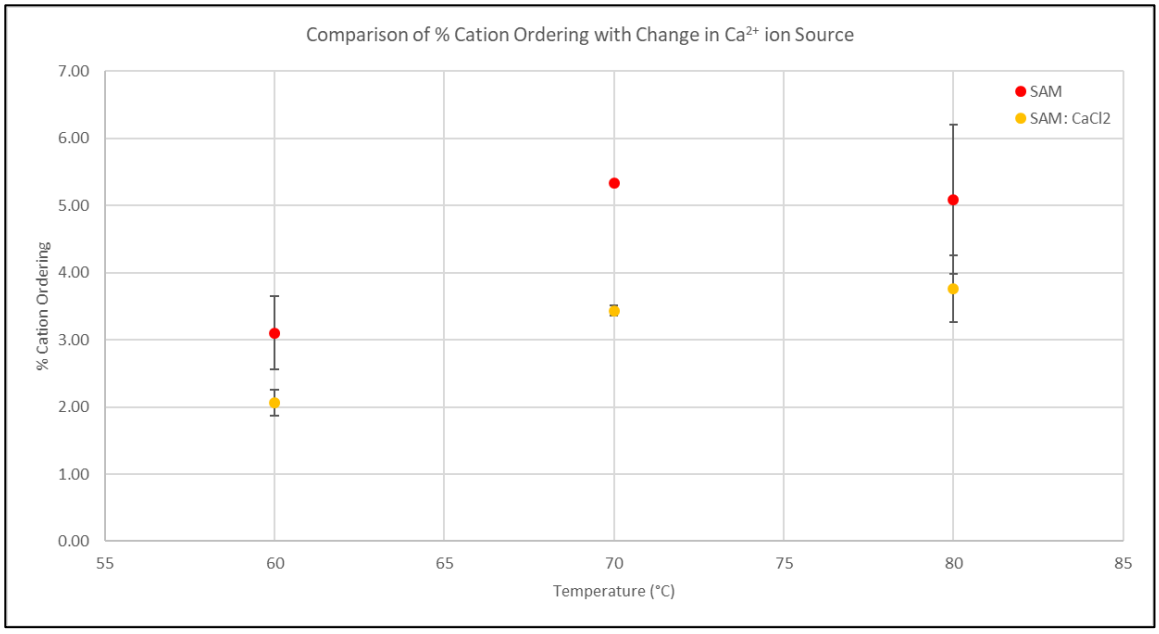

Figure 2.A8. Comparison of % cation ordering when using the typical $Ca(NO_3)_2$ as the Ca^{2+} ion source and using $CaCl_2$ as the Ca^{2+} ion source.

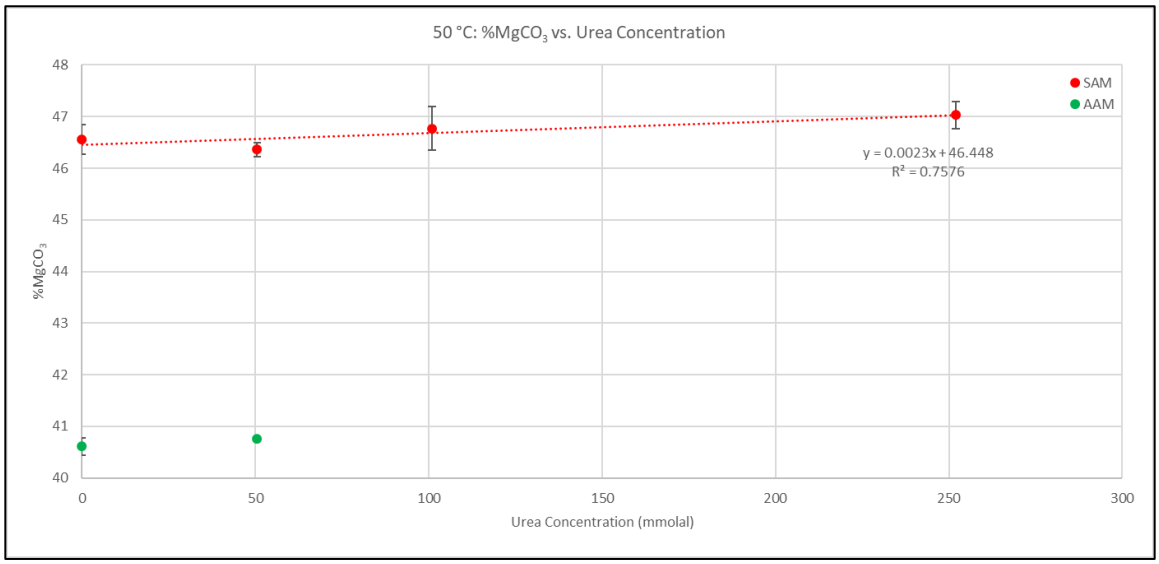

Figure 2.A9. Comparison of $\%MgCO_3$ from solid addition method precipitates (SAM) with aqueous addition method (AAM) precipitates, with increasing urea concentration and at 50 °C.

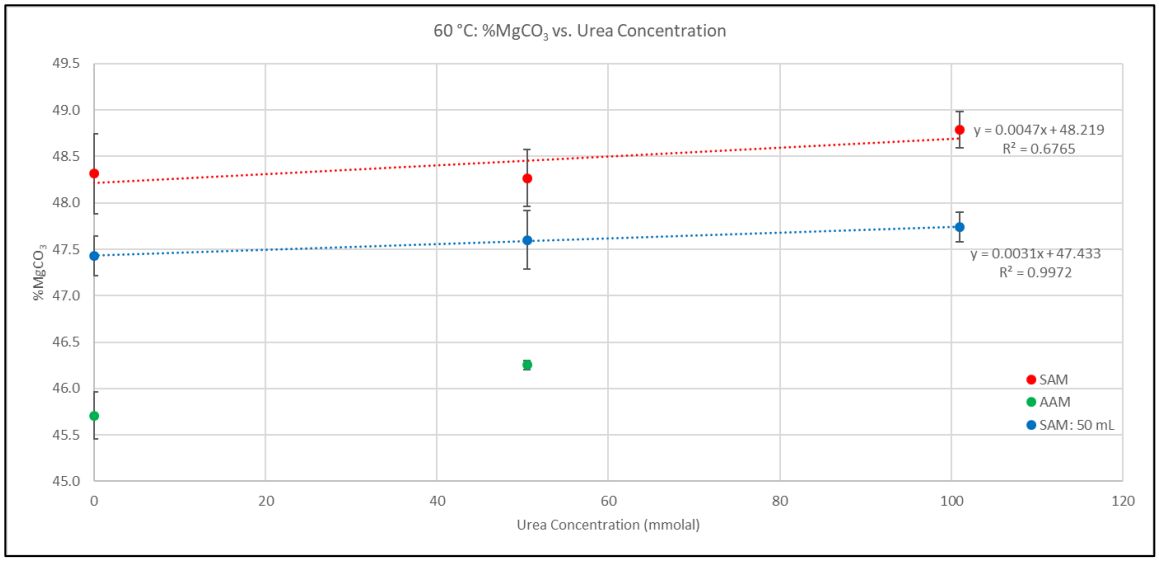

Figure 2.A10. Comparison of $\%MgCO_3$ from precipitates formed at all experimental conditions tested in this study, with increasing urea concentration and at 60 °C.

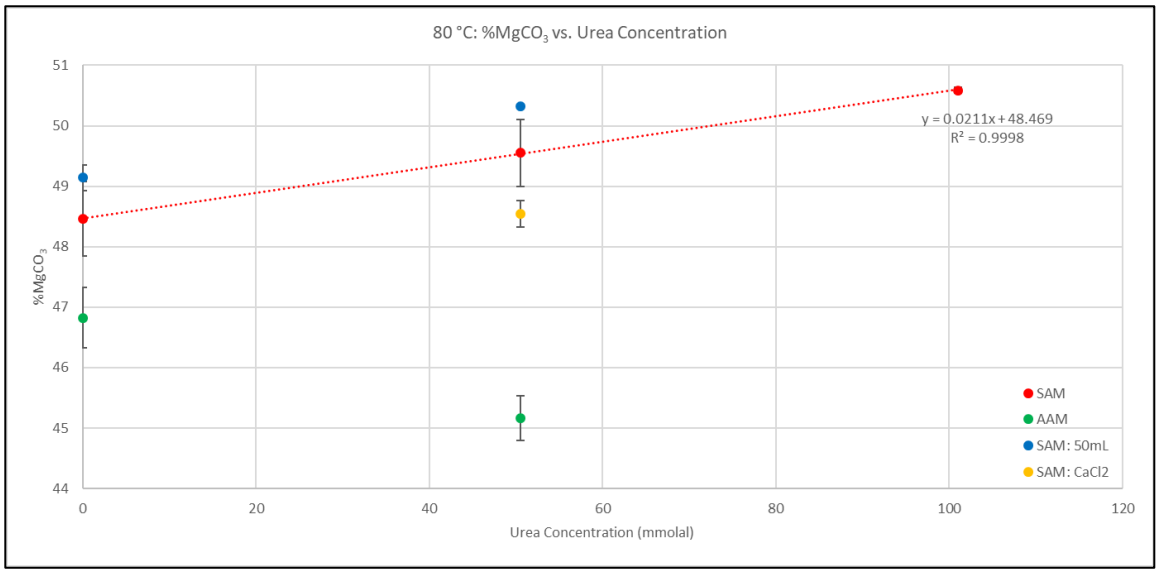

Figure 2.A11. Comparison of $\%MgCO_3$ from precipitates formed at all experimental conditions tested in this study, with increasing urea concentration and at 80 °C.

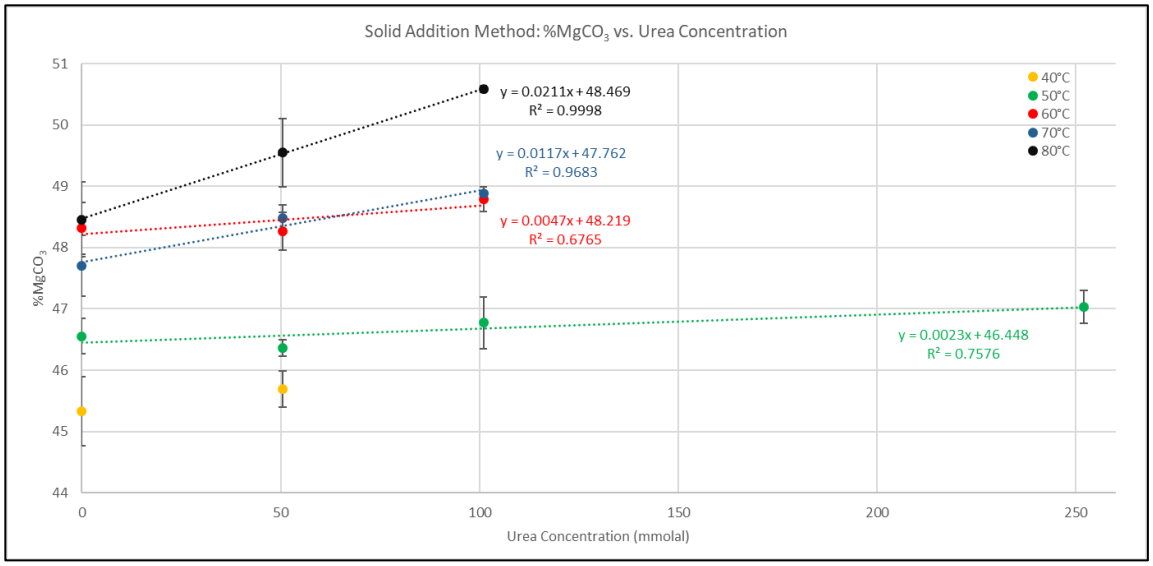

Figure 2.A12. Comparison of the influence of urea concentration on $\%MgCO_3$ for precipitates formed using the solid addition method at 40, 50, 60, 70, and 80 °C.

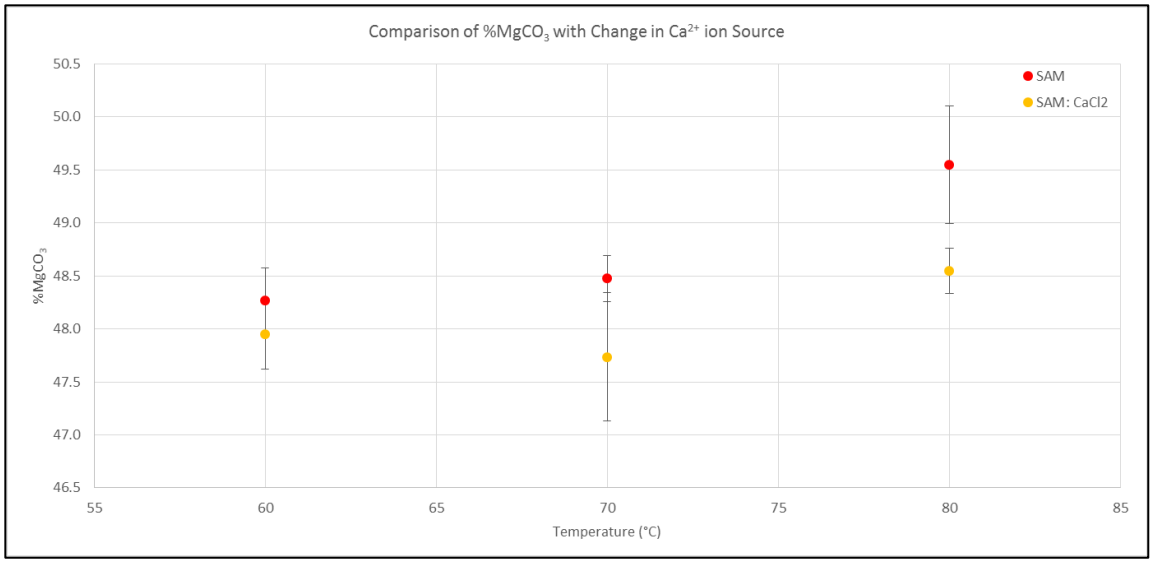

Figure 2.A13. Comparison of $\%MgCO_3$ when using the typical $Ca(NO_3)_2$ as the Ca^{2+} ion source and using $CaCl_2$ as the Ca^{2+} ion source.

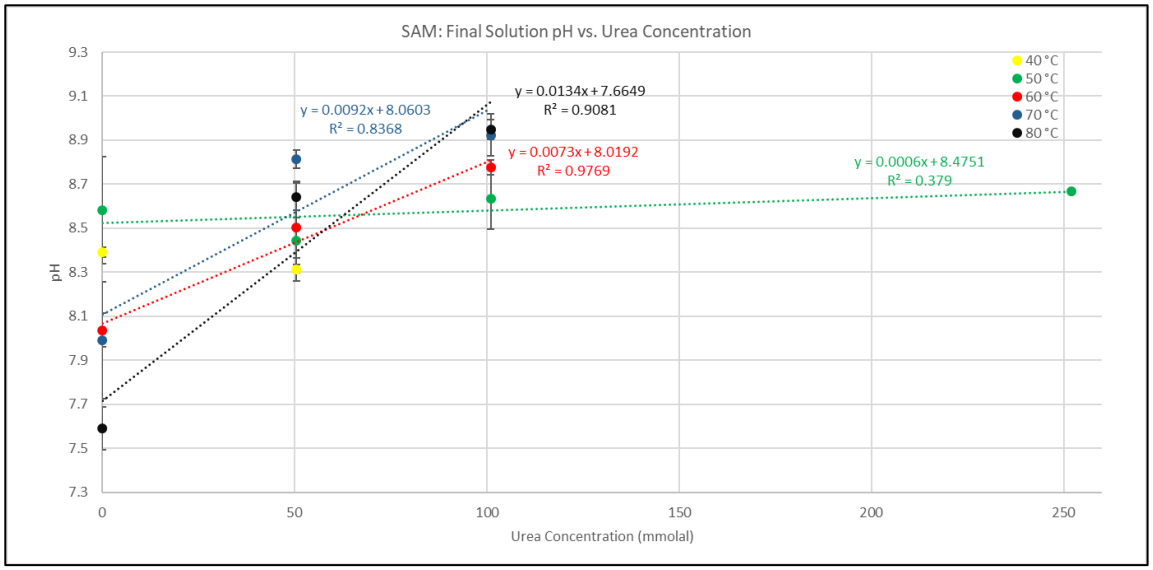

Figure 2.A14. Comparison of the final solution pH for solid addition method precipitates with increasing urea concentration at 40, 50, 60, 70, and 80 °C.

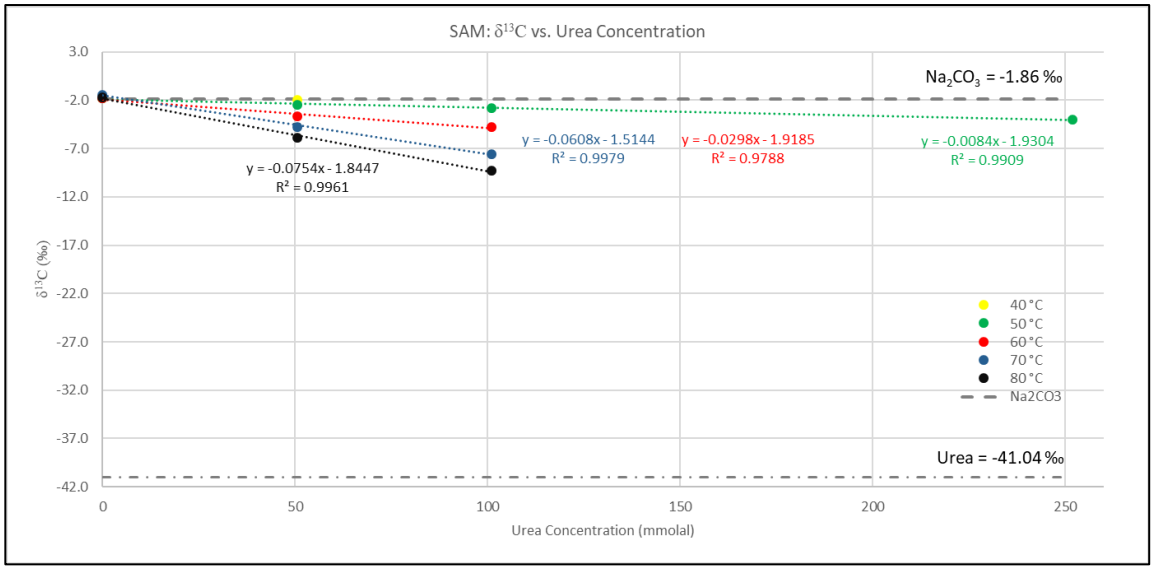

Figure 2.A15. Relation of urea concentration with $\delta^{13}C$ of solid addition method precipitates at 40, 50, 60, 70, and 80 °C.

Table 2.A1. Experimental conditions for parent solutions prepared in this study. All solutions contain 256 mmolal $MgSO_4$, 483 mmolal Na_2CO_3, and 238 mmolal $Ca(NO_3)_2$, with the exception of 238 mmolal $CaCl_2$ replacing $Ca(NO_3)_2$ (indicated in condition column).

Sample I.D	Condition	Temperature (°C)	Preparation Method	Bottle Volume (mL)	Growth Period (Days)	Urea (mmolal)	XRD %$MgCO_3$	EDS %$MgCO_3$	% Cation Ordering	pH	$\delta^{13}C$ (‰)	Product Mineralogy
BF-3-1	No U	40	SAM	250	57	0	45.9[c]		N/A	8.40	-1.83	P
BF-3-2	No U	40	SAM	250	36	0	44.8[c]		N/A	8.43	-1.74	P
BF-3-3	U	40	SAM	250	57	50.5	46.1[c]		N/A	8.53	-1.90	P
BF-3-4	U	40	SAM	250	36	50.5	45.8[c]		N/A	8.54	-2.04	P
BF-4-1	U	40	SAM	250	42	50.5	45.3[c]		N/A	8.36	-2.01	P
BF-4-2	U	40	SAM	250	42	50.5	45.6[c]		N/A	8.47	-2.01	P
BF-11-3	AAM	40	AAM	250	42	0	46.2[a]		N/A	8.34	N/A	H,A
BF-11-4	AAM	40	AAM	250	42	0	46.7[a]		N/A	8.46	N/A	H,A
BF-11-1	AAM+U	40	AAM	250	42	50.5	49.3[a]		N/A	8.28	N/A	H,A,M
BF-11-2	AAM+U	40	AAM	250	42	50.5	48.6[a]		N/A	8.23	N/A	H,A,M
BF-22-3	No U	50	SAM	250	42	0	46.7[b]		N/A	8.86	-1.87	P
BF-22-4	No U	50	SAM	250	42	0	46.2[b]	48.6[d]	N/A	8.46	-1.80	P
BF-25-1	No U	50	SAM	250	42	0	46.8[b]		N/A	8.28	-1.82	P
BF-22-1	U	50	SAM	250	42	50.5	46.3[b]		N/A	8.54	-2.33	P,A
BF-22-2	U	50	SAM	250	42	50.5	46.6[b]		N/A	8.29	-2.57	P
BF-25-2	U	50	SAM	250	42	50.5	46.3[b]		N/A	8.35	-2.43	P
BF-23-1	2X U	50	SAM	250	42	101	46.6[b]		N/A	8.47	-2.96	P
BF-23-2	2X U	50	SAM	250	42	101	47.3[b]		N/A	8.51	-2.96	P
BF-25-3	2X U	50	SAM	250	42	101	46.4[b]		N/A	8.78	-2.59	P
BF-23-3	5X U	50	SAM	250	42	252	47.1[b]		1.92	8.63	-4.09	D
BF-23-4	5X U	50	SAM	250	42	252	47.3[b]	49.3[d]	1.18	8.66	-3.93	D
BF-25-4	5X U	50	SAM	250	42	252	46.7[b]		2.59	8.57	-4.02	D
BF-24-1	AAM	50	AAM	250	42	0	40.8[b]	40.6[d]	N/A	7.32	N/A	H
BF-24-2	AAM	50	AAM	250	42	0	40.4[b]		N/A	7.34	N/A	H
BF-24-3	AAM+U	50	AAM	250	42	50.5	40.8[b]		N/A	7.41	N/A	H
BF-24-4	AAM+U	50	AAM	250	42	50.5	40.8[b]		N/A	7.42	N/A	H
BF-9-4	No U	60	SAM	250	42	0	47.6[b]	51.9	2.45	8.02	-1.83	D
BF-16-3	No U	60	SAM	250	42	0	48.5[a]		3.55	7.91	-1.82	D
BF-16-4	No U	60	SAM	250	42	0	48.3[a]		2.54	7.92	-1.72	D
BF-20-2	No U	60	SAM	250	42	0	48.8[b]		1.82	8.09	-1.78	D
BF-9-1	U	60	SAM	250	42	50.5	47.8[b]		2.34	8.39	-3.74	D
BF-16-1	U	60	SAM	250	42	50.5	48.3[a]		3.89	8.30	-3.77	D
BF-16-2	U	60	SAM	250	42	50.5	48.6[a]		3.06	8.32	-3.64	D
BF-20-1	U	60	SAM	250	42	50.5	48.4[b]		3.13	8.81	-3.58	D
BF-12-1	2X U	60	SAM	250	42	101	49.1[a]	54.0[d]	3.41	8.68	-4.79	D
BF-12-2	2X U	60	SAM	250	42	101	48.7[b]	50.7[d]	2.23	8.77	-4.71	D
BF-20-3	2X U	60	SAM	250	42	101	48.6[b]		1.21	8.73	-4.90	D
BF-14-3	AAM	60	AAM	250	42	0	46.0[a]		N/A	7.49	N/A	P
BF-14-4	AAM	60	AAM	250	42	0	45.5[a]	46.1[d]	N/A	7.84	N/A	P
BF-14-1	AAM+U	60	AAM	250	42	50.5	46.2[a]		N/A	8.25	N/A	P
BF-14-2	AAM+U	60	AAM	250	42	50.5	46.3[a]		N/A	8.49	N/A	P
BF-12-3	$CaCl_2$+U	60	SAM	250	42	50.5	48.3[a]		1.87	8.88	-3.38	D
BF-12-4	$CaCl_2$+U	60	SAM	250	42	50.5	47.6[a]		2.26	8.57	-3.76	D
BF-17-1	50mL	60	SAM	50	42	0	47.4[a]		2.79	7.74	-1.81	D
BF-17-2	50mL	60	SAM	50	42	0	47.7[a]		1.57	7.73	-1.75	D
BF-21-1	50 mL	60	SAM	50	42	0	47.2[b]		1.85	7.96	-1.73	D
BF-17-3	50mL+U	60	SAM	50	42	50.5	47.9[a]		1.63	8.66	-3.39	D
BF-17-4	50mL+U	60	SAM	50	42	50.5	47.7[a]		1.09	8.78	-3.12	D
BF-21-2	50 mL+U	60	SAM	50	42	50.5	47.2[b]		1.89	8.14	-3.91	D
BF-21-3	50mL+2X U	60	SAM	50	42	101	47.9[b]		1.83	8.81	-4.85	D
BF-21-4	50mL+2X U	60	SAM	50	42	101	47.6[b]		1.49	8.66	-4.96	D

D = dolomite; P = protodolomite; H = high magnesium calcite; A = aragonite; M = magnesium adipate glycinate

[a]: Bruker SMART6000 (CuKα); [b]: Bruker D8 Discover (CuKα); [c]: Bruker D8 Discover (CoKα); [d]: SEM Corrected

Sample I.D	Condition	Temperature (°C)	Preparation Method	Bottle Volume (mL)	Growth Period (Days)	Urea (mmol)	XRD %$MgCO_3$	EDS %$MgCO_3$	% Cation Ordering	pH	$\delta^{13}C$ (‰)	Product Mineralogy
BF-15-3	No U	70	SAM	250	42	0	47.2[a]		4.07[a]	8.21	-1.33	D
BF-15-4	No U	70	SAM	250	42	0	48.2[a]		3.64[a]	7.67	-1.54	D
BF-15-1	U	70	SAM	250	42	50.5	48.7[a]		5.33[a]	8.72	-5.04	D
BF-15-2	U	70	SAM	250	42	50.5	48.3[a]		5.35[a]	8.81	-4.46	D
BF-18-1	2X U	70	SAM	250	42	101	48.9[a]		5.44[a]	8.78	-7.74	D
BF-18-2	2X U	70	SAM	250	42	101	48.9[a]		5.60[a]	8.97	-7.42	D
BF-18-3	CaCl2+U	70	SAM	250	42	50.5	47.1[a]		3.51[a]	8.69	-4.01	D
BF-18-4	CaCl2+U	70	SAM	250	42	50.5	48.3[a]		3.36[a]	8.43	-5.12	D
BF-1-1	No U	80	SAM	250	33	0	49.1[c]	52.1[d]	4.29[c]	7.56	-1.83	D
BF-1-2	No U	80	SAM	250	33	0	47.6[c]		2.52[c]	7.53	-1.79	D
BF-28-1	No U	80	SAM	250	38	0	48.1[b]		3.47[b]	7.67	-1.46	D
BF-28-2	No U	80	SAM	250	38	0	49.0[b]		4.60[b]	7.40	-1.74	D
BF-1-3	U	80	SAM	250	33	50.5	49.7[c]		4.26[c]	8.60	-5.89	D
BF-1-4	U	80	SAM	250	33	50.5	50.1[c]		6.66[c]	8.67	-5.91	D
BF-6-1	U	80	SAM	250	41	50.5	48.8[c]		4.35[c]	8.51	-5.98	D
BF-6-2	U	80	SAM	250	41	50.5	48.3[c]		5.37[c]	8.53	-5.95	D
BF-6-5	2X U	80	SAM	250	41	101	50.5[a]	53.6	6.56[a]	8.85	-9.28	D
BF-6-6	2X U	80	SAM	250	41	101	50.6[b]		5.94[b]	8.94	-9.36	D
BF-7-3	AAM	80	AAM	250	41	0	47.3[a]	42.2[d]	N/A	6.91	-1.60	P,A
BF-7-4	AAM	80	AAM	250	41	0	46.3[a]		N/A	6.98	-1.52	P,A
BF-7-1	AAM+U	80	AAM	250	41	50.5	45.5[a]		N/A	8.06	-4.70	D,A
BF-7-2	AAM+U	80	AAM	250	41	50.5	44.8[a]		N/A	8.28	-4.36	D.A
BF-6-3	CaCl2+U	80	SAM	250	41	50.5	48.3[b]		4.26[c]	8.44	-5.91	D
BF-6-4	CaCl2+U	80	SAM	250	41	50.5	48.8[b]		3.26[c]	8.54	-5.94	D
BF-13-1	50mL	80	SAM	50	43	0	49.4[a]		5.23[a]	7.41	-1.64	D
BF-13-2	50mL	80	SAM	50	43	0	48.9[a]		4.55[a]	7.63	-1.76	D
BF-13-3	50mL+U	80	SAM	50	43	50.5	50.3[b]		4.51[b]	8.61	-5.76	D
BF-13-4	50mL+U	80	SAM	50	43	50.5	50.3[a]		4.61[a]	8.65	-5.67	D

D = dolomite; P = protodolomite; H = high magnesium calcite; A = aragonite; M = magnesium adipate glycinate

[a]: Bruker SMART6000 (CuKα); [b]: Bruker D8 Discover (CuKα); [c]: Bruker D8 Discover (CoKα); [d]: SEM Corrected

Table 2.A2. Average experimental solution and precipitate results.

Temperature (°C)	Condition	Urea (mmolal)	Avg. $\%MgCO_3$ (XRD)	$\%MgCO_3$ St. Dev	$\%MgCO_3$ (EDS)	Avg. Cation Ordering	Cation Ordering St. Dev	Avg. pH	Avg. pH St. Dev	Avg. $\delta^{13}C$	$\delta^{13}C$ St. Dev	Product Mineralogy
40	No U	0	45.3	0.57		N/A	N/A	8.34	0.02	-1.78	0.04	P
40	U	50.5	45.7	0.30		N/A	N/A	8.26	0.05	-1.99	0.05	P
40	AAM	0	46.4	0.24		N/A	N/A	8.41	0.05	N/A	N/A	H,A,M
40	AAM+U	50.5	48.9	0.36		N/A	N/A	8.53	0.01	N/A	N/A	H,A,M
50	No U	0	46.6	0.29	48.6	N/A	N/A	8.53	0.24	-1.83	-1.83	P
50	U	50.5	46.4	0.14		N/A	N/A	8.39	0.11	-2.44	-2.44	P
50	2X U	101	46.8	0.42		N/A	N/A	8.58	0.14	-2.84	-2.84	P
50	5X U	252	47.0	0.27	49.3	1.90	0.57	8.62	0.04	-4.01	-4.01	D
50	AAM	0	40.6	0.17		N/A	N/A	7.33	0.01	N/A	N/A	H
50	AAM+U	50.5	40.8	0.01	40.6	N/A	N/A	7.42	0.00	N/A	N/A	H
60	No U	0	48.3	0.43	51.9	2.60	0.71	7.97	0.08	-1.78	0.04	D
60	U	50.5	48.3	0.30		3.10	0.55	8.48	0.21	-3.66	0.08	D
60	2X U	101	48.8	0.20	52.4	2.30	0.90	8.73	0.03	-4.80	0.08	D
60	AAM	0.0	45.7	0.25	46.1	N/A	N/A	7.66	0.18	N/A	N/A	P
60	AAM+U	51	46.3	0.05		N/A	N/A	8.37	0.12	N/A	N/A	P
60	$CaCl_2$+U	50.5	48.0	0.33		2.06	0.20	8.73	0.15	-3.57	0.19	D
60	50mL	0	47.4	0.22		2.10	0.52	7.81	0.10	-1.76	0.04	D
60	50mL+U	50.5	47.6	0.31		1.50	0.33	8.53	0.28	-3.47	0.33	D
60	50mL+2X U	101	47.7	0.16		1.70	0.17	8.73	0.07	-4.90	0.05	D
70	No U	0	47.7	0.50		3.86	0.21	7.94	0.27	-1.43	0.11	D
70	U	50.5	48.5	0.22		5.34	0.01	8.76	0.04	-4.75	0.29	D
70	2X U	101	48.9	0.00		5.52	0.08	8.87	0.10	-7.58	0.16	D
70	$CaCl_2$+U	50.5	47.7	0.61		3.44	0.07	8.56	0.13	-4.56	0.55	D
80	No U	0	48.5	0.61	52.1	3.72	0.81	7.54	0.10	-1.71	0.14	D
80	U	51	49.5	0.55		5.09	1.11	8.59	0.06	-5.92	0.04	D
80	2X U	101	50.6	0.05	53.6	6.25	0.31	8.90	0.05	-9.32	0.04	D
80	AAM	0	46.8	0.50	42.2	N/A	N/A	6.95	0.03	-1.56	0.04	D,A
80	AAM+U	50.5	45.2	0.37		N/A	N/A	8.17	0.11	-4.53	0.17	D,A
80	$CaCl_2$+U	50.5	48.5	0.22		3.76	0.50	8.49	0.05	-5.92	0.02	D
80	50mL	0	49.1	0.21		4.89	0.34	7.52	0.11	-1.70	0.06	D
80	50mL+U	51	50.3	0.00		4.56	0.05	8.63	0.02	-5.71	0.04	D

D = dolomite; P = protodolomite; H = high magnesium calcite; A = aragonite; M = magnesium adipate glycinate

Table 2.A3. Comparison of $\%MgCO_3$ values calculated for identical samples analyzed by the Bruker SMART6000 and Bruker D8 with CuKα radiation. Notably, the average difference between instruments varied with temperature. Therefore, 60 °C samples analyzed by the Bruker D8 with CuKα were corrected with a value of +1.235 and 80 °C samples analyzed by the same instrument were corrected with a value of +2.316. Due to the inability to apply a similar method for samples formed at 50 °C and analyzed by the Bruker D8 with CuKα radiation, these samples were corrected with the smaller +1.235 value for greater consistency between samples.

Sample I.D	Temperature (°C)	Condition	Bruker SMART6000 (CuKα)	Bruker D8 (CuKα)	Difference
BF-16-3	60	No U	48.523	47.580	0.943
BF-12-1	60	2X U	49.068	47.950	1.118
BF-16-1	60	U	48.323	46.811	1.512
BF-17-3	60	50mL+U	47.909	45.579	2.331
BF-16-4	60	No U	48.304	47.842	0.462
BF-16-4 (2)	60	No U	48.304	47.257	1.047
				Avg. Difference	**1.235**
BF-6-5	80	2X U	50.536	47.740	2.796
BF-13-1	80	50 mL	49.355	47.124	2.232
BF-13-4	80	50 mL+U	50.325	48.405	1.920
				Avg. Difference	**2.316**

References

Arvidson, R., & Mackenzie, S. (1997). Tentative kinetic model for dolomite precipitation rate and its application to dolomite distribution. Aquatic Geochemistry, 2(3), 273-298.

Arvidson, R., & Mackenzie, F. (1999). The dolomite problem: Control of precipitation kinetics by temperature and saturation state. American Journal of Science, 299(4), 257-288.

Compton J. S. and Siever R. (1984). Stratigraphy and dolostone occurrence in the Miocene Monterey Formation, Santa Maria Basin area, California. In Dolomites of the Monterey Formation and Other Organic-Rich Units (Eds. R. R. Garrison, M. Kastner and D. H. Zenger). Society for Sedimentary Geology, Tulsa, OK, 141-154.

Deelman J. C. (1999). Low-temperature nucleation of magnesite and dolomite. Neues Jahrbuch Fur Mineralogie-Monatshefte, 7, 289-302.

Goetz, A. J., Griesshaber, E., Abel, R., Fehr, T., Ruthensteiner, B., & Schmahl, W. W. (2014). Tailored order: The mesocrystalline nature of sea urchin teeth. Acta biomaterialia, 10(9), 3885-3898.

Graf, D.L. and Goldsmith, J.R. (1956). Some hydrothermal syntheses of dolomite and protodolomite. J. Geol., 64, 173-186.

Gregg, J.M. and Shelton, K.L. (1990) Dolomitization and dolomite neomorphism in the back reef facies of the Bonneterre and Davis Formations (Cambrian), southeastern Missouri. J. Sed. Petrol., 60, 549-562.

Gregg, J., Bish, D., Kaczmarek, S., & Machel, H. (2015). Mineralogy, nucleation and growth of dolomite in the laboratory and sedimentary environment: A review. Sedimentology, 62(6), 1749-1769.

Horita, J. (2014). Oxygen and carbon isotope fractionation in the system dolomite–water–CO_2 to elevated temperatures. Geochimica et Cosmochimica Acta, 129, 111-124.

Kaczmarek, S., & Sibley, D. (2007). A Comparison of Nanometer-Scale Growth and Dissolution Features on Natural and Synthetic Dolomite Crystals: Implications for the Origin of Dolomite. Journal of Sedimentary Research, 77(5), 424-432.

Kaczmarek, & Sibley. (2011). On the evolution of dolomite stoichiometry and cation order during high-temperature synthesis experiments: An alternative model for the geochemical evolution of natural dolomites. Sedimentary Geology, 240(1), 30-40.

Kaczmarek, & Thornton. (2017). The effect of temperature on stoichiometry, cation ordering, and reaction rate in high-temperature dolomitization experiments. Chemical Geology, 468, 32-41.

Kelleher, I. J., & Redfern, S. A. (2002). Hydrous calcium magnesium carbonate, a possible precursor to the formation of sedimentary dolomite. Molecular simulation, 28(6-7), 557-572.

Kemp A. (1990). Sedimentary fabrics and variation in lamination style in Peru continental margin upwelling sediments. Proc. ODP, Sci. Results 112, 43–58.

Krause, S., Liebetrau, V., Gorb, S., Sánchez-Román, M., McKenzie, J. A., & Treude, T. (2012). Microbial nucleation of Mg-rich dolomite in exopolymeric substances under anoxic modern seawater salinity: New insight into an old enigma. Geology, 40(7), 587-590.

Land, L. (1998). Failure to Precipitate Dolomite at 25 °C from Dilute Solution Despite 1000-Fold Oversaturation after32 Years. Aquatic Geochemistry, 4(3), 361-368.

Lippmann, F. (1973). Sedimentary Carbonate Minerals, Rocks, and Inorganic Materials. Monograph Series of Theoretical and Experimental Studies Vol. 4 Springer-Verlag, Berlin (228 p).

Mansfield, C. F. (1980). A urolith of biogenic dolomite-another clue in the dolomite mystery. Geochimica et Cosmochimica Acta, 44(6), 829-839.

Morrow, D.W. & Rickets, B.D. (1988) Experimental investigation of sulfate inhibition of dolomite and its mineral analogues. In: Sedimentology and Geochemistry of Dolostones (Eds. V. Shukla and P.A. Baker), SEPM Spec. Publ., 43, 25–38.

Oomori, T., & Kitano, Y. (1987). Synthesis of protodolomite from sea water containing dioxane. Geochemical Journal, 21(2), 59-65.

Petrash, Bialik, Bontognali, Vasconcelos, Roberts, Mckenzie, & Konhauser. (2017). Microbially catalyzed dolomite formation: From near-surface to burial. Earth-Science Reviews, 171, 558-582.

Sánchez-Román, M., Vasconcelos, C., Schmid, T., Dittrich, M., McKenzie, J. A., Zenobi, R., & Rivadeneyra, M. A. (2008). Aerobic microbial dolomite at the nanometer scale: Implications for the geologic record. Geology, 36(11), 879-882.

Schmidt, M., Xeflide, S., Botz, R., & Mann, S. (2005). Oxygen isotope fractionation during synthesis of CaMg-carbonate and implications for sedimentary dolomite formation. Geochimica et Cosmochimica Acta, 69(19), 4665-4674.

Vasconcelos, C., McKenzie, J. A., Bernasconi, S., Grujic, D., & Tiens, A. J. (1995). Microbial mediation as a possible mechanism for natural dolomite formation at low temperatures. Nature, 377(6546), 220.

Wang, R. Z., Addadi, L., & Weiner, S. (1997). Design strategies of sea urchin teeth: structure, composition and micromechanical relations to function. Philosophical Transactions of the Royal Society of London B: Biological Sciences, 352(1352), 469-480.

Warren, J. (2000). Dolomite: Occurrence, evolution and economically important associations. Earth Science Reviews, 52(1), 1-81.

Zhang, Fangfu, Xu, Huifang, Konishi, Hiromi, Kemp, Joshua M., Roden, Eric E., & Shen, Zhizhang. (2012a). Dissolved sulfide-catalyzed precipitation of disordered dolomite: Implications for the formation mechanism of sedimentary dolomite. Geochimica et Cosmochimica Acta, 97, 148-165.

Zhang, F., Xu, H., Konishi, H., Shelobolina, E., & Roden, E. (2012b). Polysaccharide-catalyzed nucleation and growth of disordered dolomite: A potential precursor of sedimentary dolomite. The American Mineralogist, 97(4), 556-567.

CHAPTER 3: OXYGEN ISOTOPE EFFECTS IN THE DOLOMITE-WATER SYSTEM

CHAPTER 3: OXYGEN ISOTOPE EFFECTS IN THE DOLOMITE-WATER SYSTEM

Abstract

The current understanding of the oxygen isotopic exchange between dolomite and water has been inhibited by the failure to synthesize dolomite at low temperatures similar to those that the mineral forms in nature. As a result, current established oxygen isotope dolomite-water thermometer calibrations rely on extrapolation from high temperature synthesis experiments (> 100 °C) or analyses of synthesized protodolomite, showing no evidence of cation ordering, at more ambient temperatures (25 - 80 °C). Presented here is the first known investigation into the oxygen isotopic exchange between synthesized dolomite and water between 50 and 80 °C. Results from this study show that oxygen isotope compositions in (proto)dolomite may be influenced by potential kinetic isotope effects, relating to rapid precipitation and thus the failure for attainment of oxygen isotope equilibrium between dolomite and water. A correction for possible kinetic isotope effects is attempted by exclusion of isotopically heterogeneous (proto)dolomite in constructing the dolomite-water oxygen isotope fractionation curve. The resulting corrected curve is expressed as: $1000\ln\alpha_{\text{dolomite-water}} = 2.12(\pm0.10) \cdot (10^6/T^2) + 6.02(\pm0.90)$. The results presented in this study serve as a foundation for future isotopic analyses of dolomite and will aid in the understanding of isotopic exchange between dolomite and water in nature.

Section 3.1: Introduction

The failure to synthesize dolomite at temperatures below 100 °C has impeded the ability to establish an accurate oxygen isotope dolomite-water paleothermometer calibration at low temperatures that dolomite typically forms in nature (Vasconcelos et

al., 2005; Schmidt et al., 2005; Horita, 2014). Instead, previous studies have developed calibrations for the oxygen isotopic exchange between either HMC or protodolomite and water at low temperatures (e.g., Vasconcelos et al., 2005; Schmidt et al., 2005), or dolomite-water calibrations at high temperature (> 100 °C) (e.g., Northrop and Clayton, 1966; Katz and Matthews, 1977). Therefore, an accurate measurement to refine the low temperature oxygen isotope fractionation between dolomite and water is necessary to advance our understanding of paleoclimate throughout geologic history.

Due to the uncertainties surrounding dolomite formation at low temperatures, attempts to develop the oxygen isotope dolomite-water paleothermometer have been justifiably scarce. Northrop and Clayton (1966) used dolomite synthesized between 300 - 510 °C to develop the equation:

$$1000\ln\alpha_{\text{dolomite-water}} = 3.20 \cdot (10^6/T^2) - 2.00 \quad \text{(Equation 3.1)}$$

where T is temperature in Kelvins. This equation has also been extrapolated to lower temperatures for use in comparison with isotopic analyses from protodolomite synthesized below 100 °C, as well as dolomite formed in natural environments (Northrop and Clayton, 1966; Horita, 2014).

Following the claim by Vasconcelos et al. (1995) that dolomite synthesis was possible at near-ambient temperatures by sulfate-reducing bacteria, Vasconcelos et al. (2005) used similar methods to seemingly synthesize dolomite between 25 - 45 °C and measured an oxygen isotope dolomite-water calibration for low temperatures. However, as previously discussed in Section 1.3.4, the samples failed to display evidence of cation

ordering (Gregg et al., 2015; Petrash et al. 2017). Therefore, the study provided a calibration for protodolomite-water and did not produce a significant advancement for the understanding of oxygen isotopic exchange between dolomite and water.

Fritz and Smith (1970) synthesized, by the direct precipitation methods of Siegel (1961), a combination of protodolomite and aragonite at 40 - 70 °C. The authors attempted to obtain more accurate protodolomite $\delta^{18}O$ values by extrapolating the data to resemble pure protodolomite using a least squares refinement. Fritz and Smith (1970) proposed that natural secondary dolomite, forming by recrystallization of protodolomite, possesses $1000\ln\alpha_{dolomite\text{-}water}$ values dependent on the initially precipitated protodolomite. Similarly, Schmidt et al. (2005) synthesized mixtures of amorphous carbonates and hydrous protodolomite between 40 - 80 °C by following the synthesis methods of Kelleher and Redfern (2002). The authors recognized that dolomite formation was not achieved, but instead aimed to provide a further understanding for oxygen isotope exchange between protodolomite and water. By performing a step-wise acid reaction method, Schmidt et al. (2005) attempted to remove amorphous carbonate from the samples to retain pure protodolomite, which was analyzed for their oxygen isotopic composition to better reflect dolomite oxygen isotope compositions.

More recently, Horita (2014) provided a more thorough investigation into the oxygen isotope dolomite-water calibration over the temperature range 80 - 350 °C. The single 80 °C sample was identified as protodolomite, synthesized by direct precipitation using similar methods as Kelleher and Redfern (2002), but samples formed by dolomitization between 100 - 350 °C were claimed to be dolomite with evidence of cation

ordering (Horita, 2014). The author included the 80 °C protodolomite sample in the paleothermometer calculation because it produced a "virtually identical" equation to the one obtained using solely dolomite samples (Horita, 2014). The equation developed by Horita (2014) is the following:

$$1000\ln\alpha_{dolomite\text{-}water} = 3.14(\pm0.022) \cdot (10^6/T^2) - 3.14(\pm0.11) \quad \text{(Equation 3.2)}$$

This calibration by Horita (2014) likely represents the most accurate equation available to date for oxygen isotope studies of natural dolomite, which generally form between 25 - 50 °C.

This study aims to provide further understanding of the oxygen isotope exchange between dolomite and water at 50 - 80 °C. Investigated are possible kinetic isotope effects that may be associated with dolomite synthesized by the newly developed solid addition method. Furthermore, after attempting to correct for potential kinetic isotope effects, a new dolomite-water oxygen isotope fractionation calibration is proposed, by isotopic analysis of dolomite samples synthesized between 50 - 80 °C. This study provides foundational insight into oxygen isotope exchange between dolomite and water at low temperatures, and with further investigation into resolving kinetic isotope effects that may cause deviation from true equilibrium fractionation, the potential for the value of dolomite in paleoclimate research will become greatly enhanced.

Section 3.2: Detailed Materials and Methods

Section 3.2.1: Carbonate Synthesis

Ca-Mg carbonates were synthesized according to the detailed procedures outlined in Appendix 2.1.1, and the solution compositions and tested experimental conditions described in this study are outlined in Table 2.A1. However, it should be noted that all aqueous addition method parent solutions were prepared using a thermally and isotopically equilibrated Na_2CO_3 stock solution. Specifically, three separate 966 mmolal Na_2CO_3 stock solutions were prepared in 500 mL capped bottles. Each stock solution was placed in a convection drying oven (± 1 °C) at the corresponding temperature to which the subsequent prepared parent solutions would be placed (50, 60 and 80 °C). Each solution was allotted a minimum 14 day period to allow thermal and isotopic equilibration between the dissolved inorganic carbon (DIC) species and water (Beck et al., 2005). Following the allotted equilibration period, aqueous addition method solutions were subsequently prepared by adding 25 mL of the 966 mmolal Na_2CO_3 stock solution to 25 mL of solution containing the remaining specified chemical reagents (e.g., $MgSO_4$, $Ca(NO_3)_2$, urea) (Table 2.A1). Following this addition, the solutions were shaken vigorously for 2 minutes and immediately placed in a convection oven at the specified temperature (Table 2.A1). It was not possible for parent solutions prepared by the solid addition method to have the DIC species isotopically equilibrated with parent water prior to solution preparation, due to the nature of the method.

Section 3.2.2: Oxygen Isotope Analyses for Carbonates

Prior to oxygen isotope analyses of the carbonates synthesized in this study, the necessary reaction time between dolomite and phosphoric acid was investigated. A single synthesized dolomite sample (BF-12-1) and an internal dolomite laboratory standard (BF-Dol; natural sample) were used to establish the minimum time required for efficient (proto)dolomite conversion to CO_2 by acid reaction. The bulk proportion of BF-Dol used for this study was previous ground and sieved through a p200 mesh. Both BF-Dol and BF-12-1 were further ground using a mortar and pestle prior to weighing. Proportions of the BF-Dol and BF-12-1 were prepared for isotopic analyses as described below. Time periods of 24, 48, 72, 96, 120, 144, and 168 hours were allotted for reaction between dolomite and 105 % phosphoric acid. Samples of BF-12-1 and BF-Dol for each respective reaction time were run in quadruplicate. Results of the dolomite time series test demonstrated that a 48 hour reaction period was sufficient for phosphoric acid reaction with dolomite (discussed in Section 3.3.1).

Carbonate samples were prepared for isotopic analysis by thorough grounding using a mortar and pestle. Small proportions of the ground powder (~ 150 µm) were then weighed on a Mettler Toledo analytical balance and deposited into glass tubes (Exetainer). The $\delta^{18}O$ values for carbonate samples ($\delta^{18}O_{carb}$) were determined using a Thermo Finnigan Delta plus XP isotope mass spectrometer equipped with a Gas Bench II headspace autosampler. This instrument has a typical analytical $\delta^{18}O$ precision of ± 0.08 ‰. The tubes were first flushed and filled with He gas, then 5 drops of 105 % phosphoric acid were injected into each tube to react with sample powders and produce CO_2. All

samples were reacted within a heated block to a constant 25 ± 0.1 °C. All carbonates were given a minimum two day period for acid reaction. Once the allotted reaction time elapsed, $\delta^{18}O_{carb}$ were measured. All (proto)dolomite samples were analyzed in minimum duplicate.

The collected $\delta^{18}O_{carb}$ values were corrected following the recommended methods outlined by Kim et al. (2015). All $\delta^{18}O_{carb}$ values were calibrated to standard values for NBS 18 (7.19 ‰) and NBS 19 (28.65 ‰) on the SMOW scale. The acid fractionation factor of 1.0110 was used to correct for the remaining (proto)dolomite oxygen produced after phosphoric acid reaction (Sharma and Clayton, 1965). It should be noted that two Na_2CO_3 sources were used to prepare parent solutions in this study, due to the exhaustion of the initial Na_2CO_3 used. The two Na_2CO_3 sources possessed slightly different $\delta^{18}O_{carb}$ values (Na_2CO_3-A = 12.05 ‰; Na_2CO_3-B = 11.22 ‰); however, a comparison of final $\delta^{18}O_{carb}$ values of precipitates formed from either Na_2CO_3 source indicated that the change in Na_2CO_3 did not produce a noticeable effect on $\delta^{18}O_{carb}$ values.

Section 3.2.3: Oxygen Isotope Analyses for Solutions

Initial deionized water, used to prepare each experimental solution, and final solution samples were collected following the allotted growth period and stored in a cooling refrigerator at ~ 5 °C. Aliquots of parent solutions following initial reagent mixing were unable to be collected, due to the rapid reaction rate of solutions prepared in this study. Therefore, the oxygen isotope composition of the solution samples collected following (proto)dolomite growth ($\delta^{18}O_{final}$) were used to compare with the initial deionized water ($\delta^{18}O_{intial}$) to identify solutions affected by evaporation or other isotope

effects. All deionized water used for this study was stored in a single carboy, with aliquots removed prior to solution preparation, to ensure consistency of the water $\delta^{18}O_{intial}$ value.

The classic CO_2-water equilibration method was employed to measure the $\delta^{18}O_{intial}$ and $\delta^{18}O_{final}$ values. Solutions were measured using a Thermo Finnigan Delta plus XP isotope mass spectrometer equipped with a Gas Bench II headspace autosampler. Empty tubes were first flushed and filled with a 0.2 % CO_2 and 99.8 % He gas mixture, then injected with 0.2 mL of each solution. Each solution was measured in duplicate. Following all solution injections, a minimum 24 hour equilibration time was given at 25 ± 0.1 °C, and then the CO_2 was subsequently measured. All solution samples were calibrated to the internal laboratory standards MRSI-STD-W1 (-0.58 ‰) and MRSI-STD-W2 (-28.08 ‰), which were previously calibrated on the SMOW scale.

Section 3.3: Detailed Results and Discussion

Section 3.3.1: Time Series of $\delta^{18}O_{Dolomite}$

Results of the time series indicated that the maximum proportion of synthesized dolomite (BF-12-1) converted to CO_2 (i.e. total yield) was obtained after ~ 48 hours (Figure 3.1) (Table. 3.1). Total yields measured for longer reaction times, up to 168 hours, were identical within the expected systematic and analytical error. It is likely that the maximum total yield measured (96.78 %) indicates that the total dolomite sample was reacted with phosphoric acid, with consideration of errors associated with mass weighing, sample transfer to glass tubes, and calculations producing the deviation from 100 % total yield. In contrast to the synthetic dolomite, the total yield for the natural dolomite (BF-

Dol) standard steadily increased over the reaction period tested and reached a maximum total yield of 88.13 % after 168 hours. Since only laboratory synthesized dolomite, with a similar crystal size and properties as BF-12-1, were analyzed for oxygen isotopic compositions in this study, further tests to determine the time required to obtain near total yield were not implemented. In addition, oxygen isotope compositions were found to be independent of yield for both BF-Dol and BF-12-1 (discussed below). Therefore, a minimum 2-day acid reaction time was allotted for the analyses of all (proto)dolomite in this study.

The $\delta^{18}O_{carb}$ values of BF-Dol and BF-12-1 were found to be independent of reaction time (Figure 3.2). However, it was found that four BF-12-1 samples possessed significantly lower $\delta^{18}O_{carb}$ values (difference of 0.96 - 1.8 ‰) than the average value. Similarly, two BF-Dol samples had noticeable lower $\delta^{18}O_{carb}$ values (difference of 0.90 and 2.66 ‰) than the average value. As displayed by Figure 3.3, these values are not related to the yield of CO_2 produced. Therefore, the outlying values, depleted in ^{18}O, may represent isotopically heterogeneous crystals formed during dolomite growth. A similar trend was evident for certain samples synthesized at temperatures $\leq$ 60 °C in this study, which is presented and discussed in the following sections.

Section 3.3.2: Effect of Evaporation on Solution $\delta^{18}O$

The $1000\ln\alpha_{(proto)dolomite\text{-}water}$ values for all synthesized carbonates and associated parent solutions, collected in this study, are displayed in Supplementary Information Table S1. All carbonate samples were analyzed in minimum duplicate and the collected

$\delta^{18}O_{carb}$ are provided as individual and average values. Also outlined are $\delta^{18}O_{final}$ for all experimental solutions and the change in solution $\delta^{18}O$ ($\delta^{18}O_{final}$ - $\delta^{18}O_{initial}$).

Certain $\delta^{18}O_{final}$ values were found to deviate significantly from the $\delta^{18}O_{intial}$ value (-6.64 ‰) (Supplementary Table S1). Positive deviations likely resulted from evaporation, caused by the relatively high temperatures tested in this study and the large headspace within most experimental bottles (50 mL solution in 250 mL bottle). To account for evaporation effects, all $\delta^{18}O_{final}$ (and associated $\delta^{18}O_{carb}$) values which were $\geq$ +0.5 ‰ in relation to the $\delta^{18}O_{initial}$ value were excluded from further investigation and were not used in determination of experimental $1000\ln\alpha_{carbonate\text{-}water}$ values. Most solutions displaying evidence of evaporation were heated to 70 and 80 °C. Isotopic results for all remaining carbonates and parent solutions are provided in Table 3.2.

Section 3.3.3: Effect of Urea on Solution and Carbonate $\delta^{18}O$

In addition to $\delta^{18}O_{final}$ deviations from $\delta^{18}O_{intial}$ seemingly caused by evaporation, certain $\delta^{18}O_{final}$ values from 60, 70 and 80 °C were found to be more negative than the initial water value (Table 3.2). Comparison of the change in solution $\delta^{18}O$ ($\delta^{18}O_{final}$ - $\delta^{18}O_{initial}$) with urea concentration reveal that higher urea concentrations resulted in increasingly negative $\delta^{18}O_{final}$ values (Figure 3.4). Furthermore, the degree to which urea concentration influenced $\delta^{18}O_{final}$ was greater at higher temperatures, especially 70 and 80 °C. This observed effect is likely associated with the thermal hydrolysis of urea, which is more prominent as temperature increases, as shown by the relationship between (proto)dolomite $\delta^{13}C$ and urea concentration (Figure 2.8) (Section 2.4.2). The hydrolysis of urea in parent solutions produced CO_3^{2-} (Mansfield, 1980), following the reaction:

$$CH_4N_2O + H_2O = 2NH_3 + CO_2 \quad \text{(Equation 3.3)}$$

and the subsequent hydrolysis of CO_3^{2-} produced H_2CO_3 following the reaction:

$$CO_2 + H_2O = H_2CO_3 \quad \text{(Equation 3.4)}$$

where H_2CO_3 would likely dissociate to HCO_3^-, due to the pH range of solutions prepared in this study (6.91 – 8.97) (Beck et al., 2005; Kim et al., 2006). Urea hydrolysis in solutions heated to 60, 70, and 80 °C appear to have produced a sufficiently large proportion of DIC, possessing a $\delta^{18}O$ signature of the source urea, which effectively altered the $\delta^{18}O_{final}$ value. An analysis of $1000\ln\alpha_{(proto)dolomite\text{-}water}$ in relation to urea concentration shows that urea hydrolysis produced a notable increase in $1000\ln\alpha_{dolomite\text{-}water}$ for dolomite synthesized at 70 and 80 °C, whereas (proto)dolomite synthesized at 40 - 50 °C do not appear influenced by this effect (Figure 3.5). Therefore, to account for urea hydrolysis, only dolomite synthesized in the absence of urea at 60, 70, and 80 °C were used in construction of the dolomite-water oxygen isotope fractionation curve. Dolomite synthesized in 50 mL bottles displayed no discernable difference in $\delta^{18}O_{carb}$ to those synthesized in 250 mL bottles (Figure 3.6), and therefore dolomite formed in 50 mL bottles that contained no urea were used in constructing the dolomite-water fractionation curve.

Section 3.3.4: Effect of Preparation Method on Carbonate $\delta^{18}O$

Carbonates precipitated by the aqueous addition method possessed $1000\ln\alpha_{carbonate\text{-}water}$ values that were somewhat different from precipitates prepared by the solid addition method, but this difference varied with temperature (Figure 3.7). For example, HMC

precipitated by the aqueous addition method at 50 °C displayed $1000\ln\alpha_{carbonate\text{-}water}$ indistinguishable from (proto)dolomite formed by the solid addition method. In contrast, protodolomite formed at 60 °C by the aqueous addition method possessed slightly lower $1000\ln\alpha_{carbonate\text{-}water}$, values (~ 0.5 - 1 ‰). Finally, $1000\ln\alpha_{carbonate\text{-}water}$ values of precipitates formed by the aqueous addition method at 80 °C are notably lower than dolomite produced by the solid addition method (~ 1 ‰). A portion of the observed discrepancy between the preparation methods is likely attributed to the isotopic equilibration between DIC and water prior solution preparation for aqueous addition method experiments. It should also be noted that precipitates from the aqueous addition method at 80 °C were mixtures of (proto)dolomite and aragonite (Table 3.2), and therefore the aragonite would influence the collected $\delta^{18}O_{carb}$ value (e.g., Kim et al., 2007). Nevertheless, parent solutions prepared by the aqueous addition method did not produce dolomite at 50 or 60 °C and precipitates were not pure dolomite at 80 °C; therefore $1000\ln\alpha_{carbonate\text{-}water}$ values for precipitates by the aqueous addition method were not used in construction of the dolomite-water oxygen isotope fractionation curve.

Section 3.3.5: Effect of Non-Equilibrium Isotope Effects

The comparison of duplicate (or greater) analyses for individual carbonate samples displayed potential kinetic isotope effects. More specifically, significant variations were found between multiple analyses of the same synthesized carbonate (Table 3.2). Therefore, certain synthesized carbonates are likely not isotopically homogeneous. The apparent kinetic isotope effects were only found to occur for carbonates synthesized at 40 - 60 °C (Table 3.2). Similar isotopic heterogeneity was also

clear for sample BF-12-1 during the investigation the dolomite time series study (Figure 3.2).

The finding of isotopic heterogeneity likely indicates that isotopic equilibrium was not attained between certain growing carbonates and its associated solution, or that equilibration between the two phases was not established following carbonate formation. To investigate possible kinetic isotope effects that may produce the observed isotopic heterogeneity, the isotopic analyses for all solid addition method precipitates collected in this study were plotted against the temperature-dependent oxygen isotope fractionation curves for CO_3^{2-}-water and HCO_3^--water (Figure 3.7), established by Beck et al. (2005). This comparison shows that the respective lower $1000\ln\alpha_{(proto)dolomite\text{-}water}$ values from duplicate analyses of isotopically heterogeneous (proto)dolomites lie between the curves for CO_3^{2-}-water and HCO_3^--water. In contrast, the greater $1000\ln\alpha_{(proto)dolomite\text{-}water}$ values more closely resemble the HCO_3^--water curve (Figure 3.7). Therefore, the lower $1000\ln\alpha_{(proto)dolomite\text{-}water}$ values more closely resemble the $\delta^{18}O$ signature of the source Na_2CO_3 (Na_2CO_3-A = 12.05 ‰; Na_2CO_3-B = 11.22 ‰) and these carbonate samples were likely only partially equilibrated with the solution during growth.

Considering that Na_2CO_3 and water were equilibrated prior to preparation of aqueous addition method solutions, precipitates rapidly forming from these solutions would closely resemble the CO_3^{2-} line if equilibrium was minimally attained (Figure 3.7). However, precipitates formed by the aqueous addition method lie much closer to the HCO_3^- line, indicating a progression toward isotopic equilibrium between these samples and water (Figure 3.7). As a result, the similarity of most $1000\ln\alpha_{(proto)dolomite\text{-}water}$ values

from precipitates formed by the solid addition method to precipitates formed by the aqueous addition method suggests that solid addition method precipitates have also progressed toward oxygen isotopic equilibrium with water. Furthermore, this provides additional evidence that carbonates with $1000\ln\alpha_{(proto)dolomite\text{-}water}$ values (from duplicate analyses) that deviate significantly toward the CO_3^{2-} curve are only partially equilibrated. Therefore, the highest $1000\ln\alpha_{dolomite\text{-}water}$ values, or those that are furthest from the CO_3^{2-} curve, are likely closer to the true values for oxygen isotopic equilibrium for dolomite over this temperature range (50 - 80 °C).

The inability for attainment of isotopic equilibrium between certain (proto)dolomite samples and water in this study is likely caused by the rapid reaction and precipitation rates associated with the solid addition method. Rapid reaction rates may not have allowed sufficient time for equilibration between (proto)dolomite and water prior to mineral formation. Rapid precipitation would primarily affect the lowest temperatures tested, as equilibration between carbonates and solution is attained more slowly with decreasing temperature (Beck et al., 2005), which appears to occur here, as the deviations from the average $1000\ln\alpha_{(proto)dolomite\text{-}water}$ increase at each respective temperature increase with decreasing temperatures (Figure 3.7). A subsequent investigation into variation growth periods would be beneficial, providing insight into whether $1000\ln\alpha_{(proto)dolomite\text{-}water}$ values progress from the CO_3^{2-}-water fractionation curve to the HCO_3^{2-}-water curve with extended growth time. This test would indicate whether (proto)dolomite, especially at 40 - 60 °C, can establish equilibrium with water following initial formation.

Section 3.3.6: Temperature Dependence of Oxygen Isotope Fractionation between Dolomite and Water

The compilation of $1000\ln\alpha_{dolomite\text{-}water}$ values over the temperature range 50 - 80 °C are displayed in Figure 3.8 and the constructed curve demonstrates a strong linear trend in relation to temperature. The average $1000\ln\alpha_{dolomite\text{-}water}$ values used to construct the curve are outlined in Table 3.2. Only synthesized carbonates displaying evidence of cation ordering, and are therefore dolomite (Section 1.2.2), were used for constructing this curve (Table 3.2). Therefore, protodolomite synthesized at 40 °C was excluded from this construction of the curve. However, the attainment of oxygen isotope equilibrium between dolomite and water cannot be effectively proven for this study, especially due to the apparent isotopic heterogeneity of certain synthesized dolomite. For comparison, a curve constructed from average $1000\ln\alpha_{carbonate\text{-}water}$ values of protodolomite and HMC is displayed. It should be noted that, due to the combination of precipitates formed by the aqueous addition method and solid addition method to construct this curve, there is likely a high uncertainty for the validity of this curve for true oxygen isotope fractionation between protodolomite/HMC and water.

In an attempt to account for any potential kinetic isotope effects, and to construct a dolomite-water oxygen isotope fractionation curve that is closest to isotopic equilibrium, a second calibration was determined by excluding dolomite precipitates that were seemingly isotopically heterogeneous. With consideration of analytical error (±0.08), the rapid carbonate precipitation rate associated with the solid addition method and the relatively large precipitate yields collected from each experimental solution (~ 2.2

- 2.4 g), average $\delta^{18}O_{carb}$ values associated with a standard deviation (σ) $\geq$ 0.5 from duplicate (or greater) analyses were viewed as isotopically heterogeneous. These $\delta^{18}O_{carb}$ values were then excluded from determination of $1000\ln_{dolomite\text{-}water}$ over the temperature range 50 - 80 °C, and the resulting "Homogeneity Test Corrected" fractionation curve is displayed in Figure 3.9. This corrected curve has the form:

$$1000\ln\alpha_{dolomite\text{-}water} = 2.12(\pm0.10) \cdot (10^6/T^2) + 6.02(\pm0.90) \quad \text{(Equation 3.5)}$$

Notably, the Homogeneity Test Corrected dolomite-water fractionation curve displays a stronger linear trend with temperature (R^2 = 0.9954) in relation to the uncorrected $1000\ln\alpha_{dolomite\text{-}water}$ curve (R^2 = 0.9924) (Figure 3.9).

Section 3.3.7: Comparison of Dolomite-Water Fractionation Studies in Literature

Both dolomite-water oxygen isotope fractionation curves developed in this study have a distinctly lower slope than all previously established (proto)dolomite-water oxygen isotope fractionation curves (Figure 3.10). Displayed for comparison are: an extrapolation to slighter higher temperatures of the protodolomite curve from Vasconcelos et al. (2005) (25 - 45 °C); an extrapolation of Hortia (2014)'s dolomite-water curve, which analyzed dolomite formed through dolomitization (80 - 350 °C); and an extrapolation of the curve from Northrop and Clayton (1966), which synthesized dolomite at highly elevated temperatures (300 - 510 °C). Also included are the experimentally determined $1000\ln\alpha_{protodolomite\text{-}water}$ values obtained by Fritz and Smith (1970) and Schmidt et al. (2005) over the studied temperature range (50 - 80 °C). In addition, the theoretically obtained curves reported by Chacko and Deines (2008) for dolomite, magnesite ($MgCO_3$)

and calcite ($CaCO_3$) are displayed. As the Homogeneity Test Corrected dolomite-water fractionation curve developed from this study did not incorporate dolomite that were likely partially influenced by kinetic isotope effects, and are therefore isotopically heterogeneous, it is likely more representative of isotopic equilibrium between dolomite and water and is therefore used hereafter for comparison with previous literature.

The dolomite-water fractionation curve developed in this study intersects the extrapolated Horita (2014) curve at approximately 60 °C (Figure 3.10). Similarly, our curve is very similar to the $1000\ln\alpha_{protodolomite}$ value of the Vasconcelos et al. (2005) calibration at 50 °C. However, at 80 °C, our fractionation curve lies between the calibration from Northrop and Clayton (1966), and those from Horita (2014) and Vasconcelos et al. (2005). Unexpectedly, the curve developed here agrees well with oxygen isotope analyses of protodolomite by Fritz and Smith (1970) and Schmidt et al. (2005) at 80 °C. An explanation for this unusual trend, especially the significantly slower slope in relation to literature, is unclear. Potentially, the dolomite-water oxygen isotope fractionation curve determined in this study is more accurate at lower temperatures (50 – 60 °C) than many previous studies, due to the reliance of extrapolation by higher temperature studies (Northrop and Clayton, 1966; Horita, 2014) or analyses of protodolomite at similar low temperatures (25 - 45 °C) (Vasconcelos et al., 2005). Furthermore, the $1000\ln\alpha_{dolomite\text{-}water}$ values obtained from this study at 70 and 80 °C may be affected by isotopic deviations caused by evaporation, which may not have been entirely accounted for by the removal of precipitate data associated with a change in solution $\delta^{18}O > 0.5$. Evaporation is especially problematic due to the large headspace used

for most experimental solutions (50 mL solution in 250 mL bottle). It must also be considered that the potential kinetic isotope effects observed for precipitates from 50 and 60 °C produced lower $1000\ln\alpha_{dolomite\text{-}water}$ values, as isotopic equilibrium between dolomite and water may not have been attained. In these cases, certain dolomite crystals would retain the oxygen isotope signature resembling the source Na_2CO_3 (Na_2CO_3-A = 12.05 ‰; Na_2CO_3-B = 11.22 ‰), likely indicating that oxygen isotope equilibrium was not attained between these crystals and water, and therefore, the measured $\delta^{18}O_{carb}$ value would lie between the true dolomite $\delta^{18}O$ value and that of the Na_2CO_3.

Further investigations into dolomite synthesized below 100 °C through rapid precipitation, such as the solid addition method developed in this study, are required to effectively evaluate the isotopic exchange between dolomite and water. More specifically, potential alterations to a similar method that would permit oxygen isotope equilibrium between dolomite and water without significantly reducing the seemingly rapid reaction rates required to synthesize dolomite at low temperatures. Nevertheless, this study provides the first known evaluation of $1000\ln_{dolomite\text{-}water}$ values for synthesized dolomite below 100 °C and, therefore, the comparison of this curve with those developed by previous literature is potentially valuable for future studies to better evaluate isotopic exchange between dolomite and water.

Section 3.4: Conclusions

This study investigated the first known oxygen isotope exchange between dolomite and water at temperatures below 100 °C. Results indicate that potential kinetic isotope effects seemingly hinder accurate determination of equilibrium $1000\ln\alpha_{dolomite\text{-}water}$

values, as certain (proto)dolomite samples were found to be isotopically heterogeneous. These apparent kinetic isotope effects are limited to temperatures ≤ 60 °C and are likely caused by rapid carbonate precipitation, which may not permit isotopic equilibrium between (proto)dolomite and water. Evidence for kinetic isotope effects is evident by $1000\ln\alpha_{(proto)dolomite\text{-}water}$ values of isotopically heterogeneous (proto)dolomite with the established curves for $1000\ln\alpha_{HCO3\text{-}water}$ and $1000\ln\alpha_{CO3\text{-}water}$ curves, which reveal that certain $\delta^{18}O_{carb}$ values more closely resemble the source Na_2CO_3 (Na_2CO_3-A = 12.05 ‰; Na_2CO_3-B = 11.22 ‰).

By excluding $1000\alpha_{dolomite\text{-}water}$ values that display sufficient evidence of isotopic heterogeneity, a new dolomite-water oxygen isotope fractionation curve was developed:

$$1000\ln\alpha_{dolomite\text{-}water} = 2.12(\pm0.10) \cdot (10^6/T^2) + 6.02(\pm0.90) \quad \text{(Equation 3.6)}$$

Although this curve has a decidedly lower slope than previously established calibrations for dolomite that are extrapolated from higher temperatures, or solely utilized protodolomite at more ambient temperatures, the strong reproducibility of $1000\alpha_{dolomite\text{-}water}$ over the temperature range in this study (50 - 80 °C) is promising. However, further investigations into the influence of rapid dolomite precipitation, and the associated potential kinetic isotope effects, are required to effectively understand isotopic exchange between dolomite and water at near-Earth surface temperatures.

Figures and Tables

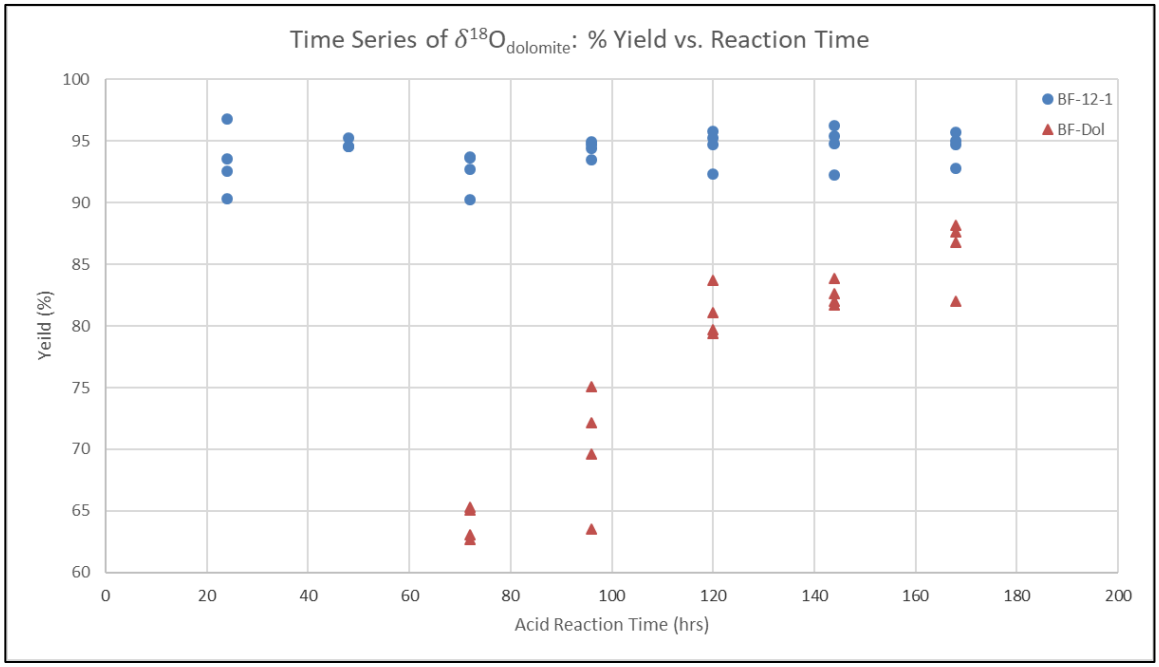

Figure 3.1. Relation of percent yield of CO_2 from dolomite following reaction with phosphoric acid. Displayed are data from our internal laboratory dolomite standard (BF-Dol), and synthesized dolomite (BF-12-1). Notice that the percent yield of BF-12-1 is indistinguishable following a 48 hr reaction period, whereas the acid reaction for BF-Dol is incomplete following a 168 hr reaction period.

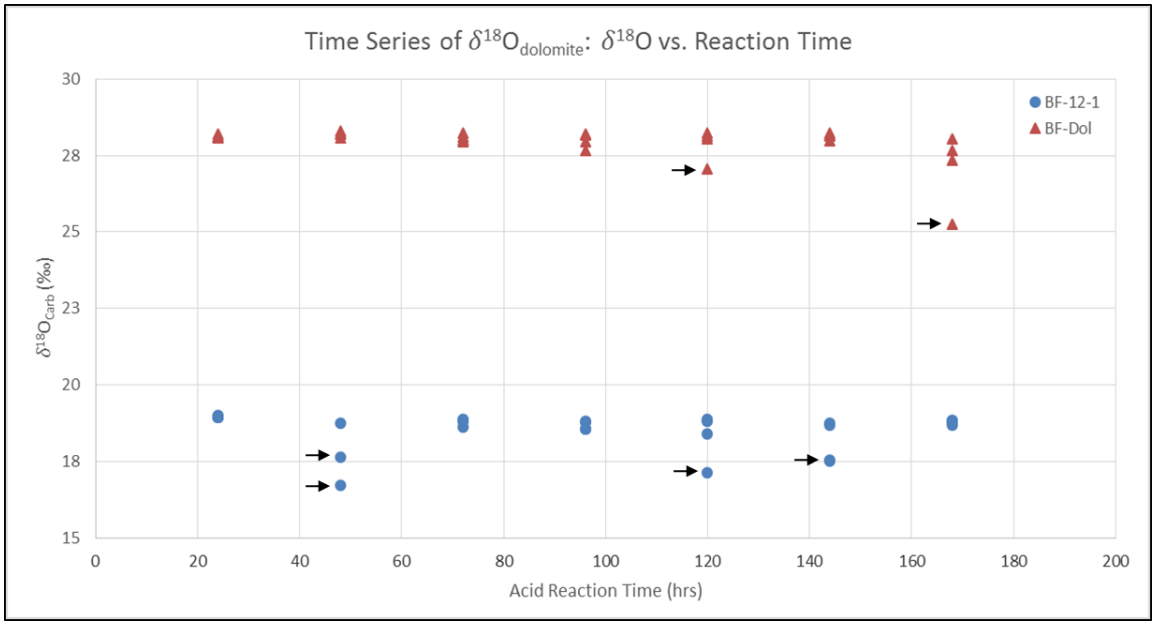

Figure 3.2. Comparison of the $\delta^{18}O_{carb}$ of BF-12-1 and BF-Dol with increasing reaction time with phosphoric acid. For both samples, there is no relationship between $\delta^{18}O_{carb}$ and acid reaction reaction. Arrows indicate $\delta^{18}O_{carb}$ values that deviate from the average value, which is likely the result of isotopic heterogeneity.

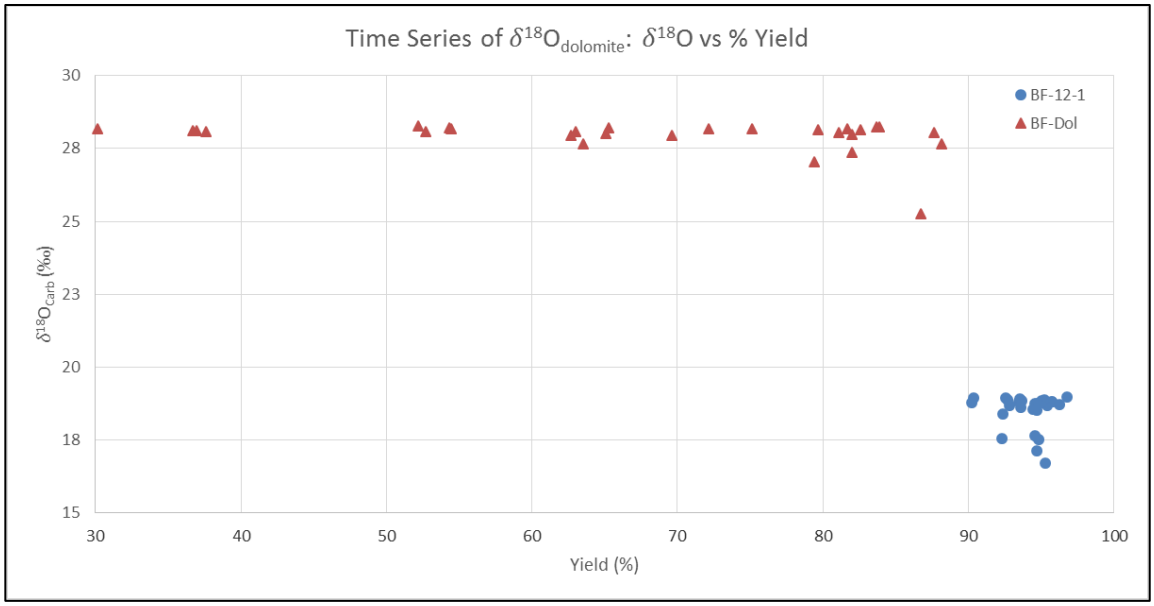

Figure 3.3. Comparison of $\delta^{18}O_{carb}$ with percent yield for BF-12-1 and BF-Dol. There appears to be no significant relationship between $\delta^{18}O_{carb}$ with percent yield.

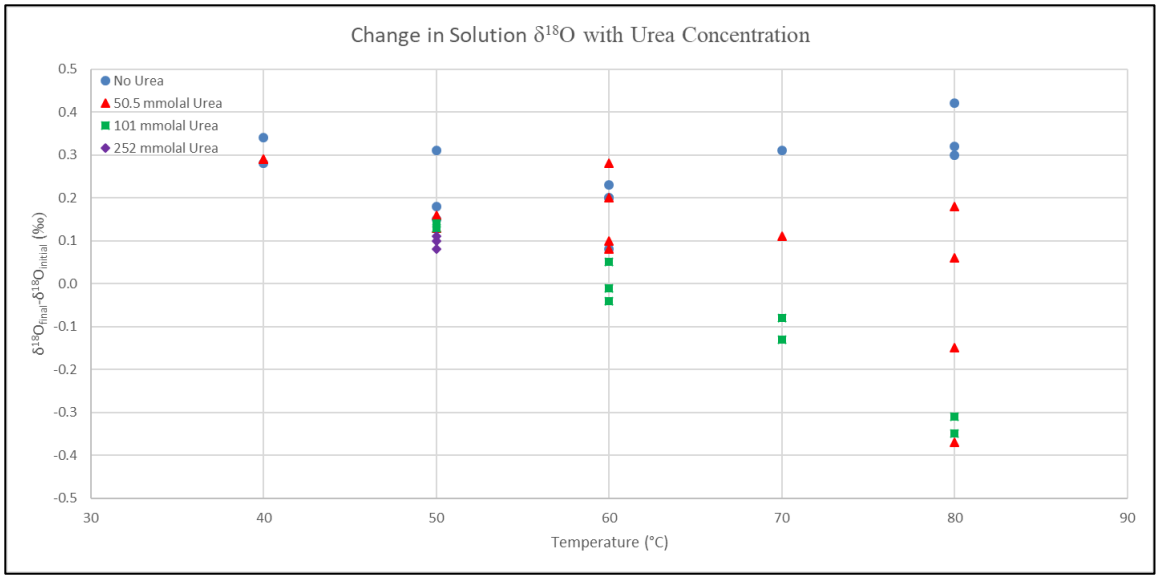

Figure 3.4. Change in solution $\delta^{18}O$ ($\delta^{18}O_{final}$ - $\delta^{18}O_{initial}$) with increasing urea concentration over the temperature range 40 - 80 °C. Notice that as urea concentration is increased, higher $\delta^{18}O_{final}$ values were recorded, resulting in solutions enriched in ^{18}O relative to the initial water used for parent solution preparation. Notably, the degree to which this effect influences $\delta^{18}O_{final}$ is greater as temperature increases.

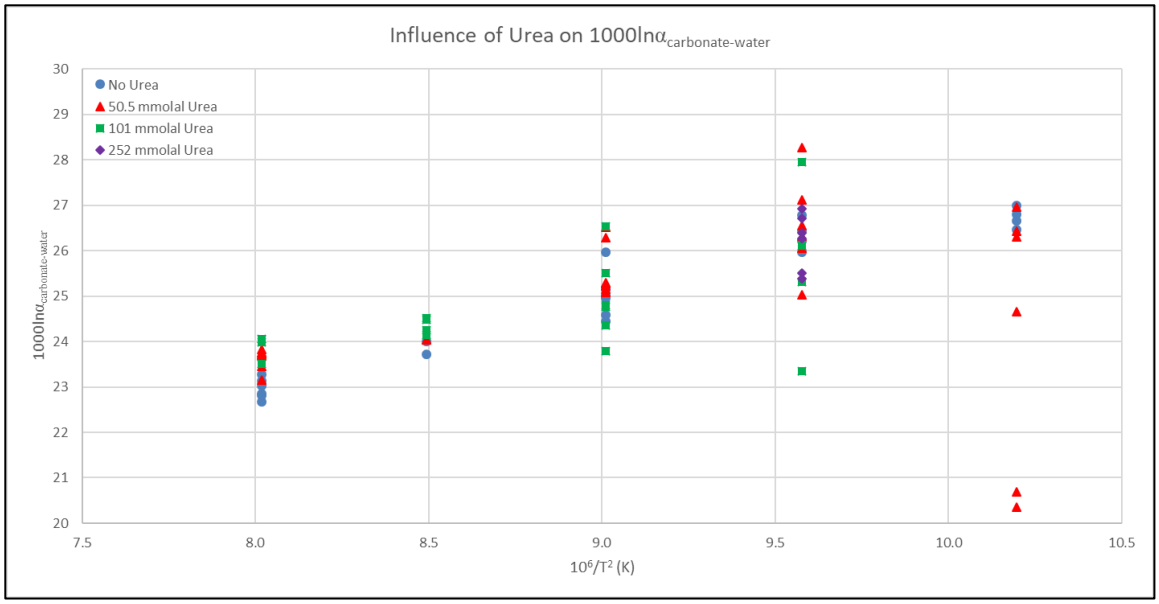

Figure 3.5. Comparison of $1000\ln\alpha_{(proto)dolomite\text{-}water}$ for precipitates formed by the solid addition method (duplicate analyses are plotted as separate values), with increasing urea concentration. Only precipitates formed in 250 mL bottles and with $Ca(NO_3)_2$ as the Ca^{2+} ion source are displayed. At 40 - 50 °C, there is no discernable difference in $1000\ln\alpha_{(proto)dolomite\text{-}water}$ between the conditions investigated in this study. However, at 70 and 80 °C, $1000\ln\alpha_{(proto)dolomite\text{-}water}$ values from parent solutions containing urea are notable higher than those with an absence of urea.

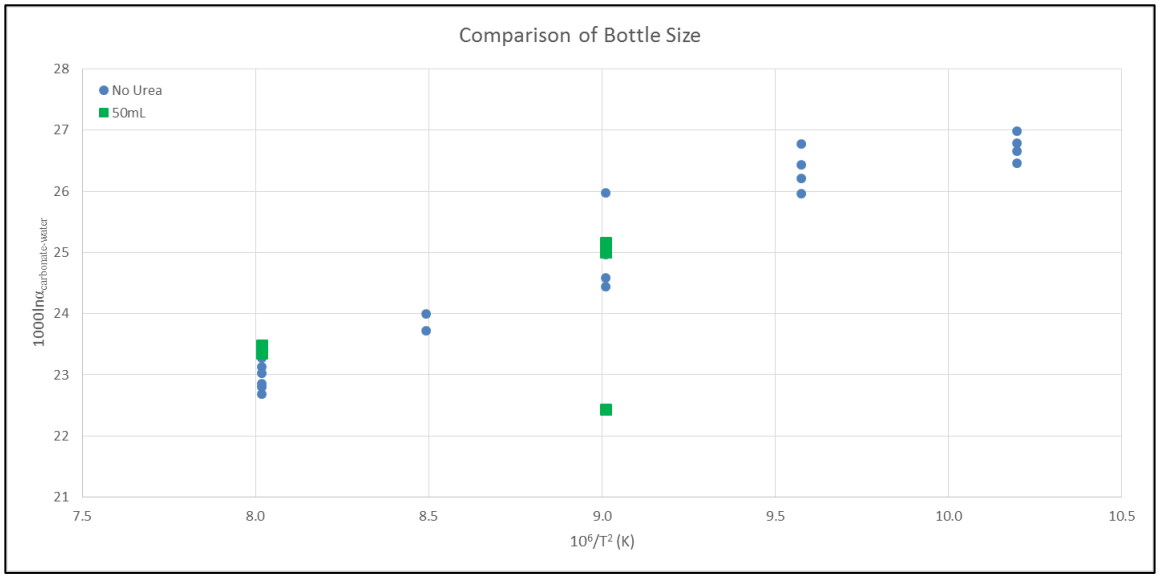

Figure 3.6. Comparison of $1000\ln\alpha_{(proto)dolomite\text{-}water}$ for precipitates formed by the solid addition method in 250 mL bottles and those formed in 50 mL bottles (duplicate analyses are plotted as separate values). There is no discernable difference in $1000\ln\alpha_{(proto)dolomite\text{-}water}$ with the varying bottle size.

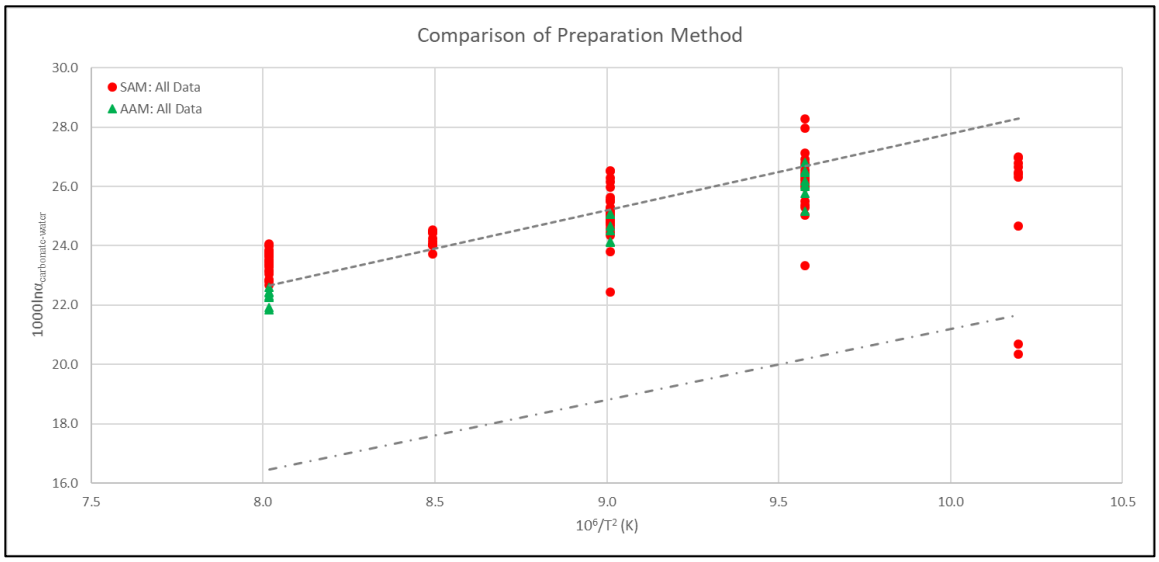

Figure 3.7. Comparison of $1000\ln\alpha_{carbonate\text{-}water}$ values (including minimum duplicates) for solid addition method precipitates (red) and aqueous addition method precipitates (green) from 40 - 80 °C. Also displayed are the oxygen isotope fractionation curves for HCO_3^- and CO_3^{2-} (Beck et al., 2005). Samples that are isotopically heterogeneous have certain $1000\ln\alpha_{(proto)dolomite\text{-}water}$ values that more closely resemble the CO_3^{2-}-water curve, whereas samples are appear closer to isotopic equilibrium lie closer to the HCO_3^--water curve.

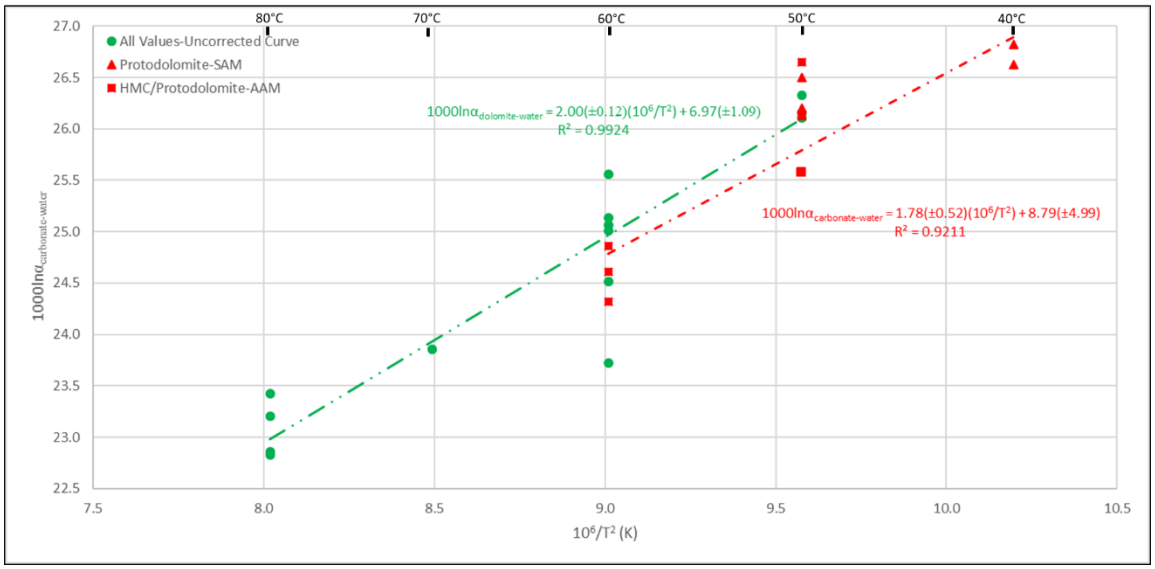

Figure 3.8. Calibration of the initial dolomite-water oxygen isotope fractionation curve developed in this study, as well as the carbonate-water oxygen isotope fraction curve, which is constructed from values of protodolomites and HMC.

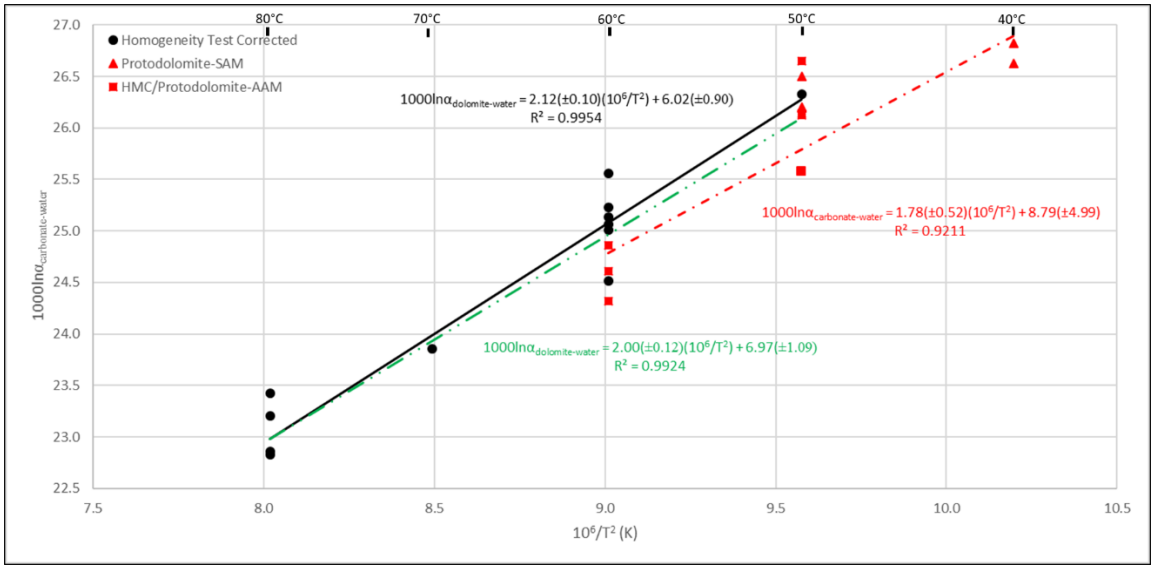

Figure 3.9. Comparison of the uncorrected (green line), "Homogeneity Test`` corrected (black line) dolomite-water oxygen isotope curves developed in this study, as well as the carbonate-water curve (protodolomite/HMC) (red). Displayed are $1000\ln\alpha_{\text{dolomite-water}}$ values used to calculate the Homogeneity Test corrected curve.

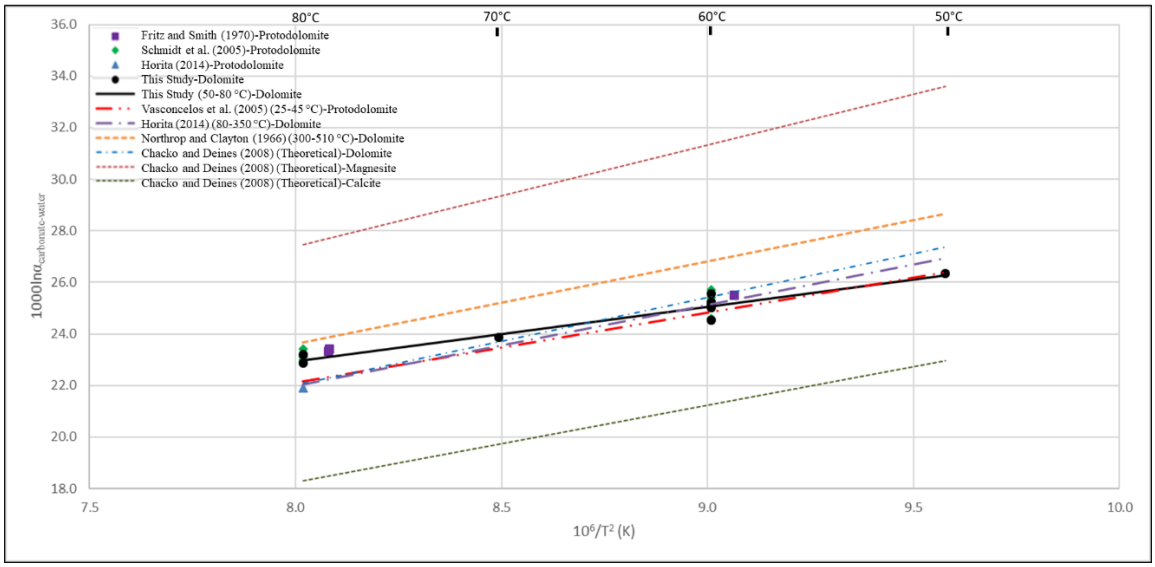

Figure 3.10. Comparison of the dolomite-water oxygen isotope fractionation curve developed from study with previous literature calibrations and analyses. Shown are: the curve from this study; calibration from Vasconcelos et al. (2005) extrapolated from 25 - 45 °C; calibration from Horita (2014) extrapolated from 80 - 350 °C and single value at 80 °C from Horita (2014) (blue triangle); calibration from Northrop and Clayton (1966) extrapolated from 300 - 510 °C; $1000\ln\alpha_{protodolomite\text{-}water}$ values collected by Fritz and Smith (1970) (purple squares) and Schmidt et al. (2005) (green diamonds). Also displayed are the theoretical curves calculated by Chacko and Deines (2008) for dolomite, magnesite and calcite.

Table 3.1. Results of the dolomite time series investigation from this study. All samples were run in quadruplicate. Standard Deviation is represented by σ.

Sample I.D	Reaction Time (hours)	$\delta^{18}O_{Carb}$ (‰)	Average	σ	Calculated % Yield	Average	σ
BF-12-1 24h r1	24	18.90	18.91	0.02	90.35	93.32	2.31
BF-12-1 24h r2	24	18.90			92.59		
BF-12-1 24h r3	24	18.88			93.54		
BF-12-1 24h r4	24	18.95			96.78		
BF-12-1 48h r2	48	18.71	17.66	0.84	94.60	94.81	0.34
BF-12-1 48h r3	48	16.66			95.29		
BF-12-1 48h r4	48	17.60			94.55		
BF-12-1 72h r1	72	18.82	18.73	0.10	92.70	92.55	1.40
BF-12-1 72h r2	72	18.57			93.61		
BF-12-1 72h r3	72	18.79			93.69		
BF-12-1 72h r4	72	18.75			90.21		
BF-12-1 96h r1	96	18.50	18.63	0.13	94.42	94.39	0.56
BF-12-1 96h r2	96	18.50			94.73		
BF-12-1 96h r3	96	18.75			94.94		
BF-12-1 96h r4	96	18.77			93.47		
BF-12-1 120h r1	120	18.35	18.26	0.70	92.35	94.51	1.30
BF-12-1 120h r2	120	17.09			94.68		
BF-12-1 120h r3	120	18.77			95.77		
BF-12-1 120h r4	120	18.83			95.24		
BF-12-1 144h r1	144	17.50	18.07	0.59	92.28	94.68	1.47
BF-12-1 144h r2	144	17.47			94.80		
BF-12-1 144h r3	144	18.63			95.39		
BF-12-1 144h r4	144	18.69			96.23		
BF-12-1 168h r1	168	18.80	18.74	0.06	95.00	94.57	1.08
BF-12-1 168h r2	168	18.78			95.75		
BF-12-1 168h r3	168	18.72			94.70		
BF-12-1 168h r4	168	18.65			92.81		
BF-Dol 24h r1	24	28.07	28.09	0.04	36.94	35.35	3.03
BF-Dol 24h r2	24	28.05			37.61		
BF-Dol 24h r3	24	28.08			36.71		
BF-Dol 24h r4	24	28.15			30.14		
BF-Dol 48h r1	48	28.05	28.15	0.07	52.70	53.42	0.99
BF-Dol 48h r2	48	28.15			54.46		
BF-Dol 48h r3	48	28.16			54.32		
BF-Dol 48h r4	48	28.25			52.20		
BF-Dol 72h r1	72	27.97	28.03	0.10	65.07	64.01	1.16
BF-Dol 72h r2	72	27.92			62.68		
BF-Dol 72h r3	72	28.18			65.26		
BF-Dol 72h r4	72	28.06			63.03		
BF-Dol 96h r1	96	27.91	27.95	0.22	69.59	70.09	4.26
BF-Dol 96h r2	96	27.61			63.54		
BF-Dol 96h r3	96	28.15			72.15		
BF-Dol 96h r4	96	28.12			75.10		
BF-Dol 120h r1	120	28.00	27.83	0.48	81.08	80.96	1.70
BF-Dol 120h r2	120	27.01			79.39		
BF-Dol 120h r3	120	28.19			83.68		
BF-Dol 120h r4	120	28.10			79.68		
BF-Dol 144h r1	144	27.93	28.09	0.10	81.97	82.53	0.85
BF-Dol 144h r2	144	28.21			83.88		
BF-Dol 144h r3	144	28.12			81.68		
BF-Dol 144h r4	144	28.10			82.60		
BF-Dol 168h r1	168	25.22	27.04	1.08	86.74	86.11	2.44
BF-Dol 168h r2	168	27.64			88.13		
BF-Dol 168h r3	168	28.00			87.61		
BF-Dol 168h r4	168	27.31			81.97		

Table 3.2. Detailed parent solution conditions and isotopic results for all samples analyzed, exclusion those displaying an evaporation effect. Experimental conditions outlined correspond to the detailed descriptions in Table 2.A1. Standard Deviation is represented by σ.

Sample ID	Temperature (°C)	Precipitation Method	Condition	Product Mineralogy	Source Na_2CO_3	$\delta^{18}O_{Carb}$ (‰)	Average	σ	$\delta^{18}O_{Final}$ (‰)	$\delta^{18}O_{Final}$ - $\delta^{18}O_{Initial}$	$1000ln\alpha_{Carbonate-Water}$	Average	σ
BF-3-1 r1	40	SAM	No U	P	A	20.88	20.71	0.17	-6.30	0.34	26.99	26.82	0.17
BF-3-1 r2	40	SAM	No U	P	A	20.54			-6.30	0.34	26.66		
BF-3-2 r1	40	SAM	No U	P	A	20.62	20.45	0.17	-6.36	0.28	26.79	26.63	0.16
BF-3-2 r2	40	SAM	No U	P	A	20.29			-6.36	0.28	26.47		
BF-3-3 r1	40	SAM	U	P	A	20.26	17.23	2.97	-6.35	0.29	26.42	23.44	3.04
BF-3-3 r2	40	SAM	U	P	A	14.08			-6.35	0.29	20.35		
BF-3-3 r3	40	SAM	U	P	A	14.43			-6.35	0.29	20.69		
BF-3-3 r4	40	SAM	U	P	A	20.13			-6.35	0.29	26.30		
BF-3-4 r1	40	SAM	U	P	A	20.80	19.63	1.18	-6.35	0.29	26.96	25.81	1.15
BF-3-4 r2	40	SAM	U	P	A	18.45			-6.35	0.29	24.65		
BF-22-2 r1	50	SAM	No U	P	B	20.46	20.17	0.29	-6.51	0.13	26.78	26.50	0.28
BF-22-2 r2	50	SAM	No U	P	B	19.88			-6.51	0.13	26.21		
BF-25-1 r1	50	SAM	No U	P	B	20.16	19.92	0.24	-6.46	0.18	26.43	26.20	0.23
BF-25-1 r2	50	SAM	No U	P	B	19.68			-6.46	0.18	25.97		
BF-22-3 r1	50	SAM	U	P	B	18.85	19.92	1.06	-6.33	0.31	25.03	26.07	1.04
BF-22-3 r2	50	SAM	U	P	B	20.98			-6.33	0.31	27.12		
BF-22-4 r1	50	SAM	U	P	B	20.24	21.12	0.88	-6.49	0.15	26.55	27.41	0.86
BF-22-4 r2	50	SAM	U	P	B	22.00			-6.49	0.15	28.27		
BF-25-2 r1	50	SAM	U	P	B	19.74	19.88	0.14	-6.48	0.16	26.05	26.19	0.14
BF-25-2 r2	50	SAM	U	P	B	20.03			-6.48	0.16	26.33		
BF-23-1 r1	50	SAM	2X U	P	B	16.96	17.96	1.00	-6.50	0.14	23.34	24.32	0.98
BF-23-1 r2	50	SAM	2X U	P	B	18.96			-6.50	0.14	25.31		
BF-23-2 r1	50	SAM	2X U	P	B	21.65	20.71	0.95	-6.51	0.13	27.96	27.03	0.93
BF-23-2 r2	50	SAM	2X U	P	B	19.76			-6.51	0.13	26.10		
BF-23-3 r1	50	SAM	5X U	D	B	20.54	19.76	0.78	-6.56	0.08	26.92	26.15[a]	0.77
BF-23-3 r2	50	SAM	5X U	D	B	18.98			-6.56	0.08	25.38		
BF-23-4 r1	50	SAM	5X U	D	B	19.91	19.98	0.06	-6.53	0.11	26.27	26.33[a+b]	0.06
BF-23-4 r2	50	SAM	5X U	D	B	20.04			-6.53	0.11	26.40		
BF-25-4 r1	50	SAM	5X U	D	B	19.13	19.74	0.61	-6.54	0.10	25.51	26.11[a]	0.60
BF-25-4 r2	50	SAM	5X U	D	B	20.35			-6.54	0.10	26.70		
BF-24-1 r1	50	AAM	AAM	H	B	19.77	19.34	0.43	-6.40	0.24	26.00	25.58	0.43
BF-24-1 r2	50	AAM	AAM	H	B	18.90			-6.40	0.24	25.15		
BF-24-2 r1	50	AAM	AAM	H	B	19.84	19.91	0.07	-6.39	0.25	26.05	26.12	0.07
BF-24-2 r2	50	AAM	AAM	H	B	19.98			-6.39	0.25	26.19		
BF-24-3 r1	50	AAM	AAM+U	H	B	20.66	20.48	0.17	-6.35	0.29	26.82	26.65	0.17
BF-24-3 r2	50	AAM	AAM+U	H	B	20.31			-6.35	0.29	26.48		
BF-24-4 r1	50	AAM	AAM+U	H	B	19.61	20.00	0.40	-6.31	0.33	25.75	26.14	0.39
BF-24-4 r2	50	AAM	AAM+U	H	B	20.40			-6.31	0.33	26.53		
BF-9-4 r1	60	SAM	No U	D	A	18.02	18.10	0.07	-6.56	0.08	24.44	24.52[a+b]	0.07
BF-9-4 r2	60	SAM	No U	D	A	18.17			-6.56	0.08	24.59		
BF-16-3 r1	60	SAM	No U	D	A	18.71	18.72	0.01	-6.44	0.20	25.00	25.01[a+b]	0.01
BF-16-3 r2	60	SAM	No U	D	A	18.72			-6.44	0.20	25.01		
BF-16-4 r1	60	SAM	No U	D	A	18.67	18.77	0.11	-6.44	0.20	24.96	25.06[a+b]	0.11
BF-16-4 r2	60	SAM	No U	D	A	18.88			-6.44	0.20	25.17		
BF-20-2 r1	60	SAM	No U	D	B	19.73	19.32	0.41	-6.41	0.23	25.97	25.57[a+b]	0.41
BF-20-2 r2	60	SAM	No U	D	B	18.90			-6.41	0.23	25.16		
BF-9-1 r1	60	SAM	U	D	A	18.75	18.82	0.07	-6.56	0.08	25.16	25.23	0.07
BF-9-1 r2	60	SAM	U	D	A	18.89			-6.56	0.08	25.30		
BF-16-1 r1	60	SAM	U	D	A	18.84	18.87	0.03	-6.54	0.10	25.22	25.25	0.03
BF-16-1 r2	60	SAM	U	D	A	18.89			-6.54	0.10	25.28		
BF-16-2 r1	60	SAM	U	D	A	7.76	13.28	5.52	-6.44	0.20	14.18	19.64	5.45
BF-16-2 r2	60	SAM	U	D	A	18.81			-6.44	0.20	25.09		
BF-20-1 r1	60	SAM	U	D	B	20.10	20.22	0.12	-6.36	0.28	26.29	26.40	0.12
BF-20-1 r2	60	SAM	U	D	B	20.34			-6.36	0.28	26.52		
BF-12-1 r1	60	SAM	2X U	D	A	17.84	18.07	0.23	-6.65	-0.01	24.35	24.58	0.23
BF-12-1 r2	60	SAM	2X U	D	A	18.30			-6.65	-0.01	24.81		
BF-12-2 r1	60	SAM	2X U	D	A	18.22	18.61	0.38	-6.68	-0.04	24.76	25.14	0.37
BF-12-2 r2	60	SAM	2X U	D	A	18.99			-6.68	-0.04	25.51		
BF-20-3 r1	60	SAM	2X U	D	B	20.12	18.72	1.40	-6.59	0.05	26.53	25.16	1.37
BF-20-3 r2	60	SAM	2X U	D	B	17.32			-6.59	0.05	23.79		
BF-12-4 r1	60	SAM	CaCl2+U	D	A	18.41	18.35	0.06	-6.78	-0.14	25.04	24.99	0.06
BF-12-4 r2	60	SAM	CaCl2+U	D	A	18.29			-6.78	-0.14	24.93		
BF-17-1 r1	60	SAM	50mL	D	A	18.74	18.71	0.02	-6.57	0.07	25.16	25.14[a+b]	0.02
BF-17-1 r2	60	SAM	50mL	D	A	18.69			-6.57	0.07	25.12		
BF-17-2 r1	60	SAM	50mL	D	A	18.60	17.30	1.31	-6.55	0.09	25.01	23.72[a]	1.29
BF-17-2 r2	60	SAM	50mL	D	A	15.99			-6.55	0.09	22.44		
BF-17-3 r1	60	SAM	50mL+U	D	A	18.77	18.66	0.11	-6.29	0.35	24.91	24.80	0.11
BF-17-3 r2	60	SAM	50mL+U	D	A	18.56			-6.29	0.35	24.70		
BF-21-2 r1	60	SAM	50mL+U	D	B	19.13	18.98	0.15	-6.54	0.10	25.51	25.36	0.15
BF-21-2 r2	60	SAM	50mL+U	D	B	18.82			-6.54	0.10	25.21		
BF-21-3 r1	60	SAM	50mL+2X U	D	B	19.21	19.25	0.04	-6.50	0.14	25.55	25.59	0.04
BF-21-3 r2	60	SAM	50mL+2X U	D	B	19.29			-6.50	0.14	25.63		
BF-21-4 r1	60	SAM	50mL+2X U	D	B	18.80	19.47	0.67	-6.20	0.44	24.84	25.50	0.66
BF-21-4 r2	60	SAM	50mL+2X U	D	B	20.15			-6.20	0.44	26.16		
BF-14-3 r1	60	AAM	AAM	P	A	18.96	18.76	0.20	-6.26	0.38	25.06	24.87	0.20
BF-14-3 r2	60	AAM	AAM	P	A	18.56			-6.26	0.38	24.67		
BF-14-1 r1	60	AAM	AAM+U	P	A	18.91	18.42	0.49	-6.34	0.30	25.09	24.60	0.48
BF-14-1 r2	60	AAM	AAM+U	P	A	17.92			-6.34	0.30	24.12		
BF-14-2 r1	60	AAM	AAM+U	P	A	18.40	18.22	0.18	-6.25	0.39	24.50	24.32	0.18
BF-14-2 r2	60	AAM	AAM+U	P	A	18.03			-6.25	0.39	24.14		

Na_2CO_3-A $\delta^{18}O$ = 12.05 ‰ ; Na_2CO_3-B $\delta^{18}O$ = 11.22 ‰ ; $\delta^{18}O_{initial}$ = -6.64 ‰ ; H: HMC; P: protodolomite; D: dolomite; A: aragonite

[a]: value used for uncorrected curve; [b]: value used for Homogeneity Test corrected curve

Sample ID	Temperature (°C)	Precipitation Method	Condition	Product Mineralogy	Source Na_2CO_3	$\delta^{18}O_{Carb}$ (‰)	Average	σ	$\delta^{18}O_{Final}$ (‰)	$\delta^{18}O_{Final}$ - $\delta^{18}O_{Initial}$	$1000ln\alpha_{Carbonate-Water}$	Average	σ
BF-15-4 r1	70	SAM	No U	D	A	17.52	17.66	0.14	-6.33	0.31	23.72	23.86[a+b]	0.14
BF-15-4 r2	70	SAM	No U	D	A	17.81			-6.33	0.31	24.00		
BF-15-1 r1	70	SAM	U	D	A	17.64	17.64	0.00	-6.53	0.11	24.04	24.04	0.00
BF-15-1 r2	70	SAM	U	D	A	17.65			-6.53	0.11	24.04		
BF-18-1 r1	70	SAM	2X U	D	A	17.85	17.68	0.17	-6.77	-0.13	24.48	24.31	0.17
BF-18-1 r2	70	SAM	2X U	D	A	17.51			-6.77	-0.13	24.14		
BF-18-2 r1	70	SAM	2X U	D	A	17.94	17.80	0.14	-6.72	-0.08	24.52	24.39	0.13
BF-18-2 r2	70	SAM	2X U	D	A	17.66			-6.72	-0.08	24.25		
BF-18-4 r1	70	SAM	CaCl2+U	D	A	17.73	17.75	0.02	-6.83	-0.19	24.43	24.45	0.02
BF-18-4 r2	70	SAM	CaCl2+U	D	A	17.77			-6.83	-0.19	24.47		
BF-1-1 r1	80	SAM	No U	D	A	17.08	17.01	0.07	-6.32	0.32	23.27	23.20[a+b]	0.07
BF-1-1 r2	80	SAM	No U	D	A	16.94			-6.32	0.32	23.13		
BF-1-2 r1	80	SAM	No U	D	A	16.58	16.76	0.18	-6.22	0.42	22.68	22.86[a+b]	0.17
BF-1-2 r2	80	SAM	No U	D	A	16.93			-6.22	0.42	23.03		
BF-28-2 r1	80	SAM	No U	D	B	16.63	16.60	0.02	-6.34	0.30	22.85	22.83[a+b]	0.02
BF-28-2 r2	80	SAM	No U	D	B	16.58			-6.34	0.30	22.81		
BF-1-3 r1	80	SAM	U	D	A	17.11	16.96	0.15	-6.46	0.18	23.44	23.30	0.14
BF-1-3 r2	80	SAM	U	D	A	16.82			-6.46	0.18	23.16		
BF-1-4 r1	80	SAM	U	D	A	17.30	17.30	0.00	-6.58	0.06	23.76	23.76	0.00
BF-1-4 r2	80	SAM	U	D	A	17.31			-6.58	0.06	23.76		
BF-6-1 r1	80	SAM	U	D	A	16.80	16.87	0.07	-7.01	-0.37	23.70	23.76	0.07
BF-6-1 r2	80	SAM	U	D	A	16.93			-7.01	-0.37	23.83		
BF-6-2 r1	80	SAM	U	D	A	17.02	17.04	0.02	-6.79	-0.15	23.69	23.71	0.02
BF-6-2 r2	80	SAM	U	D	A	17.06			-6.79	-0.15	23.72		
BF-6-3 r1	80	SAM	CaCl2+U	D	A	16.96	17.01	0.05	-6.88	-0.24	23.72	23.77	0.05
BF-6-3 r2	80	SAM	CaCl2+U	D	A	17.06			-6.88	-0.24	23.82		
BF-6-4 r1	80	SAM	CaCl2+U	D	A	16.04	16.57	0.34	-6.88	-0.24	22.81	23.34	0.34
BF-6-4 r2	80	SAM	CaCl2+U	D	A	16.97			-6.88	-0.24	23.73		
BF-6-4 r3	80	SAM	CaCl2+U	D	A	16.58			-6.88	-0.24	23.35		
BF-6-4 r4	80	SAM	CaCl2+U	D	A	16.71			-6.88	-0.24	23.48		
BF-6-5 r1	80	SAM	2X U	D	A	17.16	17.20	0.04	-6.95	-0.31	23.99	24.02	0.04
BF-6-5 r2	80	SAM	2X U	D	A	17.24			-6.95	-0.31	24.06		
BF-6-6 r1	80	SAM	2X U	D	A	17.18	16.91	0.27	-6.99	-0.35	24.05	23.78	0.27
BF-6-6 r2	80	SAM	2X U	D	A	16.63			-6.99	-0.35	23.51		
BF-13-2 r1	80	SAM	50mL	D	A	17.08	17.01	0.07	-6.53	0.11	23.49	23.42[a+b]	0.07
BF-13-2 r2	80	SAM	50mL	D	A	16.94			-6.53	0.11	23.35		
BF-13-3 r1	80	SAM	50mL+U	D	A	17.07	16.99	0.08	-6.87	-0.23	23.82	23.74	0.08
BF-13-3 r2	80	SAM	50mL+U	D	A	16.91			-6.87	-0.23	23.66		
BF-13-4 r1	80	SAM	50mL+U	D	A	17.11	17.03	0.08	-6.79	-0.15	23.78	23.70	0.08
BF-13-4 r2	80	SAM	50mL+U	D	A	16.94			-6.79	-0.15	23.62		
BF-7-3 r1	80	AAM	AAM	P,A	A	15.79	16.17	0.38	-6.16	0.48	21.85	22.22	0.37
BF-7-3 r2	80	AAM	AAM	P,A	A	16.55			-6.16	0.48	22.59		
BF-7-4 r1	80	AAM	AAM	P,A	A	16.18	16.27	0.09	-6.18	0.46	22.25	22.34	0.09
BF-7-4 r2	80	AAM	AAM	P,A	A	16.36			-6.18	0.46	22.43		
BF-7-1 r1	80	AAM	AAM+U	D,A	A	16.20	15.95	0.25	-6.32	0.32	22.41	22.17	0.24
BF-7-1 r2	80	AAM	AAM+U	D,A	A	15.71			-6.32	0.32	21.92		
BF-7-2 r1	80	AAM	AAM+U	D,A	A	16.28	16.30	0.03	-6.08	0.56	22.25	22.27	0.03
BF-7-2 r2	80	AAM	AAM+U	D,A	A	16.33			-6.08	0.56	22.30		

Na_2CO_3-A $\delta^{18}O$ = 12.05 ‰ ; Na_2CO_3-B $\delta^{18}O$ = 11.22 ‰ ; $\delta^{18}O_{initial}$ = -6.64 ‰ ; H: HMC; P: protodolomite; D: dolomite; A: aragonite

[a]: value used for uncorrected curve; [b]: value used for Homogeneity Test corrected curve

References

Beck, W. C., Grossman, E. L., & Morse, J. W. (2005). Experimental studies of oxygen isotope fractionation in the carbonic acid system at 15, 25, and 40 C. Geochimica et Cosmochimica Acta, 69(14), 3493-3503.

Fritz, P., & Smith, D. G. W. (1970). The isotopic composition of secondary dolomites. Geochimica et Cosmochimica Acta, 34(11), 1161-1173.

Gregg, J., Bish, D., Kaczmarek, S., & Machel, H. (2015). Mineralogy, nucleation and growth of dolomite in the laboratory and sedimentary environment: A review. Sedimentology, 62(6), 1749-1769.

Horita, J. (2014). Oxygen and carbon isotope fractionation in the system dolomite-water-CO_2 to elevated temperatures. Geochimica et Cosmochimica Acta, 129, 111-124.

Katz, A., & Matthews, A. (1977). The dolomitization of CaCO3: an experimental study at 252–295 C. Geochimica et Cosmochimica Acta, 41(2), 297-308.

Kelleher, I. J., & Redfern, S. A. (2002). Hydrous calcium magnesium carbonate, a possible precursor to the formation of sedimentary dolomite. Molecular simulation, 28(6-7), 557-572.

Kim, S. T., Coplen, T. B., & Horita, J. (2015). Normalization of stable isotope data for carbonate minerals: Implementation of IUPAC guidelines. Geochimica et Cosmochimica Acta, 158, 276-289.

Kim, S. T., O'Neil, J. R., Hillaire-Marcel, C., & Mucci, A. (2007). Oxygen isotope fractionation between synthetic aragonite and water: influence of temperature and Mg2+ concentration. Geochimica et Cosmochimica Acta, 71(19), 4704-4715.

Northrop, D. A., & Clayton, R. N. (1966). Oxygen-isotope fractionations in systems containing dolomite. The Journal of Geology, 74(2), 174-196.

Petrash, D. A., Bialik, O. M., Bontognali, T. R., Vasconcelos, C., Roberts, J. A., McKenzie, J. A., & Konhauser, K. O. (2017). Microbially catalyzed dolomite formation: from near-surface to burial. Earth-Science Reviews, 171, 558-582.

Schmidt, M., Xeflide, S., Botz, R., & Mann, S. (2005). Oxygen isotope fractionation during synthesis of CaMg-carbonate and implications for sedimentary dolomite formation. Geochimica et Cosmochimica Acta, 69(19), 4665-4674.

Siegel, F.R., 1961. Factors influencing the precipitation of dolomitic carbonates. Geol. Surv. Kansas Bull. 152, 129–158.

Vasconcelos, C., McKenzie, J. A., Bernasconi, S., Grujic, D., & Tiens, A. J. (1995). Microbial mediation as a possible mechanism for natural dolomite formation at low temperatures. Nature, 377(6546), 220.

Vasconcelos, C., McKenzie, J. A., Warthmann, R., & Bernasconi, S. M. (2005). Calibration of the δ18O paleothermometer for dolomite precipitated in microbial cultures and natural environments. Geology, 33(4), 317-320.

CHAPTER 4: CONCLUSIONS AND FUTURE RESEARCH

CHAPTER 4: CONCLUSIONS AND FUTURE RESEARCH

Section 4.1: Principal Findings

This study is the first known instance of dolomite synthesis at temperatures below 100 °C, displaying an ability to synthesize dolomite at temperatures as low as 60 °C without urea catalysis. Developed is a method capable of producing dolomite simply and under relatively short time periods (~ 42 days). The "solid addition" method, based on the addition of solid phase Na_2CO_3 to $MgSO_4$-$Ca(NO_3)_2$ solutions, likely expedites reaction kinetics by the rapid replacement of undissolved Na_2CO_3 with Ca^{2+} and Mg^{2+} ions. By doing so, dolomite formation may occur quickly by evading the rate-determining nucleation phase and instead forming analogously to the previously described "calcite seed effect". This method has the potential for use as a foundational tool for further investigations of possible solution chemistry or catalysts that facilitate dolomite formation and thereby provide possible answers to finally solve the elusive "dolomite problem".

Urea was found to have an apparent facilitating effect on dolomite formation. Although previously proposed to encourage dolomite synthesis (Mansfield, 1980; Deelman, 1999), a clear relationship has been established between increasing urea concentration and dolomite formation. Increasing urea concentrations resulted in both elevated stoichiometry and cation ordering of synthesized dolomite. Urea catalysis is validated by distinct trends in carbon stable isotopes, displaying that ^{13}C depletion is controlled by the urea concentration and indicating that urea carbon is incorporated into the dolomite crystal structure. Importantly, the degree to which urea influences dolomite synthesis is dependent on formation temperature, likely indicating that thermal urea

hydrolysis is occurring. Furthermore, increasing urea concentration was generally associated with an increase in pH, which was also dependent on temperature. The exact mechanism by which urea catalysis facilitates dolomite formation is unclear at this time, although it is likely that the effect is related to one or more of: elevated pH, elevated alkalinity, or a comparable catalytic effect as those displayed by other biogenic substances and certain microorganisms.

The role of the solid addition method on dolomite formation, as opposed to the larger headspace used in this study, was confirmed by experiments conducted in smaller 50 mL bottles. Although the variation in headspace caused a limited effect at 80 °C, decreased headspace at 60 °C resulted in weaker dolomite cation ordering and a reduction in $\%MgCO_3$ of ~ 1 %. Elevated headspace appears to allow more efficient solution mixing during daily shaking periods by a greater surface area at the solution-air boundary. Furthermore, although a small sample size was tested, initial results found that $CaCl_2$ replacement for $Ca(NO_3)_2$ in solutions containing 50.5 mmolal urea caused a slight decrease in both dolomite cation ordering and stoichiometry between 60 - 80 °C.

A new dolomite-water oxygen isotope calibration was developed by analyzing (proto)dolomite samples synthesized by the solid addition method. This calibration is somewhat similar to those previously published for low temperature protodolomite, although the slope is decidedly higher. While the calibration presented in this study is the first to use dolomite synthesized at temperatures below 100 °C, potential kinetic effects were likely found that may hinder the accuracy of equilibrium values. Therefore, further

investigations into dolomite synthesized by this method are required to effectively evaluate possible isotopic kinetic effects caused by rapid mineral formation.

Section 4.2: Candidate's Contribution to the Field

The candidate carried out the bulk of experimental procedures and analyses outlined in this study. These include all the preparation of experimental solutions described, precipitate filtrations, and XRD analyses and associated processing of XRD patterns. The candidate carried out most ICP-MS analyses, although certain isotopic analysis procedures were performed by either Martin Knyf or Kate Allan, due to unforeseen circumstances. SEM and SEM-EDS analyses were partially conducted by the candidate; however, the candidate was present during each procedure that was carried out by Chris Butcher at the Canadian Centre for Electron Microscopy (CCEM). All data analyses presented here were conducted by the candidate, as well as the writing of this study. Incorporated are also scientific insight and editorial guidance given by the candidate's supervisor, Dr. Sang-Tae Kim.

The findings presented by the candidate should greatly benefit the field of dolomite formation research and geology/geochemistry in general. The inability to synthesize dolomite has developed into a widely recognized issue and the solid addition method described here should provide a foundational tool for numerous subsequent studies investigating conditions that encourage dolomite formation. The verification of urea catalysis on dolomite formation should lead to studies that attempt to connect the role of urea to natural dolomite formation environments. Finally, establishment of the first dolomite-water oxygen isotope thermometry calibration at low temperatures (< 100 °C)

using partially-ordered dolomite should be a valuable next step in developing a calibration with true equilibrium values, which will allow estimation of the temperatures that dolomite has formed in certain depositional environments and throughout geologic history.

Section 4.3: Future Research Requirements

Numerous investigations are necessary to build upon the findings presented here. First and foremost, the underlying mechanisms that enable the solid addition method to synthesize dolomite are currently unconfirmed and an in-depth study into the exact reaction processes would benefit the scientific community greatly. This includes identifying if dolomite is formed by rapid reaction kinetics associated with the addition of solid phase Na_2CO_3 and if this reaction is analogous to either a "calcite seed effect" or high temperature dolomitization.

Experiments targeting various dolomite growth periods (i.e. intervals between 0 and 42 days) using this method would provide insight into the development of cation ordering and stoichiometry. More specifically, this form of investigation would reveal if cation ordering evolves with reaction progress, as proposed in this study. As well, testing variations in the molar Mg/Ca ratio in conjunction with the solid addition method would demonstrate if the previous finding that dolomite stoichiometry is dependent on the molar Mg/Ca ratio template of the parent solution (Kaczmarek and Sibley, 2011) is applicable at temperatures below 100 °C.

Additional studies into the effect urea of catalysis on dolomite formation are required. This includes determining if a potential urea concentration threshold exists at which dolomite %$MgCO_3$ no longer increases (e.g., at 70 and 80 °C). More importantly, further tests into dolomite synthesis using the solid addition method in conjunction with urea addition are required at 40 °C and 50 °C. Primarily, potential dolomite synthesis at 40 °C, or lower temperatures, should be targeted by applying both higher urea concentrations (i.e., > 252 mmolal) and longer growth periods (i.e., > 42 days). The minimal temperature at which thermal hydrolysis of urea is possible should also be investigated.

Finally, confirmation of any potential oxygen isotope kinetic effects associated with dolomite formation by the solid addition method should be targeted. Similarly, investigations into modifications of the solid addition method should target synthesizing dolomite in isotopic equilibrium, if possible. By doing so, a more accurate dolomite-water oxygen isotope thermometer could be developed, and the scientific field of carbonate geochemistry would greatly benefit.

References

Deelman J. C. (1999). Low-temperature nucleation of magnesite and dolomite. Neues Jahrbuch Fur Mineralogie-Monatshefte, 7, 289–302.

Kaczmarek, & Sibley. (2011). On the evolution of dolomite stoichiometry and cation order during high-temperature synthesis experiments: An alternative model for the geochemical evolution of natural dolomites. Sedimentary Geology, 240(1), 30-40.

Mansfield, C. F. (1980). A urolith of biogenic dolomite - another clue in the dolomite mystery. Geochimica et Cosmochimica Acta, 44(6), 829-839.

Supplementary Information

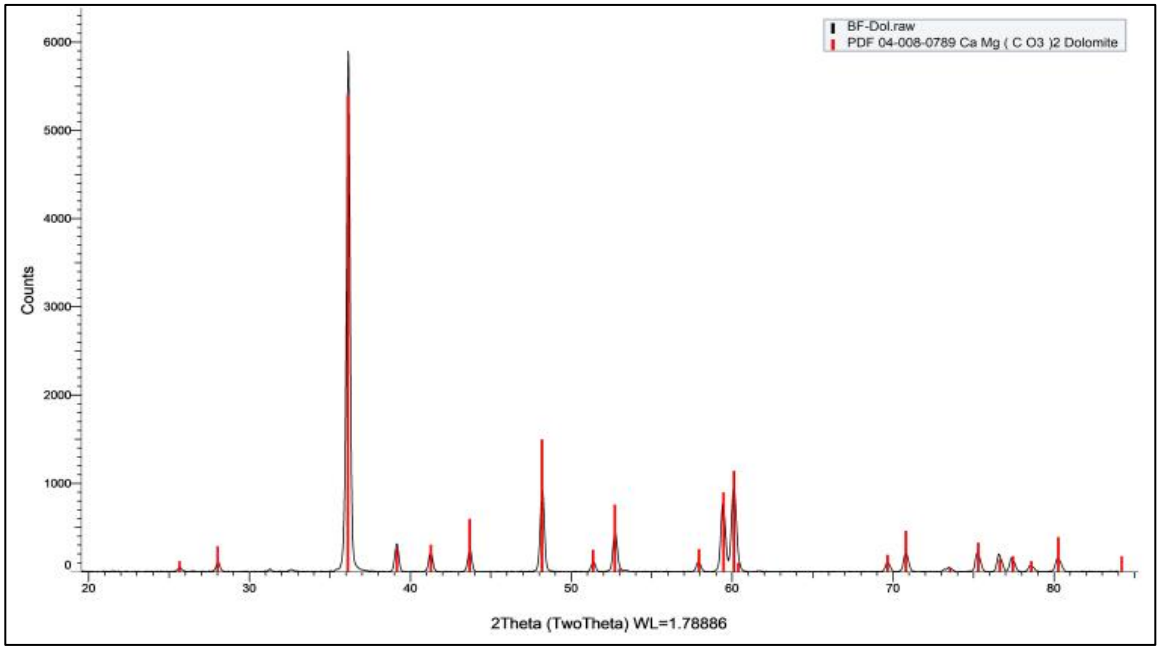

Figure S1. XRD pattern for internal laboratory dolomite standard (BF-Dol), obtained by CoKα radiation.

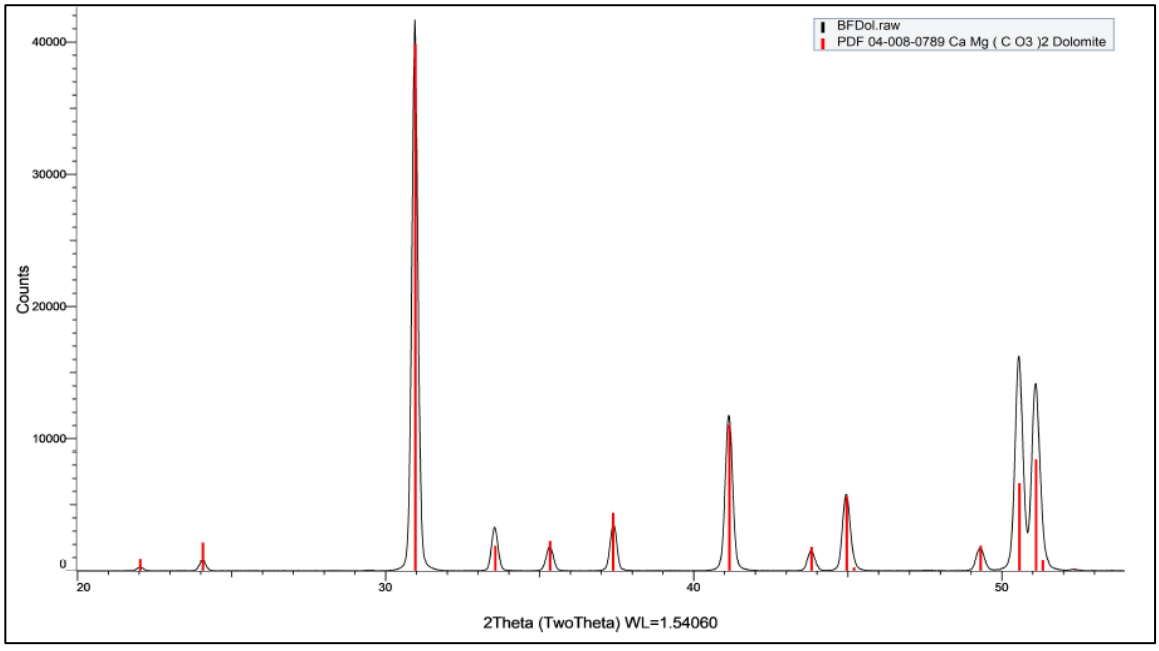

Figure S2. XRD pattern for internal laboratory dolomite standard (BF-Dol), obtained by CuKα radiation.

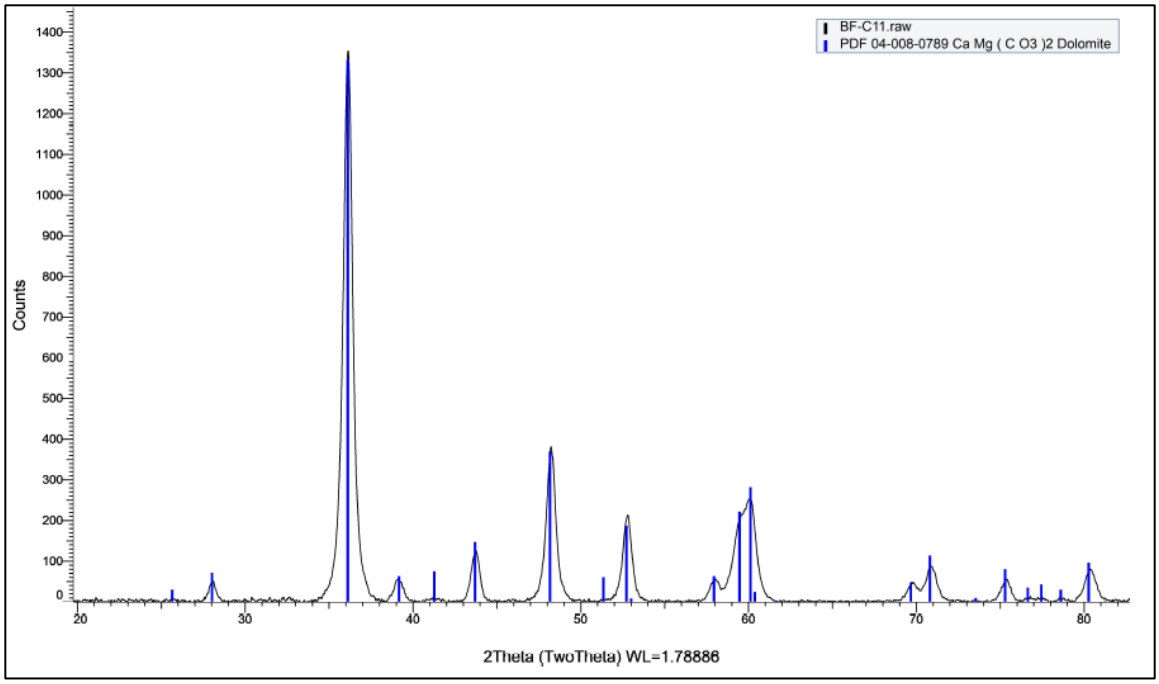

Figure S3. XRD pattern for sample BF-1-1, obtained by CoKα radiation.

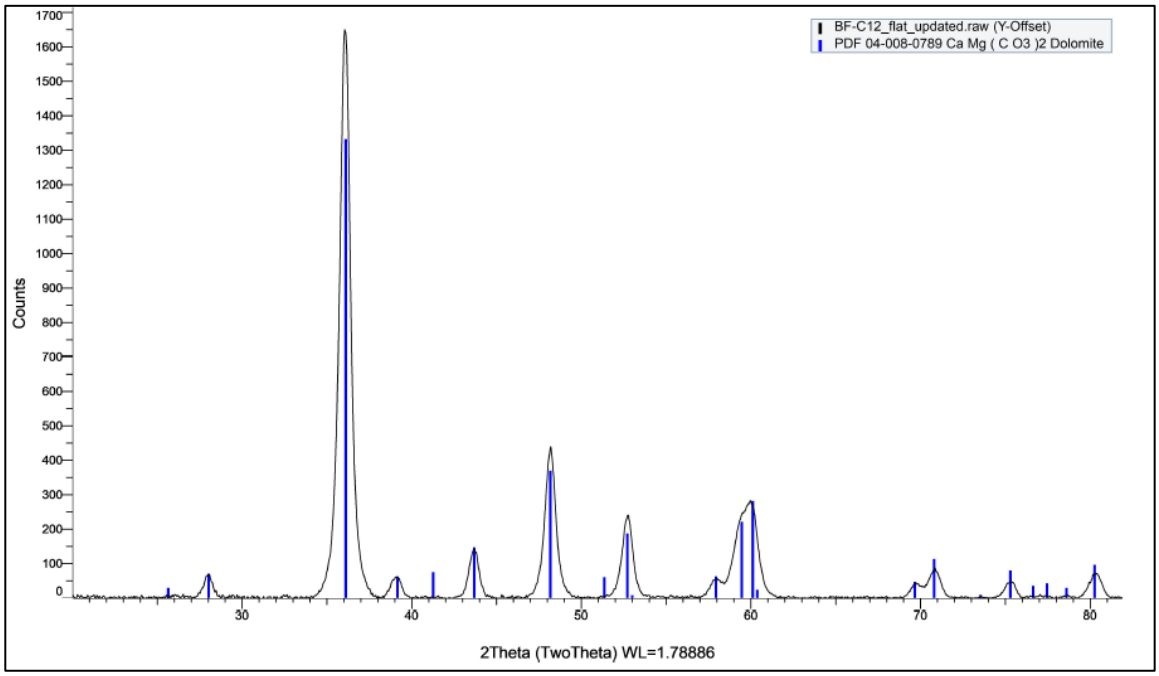

Figure S4. XRD pattern for sample BF-1-2, obtained by CoKα radiation.

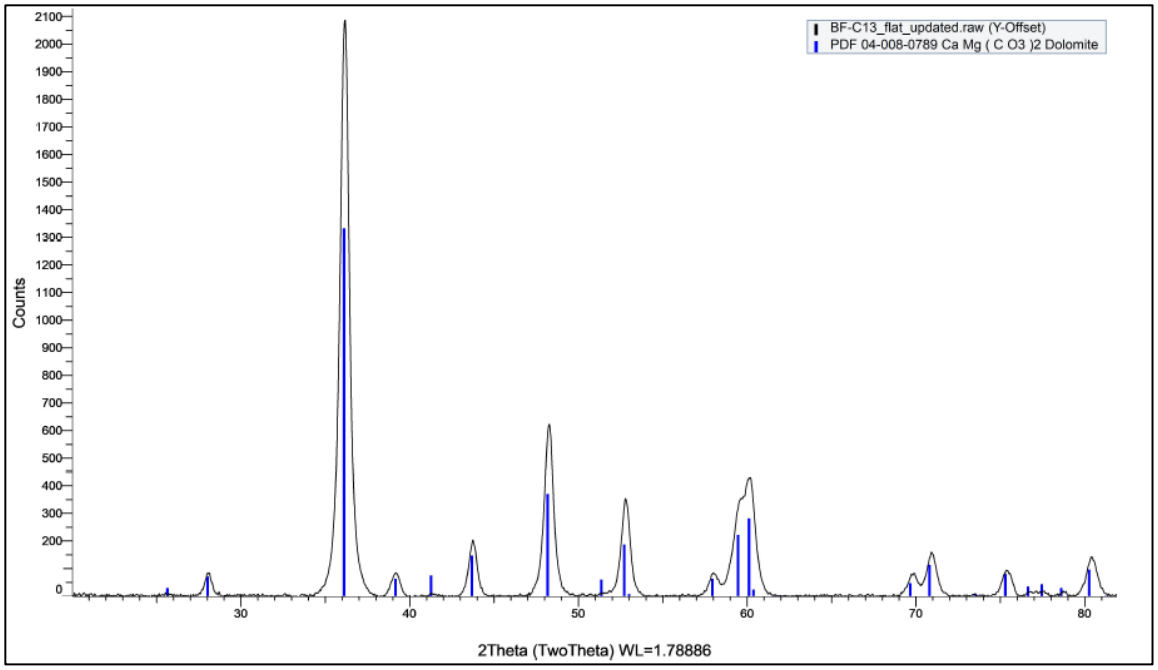

Figure S5. XRD pattern for sample BF-1-3, obtained by CoKα radiation.

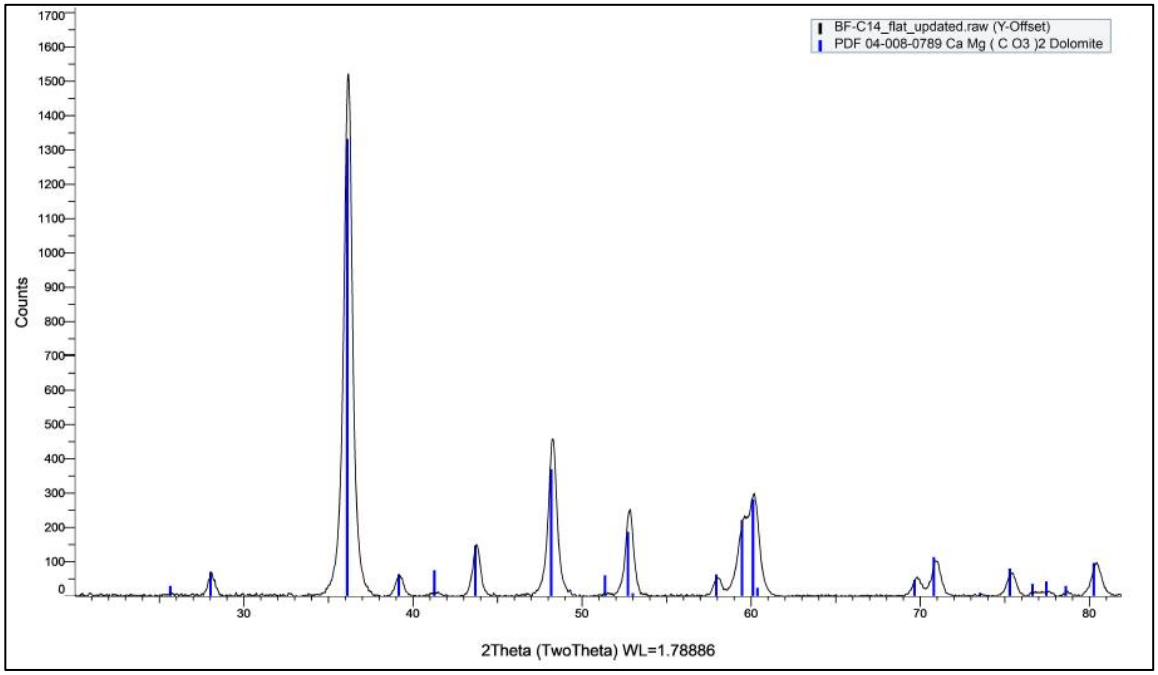

Figure S6. XRD pattern for sample BF-1-4, obtained by CoKα radiation.

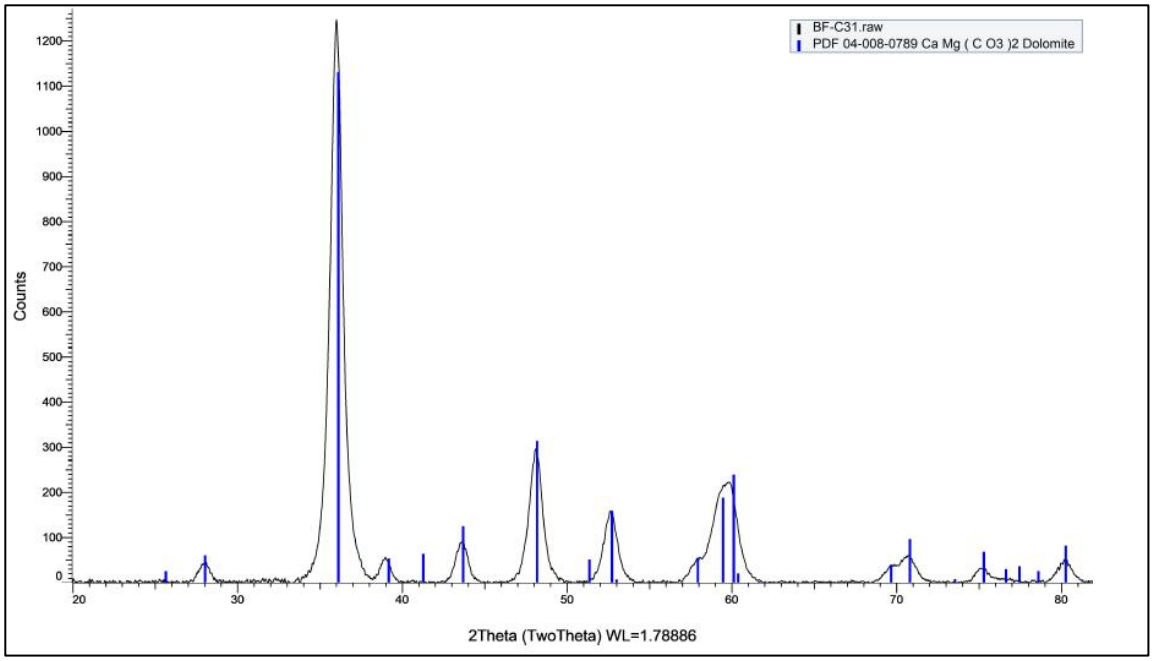

Figure S7. XRD pattern for sample BF-3-1, obtained by CoKα radiation.

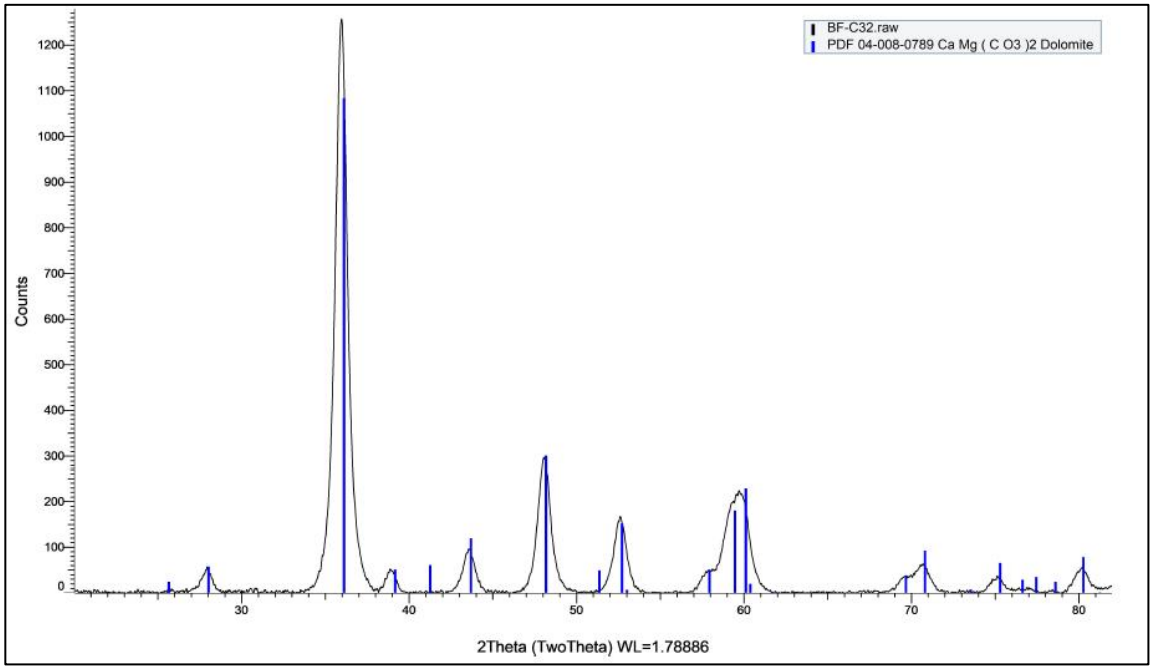

Figure S8. XRD pattern for sample BF-3-2, obtained by CoKα radiation.

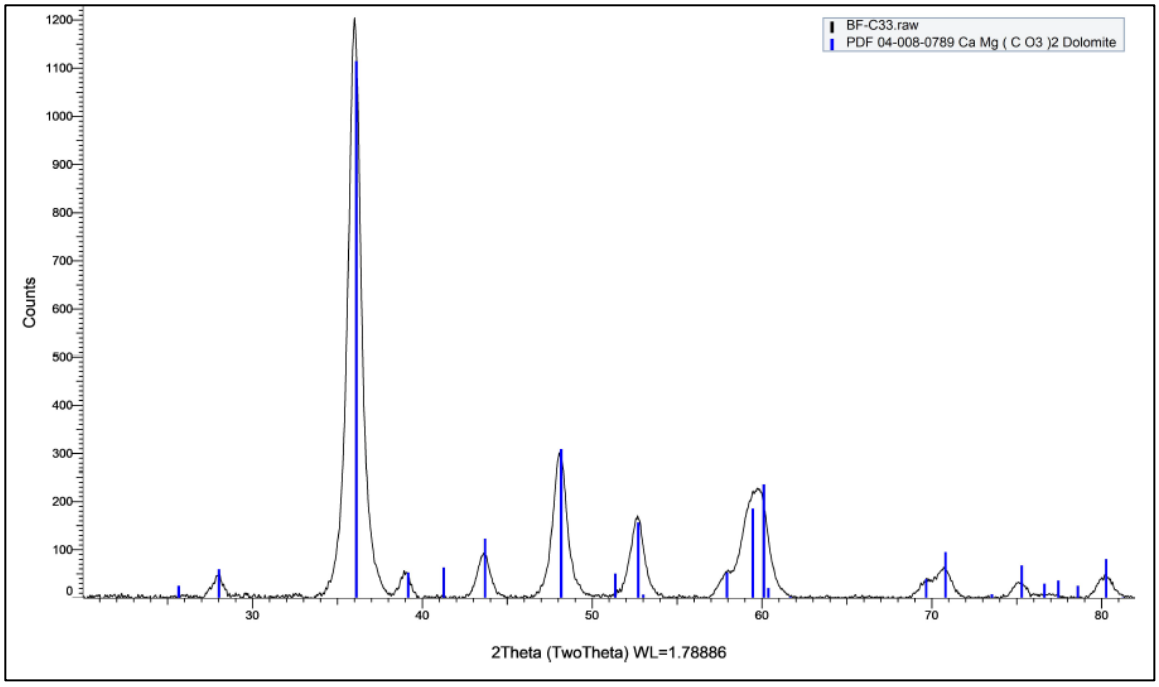

Figure S9. XRD pattern for sample BF-3-3, obtained by CoKα radiation.

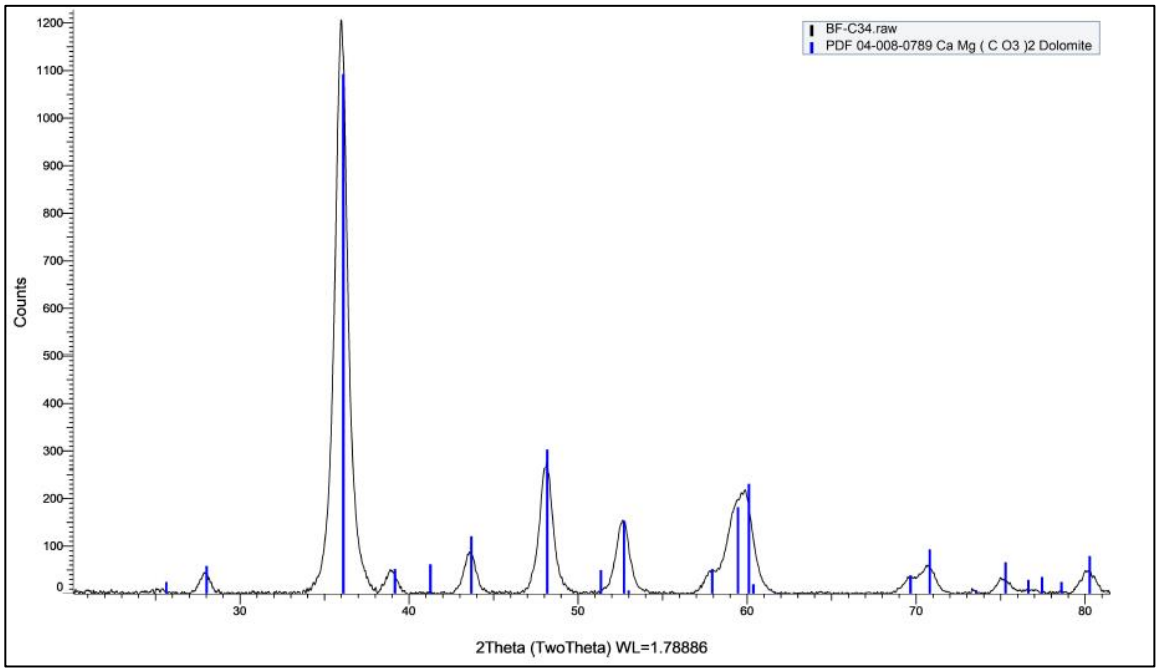

Figure S10. XRD pattern for sample BF-3-4, obtained by CoKα radiation.

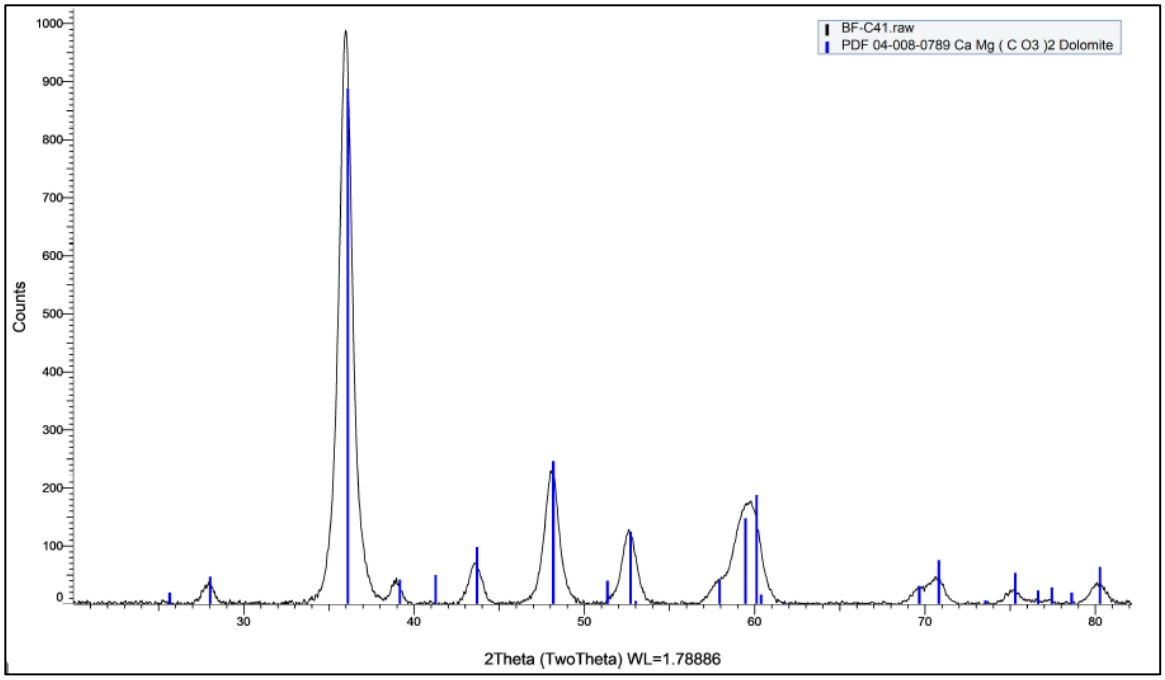

Figure S11. XRD pattern for sample BF-4-1, obtained by CoKα radiation.

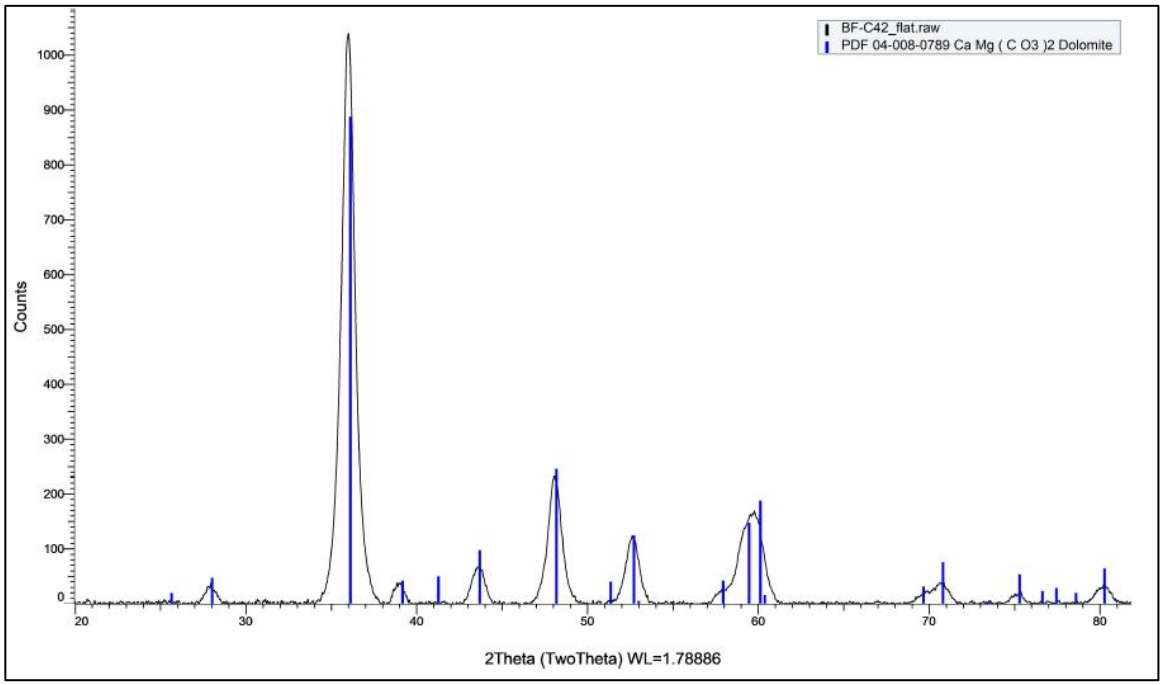

Figure S12. XRD pattern for sample BF-4-2, obtained by CoKα radiation.

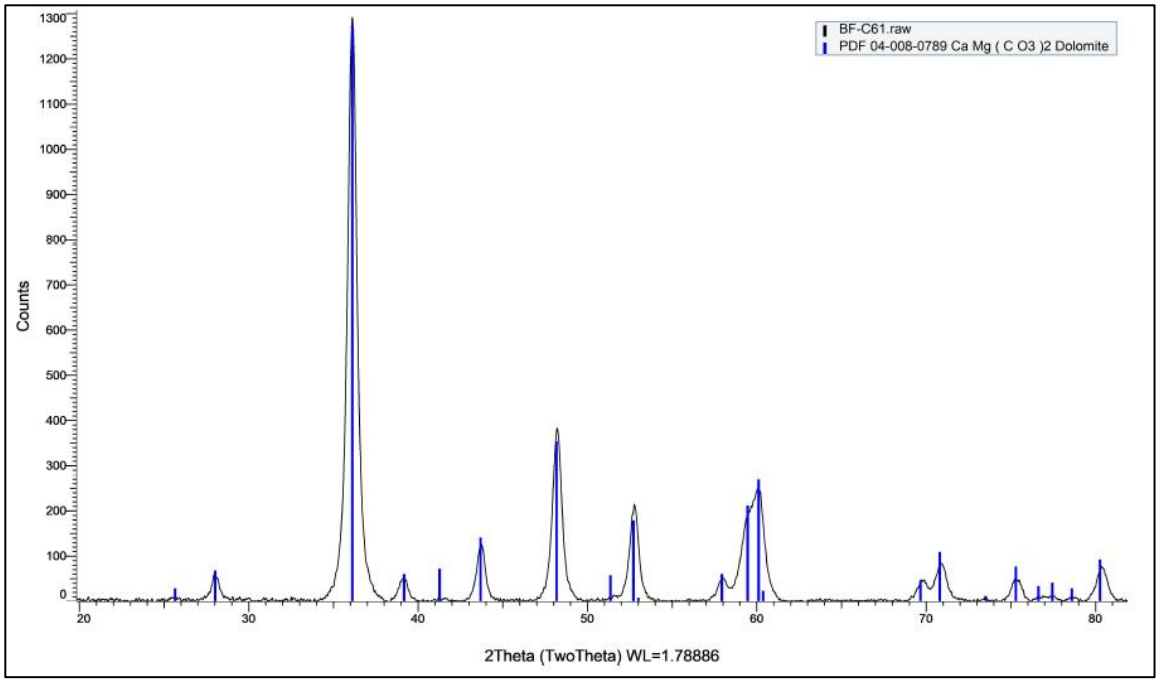

Figure S13. XRD pattern for sample BF-6-1, obtained by CoKα radiation.

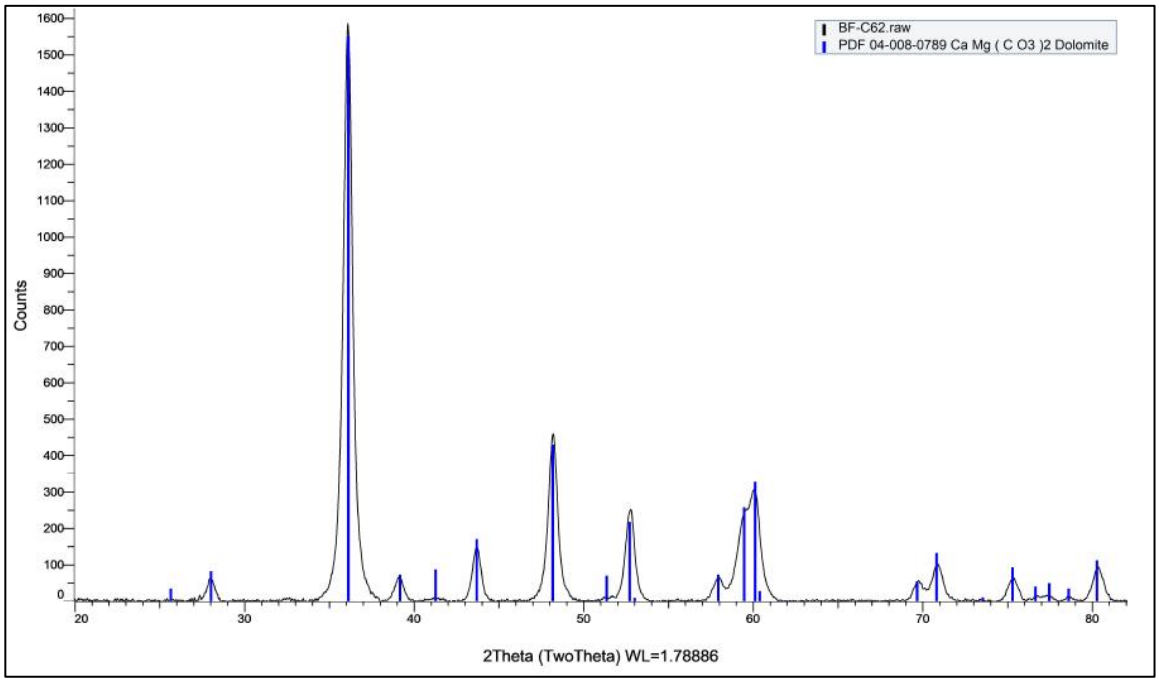

Figure S14. XRD pattern for sample BF-6-2, obtained by CoKα radiation.

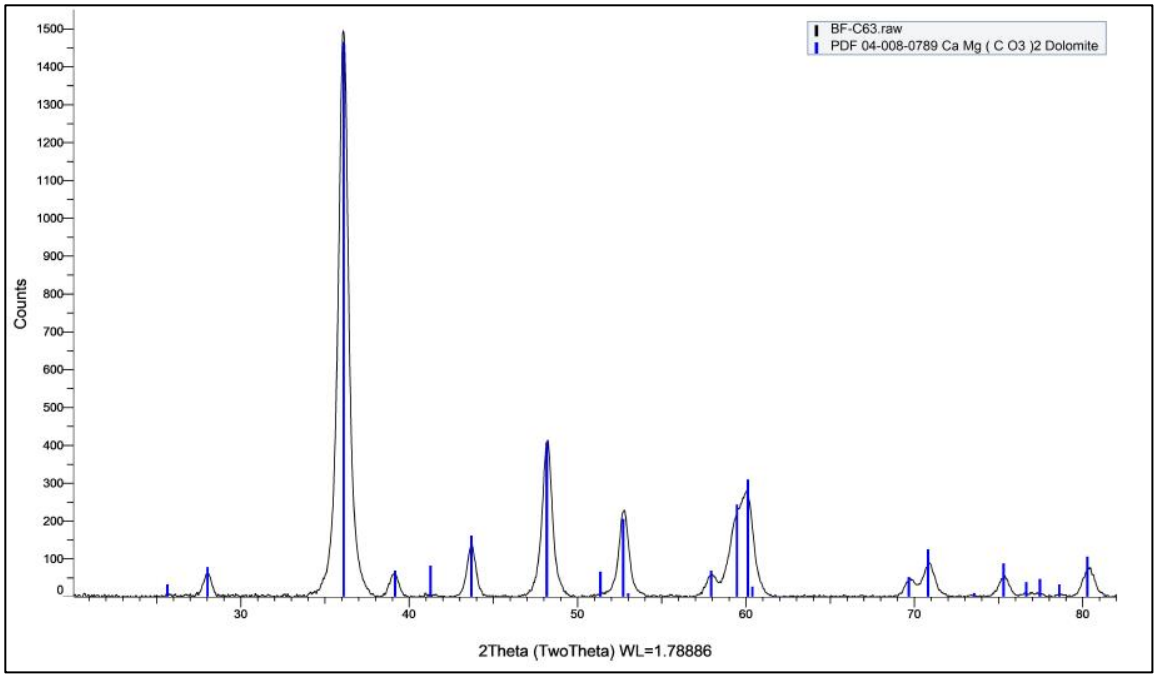

Figure S15. XRD pattern for sample BF-6-3, obtained by CoKα radiation.

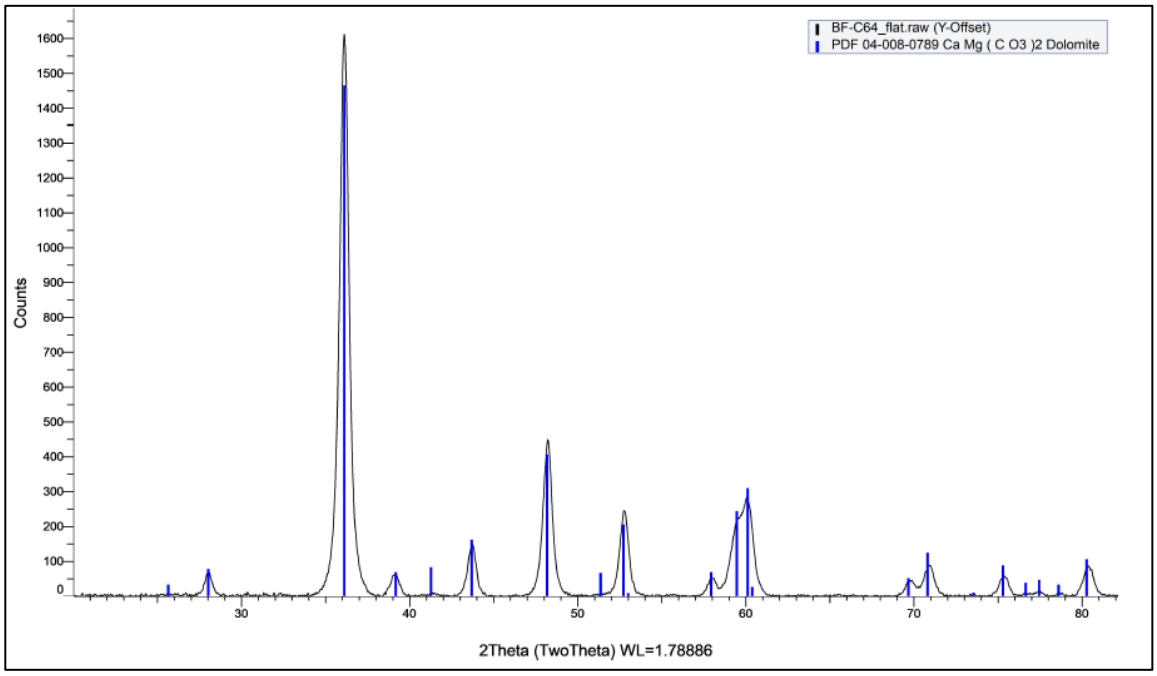

Figure S16. XRD pattern for sample BF-6-4, obtained by CoKα radiation.

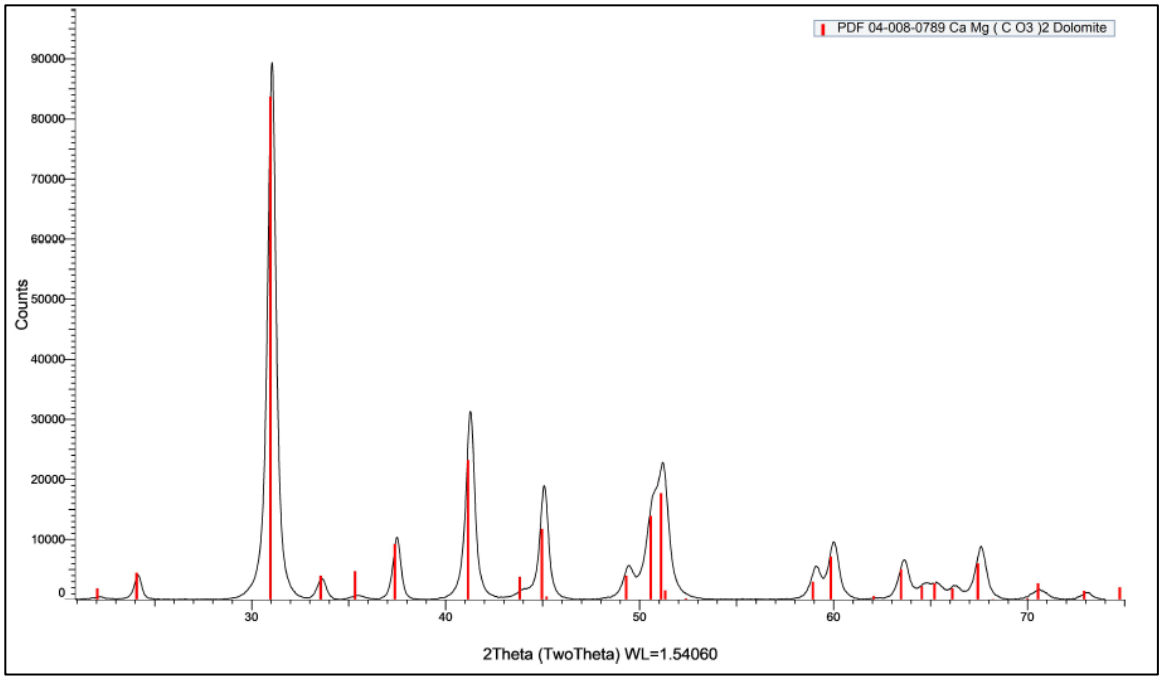

Figure S17. XRD pattern for sample BF-6-5, obtained by CuKα radiation.

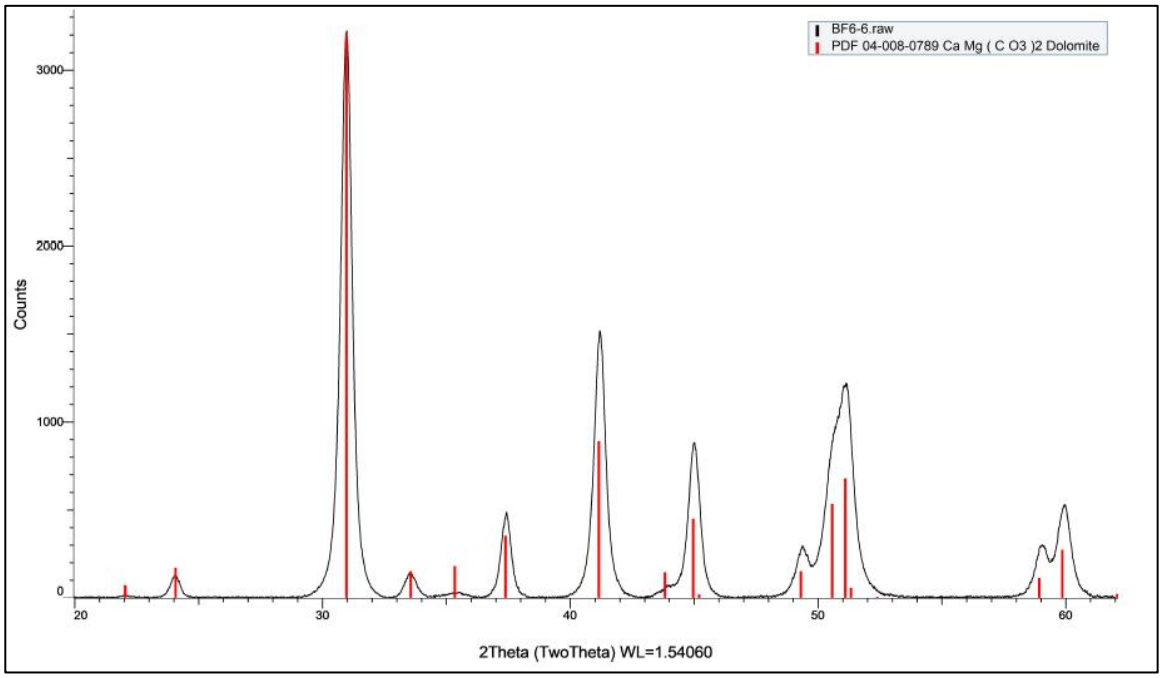

Figure S18. XRD pattern for sample BF-6-6, obtained by CuKα radiation.

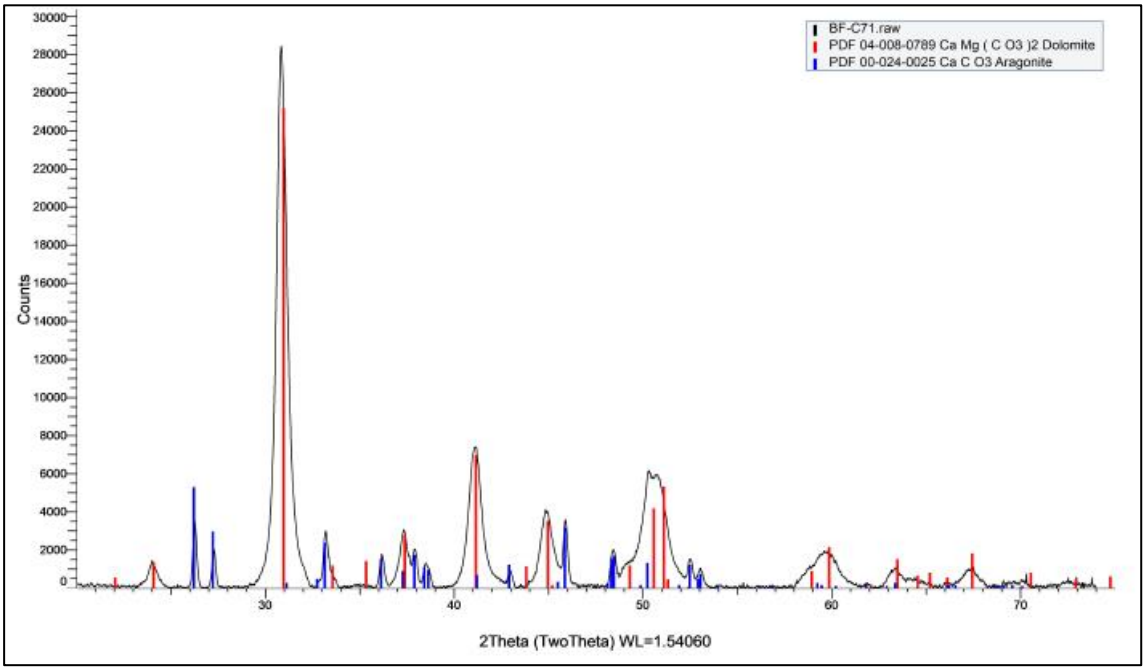

Figure S19. XRD pattern for sample BF-7-1, obtained by CuKα radiation.

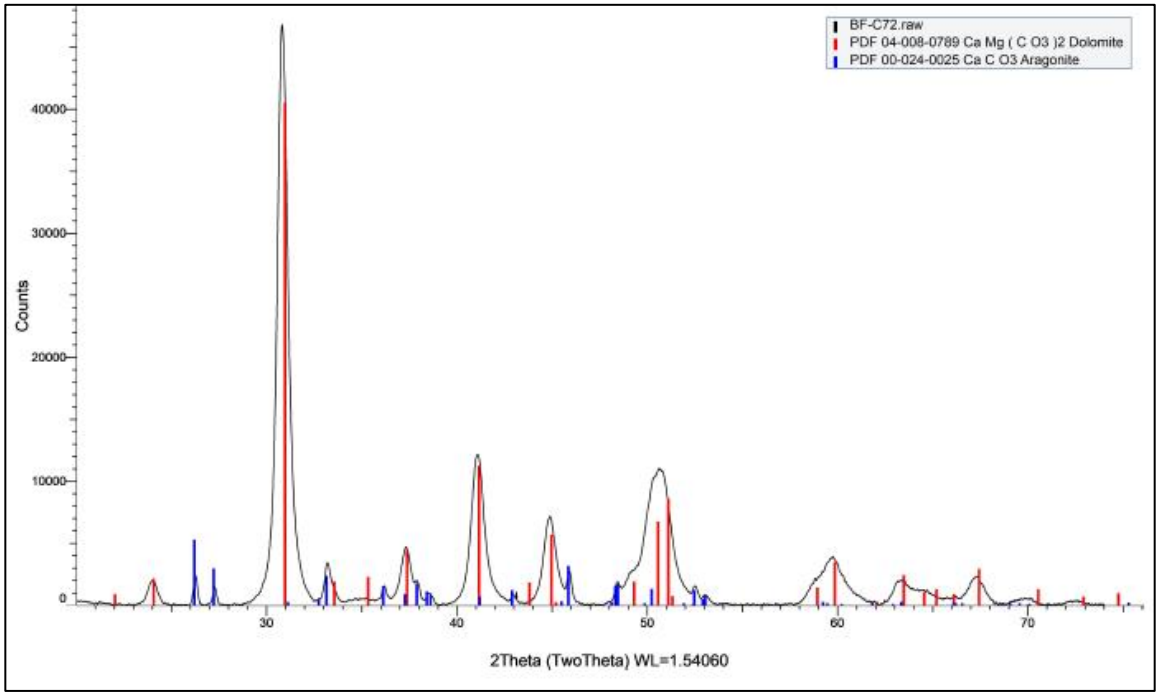

Figure S20. XRD pattern for sample BF-7-2, obtained by CuKα radiation.

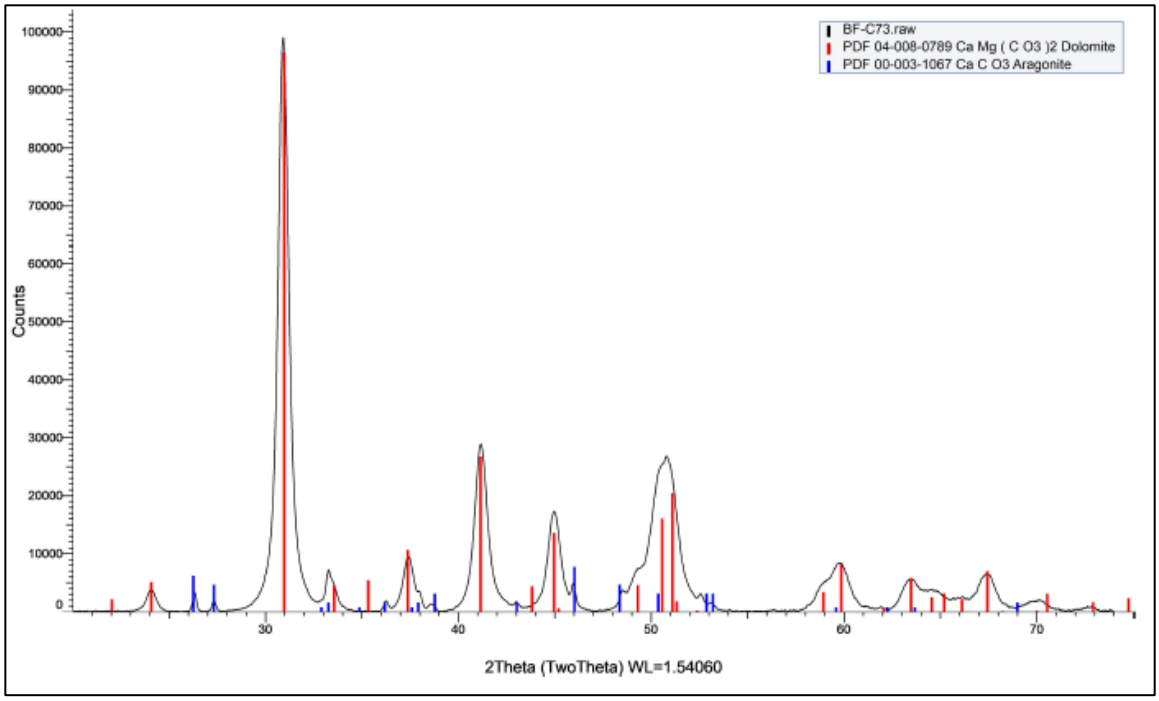

Figure S21. XRD pattern for sample BF-7-3, obtained by CuKα radiation.

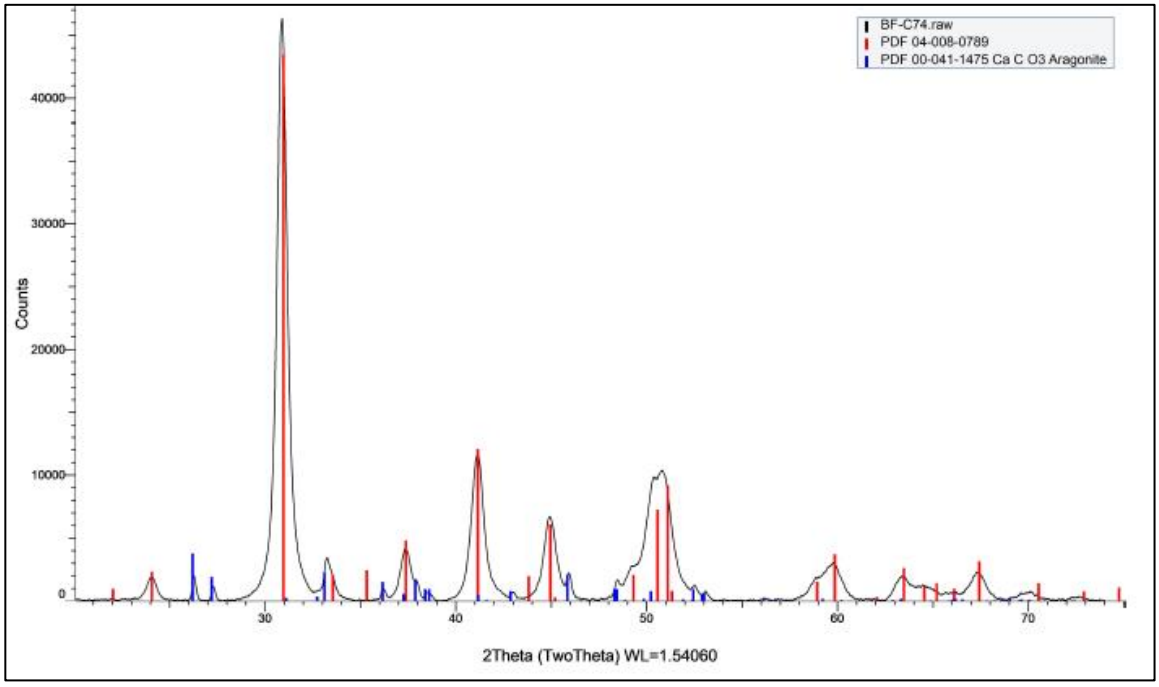

Figure S22. XRD pattern for sample BF-7-4, obtained by CuKα radiation.

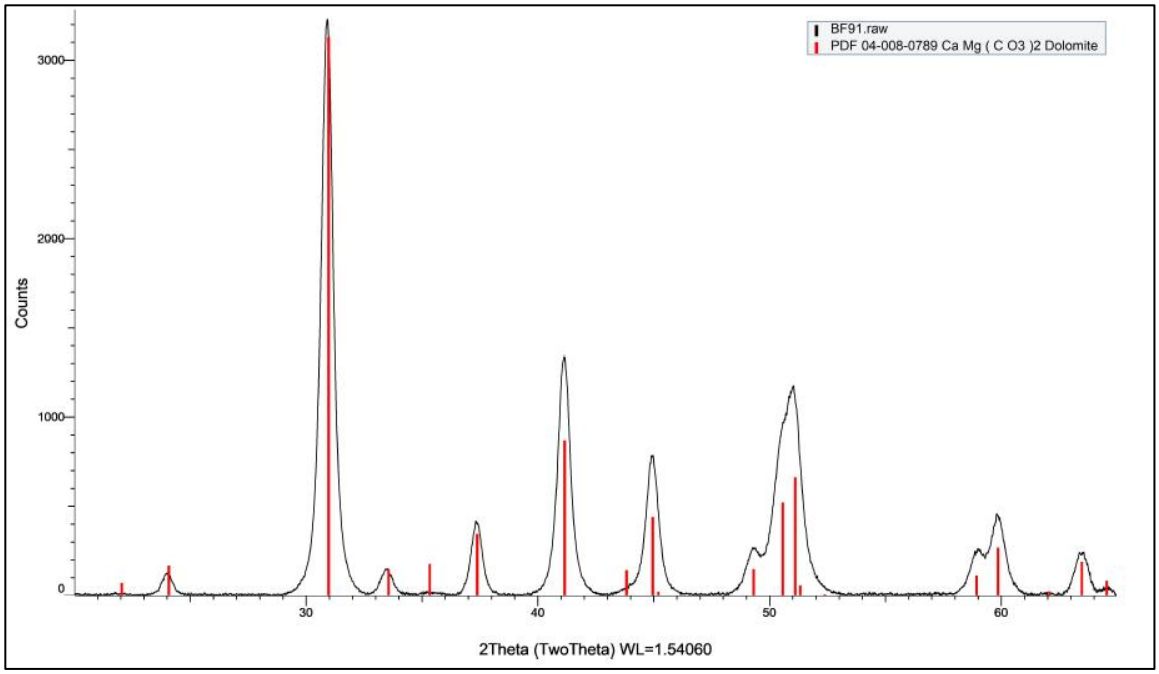

Figure S23. XRD pattern for sample BF-9-1, obtained by CuKα radiation.

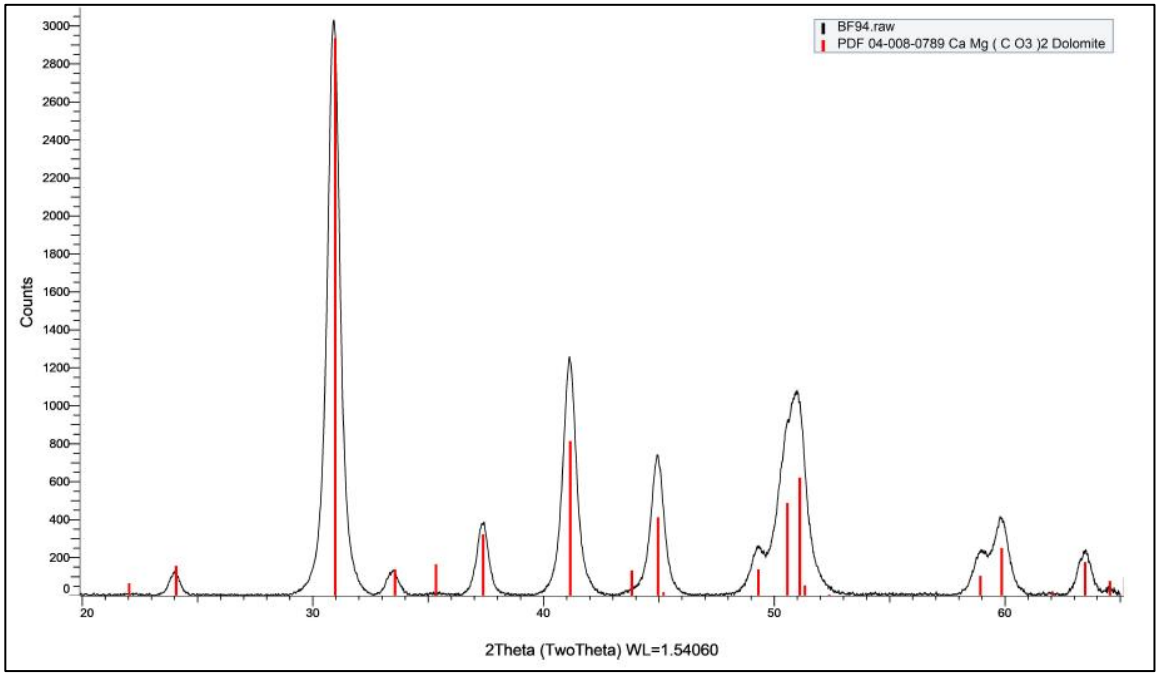

Figure S24. XRD pattern for sample BF-9-4, obtained by CuKα radiation.

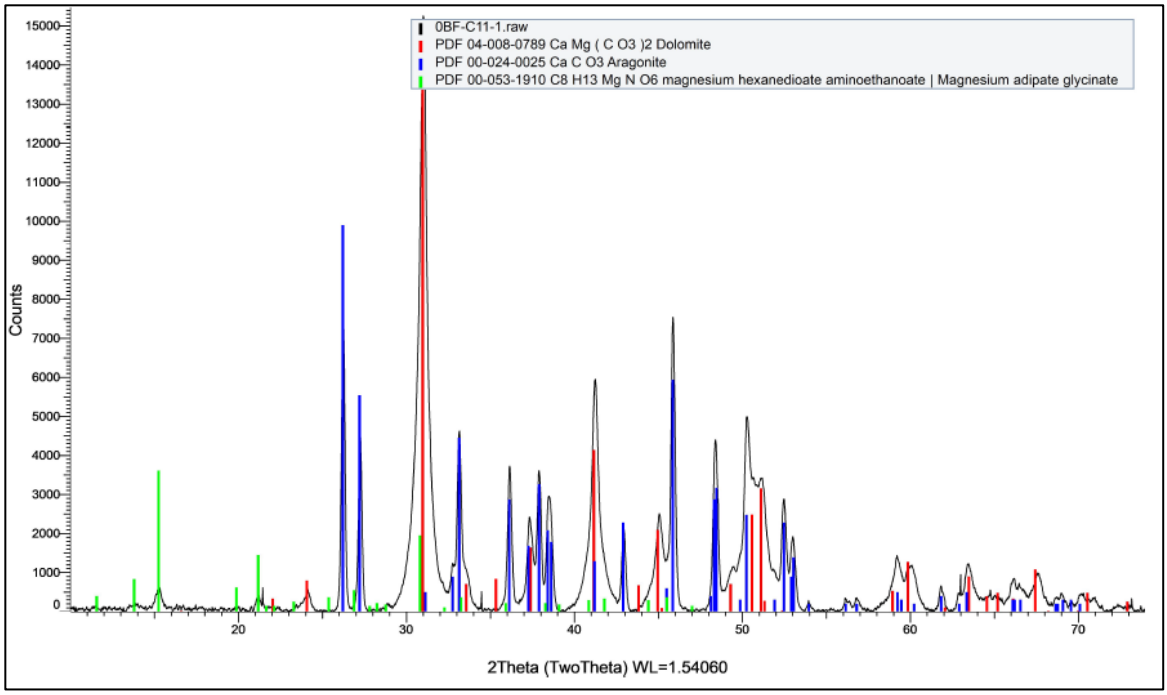

Figure S25. XRD pattern for BF-11-1, obtained by CuKα radiation.

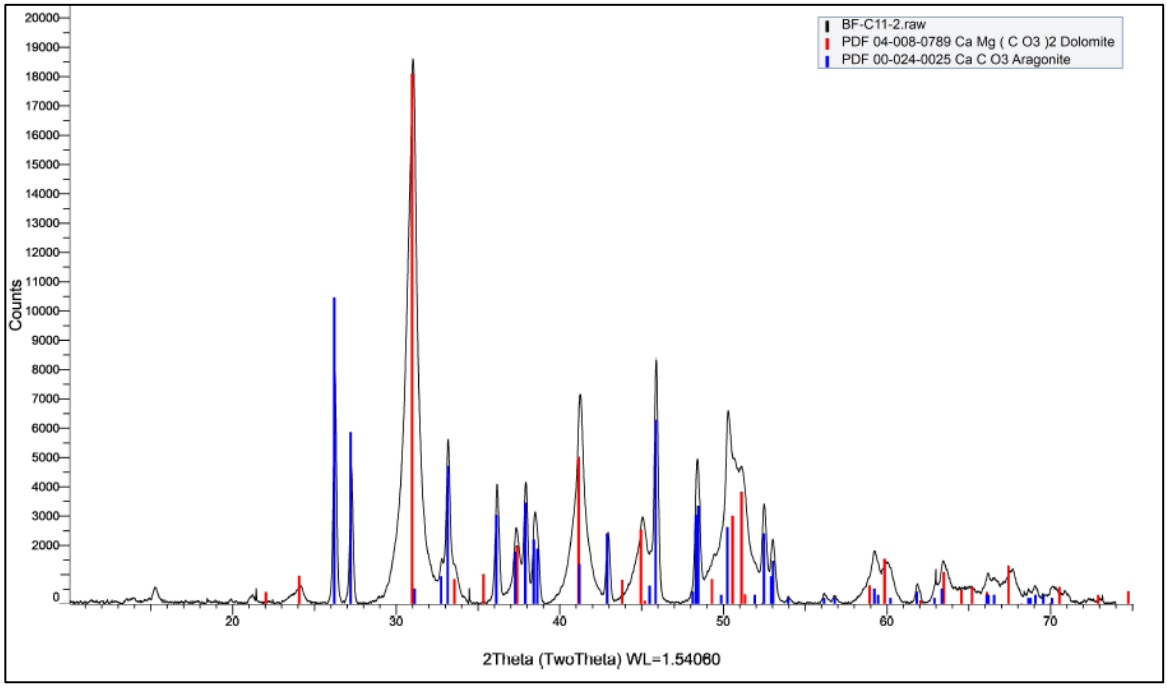

Figure S26. XRD pattern for BF-11-2, obtained by CuKα radiation.

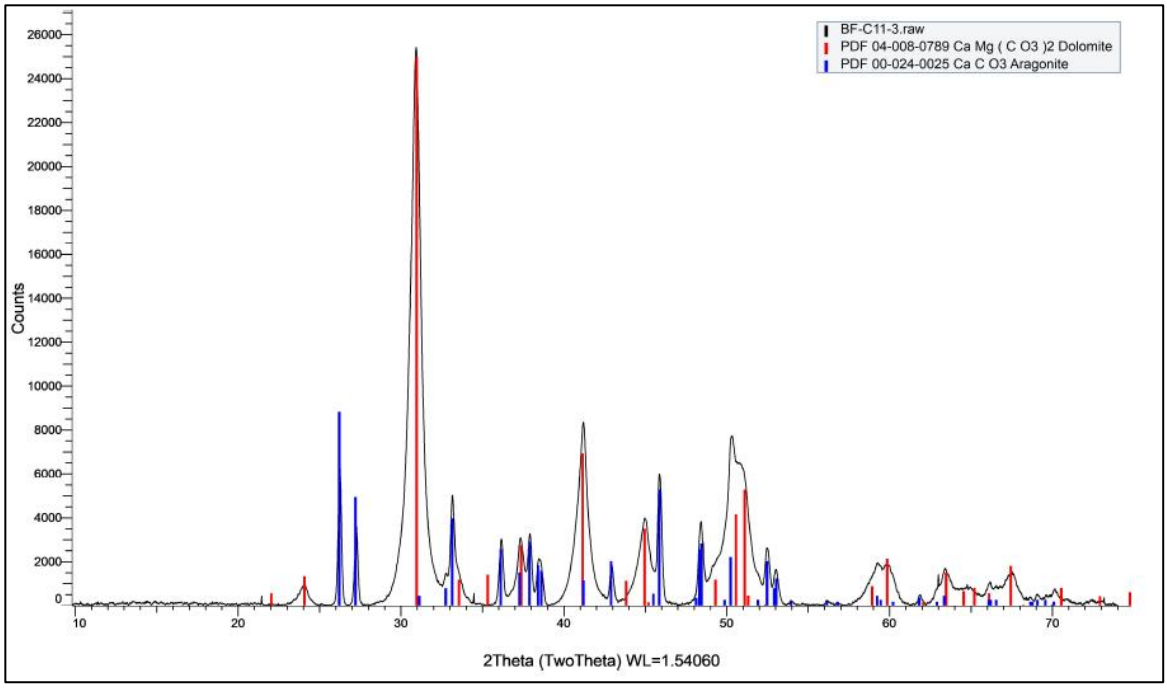

Figure S27. XRD pattern for BF-11-3, obtained by CuKα radiation.

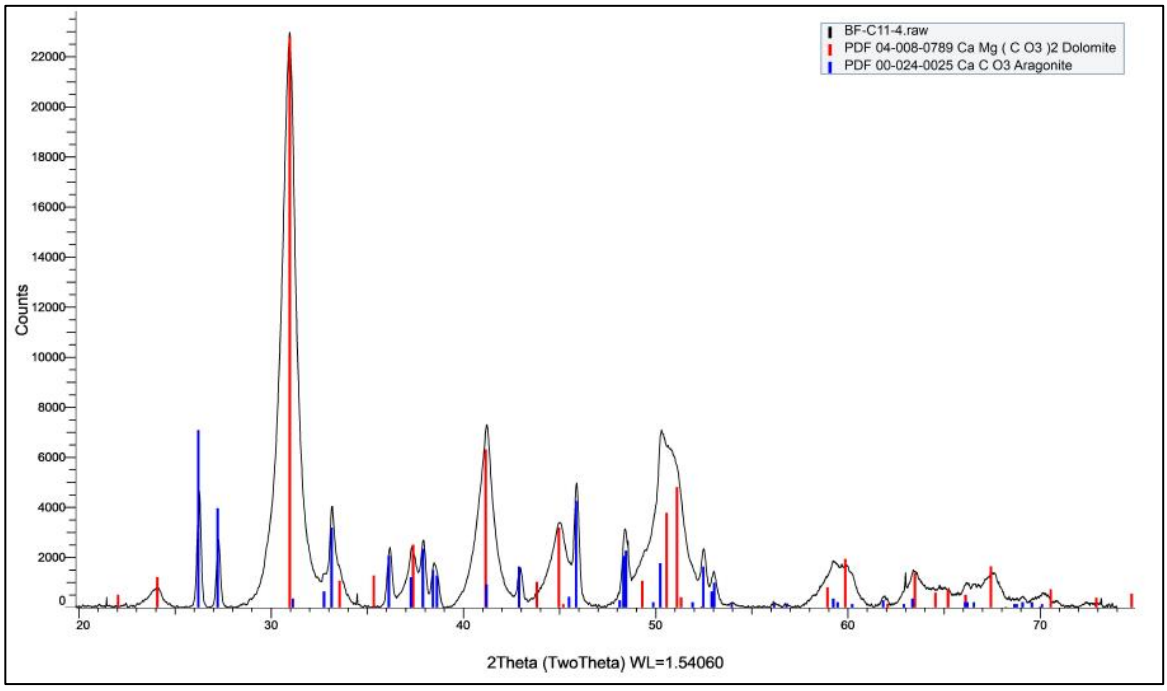

Figure S28. XRD pattern for BF-11-4, obtained by CuKα radiation.

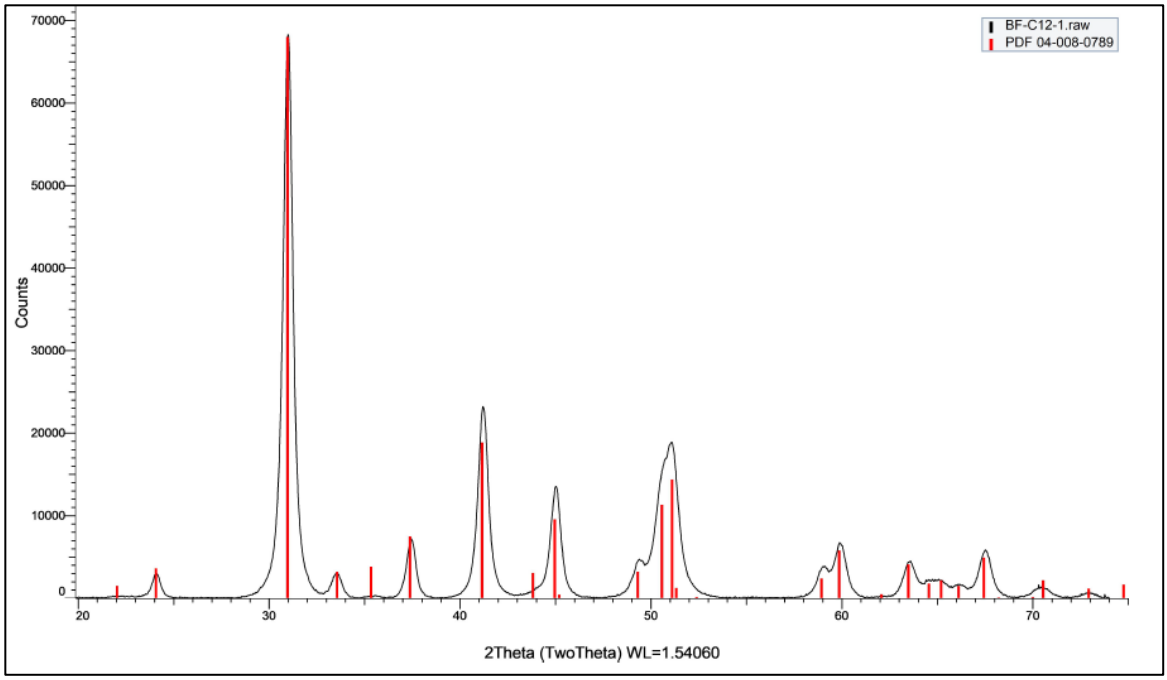

Figure S29. XRD pattern for BF-12-1, obtained by CuKα radiation.

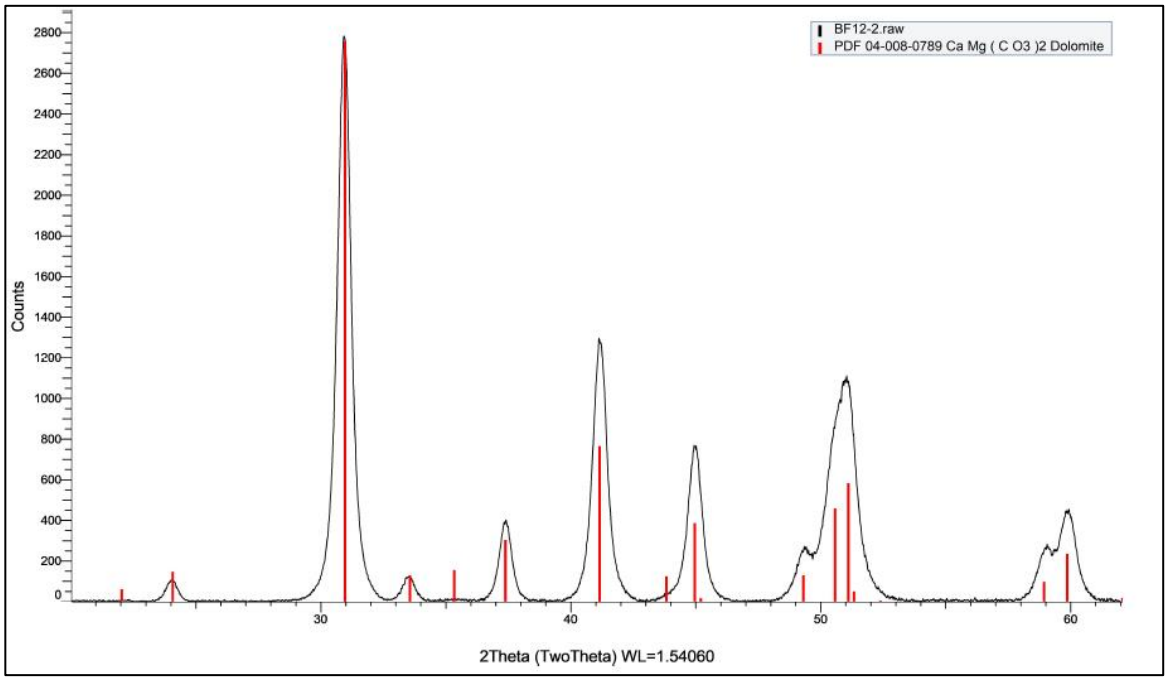

Figure S30. XRD pattern for BF-12-2, obtained by CuKα radiation.

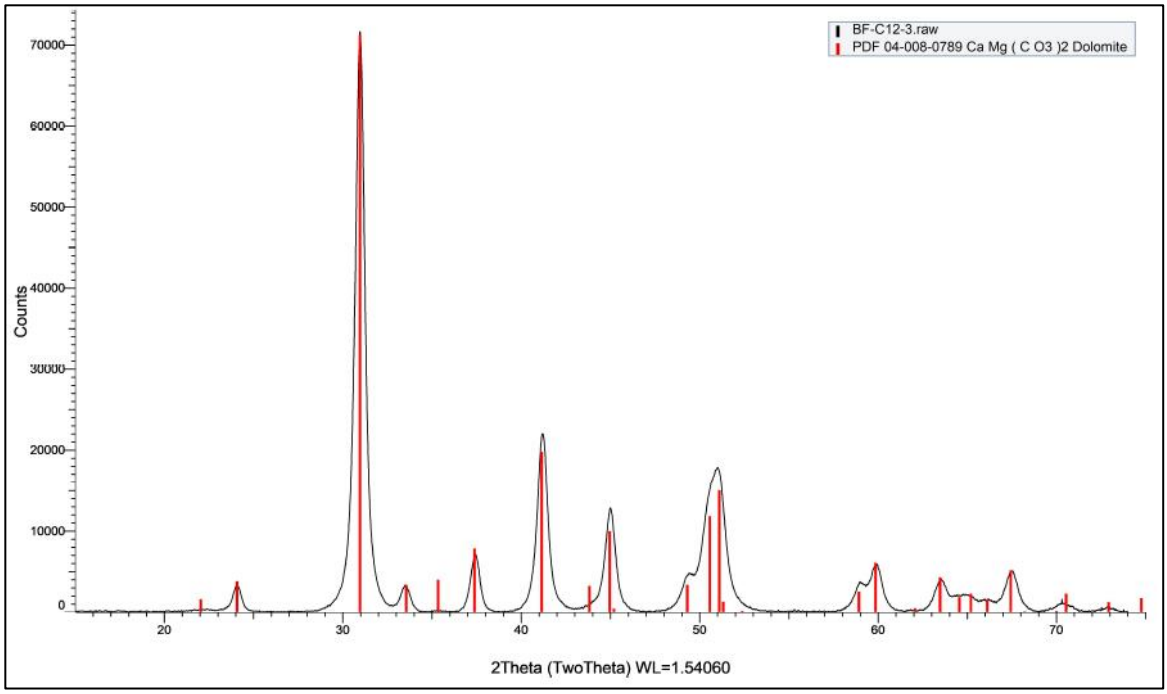

Figure S31. XRD pattern for BF-12-3, obtained by CuKα radiation.

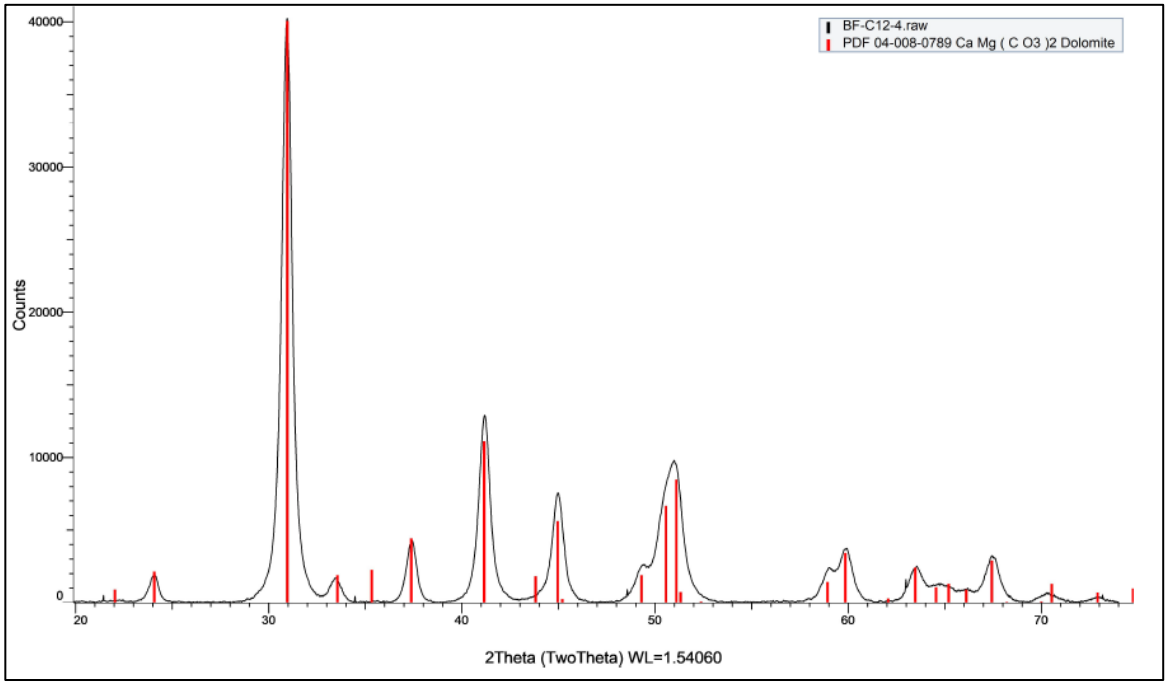

Figure S32. XRD pattern for BF-12-4, obtained by CuKα radiation.

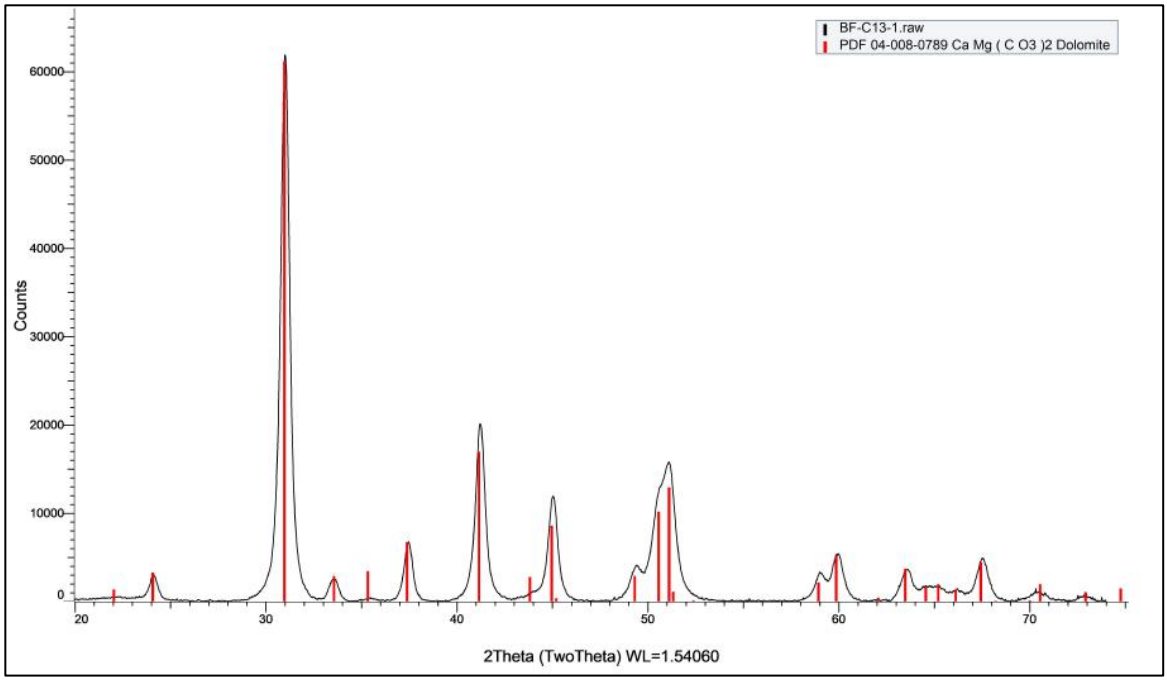

Figure S33. XRD pattern for BF-13-1, obtained by CuKα radiation.

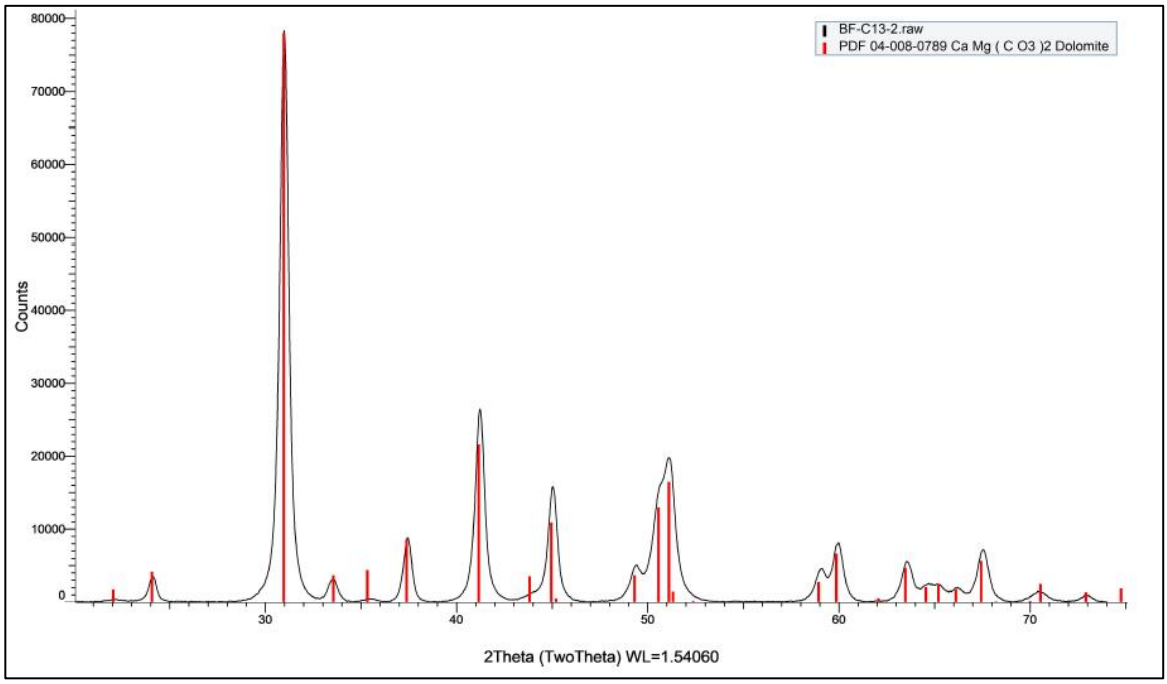

Figure S34. XRD pattern for BF-13-2, obtained by CuKα radiation.

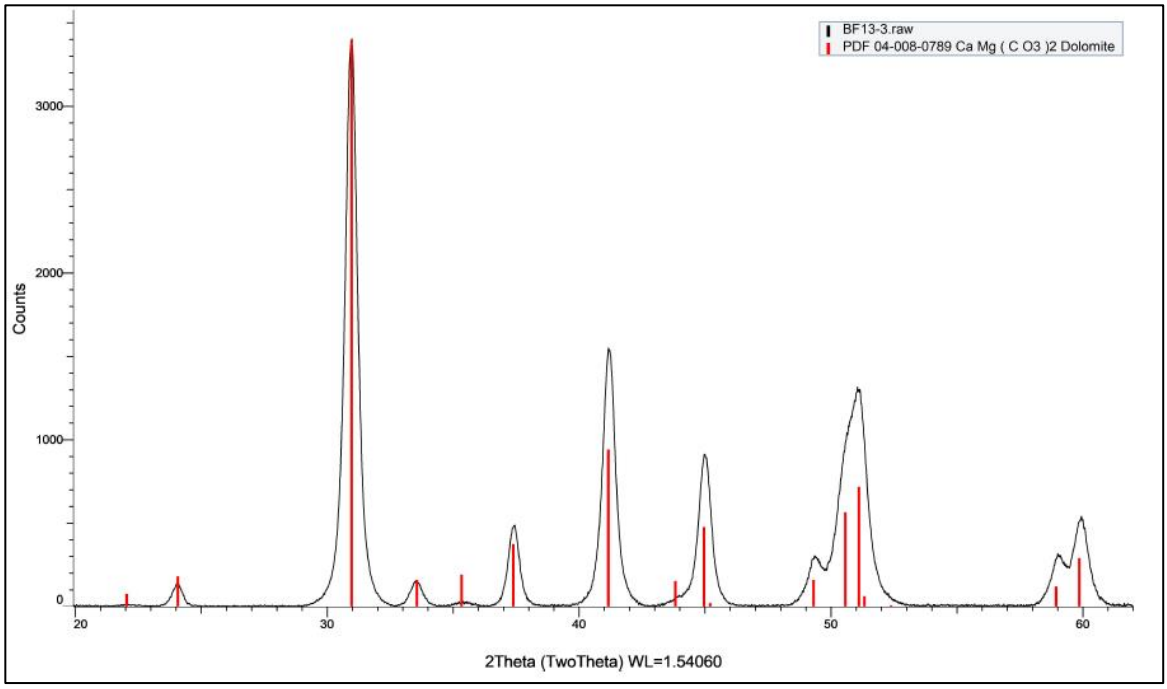

Figure S35. XRD pattern for BF-13-3, obtained by CuKα radiation.

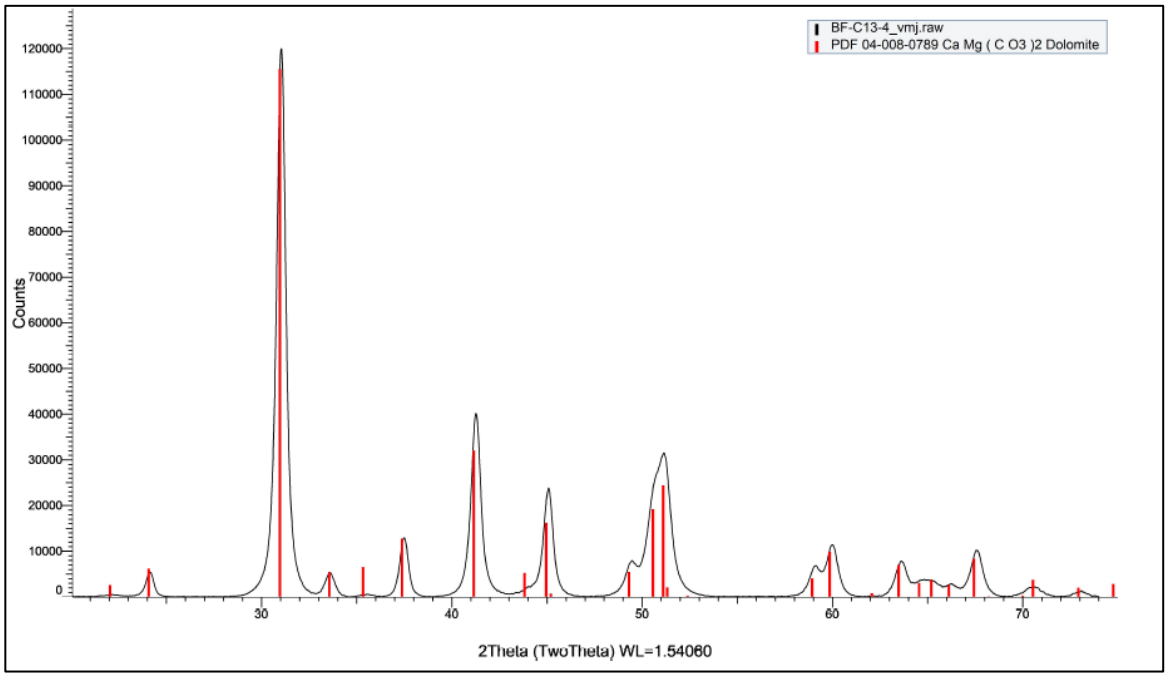

Figure S36. XRD pattern for BF-13-4, obtained by CuKα radiation.

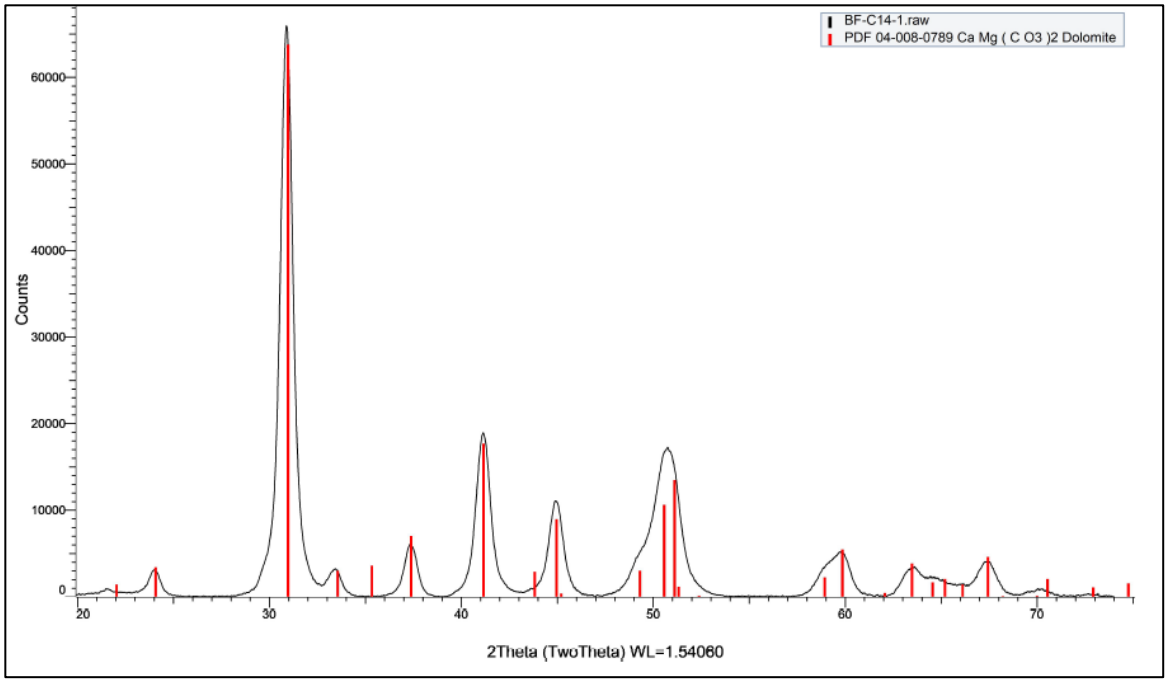

Figure S37. XRD pattern for BF-14-1, obtained by CuKα radiation.

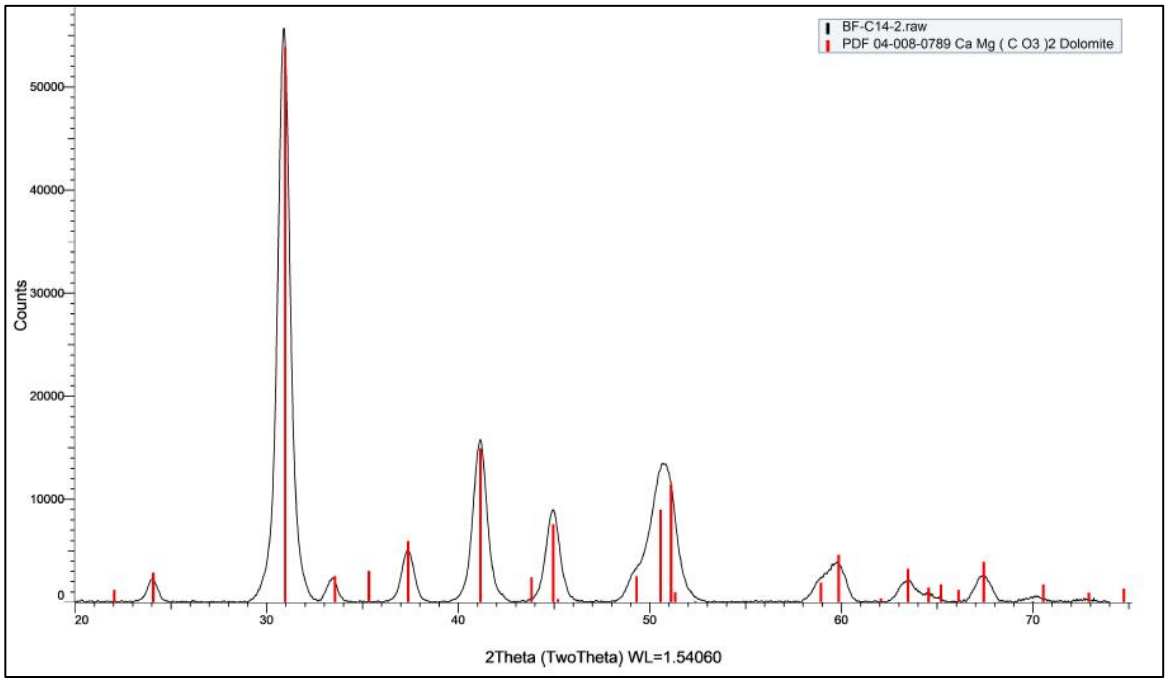

Figure S38. XRD pattern for BF-14-2, obtained by CuKα radiation.

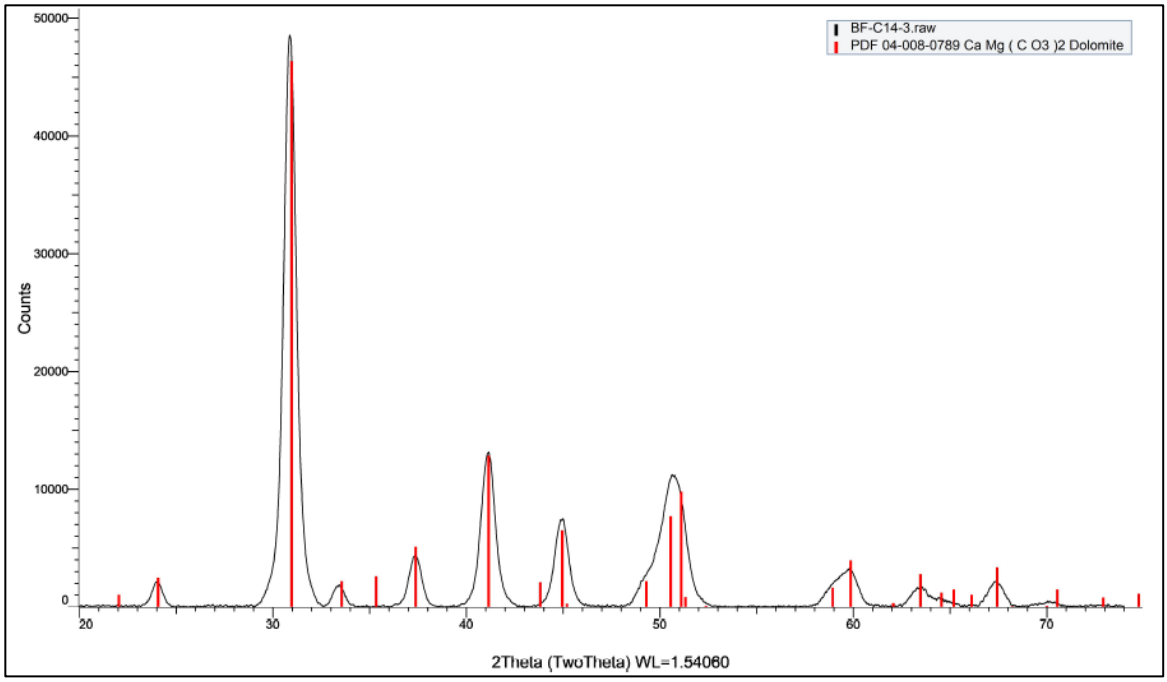

Figure S39. XRD pattern for BF-14-3, obtained by CuKα radiation.

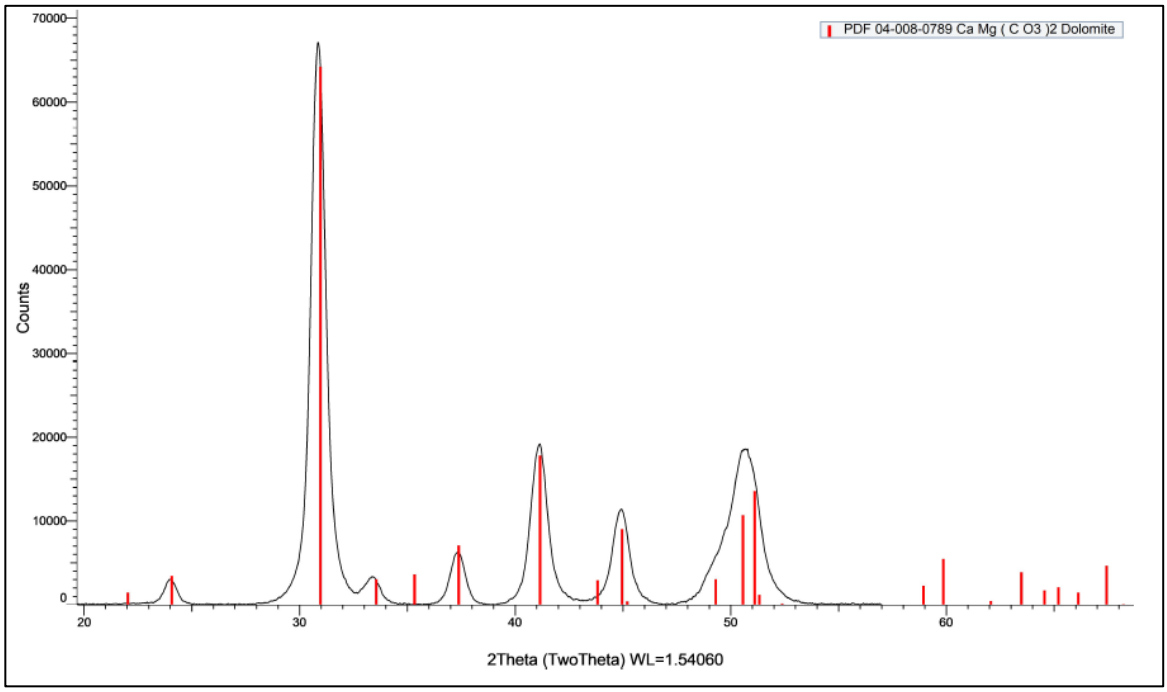

Figure S40. XRD pattern for BF-14-4, obtained by CuKα radiation.

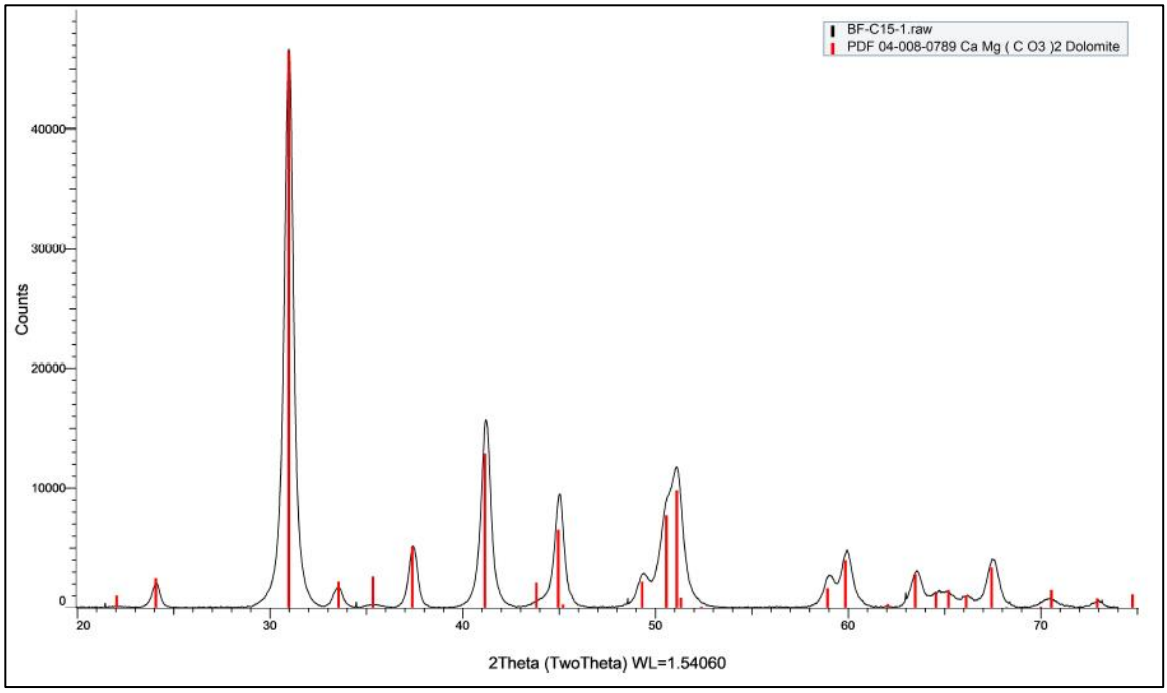

Figure S41. XRD pattern for BF-15-1, obtained by CuKα radiation.

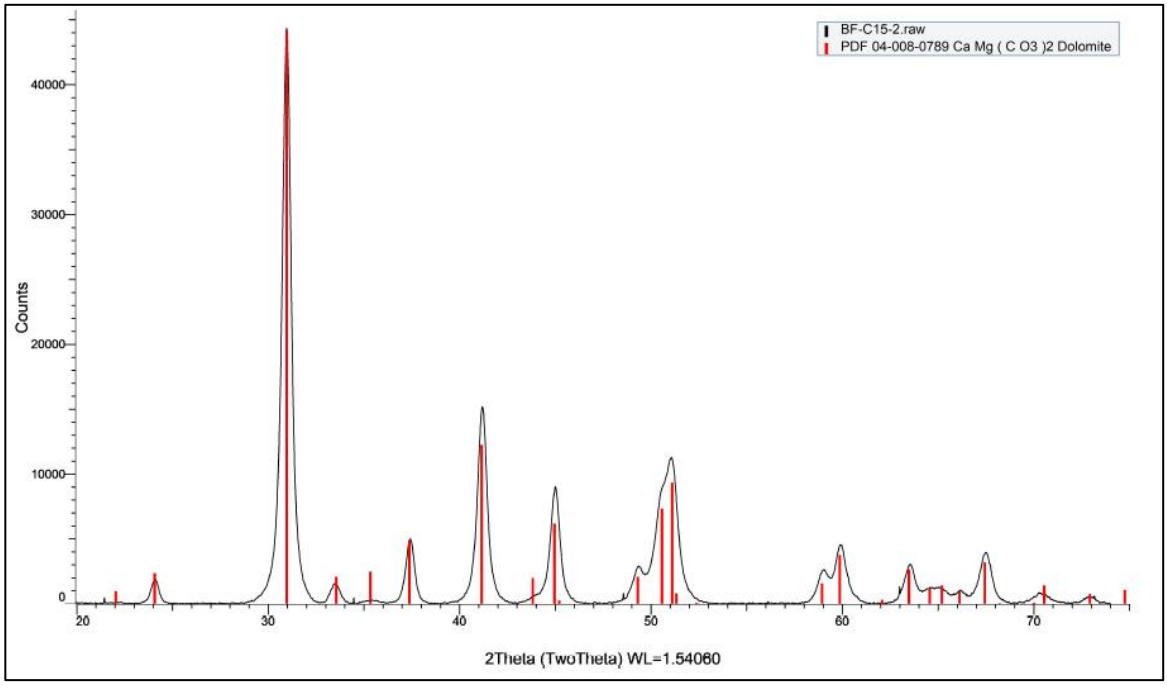

Figure S42. XRD pattern for BF-15-2, obtained by CuKα radiation.

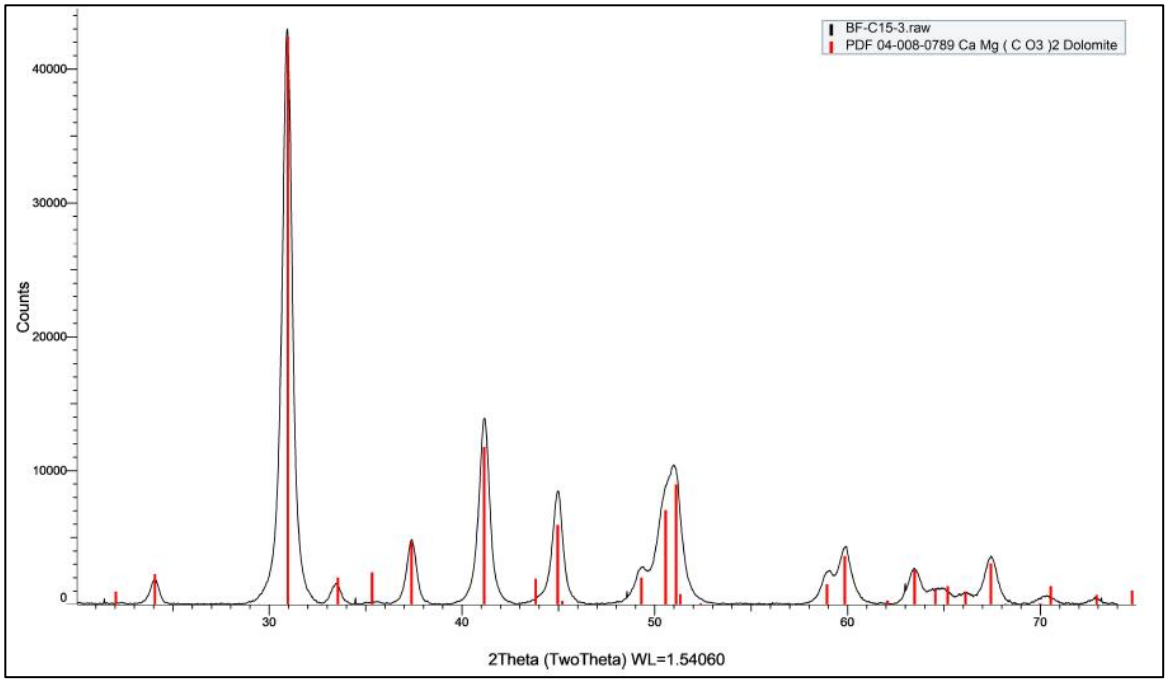

Figure S43. XRD pattern for BF-15-3, obtained by CuKα radiation.

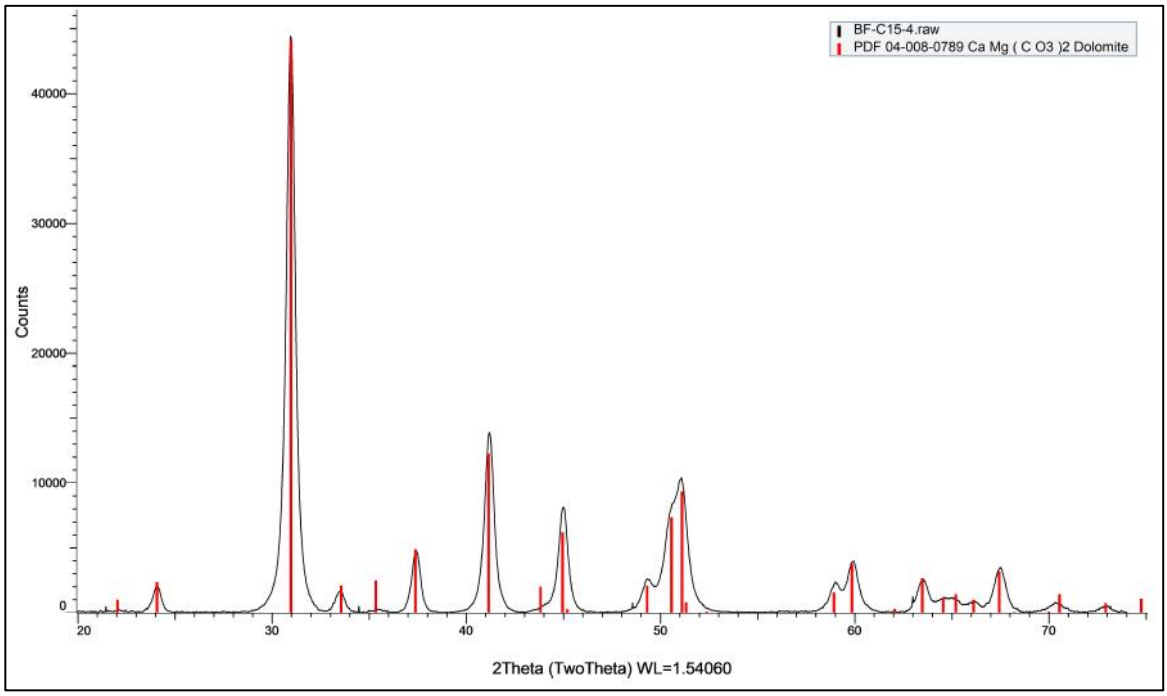

Figure S44. XRD pattern for BF-15-4, obtained by CuKα radiation.

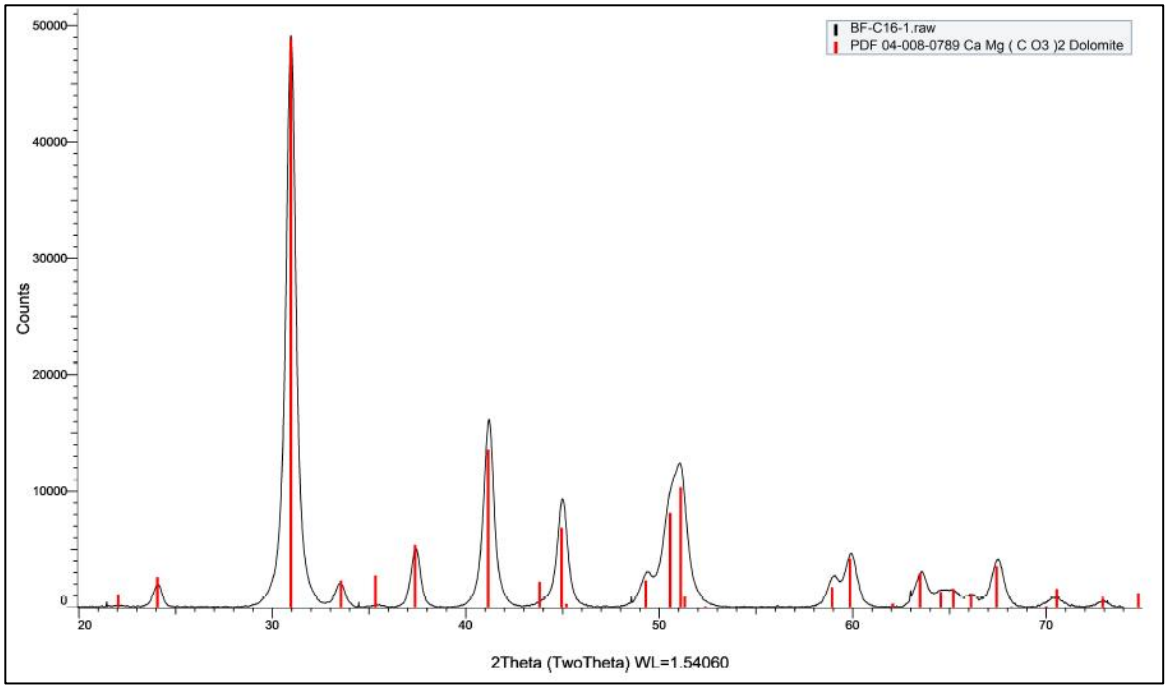

Figure S45. XRD pattern for BF-16-1, obtained by CuKα radiation.

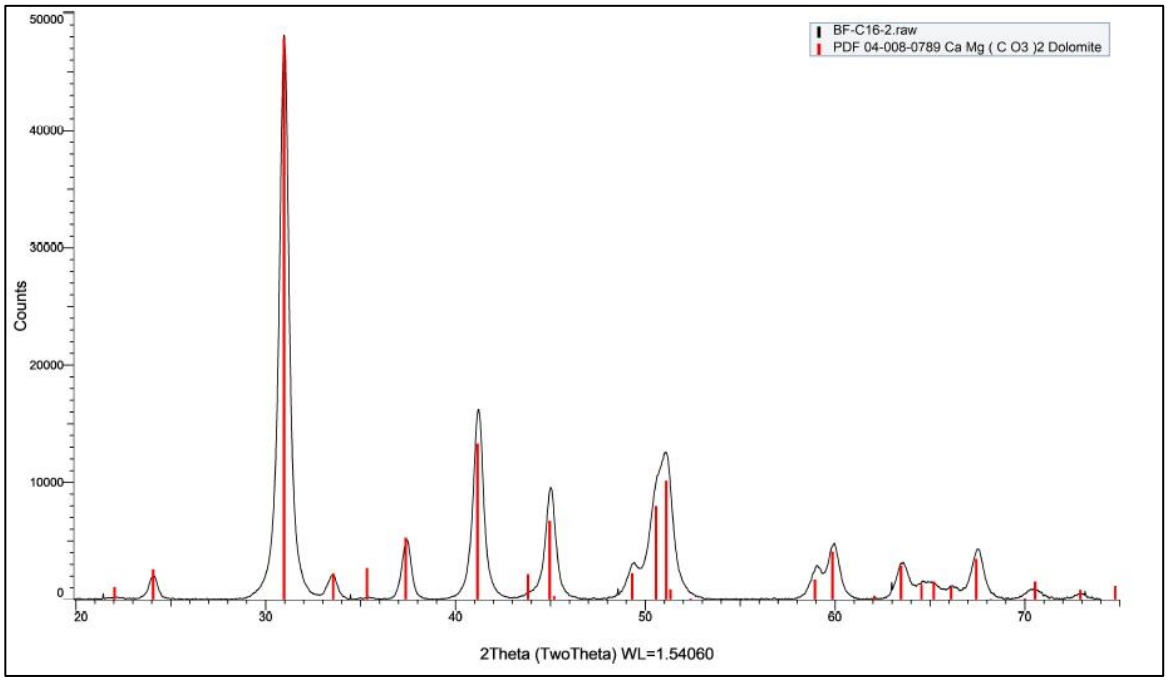

Figure S46. XRD pattern for BF-16-2, obtained by CuKα radiation.

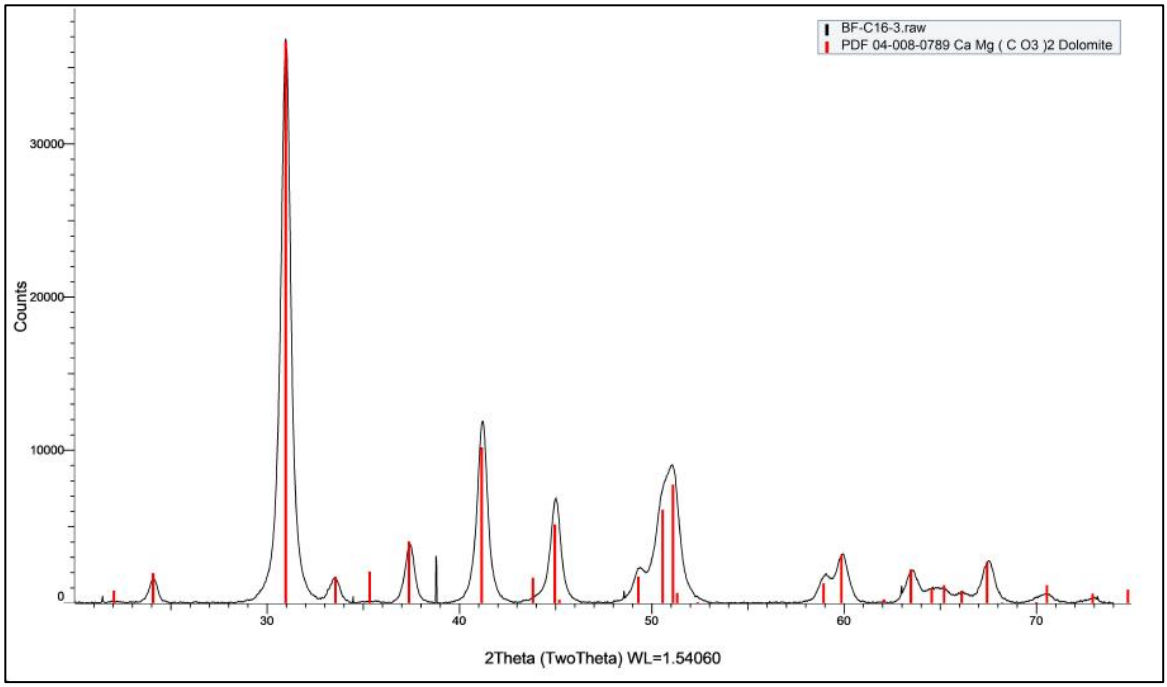

Figure S47. XRD pattern for BF-16-3, obtained by CuKα radiation.

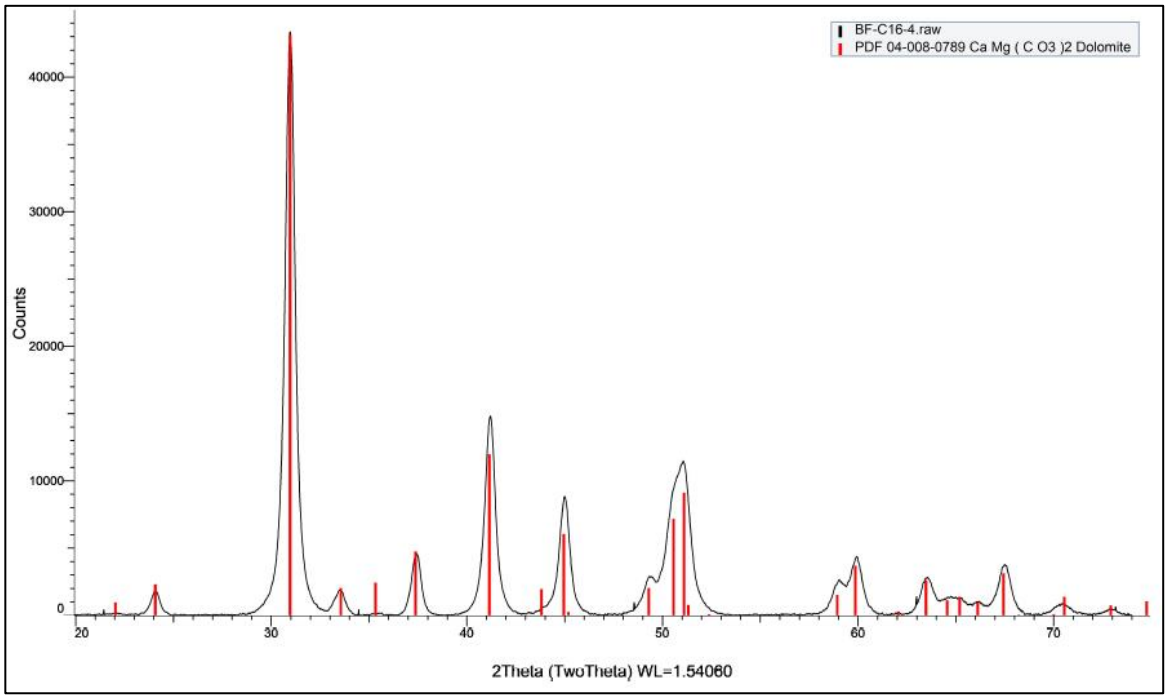

Figure S48. XRD pattern for BF-16-4, obtained by CuKα radiation.

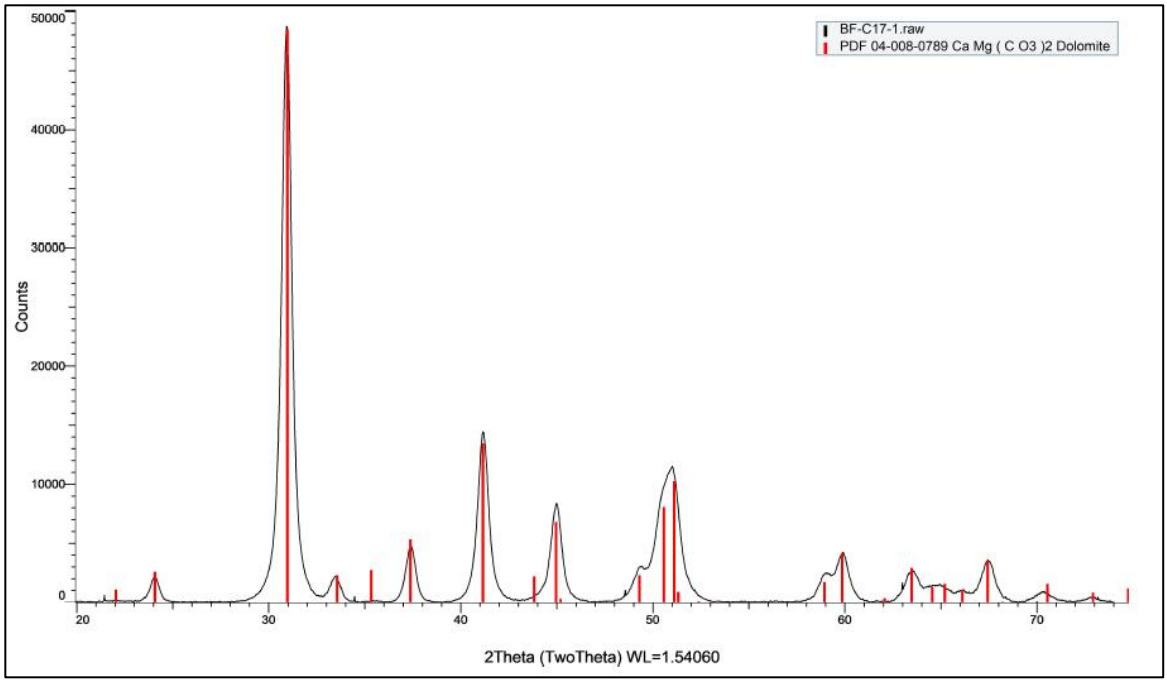

Figure S49. XRD pattern for BF-17-1, obtained by CuKα radiation.

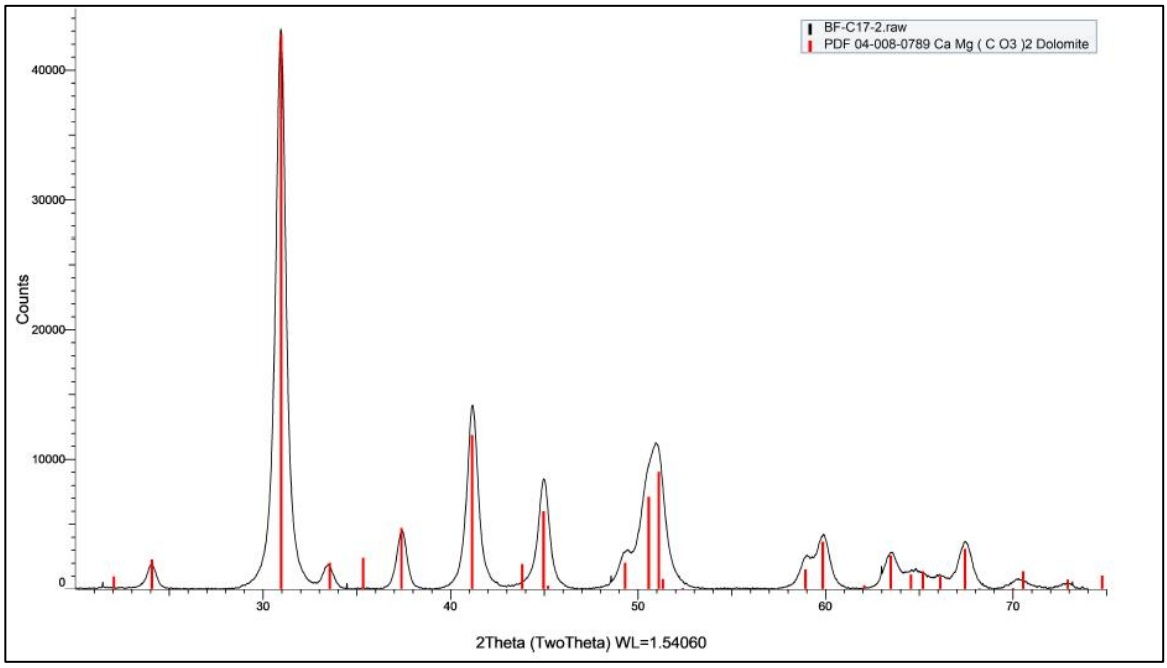

Figure S50. XRD pattern for BF-17-2, obtained by CuKα radiation.

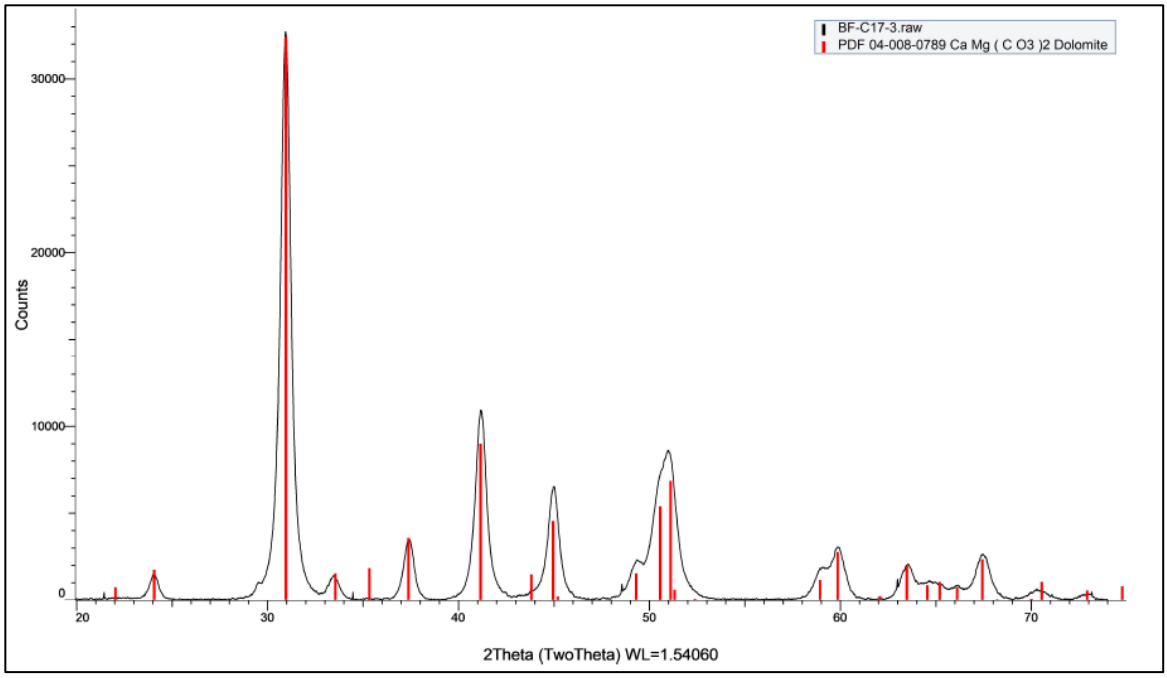

Figure S51. XRD pattern for BF-17-3, obtained by CuKα radiation.

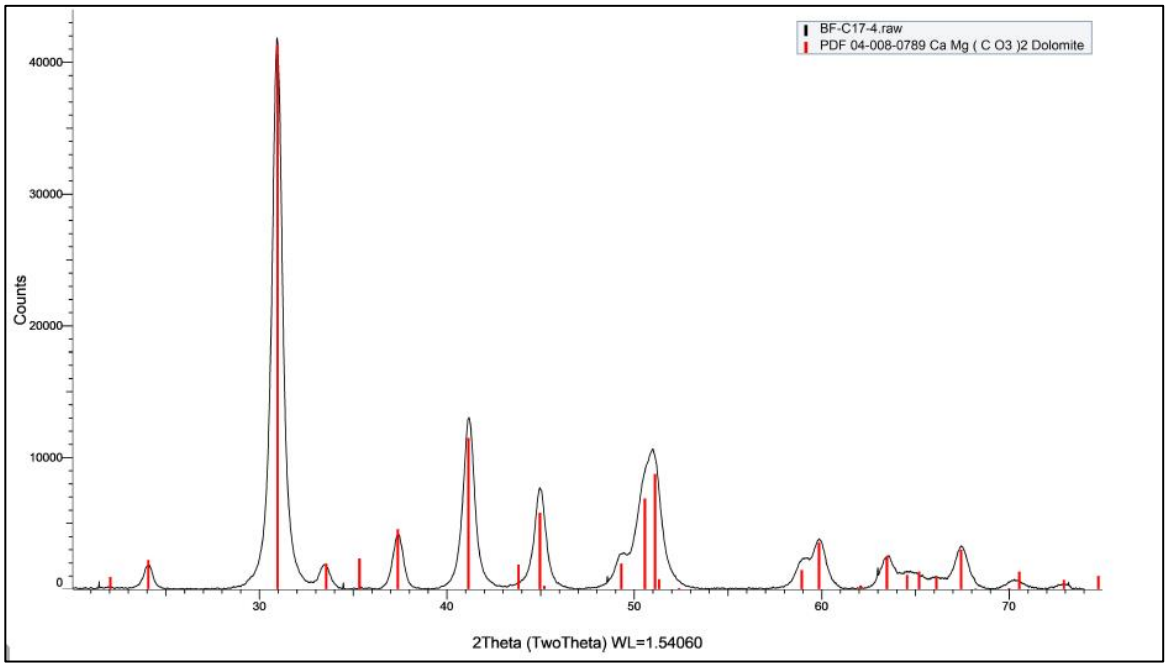

Figure S52. XRD pattern for BF-17-4, obtained by CuKα radiation.

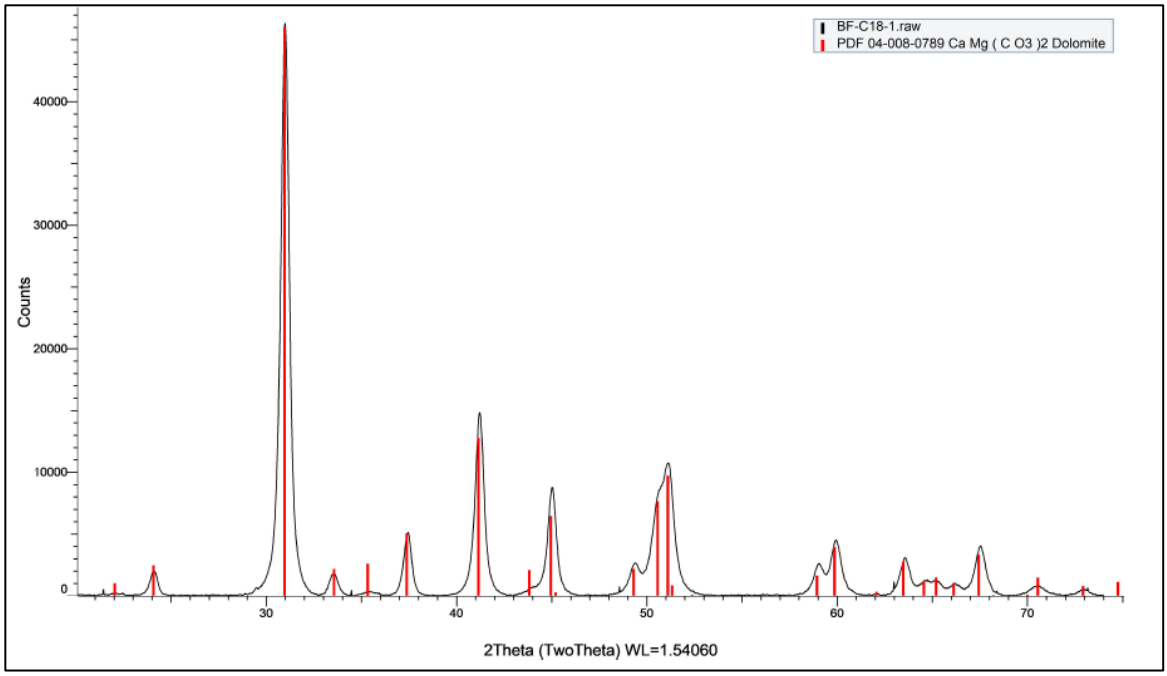

Figure S53. XRD pattern for BF-18-1, obtained by CuKα radiation.

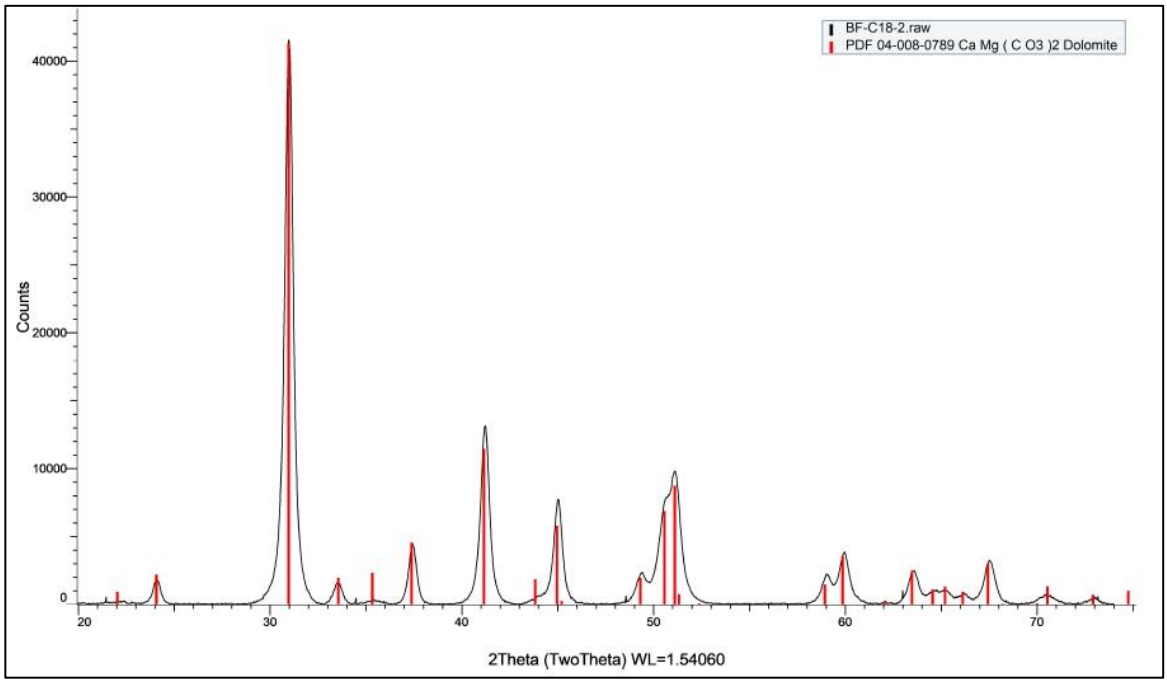

Figure S54. XRD pattern for BF-18-2, obtained by CuKα radiation.

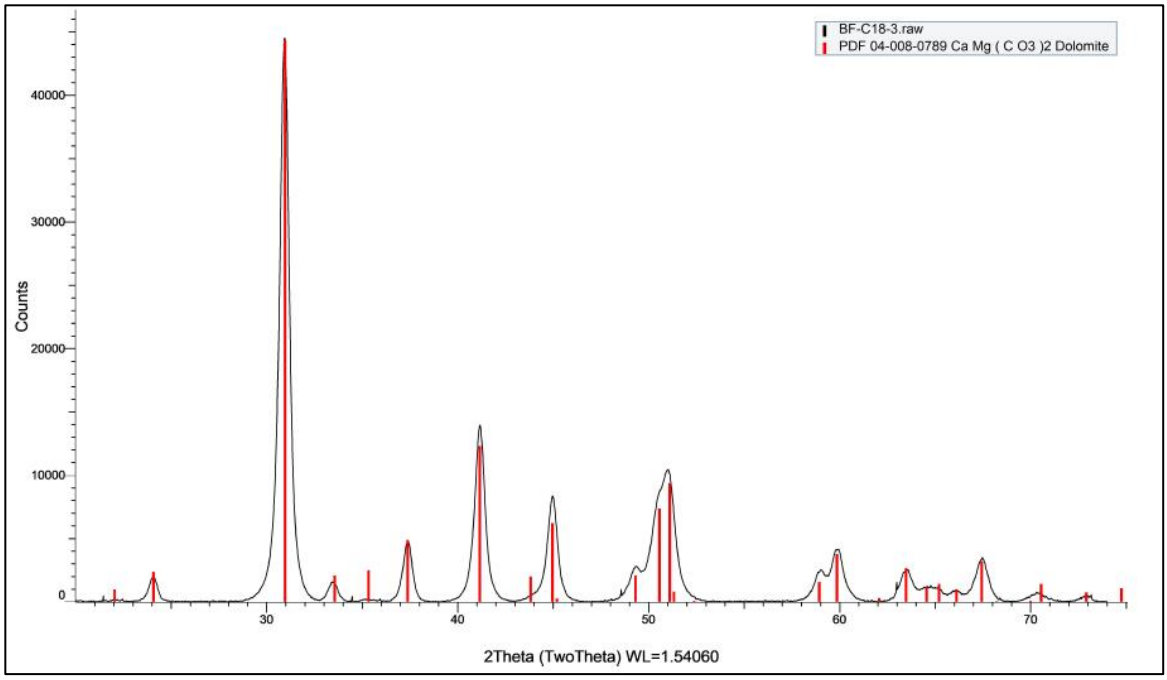

Figure S55. XRD pattern for BF-18-3, obtained by CuKα radiation.

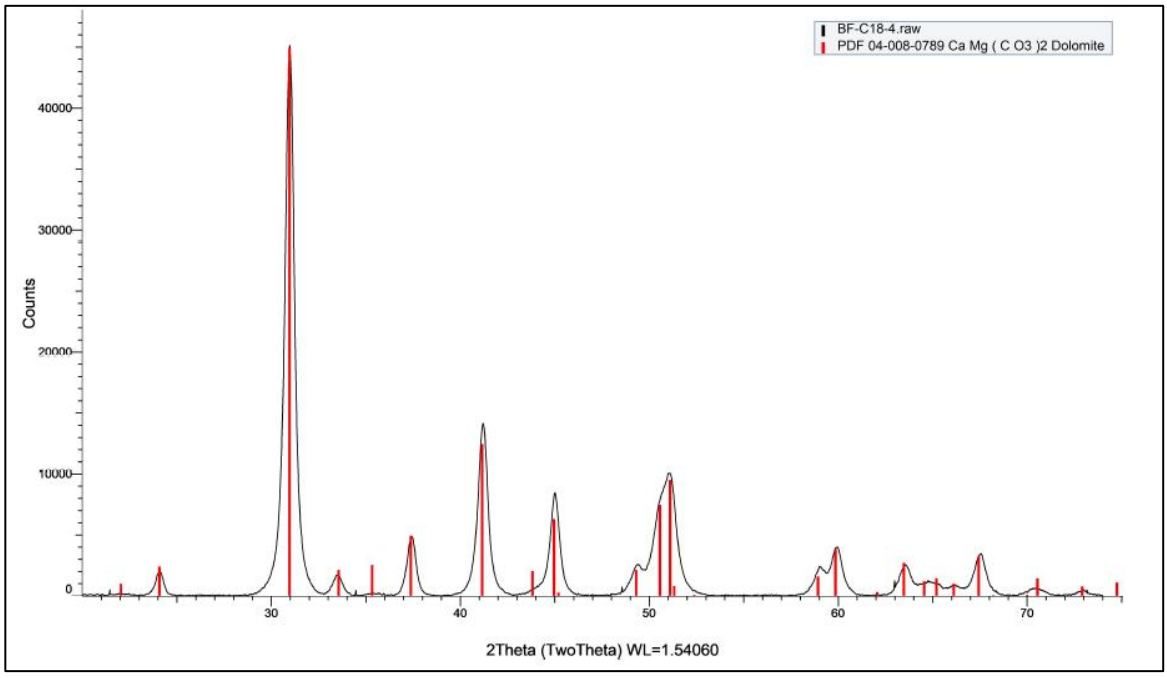

Figure S56. XRD pattern for BF-18-4, obtained by CuKα radiation.

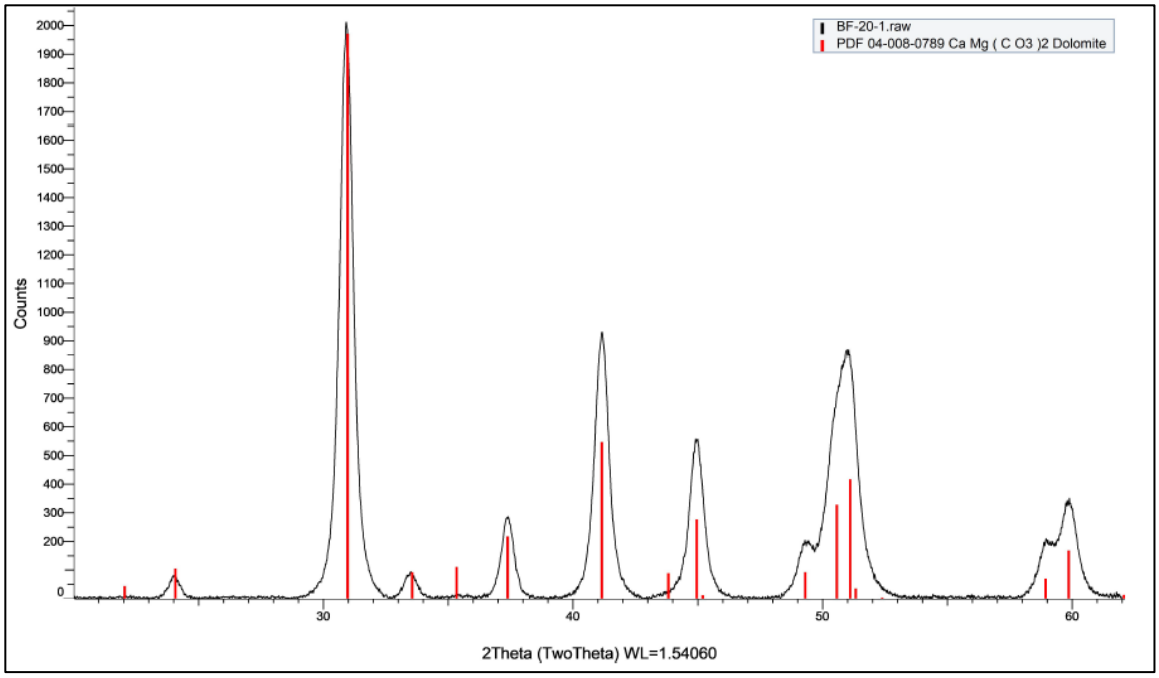

Figure S57. XRD pattern for BF-20-1, obtained by CuKα radiation.

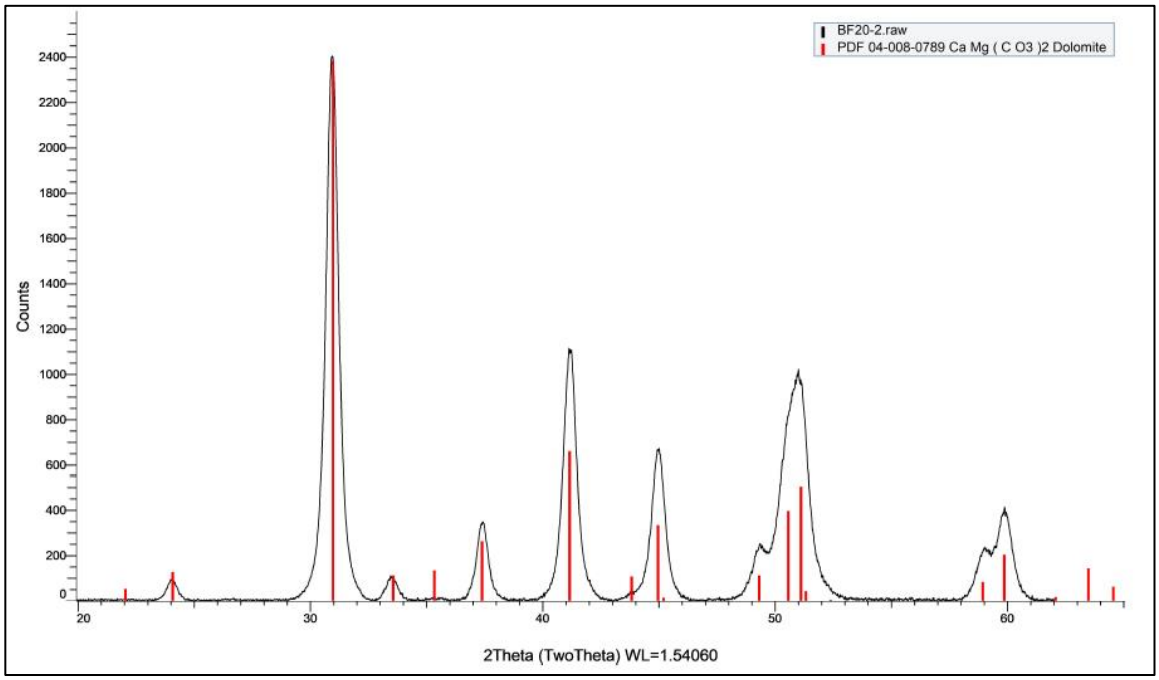

Figure S58. XRD pattern for BF-20-2, obtained by CuKα radiation.

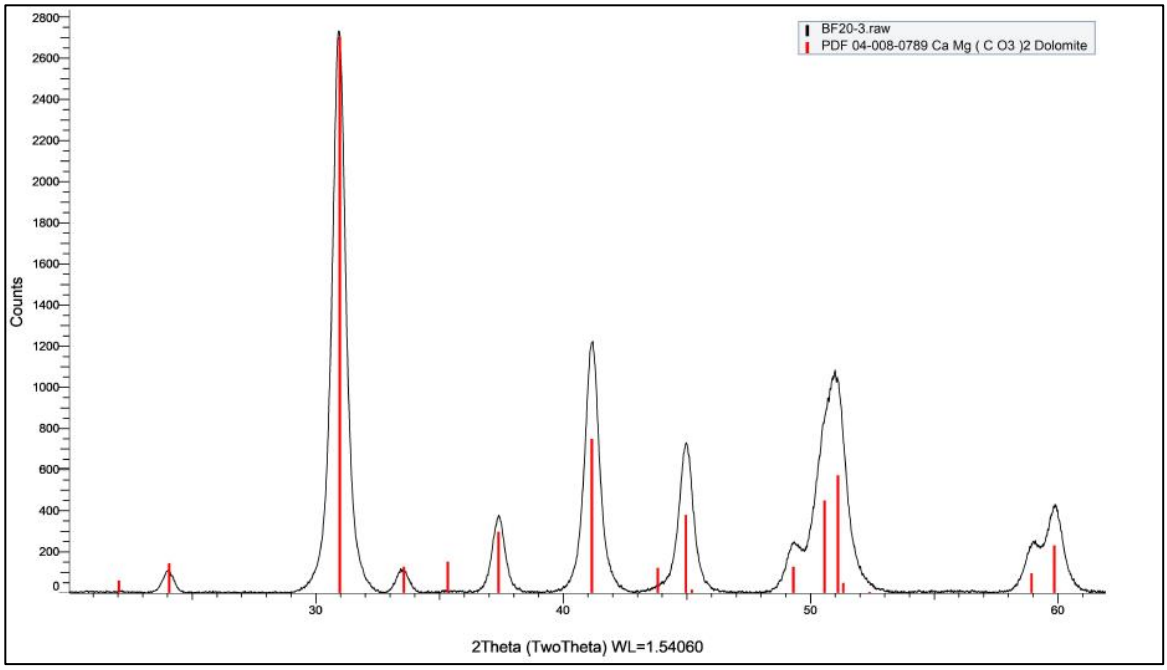

Figure S59. XRD pattern for BF-20-3, obtained by CuKα radiation.

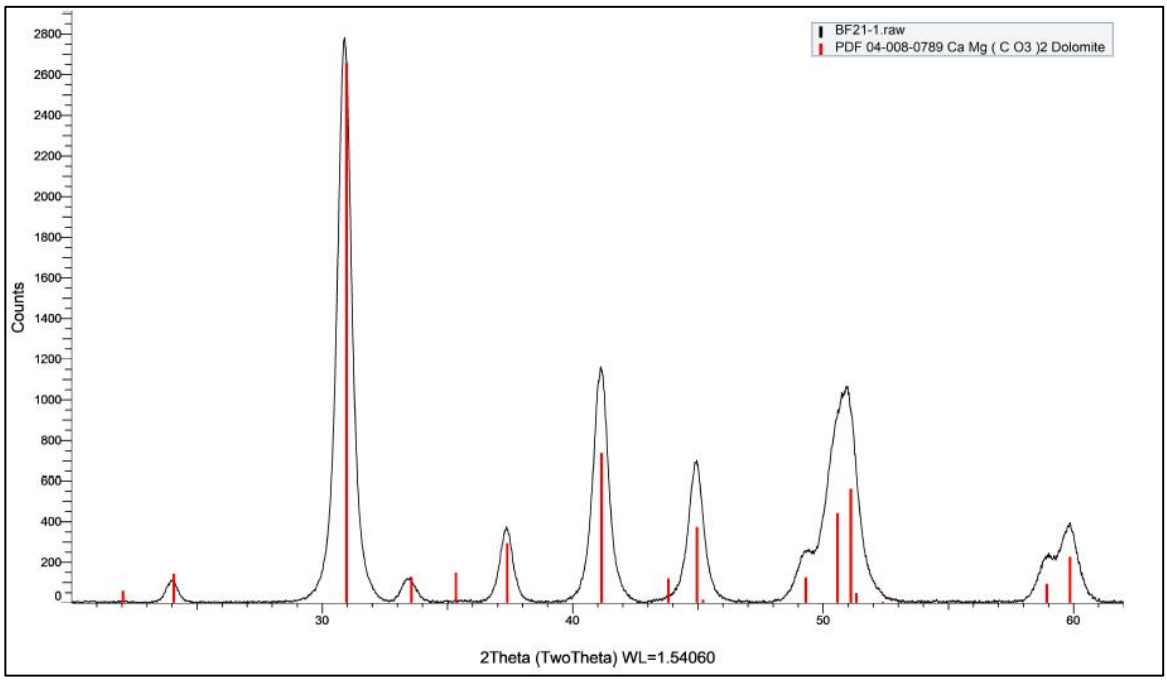

Figure S60. XRD pattern for BF-21-1, obtained by CuKα radiation.

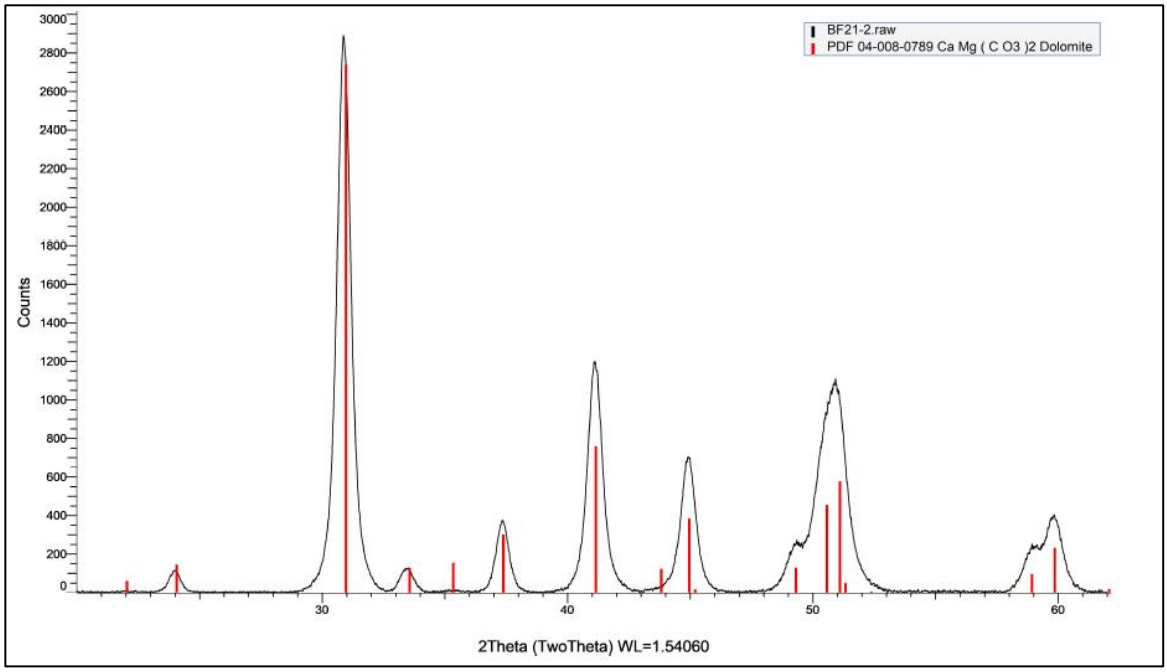

Figure S61. XRD pattern for BF-21-2, obtained by CuKα radiation.

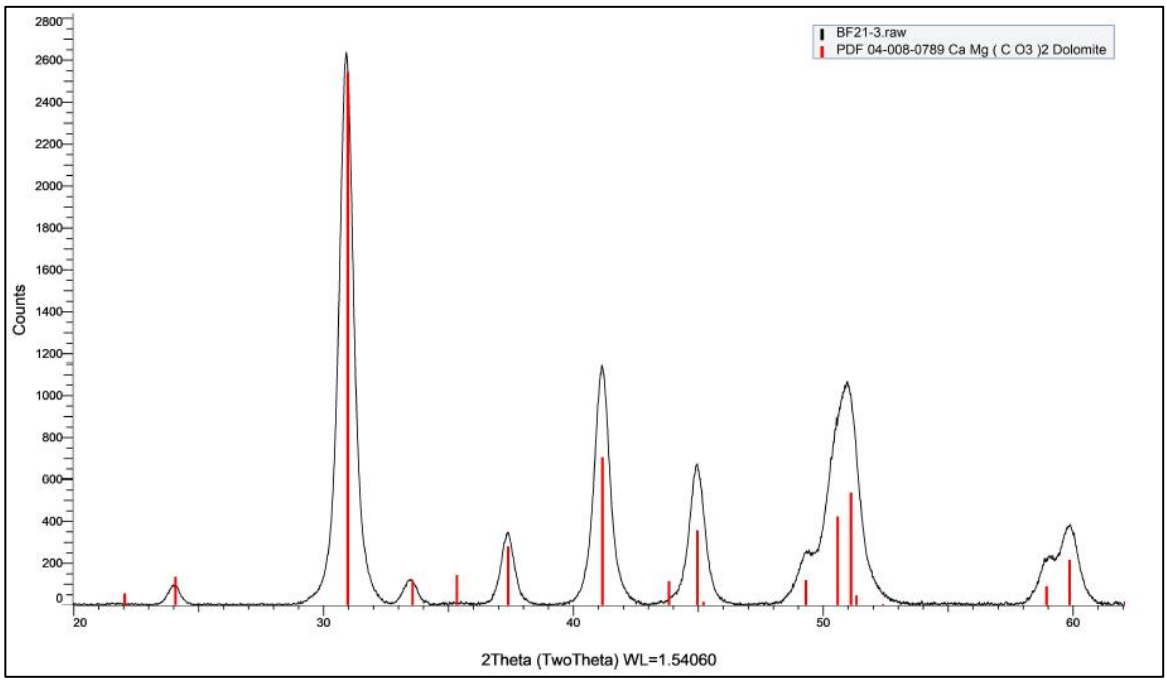

Figure S62. XRD pattern for BF-21-3, obtained by CuKα radiation.

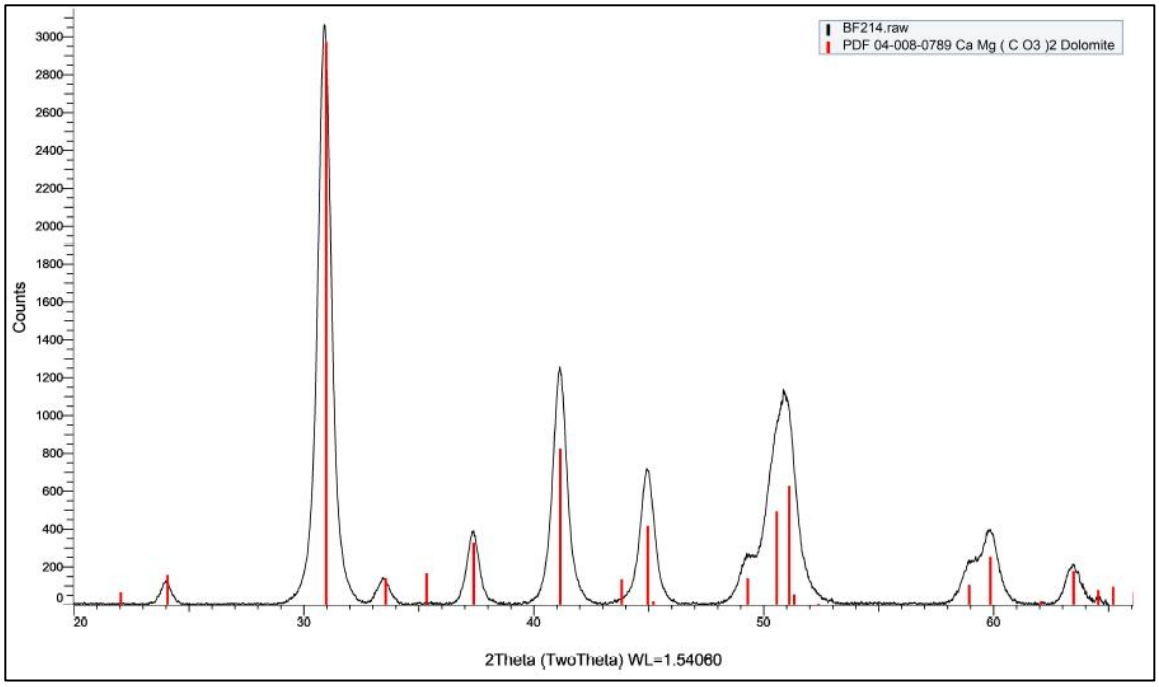

Figure S63. XRD pattern for BF-22-4, obtained by CuKα radiation.

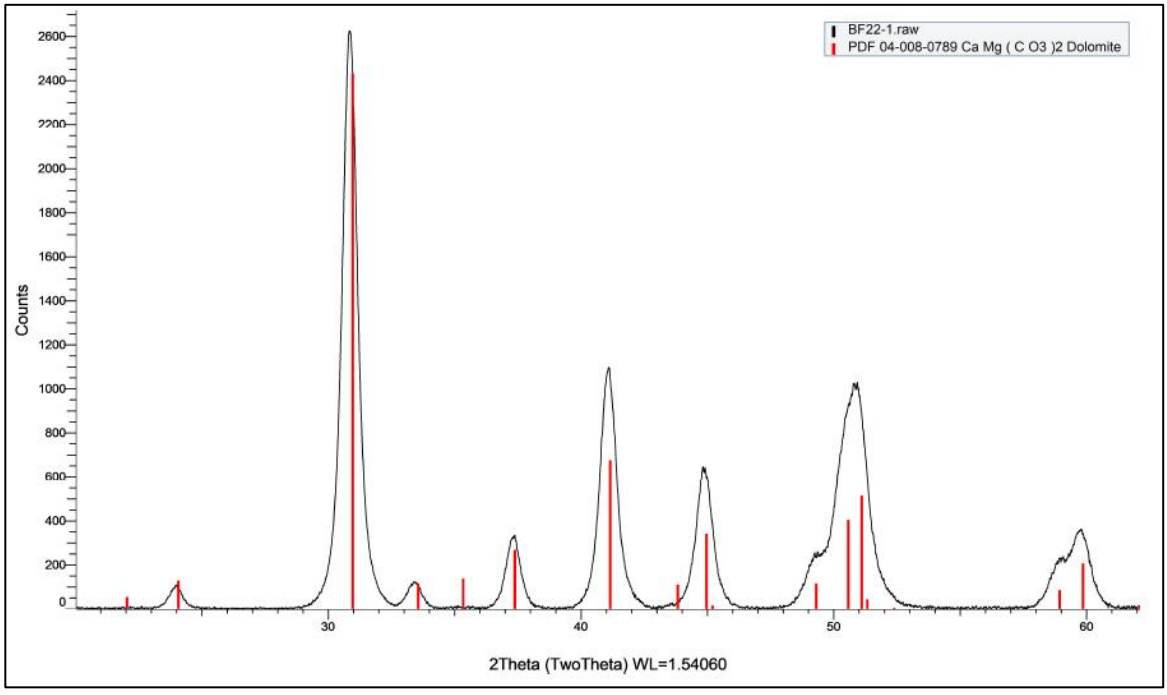

Figure S64. XRD pattern for BF-22-1, obtained by CuKα radiation.

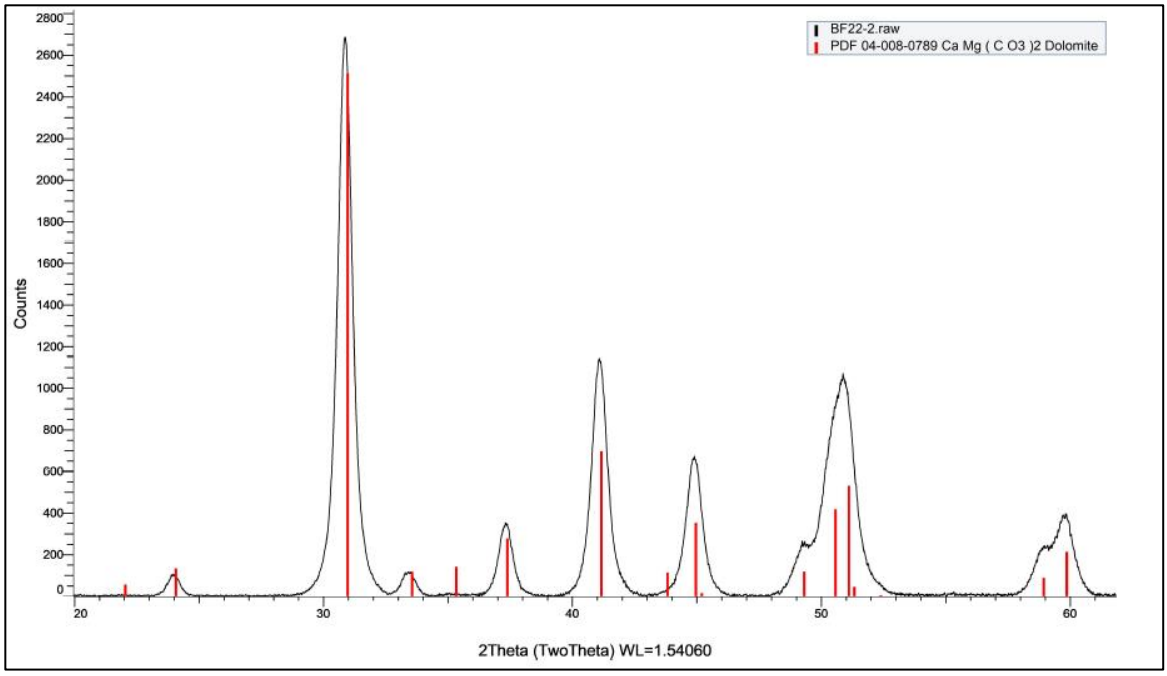

Figure S65. XRD pattern for BF-22-2, obtained by CuKα radiation.

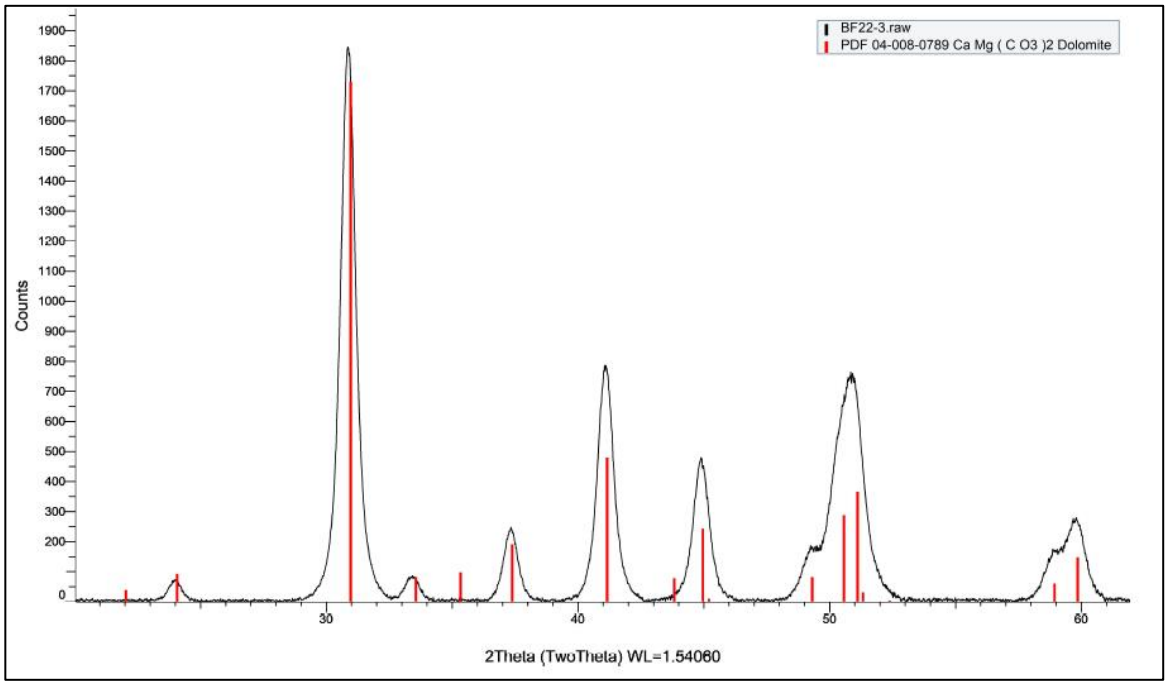

Figure S66. XRD pattern for BF-22-3, obtained by CuKα radiation.

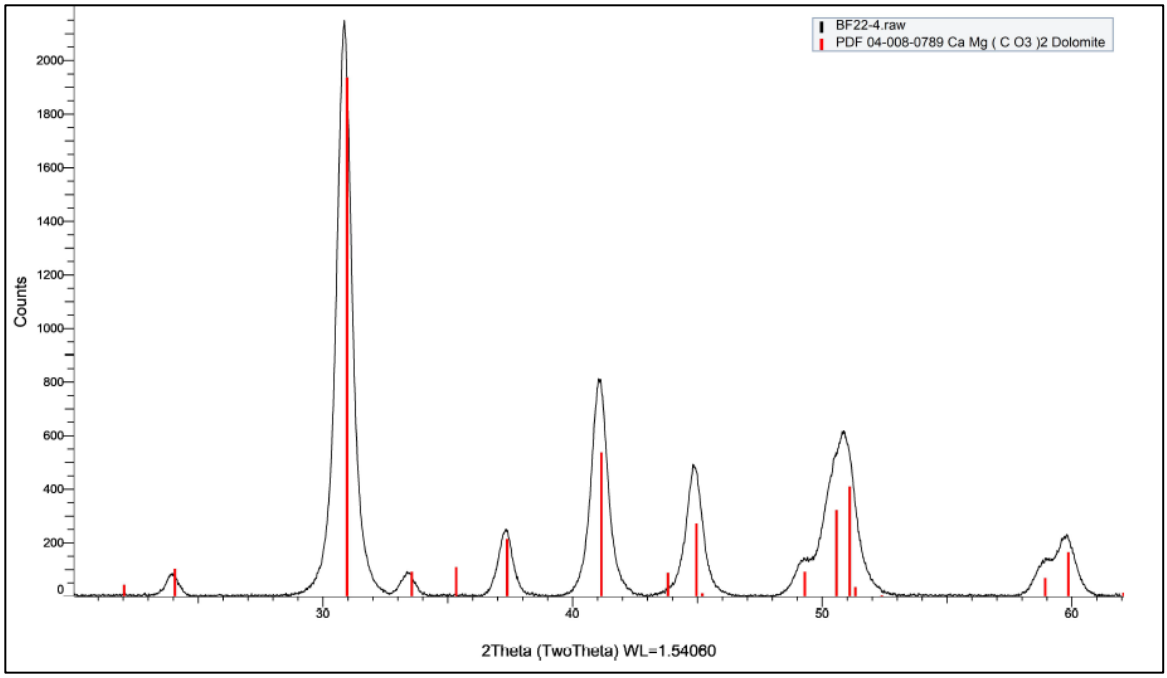

Figure S67. XRD pattern for BF-22-4, obtained by CuKα radiation.

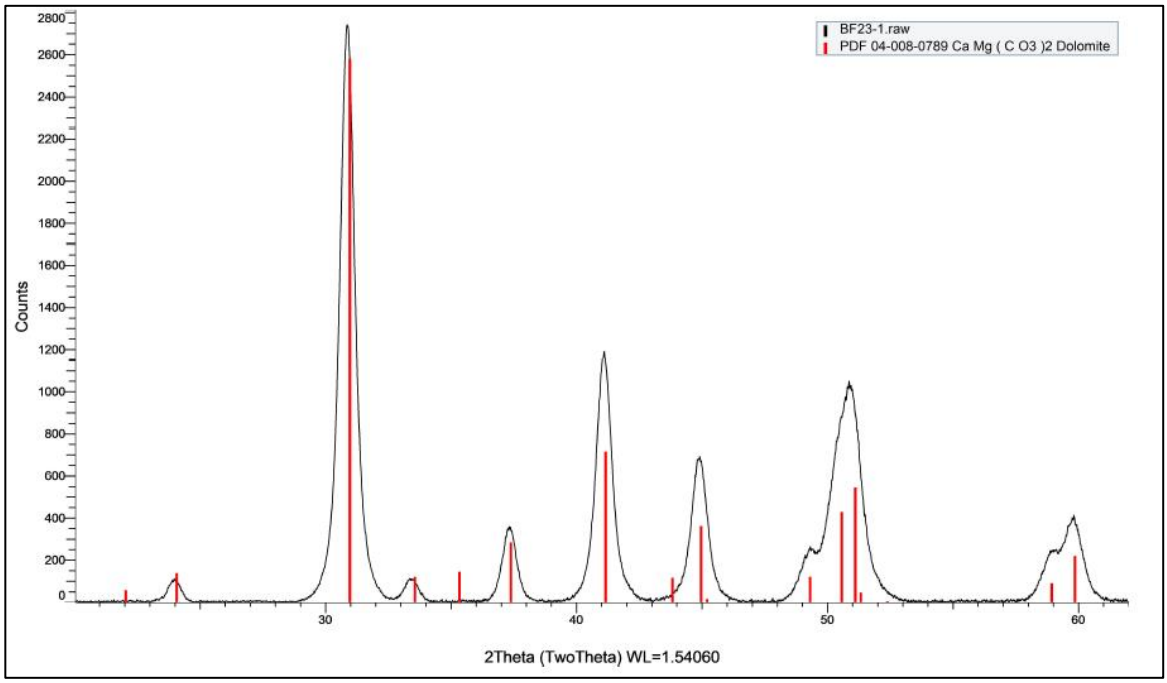

Figure S68. XRD pattern for BF-23-1, obtained by CuKα radiation.

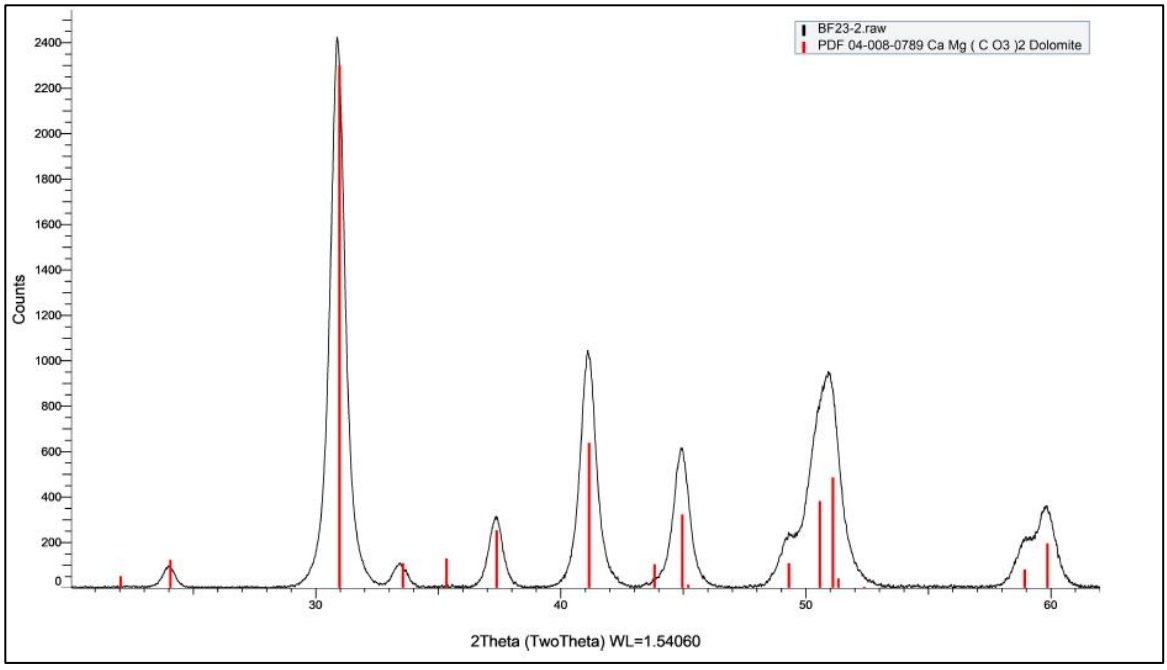

Figure S69. XRD pattern for BF-23-2, obtained by CuKα radiation.

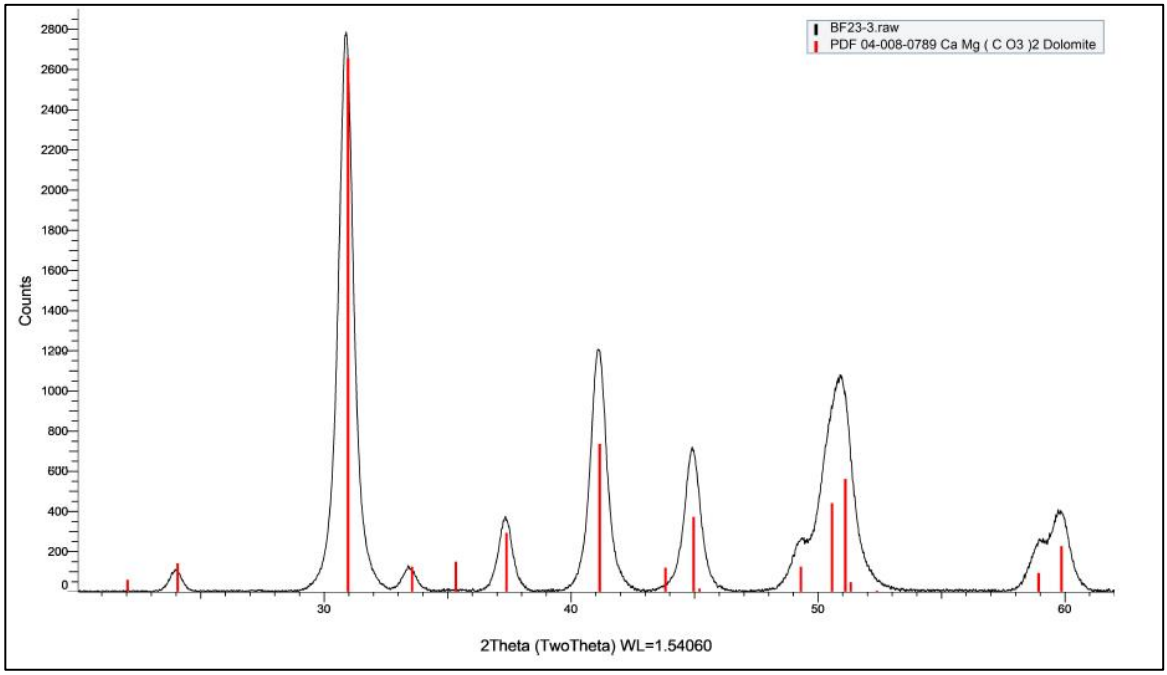

Figure S70. XRD pattern for BF-23-3, obtained by CuKα radiation.

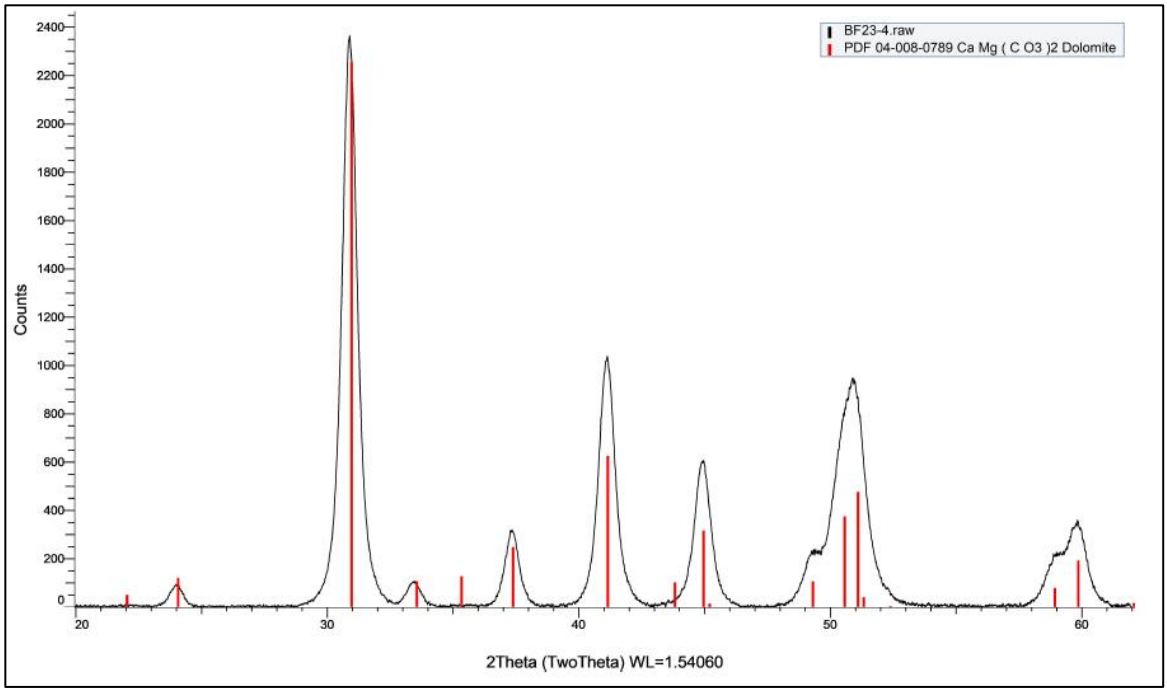

Figure S71. XRD pattern for BF-23-4, obtained by CuKα radiation.

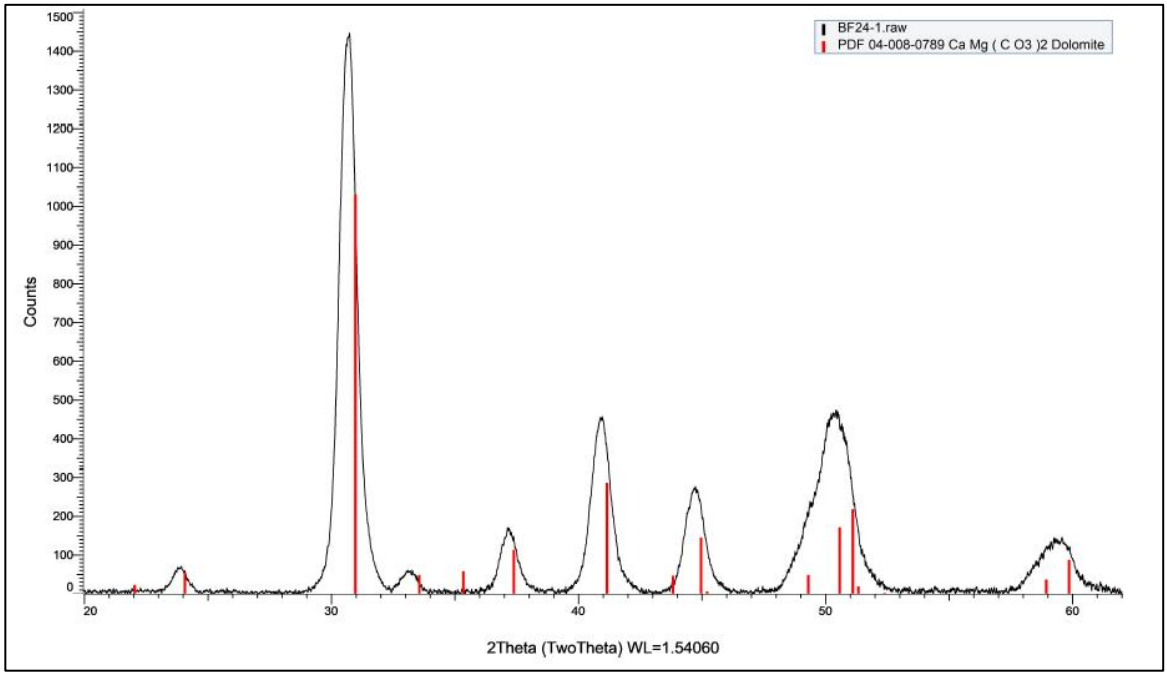

Figure S72. XRD pattern for BF-24-1, obtained by CuKα radiation.

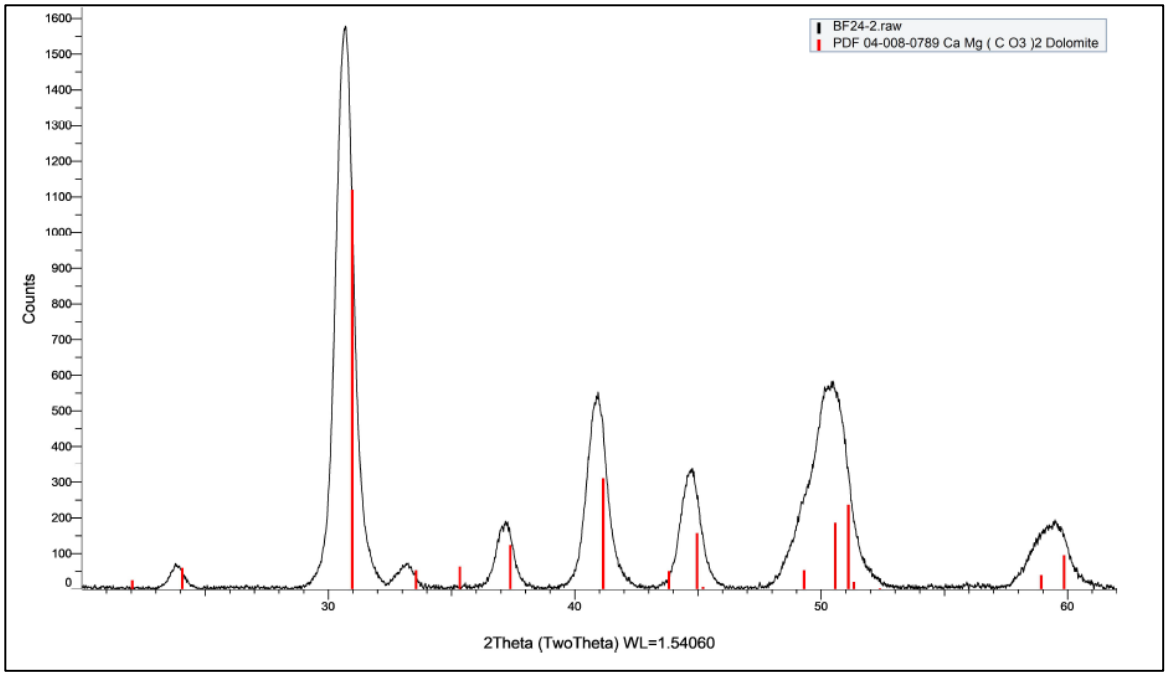

Figure S73. XRD pattern for BF-24-2, obtained by CuKα radiation.

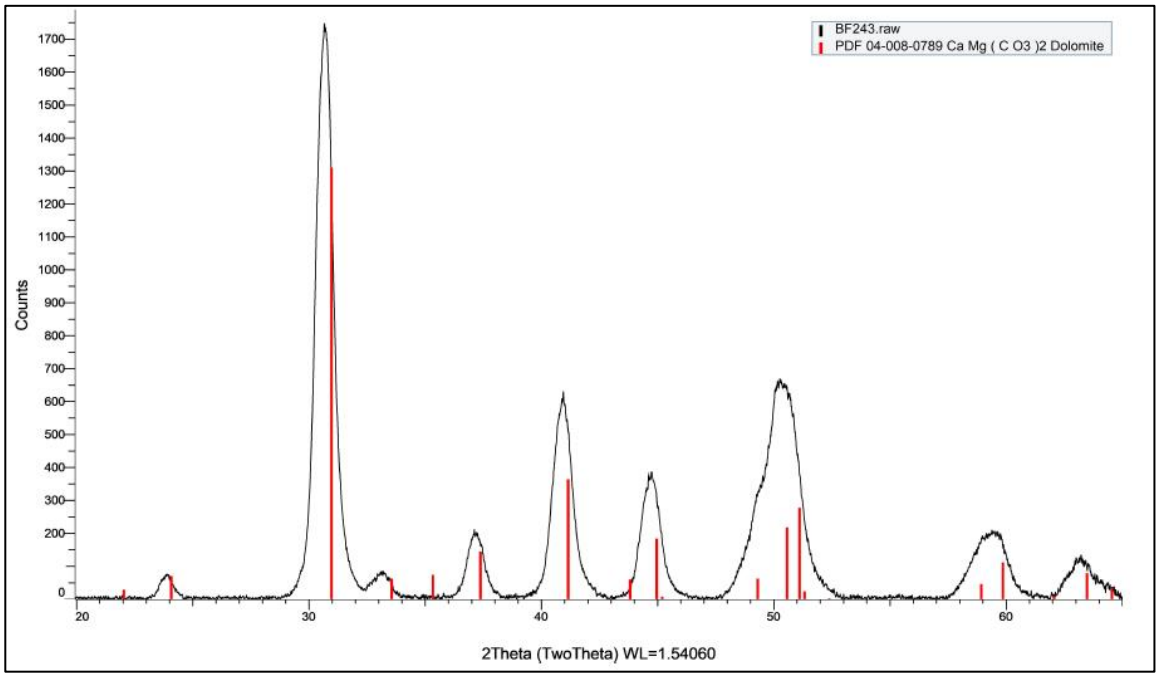

Figure S74. XRD pattern for BF-24-3, obtained by CuKα radiation.

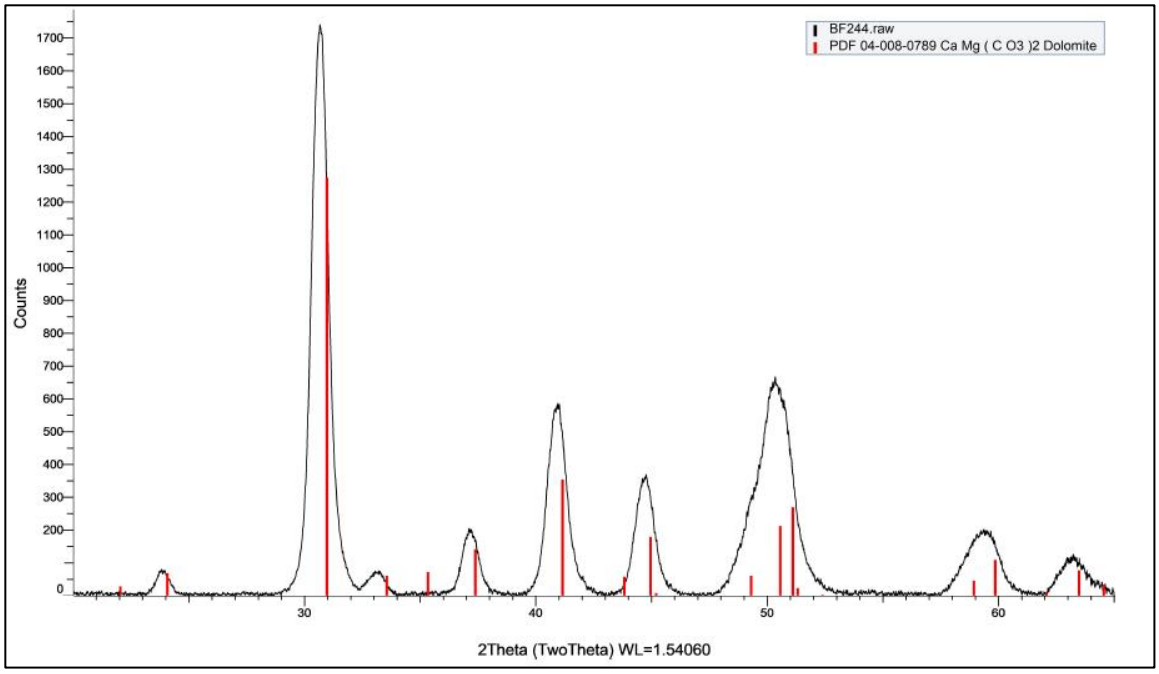

Figure S75. XRD pattern for BF-24-4, obtained by CuKα radiation.

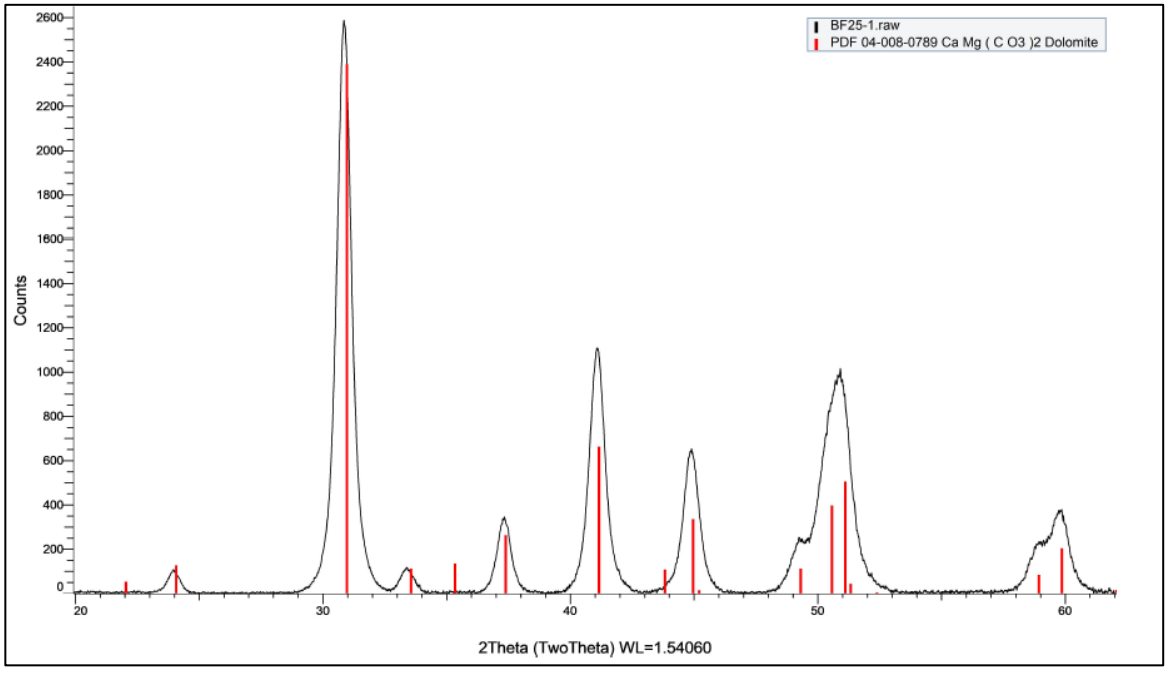

Figure S76. XRD pattern for BF-25-1, obtained by CuKα radiation.

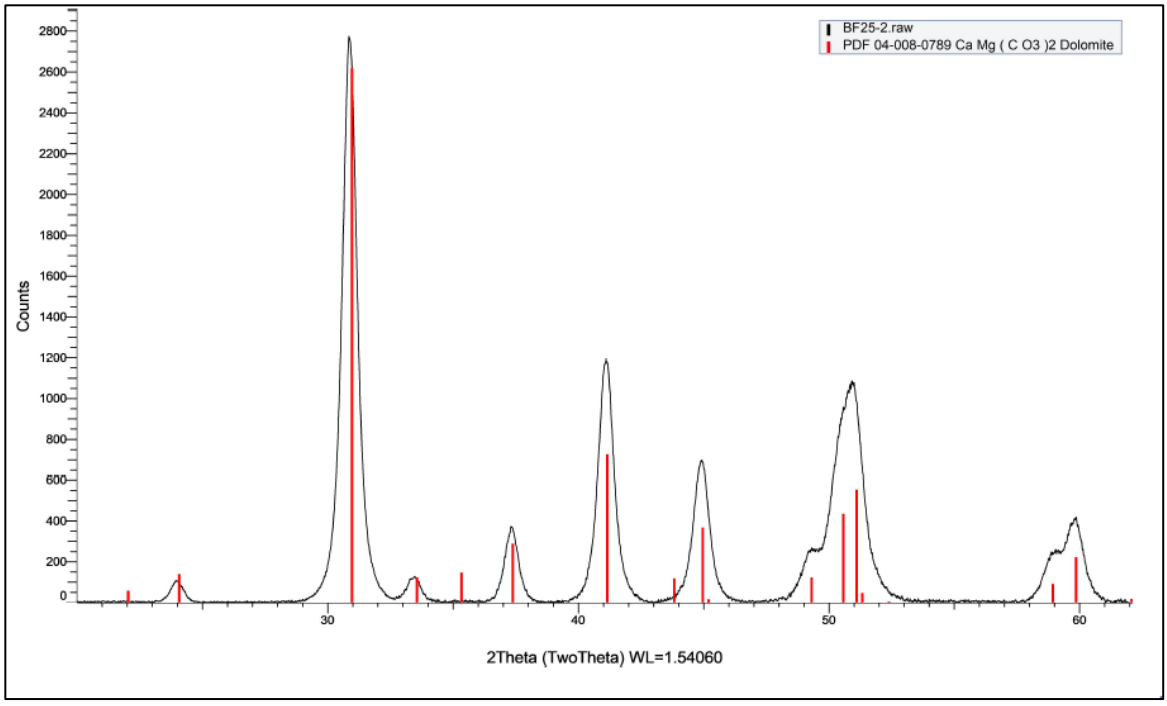

Figure S77. XRD pattern for BF-25-2, obtained by CuKα radiation.

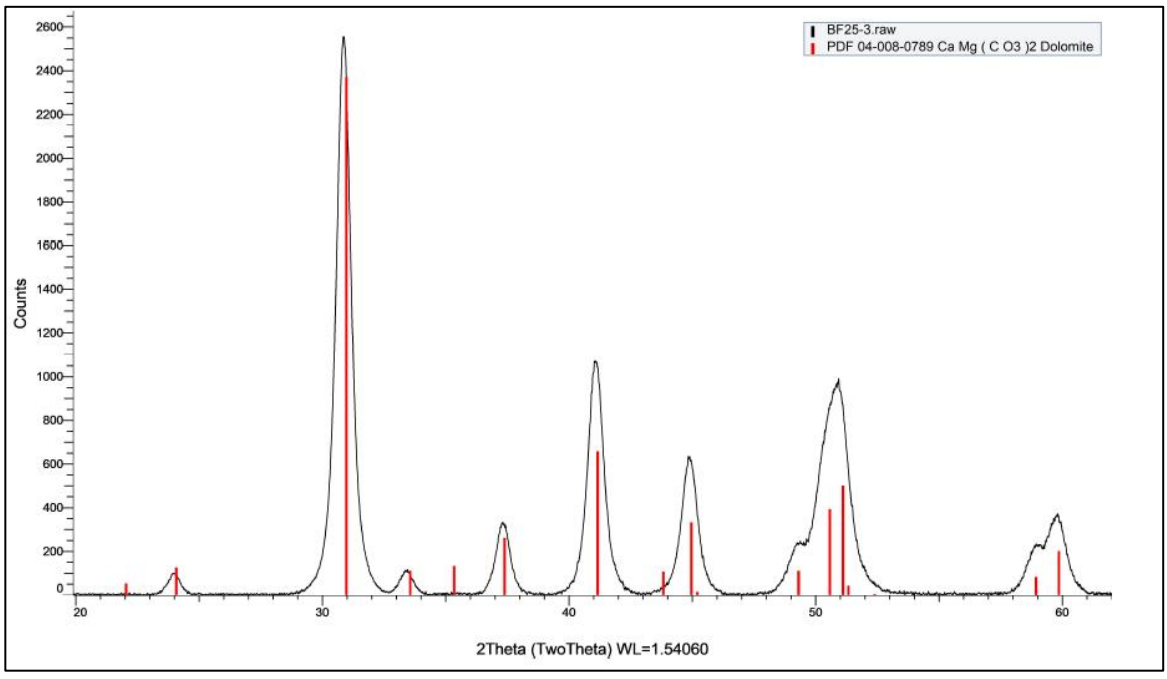

Figure S78. XRD pattern for BF-25-3, obtained by CuKα radiation.

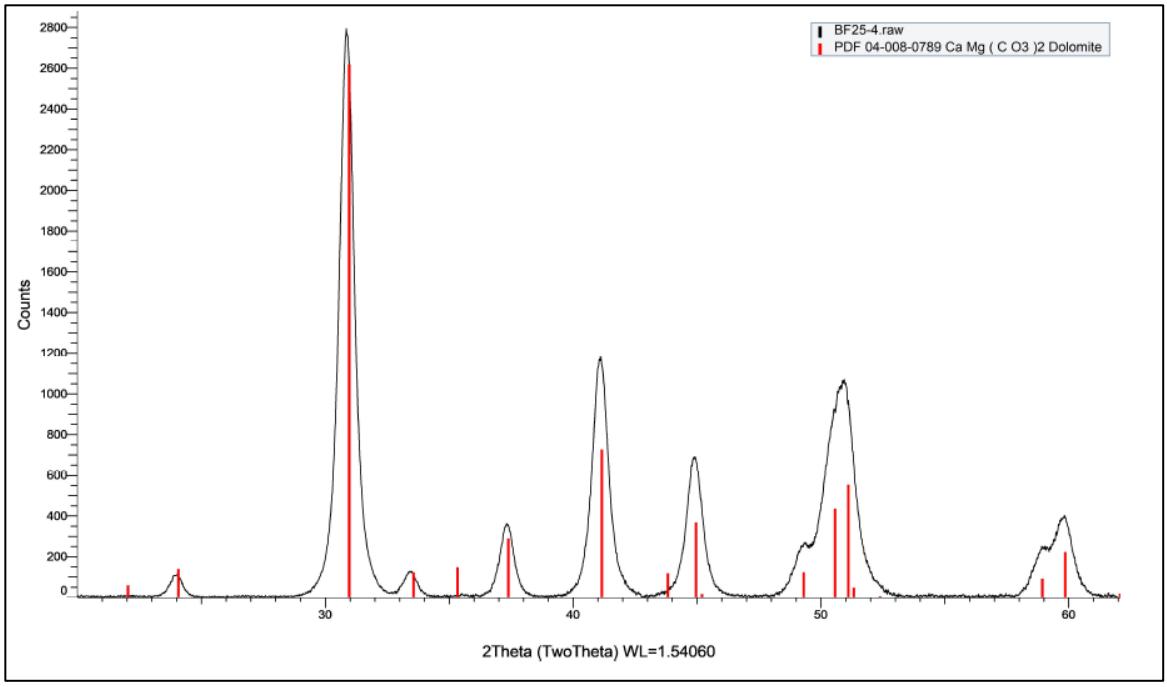

Figure S79. XRD pattern for BF-25-4, obtained by CuKα radiation.

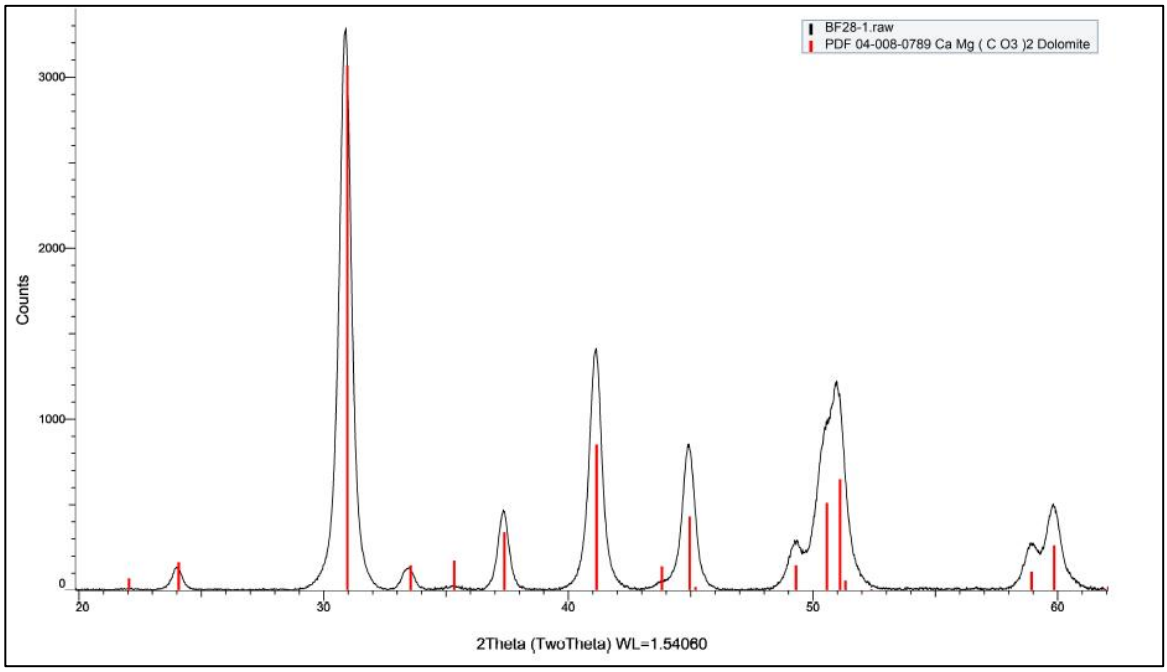

Figure S80. XRD pattern for BF-28-1, obtained by CuKα radiation.

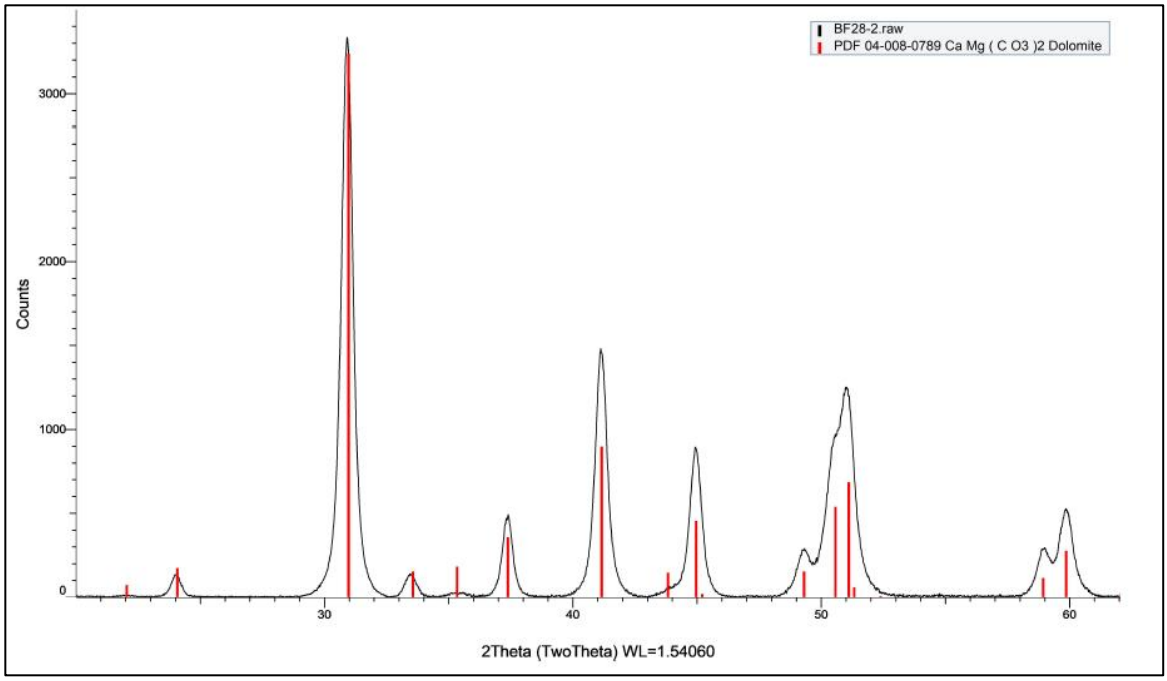

Figure S81. XRD pattern for BF-28-2, obtained by CuKα radiation.

Table S1. Detailed parent solution conditions and isotopic results for all samples analyzed. Samples removed due to evaporation effects are highlighted in grey.

Sample ID	Temperature (°C)	Precipitation Method	Condition	Product Mineralogy	Source Na_2CO_3	$\delta^{18}O_{Carb}$ (‰)	Average	σ	$\delta^{18}O_{Final}$ (‰)	$\delta^{18}O_{Final}$ - $\delta^{18}O_{Initial}$	$1000ln\alpha_{Carbonate-Water}$	Average	σ
BF-3-1 r1	40	SAM	No U	P	A	20.88	20.71	0.17	-6.30	0.34	26.99	26.82	0.17
BF-3-1 r2	40	SAM	No U	P	A	20.54			-6.30	0.34	26.66		
BF-3-2 r2	40	SAM	No U	P	A	20.62	20.45	0.17	-6.36	0.28	26.79	26.63	0.16
BF-3-2 r2	40	SAM	No U	P	A	20.29			-6.36	0.28	26.47		
BF-3-3 r1	40	SAM	U	P	A	20.26	17.23	2.97	-6.35	0.29	26.42	23.44	3.04
BF-3-3 r2	40	SAM	U	P	A	14.08			-6.35	0.29	20.35		
BF-3-3 r3	40	SAM	U	P	A	14.43			-6.35	0.29	20.69		
BF-3-3 r4	40	SAM	U	P	A	20.13			-6.35	0.29	26.30		
BF-3-4 r1	40	SAM	U	P	A	20.80	19.63	1.18	-6.35	0.29	26.96	25.81	1.15
BF-3-4 r2	40	SAM	U	P	A	18.45			-6.35	0.29	24.65		
BF-22-1 r1	50	SAM	U	P	B	20.36	20.31	0.06	-6.03	0.61	26.21	26.15	0.05
BF-22-1 r2	50	SAM	U	P	B	20.25			-6.03	0.61	26.10		
BF-22-2 r1	50	SAM	No U	P	B	20.46	20.17	0.29	-6.51	0.13	26.78	26.50	0.28
BF-22-2 r2	50	SAM	No U	P	B	19.88			-6.51	0.13	26.21		
BF-22-3 r1	50	SAM	U	P	B	18.85	19.92	1.06	-6.33	0.31	25.03	26.07	1.04
BF-22-3 r2	50	SAM	U	P	B	20.98			-6.33	0.31	27.12		
BF-22-4 r1	50	SAM	U	P	B	20.24	21.12	0.88	-6.49	0.15	26.55	27.41	0.86
BF-22-4 r2	50	SAM	U	P	B	22.00			-6.49	0.15	28.27		
BF-23-1 r1	50	SAM	2X U	P	B	16.96	17.96	1.00	-6.50	0.14	23.34	24.32	0.98
BF-23-1 r2	50	SAM	2X U	P	B	18.96			-6.50	0.14	25.31		
BF-23-2 r1	50	SAM	2X U	P	B	21.65	20.71	0.95	-6.51	0.13	27.96	27.03	0.93
BF-23-2 r2	50	SAM	2X U	P	B	19.76			-6.51	0.13	26.10		
BF-23-3 r1	50	SAM	5X U	D	B	20.54	19.76	0.78	-6.56	0.08	26.92	26.15	0.77
BF-23-3 r2	50	SAM	5X U	D	B	18.98			-6.56	0.08	25.38		
BF-23-4 r1	50	SAM	5X U	D	B	19.91	19.98	0.06	-6.53	0.11	26.27	26.33	0.06
BF-23-4 r2	50	SAM	5X U	D	B	20.04			-6.53	0.11	26.40		
BF-25-1 r1	50	SAM	No U	P	B	20.16	19.92	0.24	-6.46	0.18	26.43	26.20	0.23
BF-25-1 r2	50	SAM	No U	P	B	19.68			-6.46	0.18	25.97		
BF-25-2 r1	50	SAM	U	P	B	19.74	19.88	0.14	-6.48	0.16	26.05	26.19	0.14
BF-25-2 r2	50	SAM	U	P	B	20.03			-6.48	0.16	26.33		
BF-25-3 r1	50	SAM	2X U	P	B	19.66	20.06	0.40	-5.27	1.37	24.76	25.15	0.39
BF-25-3 r2	50	SAM	2X U	P	B	20.46			-5.27	1.37	25.54		
BF-25-4 r1	50	SAM	5X U	D	B	19.13	19.74	0.61	-6.54	0.10	25.51	26.11	0.60
BF-25-4 r2	50	SAM	5X U	D	B	20.35			-6.54	0.10	26.70		
BF-24-1 r1	50	AAM	AAM	H	B	19.77	19.34	0.43	-6.40	0.24	26.00	25.58	0.43
BF-24-1 r2	50	AAM	AAM	H	B	18.90			-6.40	0.24	25.15		
BF-24-2 r1	50	AAM	AAM	H	B	19.84	19.91	0.07	-6.39	0.25	26.05	26.12	0.07
BF-24-2 r2	50	AAM	AAM	H	B	19.98			-6.39	0.25	26.19		
BF-24-3 r1	50	AAM	AAM+U	H	B	20.66	20.48	0.17	-6.35	0.29	26.82	26.65	0.17
BF-24-3 r2	50	AAM	AAM+U	H	B	20.31			-6.35	0.29	26.48		
BF-24-4 r1	50	AAM	AAM+U	H	B	19.61	20.00	0.40	-6.31	0.33	25.75	26.14	0.39
BF-24-4 r2	50	AAM	AAM+U	H	B	20.40			-6.31	0.33	26.53		
BF-9-1 r1	60	SAM	U	D	A	18.75	18.82	0.07	-6.56	0.08	25.16	25.23	0.07
BF-9-1 r2	60	SAM	U	D	A	18.89			-6.56	0.08	25.30		
BF-9-4 r1	60	SAM	No U	D	A	18.02	18.10	0.07	-6.56	0.08	24.44	24.52	0.07
BF-9-4 r2	60	SAM	No U	D	A	18.17			-6.56	0.08	24.59		
BF-12-1 r1	60	SAM	2X U	D	A	17.84	18.07	0.23	-6.65	-0.01	24.35	24.58	0.23
BF-12-1 r2	60	SAM	2X U	D	A	18.30			-6.65	-0.01	24.81		
BF-12-2 r1	60	SAM	2X U	D	A	18.22	18.61	0.38	-6.68	-0.04	24.76	25.14	0.37
BF-12-2 r2	60	SAM	2X U	D	A	18.99			-6.68	-0.04	25.51		
BF-12-3 r1	60	SAM	CaCl2+U	D	A	17.98	17.91	0.07	-5.71	0.93	23.55	23.48	0.06
BF-12-3 r2	60	SAM	CaCl2+U	D	A	17.85			-5.71	0.93	23.42		
BF-12-4 r1	60	SAM	CaCl2+U	D	A	18.41	18.35	0.06	-6.78	-0.14	25.04	24.99	0.06
BF-12-4 r2	60	SAM	CaCl2+U	D	A	18.29			-6.78	-0.14	24.93		
BF-16-1 r1	60	SAM	U	D	A	18.84	18.87	0.03	-6.54	0.10	25.22	25.25	0.03
BF-16-1 r2	60	SAM	U	D	A	18.89			-6.54	0.10	25.28		
BF-16-2 r1	60	SAM	U	D	A	7.76	13.28	5.52	-6.44	0.20	14.18	19.64	5.45
BF-16-2 r2	60	SAM	U	D	A	18.81			-6.44	0.20	25.09		
BF-16-3 r1	60	SAM	No U	D	A	18.71	18.72	0.01	-6.44	0.20	25.00	25.01	0.01
BF-16-3 r2	60	SAM	No U	D	A	18.72			-6.44	0.20	25.01		
BF-16-4 r1	60	SAM	No U	D	A	18.67	18.77	0.11	-6.44	0.20	24.96	25.06	0.11
BF-16-4 r2	60	SAM	No U	D	A	18.88			-6.44	0.20	25.17		
BF-17-1 r1	60	SAM	50mL	D	A	18.74	18.71	0.02	-6.57	0.07	25.16	25.14	0.02
BF-17-1 r2	60	SAM	50mL	D	A	18.69			-6.57	0.07	25.12		
BF-17-2 r1	60	SAM	50mL	D	A	18.60	17.30	1.31	-6.55	0.09	25.01	23.72	1.29
BF-17-2 r2	60	SAM	50mL	D	A	15.99			-6.55	0.09	22.44		
BF-17-3 r1	60	SAM	50mL+U	D	A	18.77	18.66	0.11	-6.29	0.35	24.91	24.80	0.11
BF-17-3 r2	60	SAM	50mL+U	D	A	18.56			-6.29	0.35	24.70		
BF-17-4 r1	60	SAM	50mL+U	D	A	18.73	18.41	0.31	-5.21	1.43	23.78	23.47	0.31
BF-17-4 r2	60	SAM	50mL+U	D	A	18.10			-5.21	1.43	23.16		
BF-20-1 r1	60	SAM	U	D	B	20.10	20.22	0.12	-6.36	0.28	26.29	26.40	0.12
BF-20-1 r2	60	SAM	U	D	B	20.34			-6.36	0.28	26.52		
BF-20-2 r1	60	SAM	No U	D	B	19.73	19.32	0.41	-6.41	0.23	25.97	25.57	0.41
BF-20-2 r2	60	SAM	No U	D	B	18.90			-6.41	0.23	25.16		
BF-20-3 r1	60	SAM	2X U	D	B	20.12	18.72	1.40	-6.59	0.05	26.53	25.16	1.37
BF-20-3 r2	60	SAM	2X U	D	B	17.32			-6.59	0.05	23.79		
BF-21-1 r1	60	SAM	50mL	D	B	19.91	19.57	0.34	-5.84	0.80	25.58	25.24	0.34
BF-21-1 r2	60	SAM	50mL	D	B	19.22			-5.84	0.80	24.90		
BF-21-2 r1	60	SAM	50mL+U	D	B	19.13	18.98	0.15	-6.54	0.10	25.51	25.36	0.15
BF-21-2 r2	60	SAM	50mL+U	D	B	18.82			-6.54	0.10	25.21		
BF-21-3 r1	60	SAM	50mL+2X U	D	B	19.21	19.25	0.04	-6.50	0.14	25.55	25.59	0.04
BF-21-3 r2	60	SAM	50mL+2X U	D	B	19.29			-6.50	0.14	25.63		
BF-21-4 r1	60	SAM	50mL+2X U	D	B	18.80	19.47	0.67	-6.20	0.44	24.84	25.50	0.66
BF-21-4 r2	60	SAM	50mL+2X U	D	B	20.15			-6.20	0.44	26.16		
BF-14-1 r1	60	AAM	AAM+U	P	A	18.91	18.42	0.49	-6.34	0.30	25.09	24.60	0.48
BF-14-1 r2	60	AAM	AAM+U	P	A	17.92			-6.34	0.30	24.12		
BF-14-2 r1	60	AAM	AAM+U	P	A	18.40	18.22	0.18	-6.25	0.39	24.50	24.32	0.18
BF-14-2 r2	60	AAM	AAM+U	P	A	18.03			-6.25	0.39	24.14		
BF-14-3 r1	60	AAM	AAM	P	A	18.96	18.76	0.20	-6.26	0.38	25.06	24.87	0.20
BF-14-3 r2	60	AAM	AAM	P	A	18.56			-6.26	0.38	24.67		
BF-14-4 r1	60	AAM	AAM	P	A	18.88	18.81	0.07	-6.13	0.51	24.86	24.79	0.07
BF-14-4 r2	60	AAM	AAM	P	A	18.74			-6.13	0.51	24.72		

Sample ID	Temperature (°C)	Precipitation Method	Condition	Product Mineralogy	Source Na_2CO_3	$\delta^{18}O_{Carb}$ (‰)	Average	σ	$\delta^{18}O_{Final}$ (‰)	$\delta^{18}O_{Final}$- $\delta^{18}O_{Initial}$	$1000\ln\alpha_{Carbonate\text{-}Water}$	Average	σ
BF-15-1 r1	70	SAM	U	D	A	17.64	17.64	0.00	-6.53	0.11	24.04	24.04	0.00
BF-15-1 r2	70	SAM	U	D	A	17.65			-6.53	0.11	24.04		
BF-15-2 r1	70	SAM	U	D	A	18.04	18.08	0.04	-5.78	0.86	23.68	23.72	0.04
BF-15-2 r2	70	SAM	U	D	A	18.11			-5.78	0.86	23.75		
BF-15-3 r1	70	SAM	No U	D	A	18.23	18.26	0.03	-2.19	4.45	20.26	20.29	0.03
BF-15-3 r2	70	SAM	No U	D	A	18.30			-2.19	4.45	20.33		
BF-15-4 r1	70	SAM	No U	D	A	17.52	17.66	0.14	-6.33	0.31	23.72	23.86	0.14
BF-15-4 r2	70	SAM	No U	D	A	17.81			-6.33	0.31	24.00		
BF-18-1 r1	70	SAM	2X U	D	A	17.85	17.68	0.17	-6.77	-0.13	24.48	24.31	0.17
BF-18-1 r2	70	SAM	2X U	D	A	17.51			-6.77	-0.13	24.14		
BF-18-2 r1	70	SAM	2X U	D	A	17.94	17.80	0.14	-6.72	-0.08	24.52	24.39	0.13
BF-18-2 r2	70	SAM	2X U	D	A	17.66			-6.72	-0.08	24.25		
BF-18-3 r1	70	SAM	CaCl2+U	D	A	18.60	18.67	0.06	0.75	7.39	17.68	17.74	0.06
BF-18-3 r2	70	SAM	CaCl2+U	D	A	18.73			0.75	7.39	17.80		
BF-18-4 r1	70	SAM	CaCl2+U	D	A	17.73	17.75	0.02	-6.83	-0.19	24.43	24.45	0.02
BF-18-4 r2	70	SAM	CaCl2+U	D	A	17.77			-6.83	-0.19	24.47		
BF-1-1 r1	80	SAM	No U	D	A	17.08	17.01	0.07	-6.32	0.32	23.27	23.20	0.07
BF-1-1 r2	80	SAM	No U	D	A	16.94			-6.32	0.32	23.13		
BF-1-2 r1	80	SAM	No U	D	A	16.58	16.76	0.18	-6.22	0.42	22.68	22.86	0.17
BF-1-2 r2	80	SAM	No U	D	A	16.93			-6.22	0.42	23.03		
BF-1-3 r1	80	SAM	U	D	A	17.11	16.96	0.15	-6.46	0.18	23.44	23.30	0.14
BF-1-3 r2	80	SAM	U	D	A	16.82			-6.46	0.18	23.16		
BF-1-4 r1	80	SAM	U	D	A	17.30	17.30	0.00	-6.58	0.06	23.76	23.76	0.00
BF-1-4 r2	80	SAM	U	D	A	17.31			-6.58	0.06	23.76		
BF-6-1 r1	80	SAM	U	D	A	16.80	16.87	0.07	-7.01	-0.37	23.70	23.76	0.07
BF-6-1 r2	80	SAM	U	D	A	16.93			-7.01	-0.37	23.83		
BF-6-2 r1	80	SAM	U	D	A	17.02	17.04	0.02	-6.79	-0.15	23.69	23.71	0.02
BF-6-2 r2	80	SAM	U	D	A	17.06			-6.79	-0.15	23.72		
BF-6-3 r1	80	SAM	CaCl2+U	D	A	16.96	17.01	0.05	-6.88	-0.24	23.72	23.77	0.05
BF-6-3 r2	80	SAM	CaCl2+U	D	A	17.06			-6.88	-0.24	23.82		
BF-6-4 r1	80	SAM	CaCl2+U	D	A	16.04	16.57	0.34	-6.88	-0.24	22.81	23.34	0.34
BF-6-4 r2	80	SAM	CaCl2+U	D	A	16.97			-6.88	-0.24	23.73		
BF-6-4 r3	80	SAM	CaCl2+U	D	A	16.58			-6.88	-0.24	23.35		
BF-6-4 r4	80	SAM	CaCl2+U	D	A	16.71			-6.88	-0.24	23.48		
BF-6-5 r1	80	SAM	2X U	D	A	17.16	17.20	0.04	-6.95	-0.31	23.99	24.02	0.04
BF-6-5 r2	80	SAM	2X U	D	A	17.24			-6.95	-0.31	24.06		
BF-6-6 r1	80	SAM	2X U	D	A	17.18	16.91	0.27	-6.99	-0.35	24.05	23.78	0.27
BF-6-6 r2	80	SAM	2X U	D	A	16.63			-6.99	-0.35	23.51		
BF-13-1 r1	80	SAM	50mL	D	A	17.31	17.24	0.06	-5.71	0.93	22.88	22.82	0.06
BF-13-1 r2	80	SAM	50mL	D	A	17.18			-5.71	0.93	22.76		
BF-13-2 r1	80	SAM	50mL	D	A	17.08	17.01	0.07	-6.53	0.11	23.49	23.42	0.07
BF-13-2 r2	80	SAM	50mL	D	A	16.94			-6.53	0.11	23.35		
BF-13-3 r1	80	SAM	50mL+U	D	A	17.07	16.99	0.08	-6.87	-0.23	23.82	23.74	0.08
BF-13-3 r2	80	SAM	50mL+U	D	A	16.91			-6.87	-0.23	23.66		
BF-13-4 r1	80	SAM	50mL+U	D	A	17.11	17.03	0.08	-6.79	-0.15	23.78	23.70	0.08
BF-13-4 r2	80	SAM	50mL+U	D	A	16.94			-6.79	-0.15	23.62		
BF-28-1 r1	80	SAM	No U	D	B	17.89	17.49	0.40	-4.25	2.39	21.99	21.60	0.39
BF-28-1 r2	80	SAM	No U	D	B	17.09			-4.25	2.39	21.21		
BF-28-2 r1	80	SAM	No U	D	B	16.63	16.60	0.02	-6.34	0.30	22.85	22.83	0.02
BF-28-2 r2	80	SAM	No U	D	B	16.58			-6.34	0.30	22.81		
BF-7-1 r1	80	AAM	AAM+U	D,A	A	16.20	15.95	0.25	-6.32	0.32	22.41	22.17	0.24
BF-7-1 r2	80	AAM	AAM+U	D,A	A	15.71			-6.32	0.32	21.92		
BF-7-2 r1	80	AAM	AAM+U	D,A	A	16.28	16.30	0.03	-6.08	0.56	22.25	22.27	0.03
BF-7-2 r2	80	AAM	AAM+U	D,A	A	16.33			-6.08	0.56	22.30		
BF-7-3 r1	80	AAM	AAM	P,A	A	15.79	16.17	0.38	-6.16	0.48	21.85	22.22	0.37
BF-7-3 r2	80	AAM	AAM	P,A	A	16.55			-6.16	0.48	22.59		
BF-7-4 r1	80	AAM	AAM	P,A	A	16.18	16.27	0.09	-6.18	0.46	22.25	22.34	0.09
BF-7-4 r2	80	AAM	AAM	P,A	A	16.36			-6.18	0.46	22.43		